frontiers | Research Topics

Emerging talents in toxicology

Edited by
Ana Luiza Ziulkoski, Samson Amos, Yuseok Moon, Alessandro Venosa, Iseult Lynch, Neus Feliu, Francesca Larese Filon, Salik Hussain, Lena Smirnova, Monica Renee Langley, Onyenmechi Afonne, Tara McMorrow, Luigi Margiotta-Casaluci, Alexa C. Alexander, Juliana Perobelli, Marina Trevizan Guerra, Dilek Battal, Vera Marisa Costa, Takamitsu A. Kato and Xiaohui Fan

Published in
Frontiers in Toxicology

ISSN 1664-8714
ISBN 978-2-8325-4463-1
DOI 10.3389/978-2-8325-4463-1

About Frontiers

Frontiers is more than just an open access publisher of scholarly articles: it is a pioneering approach to the world of academia, radically improving the way scholarly research is managed. The grand vision of Frontiers is a world where all people have an equal opportunity to seek, share and generate knowledge. Frontiers provides immediate and permanent online open access to all its publications, but this alone is not enough to realize our grand goals.

Frontiers journal series

The Frontiers journal series is a multi-tier and interdisciplinary set of open-access, online journals, promising a paradigm shift from the current review, selection and dissemination processes in academic publishing. All Frontiers journals are driven by researchers for researchers; therefore, they constitute a service to the scholarly community. At the same time, the *Frontiers journal series* operates on a revolutionary invention, the tiered publishing system, initially addressing specific communities of scholars, and gradually climbing up to broader public understanding, thus serving the interests of the lay society, too.

Dedication to quality

Each Frontiers article is a landmark of the highest quality, thanks to genuinely collaborative interactions between authors and review editors, who include some of the world's best academicians. Research must be certified by peers before entering a stream of knowledge that may eventually reach the public - and shape society; therefore, Frontiers only applies the most rigorous and unbiased reviews. Frontiers revolutionizes research publishing by freely delivering the most outstanding research, evaluated with no bias from both the academic and social point of view. By applying the most advanced information technologies, Frontiers is catapulting scholarly publishing into a new generation.

What are Frontiers Research Topics?

Frontiers Research Topics are very popular trademarks of the *Frontiers journals series*: they are collections of at least ten articles, all centered on a particular subject. With their unique mix of varied contributions from Original Research to Review Articles, Frontiers Research Topics unify the most influential researchers, the latest key findings and historical advances in a hot research area.

Find out more on how to host your own Frontiers Research Topic or contribute to one as an author by contacting the Frontiers editorial office: frontiersin.org/about/contact

Emerging talents in toxicology

Citation

Ziulkoski, A. L., Amos, S., Moon, Y., Venosa, A., Lynch, I., Feliu, N., Filon, F. L., Hussain, S., Smirnova, L., Langley, M. R., Afonne, O., McMorrow, T., Margiotta-Casaluci, L., Alexander, A. C., Perobelli, J., Guerra, M. T., Battal, D., Costa, V. M., Kato, T. A., Fan, X., eds. (2024). *Emerging talents in toxicology*. Lausanne: Frontiers Media SA. doi: 10.3389/978-2-8325-4463-1

Table of contents

frontiers | Frontiers in Toxicology

TYPE Editorial
PUBLISHED 01 February 2024
DOI 10.3389/ftox.2024.1369297

OPEN ACCESS

EDITED AND REVIEWED BY
Robert Landsiedel,
BASF, Germany

*CORRESPONDENCE
Takamitsu A. Kato,
takamitsu.kato@colostate.edu

RECEIVED 12 January 2024
ACCEPTED 24 January 2024
PUBLISHED 01 February 2024

CITATION
Kato TA (2024), Editorial: Emerging talents in toxicology.
Front. Toxicol. 6:1369297.
doi: 10.3389/ftox.2024.1369297

Editorial: Emerging talents in toxicology

Takamitsu A. Kato*

Department of Environmental and Radiological Health Sciences, Colorado State University, Fort Collins, CO, United States

KEYWORDS

nanoparticle, Corona formation, model organisms, risk assessment, nanodebris

Editorial on the Research Topic
Emerging talents in toxicology

In this editorial, I summarize six articles associated with nanoparticle research in the Research Topic "Emerging Talents in Toxicology" of the Journal of Frontiers in Toxicology.

The Research Topic, titled "Emerging talents in Toxicology" highlights recent advancements in toxicology, not limited to nanoparticle toxicology. The Research Topic comprises nine papers, with six of them specifically addressing nanoparticles. The growing use of nanomaterials indeed brings both benefits and concerns. Nanomaterials, due to their unique properties, have applications in various fields such as medicine, electronics, and materials science. However, the potential exposure to nanodebris raises questions about their impact on human health and the environment. It is crucial to distinguish between intentionally produced (engineered) nanomaterials and nonodebris. The term of 'nanodebris' refers to nanoparticles originating from the decomposition and wear-off materials a Research Topic specifically addressed in nanoplastics by Cunningham et al. This distinction is essential for a comprehensive understanding of the implications associated with nanomaterial usage. The specific risks associated with nanomaterial exposure depend on factors like the types of nanomaterial, its size, shape, and the route of exposure. Research is ongoing to understand the potential health and environmental effects of nanomaterials. In the context of human exposure, concerns include inhalation of airborne nanoparticles, ingestion through contaminated food or water, and skin contact. Similarly, environmental exposure can occur through the release of nanomaterials into air, water, or soil. Although nanoparticle research is expanding rapidly, there remain many unanswered questions in the fields. The six articles contribute insights into various nanoparticles, including Silver nanoparticle, Titanium dioxide nanoparticle, Cadmium Tellurium Quantum dots, and nanoplastics.

This editorial briefly introduces these papers, with three research papers investigating the detection and toxicology of nanoparticle and protein interactions. Another research article explores the transgenerational effects of nanoparticle exposure. Two review papers are included, with one summarizing the current status and problems of nanoplastics pollution and risk assessment, which the other proposes a unique model organism for ecotoxicology research.

The study by Park et al. investigates *in vitro* nanoparticle toxicology with protein modification, specifically examining the impact of glycation on nanoparticle-protein interactions, known as Corona formation. Silver nanoparticles, wildly used in the medical field for their antimicrobial properties, were studied in relation to their interaction with Human serum albumin (HSA) in human liver carcinoma HepG2 cells.

The study found that HAS interaction increased the toxicity of silver nanoparticles to HepG2 cells without dissolving silver ions, suggesting potential novel properties in Corona formation. In the study by Griffith et al., *in vivo* nanoparticle toxicology with nano-Titanium dioxide is explored through an inhalation study using pregnant Sprague-Dawley rats. The study hypothesizes a sex-dependent toxic effect of nanoparticles on the fetus through the placenta. Maternal inhalation exposure to nano-Titanium dioxide was found to have a greater effect on fetal females, potentially influencing their growth and development in a sex-dependent manner. Bosch et al. investigated *in vivo* toxicity of cadmium tellurium quantum dot nanomaterials with different functional groups (carboxylate, ammonia, polyethylene glycol) in zebrafish embryos. Quantum dots, fluorescent nanocrystals with a semiconductor metal core, are used as contrasting agents for bio-imaging applications. The study showed that ammonia functionalized cadmium tellurium quantum dot nanoparticles caused the most severe effects, including respiration inhibition and developmental defects. Cunningham et al. provided a review highlighting critical gaps between nanoplastics research and risk assessment. Plastic pollution is a global issue, with research focusing more on macroplatics than nanoplastics due to detection challenges. The limited knowledge about the introduction and transport of nanoplastics in the environment suggests a potential underestimation of nanoplastics pollution. The authors emphasize the need for improved ecological risk assessment for nanoplastics. Reilly et al. reviewed and proposed Daphnia as a model organism to study biological responses to nanomaterials. Daphnia has been established as a model organism for ecotoxicity testing, and recent advancements such as the completion of the Daphnia genome project, enable molecular ecotoxicology approaches to understand human health implications through conserved biochemical pathways Daphnia, a legacy model organism, combined with innovative approach such as microfluidics, allows for real time analysis of nanomaterial toxicity. Umezawa et al. investigated the secondary structure change in albumin with cerium oxide nanoparticles using an IR spectroscopy-based method. Cerium oxide is crucial industrial materials with unique anti-oxide activities with cytotoxicity. The study focuses on detecting protein structure changes potentially associated with nanoparticle toxicity, which may alter cellular interaction.

It is interesting to note that the theme of "Emerging Talents in Toxicology" implies that the first authors of the articles are likely scholars in training, showcasing the involvement of young researchers in the field of toxicology. The diversity of nanoparticles and Research Topic covered in the six articles suggests a broad range of research areas within nanoparticle studies. This diversity not only reflects the expanding scope of nanoparticle research but also indicates that there are ample opportunities for further exploration and advancement in this field. As emerging talents delve into various aspects of toxicology related to nanoparticles, they contribute to the overall understanding of the potential risks and benefits associated with nanomaterials. Nanoparticle research is interdisciplinary, involving fields such as toxicology, materials science, and environmental science. The collaboration of emerging talents across these disciplines can lead to innovative approaches and insights. It is crucial to support and encourage young researchers in this area to foster continued growth and progress in nanoparticle research.

Author contributions

TK: Writing–original draft, Writing–review and editing.

Funding

The author(s) declare financial support was received for the research, authorship, and/or publication of this article. This work was partially supported by Dr. Akiko Ueno Radiobiology Research Fund.

Acknowledgments

I thank authors of the papers published in this research topics for their valuable contributions and the referees for their review.

Conflict of interest

The author declares that the research was conducted in the absence of any commercial or financial relationships that could be construed as a potential conflict of interest.

The author(s) declared that they were an editorial board member of Frontiers, at the time of submission. This had no impact on the peer review process and the final decision.

Publisher's note

frontiers | Frontiers in Toxicology

TYPE Original Research
PUBLISHED 21 February 2023
DOI 10.3389/ftox.2023.1113032

OPEN ACCESS

EDITED BY
Ana Luiza Ziulkoski,
Feevale University, Brazil

REVIEWED BY
Caroline Rigotto,
Feevale University, Brazil
Sabrina Almeida,
Universidade Atlântica, Portugal

*CORRESPONDENCE
Aditya N. Bade,
aditya.bade@unmc.edu

SPECIALTY SECTION
This article was submitted to In Vitro Toxicology, a section of the journal Frontiers in Toxicology

RECEIVED 30 November 2022
ACCEPTED 03 February 2023
PUBLISHED 21 February 2023

CITATION
Foster EG, Palermo NY, Liu Y, Edagwa B, Gendelman HE and Bade AN (2023), Inhibition of matrix metalloproteinases by HIV-1 integrase strand transfer inhibitors. *Front. Toxicol.* 5:1113032. doi: 10.3389/ftox.2023.1113032

Inhibition of matrix metalloproteinases by HIV-1 integrase strand transfer inhibitors

Emma G. Foster[1], Nicholas Y. Palermo[2], Yutong Liu[3], Benson Edagwa[1], Howard E. Gendelman[1,4] and Aditya N. Bade[1]*

[1]Department of Pharmacology and Experimental Neuroscience, University of Nebraska Medical Center, Omaha, NE, United States, [2]Computational Chemistry Core, University of Nebraska Medical Center, Omaha, NE, United States, [3]Department of Radiology, University of Nebraska Medical Center, Omaha, NE, United States, [4]Department of Pharmaceutical Sciences, University of Nebraska Medical Center, Omaha, NeE, United States

More than fifteen million women with the human immunodeficiency virus type-1 (HIV-1) infection are of childbearing age world-wide. Due to improved and affordable access to antiretroviral therapy (ART), the number of *in utero* antiretroviral drug (ARV)-exposed children has exceeded a million and continues to grow. While most recommended ART taken during pregnancy suppresses mother to child viral transmission, the knowledge of drug safety linked to fetal neurodevelopment remains an area of active investigation. For example, few studies have suggested that ARV use can be associated with neural tube defects (NTDs) and most notably with the integrase strand transfer inhibitor (INSTI) dolutegravir (DTG). After risk benefit assessments, the World Health Organization (WHO) made recommendations for DTG usage as a first and second-line preferred treatment for infected populations including pregnant women and those of childbearing age. Nonetheless, long-term safety concerns remain for fetal health. This has led to a number of recent studies underscoring the need for biomarkers to elucidate potential mechanisms underlying long-term neurodevelopmental adverse events. With this goal in mind, we now report the inhibition of matrix metalloproteinases (MMPs) activities by INSTIs as an ARV class effect. Balanced MMPs activities play a crucial role in fetal neurodevelopment. Inhibition of MMPs activities by INSTIs during neurodevelopment could be a potential mechanism for adverse events. Thus, comprehensive molecular docking testing of the INSTIs, DTG, bictegravir (BIC), and cabotegravir (CAB), against twenty-three human MMPs showed broad-spectrum inhibition. With a metal chelating chemical property, each of the INSTI were shown to bind Zn++ at the MMP's catalytic domain leading to MMP inhibition but to variable binding energies. These results were validated in myeloid cell culture experiments demonstrating MMP-2 and 9 inhibitions by DTG, BIC and CAB and even at higher degree than doxycycline (DOX). Altogether, these data provide a potential mechanism for how INSTIs could affect fetal neurodevelopment.

KEYWORDS

HIV-1, pregnancy, antiretroviral drugs, integrase strand transfer inhibitors, neurodevelopment, drug-induced adverse events

Introduction

Pregnant women and women of child bearing age infected with the human immunodeficiency virus type-1 (HIV-1) infection have benefited by antiretroviral therapy (ART) in the reduction of maternal fetal viral transmission (The U.S. Department of Health and Human Services, 2015; World Health Organization (WHO), 2019a). Currently, more than 15.5 million women of child-bearing age are HIV-1 infected, worldwide (The Joint United Nations Programme on HIV/AIDS (UNAIDS), 2021a). In 2020, eighty five percent of HIV-1-infected pregnant women were on ART (The Joint United Nations Programme on HIV/AIDS (UNAIDS), 2021a). Due to such broad usage of ART during pregnancy, the rate of vertical transmission of HIV-1 has reduced to less than 1% (The Centers for Disease Control and Prevention (CDC), 2018; Peters et al., 2017; Schnoll et al., 2019; Rasi et al., 2022; The Joint United Nations Programme on HIV/AIDS (UNAIDS), 2021b). This includes resource-limited countries (RLCs), which currently hold up to two-thirds of the world's total HIV-1 infected population (The Joint United Nations Programme on HIV/AIDS (UNAIDS), 2021b). However, along with the significant benefits in reducing infection-associated morbidities and mortalities, there remains risks of ART-linked adverse events (Hill et al., 2018). As over a million ARV-exposed HIV-1 uninfected children are born each year (Ramokolo et al., 2019; Crowell et al., 2020), an appreciation of adverse pregnancy events, in particular, related to ARVs is certainly warranted.

Herein, we particularly focused on HIV-1 integrase strand transfer inhibitors (INSTIs), a relatively new class of ARVs. Raltegravir (RAL), elvitegravir (EVG), dolutegravir (DTG), bictegravir (BIC), and cabotegravir (CAB) are the US Food and Drug Administration (FDA) approved INSTIs for the treatment of HIV-1 infected patients (Smith et al., 2021). In recent years, widespread usage of INSTIs have emerged related to their efficacy and high barrier to viral drug resistance (Smith et al., 2021). Indeed, these antiretrovirals are currently part of preferred first- and second-line ART regimens (World Health Organization (WHO), 2016; Department of Health and Human Services (DHHS), 2022). Moreover, increasing pretreatment resistance to non-nucleoside reverse transcriptase inhibitors (NNRTIs) in RLCs, especially in women, increases usage of INSTI-based regimens (World Health Organization (WHO), 2019a; World Health Organization (WHO), 2019b). During pregnancy, DTG and RAL are preferred drugs in combination therapy with a preferred dual-nucleoside reverse transcriptase inhibitor (NRTI) backbone. EVG, BIC or CAB are not recommended during pregnancy due to limited safety data (The U.S. Department of Health and Human Services, 2015). Recently DTG was found to be potentially associated with birth defects (NTDs) and postnatal neurodevelopmental abnormalities (Hill et al., 2018; Cabrera et al., 2019; Zash et al., 2019; Crowell et al., 2020; Mohan et al., 2020; Bade et al., 2021). Given the widescale usage of DTG as a part of first-line regimens worldwide (Hill et al., 2018; Dorward et al., 2018; World Health Organization (WHO), 2018; The Lancet, 2020) and emerging potent INSTIs such as BIC and CAB, uncovering any INSTIs-associated adverse effects and thus, the underlying mechanisms is of importance.

Pre-clinical and clinical research have served to evaluate interaction between folate levels or transport pathways and DTG or other INSTIs for any developmental toxicity (Cabrera et al., 2019; Chandiwana et al., 2020; Gilmore et al., 2022). However, results have failed to conclusively establish cause-and-effect relationships (Cabrera et al., 2019; Chandiwana et al., 2020; Gilmore et al., 2022). No other biomarker linked to INSTI drug-induced adverse events has been explored. We demonstrated that DTG is a broad-spectrum inhibitor of matrix metalloproteinases (MMPs) (Bade et al., 2021). MMPs are known to play a role in many neurodevelopmental processes, including, but not limited to axonal growth and guidance, synaptic development and plasticity (Ethell and Ethell, 2007; Agrawal et al., 2008; Fujioka et al., 2012; Reinhard et al., 2015; De Stefano and Herrero, 2017). Therefore, dysregulation of their activities could affect fetal neurodevelopment (Reinhard et al., 2015; Bade et al., 2021). Docking assessments against five MMPs showed that DTG binds to Zn++ at the catalytic domain of an MMP to inhibit the enzyme's activity. Moreover, such MMPs inhibition can affect mice fetal neurodevelopment following DTG administration to pregnant dams at the time of conception. Clinical reports of adverse events associated with INSTIs have demonstrated class effects. Therefore, it is prudent to determine whether other ARVs from the INSTI class are inhibitors of MMPs and consider this as a potential mechanism of INSTIs-related adverse neurodevelopmental outcomes. Moreover, such biomarker discovery against MMP enzymes will help to understand potential genetic susceptibility. Herein, we show, for the first time, comprehensive computational molecular docking assessments of DTG, BIC or CAB against each one of the twenty-three human MMP enzymes. Further, inhibition potency of each INSTI was validated using a cell culture model. To this end, we show that inhibition of MMPs activities is an INSTI class effect and warranting assessments to determine the effect of drug-induced effects on the gestational environment and fetal neurodevelopment.

Methods

Molecular docking

Homology models of all 23 known human MMPs (MMP-1, 2, 3, 7, 8, 9, 10, 11, 12, 13, 14, 15, 16, 17, 19, 20, 21, 23, 24, 25, 26, 27, and 28) were generated. This was done on a template of MMP-2 (PDB ID: 1HOV) using the Homology Modeling module of the YASARA Structure program package (Krieger and Vriend, 2014). The Schrodinger software suite release 2020–4 (New York, NY) was used for all molecular dynamic simulations and molecular docking calculations. All molecules were parametrized using the OPLS3e force field (Harder et al., 2016). Each homology model was placed in an orthorhombic box of TIP4P water with periodic boundaries; at least 10 Å from any solute molecule. The simulation cells were neutralized with the addition of Na + or Cl− ions. Production molecular dynamics were run for 500 ns with default settings. The representative structure of the largest cluster from each simulation was chosen for docking calculations. Induced-fit binding as implemented in Schrodinger was used with default settings, except that the high-accuracy XP mode was chosen for Glide docking. All ranked poses were required to have at least one bond with the active site zinc ion; other poses were not considered.

Gelatin zymography

Gelatin zymography was performed to assess MMP-9 and -2 activity following treatment of THP-1 cells with DTG, CAB,

BIC, or DOX. This assay was used as preliminary confirmation of the inhibition of MMPs by individual INSTIs. Due to the nature of this assay, only the gelatinases, MMP-2 and -9, could be assessed. Cells were plated at a density of 1×10^6 in 12 well plates and treated with phorbol-12-myristate-13-acetate (PMA) for 24 h. This was done to promote cell differentiation to stimulate MMP secretion. Following PMA treatment, cells were treated with DTG, CAB, BIC, or DOX at concentrations of 25, 50, 75, or 100 μM or control vehicle for 24 h. In our previous study, no DTG-induced cytotoxicity was recorded in PMA-stimulated THP-1 cells up to 100 μM (Bade et al., 2021). Thus, for comparative assessments among different INSTIs (DTG, BIC, and CAB) and DOX (positive control) drug concentrations of up to 100 μM were utilized. Each of the experimental tests were performed in triplicate. Following treatment, media was collected and centrifuged at 15,000 x g for 10 min at 4°C. Supernatant was collected and stored at −80°C for further analysis. For gelatin zymography, 3 μg of protein from cell medium was loaded in a 10% SDS-polyacrylamide gel containing 0.1% gelatin. Gels were ran at 55 V until the loading dye passed through its bottom. The gel was then removed and washed with water for 15 min, then incubated with renaturation buffer [2.5% (v/v) Triton X-100 in Milli-Q water] for 90 min at room temperature. The used renaturation buffer was replaced with fresh buffer every 30 min. Renaturation buffer was then replaced with developing buffer (50 mM Tris–HCl, pH 7.5, 5 mM CaCl2, 0.2 M NaCl, and 0.02% Brij-35) and the gel was incubated at 37°C in a shaker (Innova 42, New Brunswick Scientifc, Edison, NJ) for 48 h. After 48 h, the gel was washed with water for 15 min and then stained using 0.2% Coomassie Brilliant Blue R-250 (BIO-RAD, Hercules, CA) for 1 h. After staining, the gel was washed with water for 15 min before washing with destaining solution (30% methanol, 10% acetic acid, 60% water) for 45 min. The gel was then washed with water for 20 min to remove any destaining solution. Finally, the stained gel was imaged using the iBright 750 Imaging System (Invitrogen, Carlsbad, CA). ImageJ software was used to quantitate band density recorded as a measure of relative MMP activity.

Statistical analysis

Statistical analyses were conducted using GraphPad Prism 7.0 software (La Jolla, CA). Data from *in vitro* studies were expressed as mean ± standard error of the mean (SEM) with a minimum of 3 biological replicates. A one-way ANOVA followed by Tukey's or Dunnett's test was used to compare three or more groups. Statistical significance was denoted as $^*p < 0.05$, $^{**}p < 0.01$, $^{***}p < 0.001$, $^{****}p < 0.0001$.

Results

INSTIs chelate Zn++ at the catalytic domain of MMPs

Molecular dockings were completed using Schrodinger's software to identify the mechanism through which each INSTI interacts with the catalytic domain structures of the human MMPs. Here, we used DTG, BIC and CAB for assessments. MMPs are Zn++ dependent endopeptidases. INSTIs possess a prominent metal-binding pharmacophore (MBP) also, referred to as a metal-binding group or MBG in their chemical structure. Based on these chemical abilities for binding to the metal ions we hypothesized that DTG, BIC or CAB can inhibit MMPs activities by binding to Zn++ at the catalytic domain of the protein structure. Herein, induced fit docking used a combination of the Glide and Prime programs in the Schrodinger suite. All docking scores used the highest accuracy Glide XP mode. Previously, we reported interaction of DTG with five MMPs, MMP-2, 8, 9, 14, and 19 and interaction of CAB or BIC with MMP-2 and -14 as proof-of-concept evaluations (Bade et al., 2021). Herein, as 23 MMPs are known to be found in humans, molecular docking interaction was tested against each of these enzymes to find the highest binding interaction for DTG, BIC or CAB and determine whether any individual MMP could have genetic susceptibility against these INSTIs.

DTG formed a metal coordination complex with Zn^{++}. This was recorded in the catalytic domain of each of the MMPs tested. Metal coordination of DTG with Zn++ occurred at Zn 166, 166, 479, 269, 469, 709, 478, 490, 472, 473, 584, 671, 609, 605, 510, 485, 571, 485, 647, 564, 263, 515, and 522 receptors of MMP-1, 2, 3, 7, 8, 9, 10, 11, 12, 13, 14, 15, 16, 17, 19, 20, 21, 23, 24, 25, 26, 27, and 28, respectively. DTG also formed other interactions with Zn^{++}, which included cation pi interactions. These interactions occurred at Zn 490, 605, and 522 receptors of MMP-11, 17, and 28 respectively. Other interactions included pi stacking and hydrogen bonding. Pi stacking occurred with histidine amino acids of all tested MMPs except MMP-7, 9, 19, and 27. Pi stacking also occurred with tyrosine amino acids, but only with MMP-3, 11, and 16. Hydrogen bond interactions occurred at glutamate amino acid residues of MMP-1, 3, 10, 12, 15, 16, 19, 20, 21, 23, 24, 25, and 26; alanine amino acid residues of MMP-2, 7, 8, 11, 14, 17, and 19; leucine amino acid residues of MMP-7, 8, 9, 10, 12, 15, 16, 20, 23, 24, 25, and 26; glycine amino acid residues of MMP-9 and 27; tyrosine amino acid residues of MMP-9 and 27; asparagine 170 amino acid residue of MMP-8; proline 421 amino acid residue of MMP-9; phenylalanine 249 of MMP-21; and glutamine 247 of MMP-21. The distances of all the receptor-ligand bonds are shown in the respective DTG-MMP interaction table (Table 1). Docking simulation of DTG into individual MMP showed binding energy of −6.032, −6.450, −6.253, −7.243, −8.330, −9.430, −6.686, −6.210, −6.713, −6.461, −9.040, −5.885, −7.325, −6.810, −7.130, −6.097, −6.179, −6.213, −6.917, −6.865, −7.198, −7.427 or −6.012 kcal/mol for MMP-1 to −28, respectively (Table 4). Overall, observed high binding energies from the docking simulation validated docking interactions in Table 1. Moreover, these docking assessments confirmed that DTG is a broad-spectrum inhibitor, and it inhibits all MMPs activities by chelating Zn++ at the catalytic domain.

Notably, CAB also formed a metal coordination complex with Zn^{++} in the catalytic domain of all tested MMPs. Metal coordination of CAB with Zn++ occurred at Zn 471, 166, 479, 269, 469, 709, 478, 490, 472, 473, 584, 671, 609, 605, 510, 485, 571, 392, 647, 564, 263, 515, and 522 receptors of MMP-1, 2, 3, 7, 8, 9, 10, 11, 12, 13, 14, 15, 16, 17, 19, 20, 21, 23, 24, 25, 26, 27, and 28, respectively. However, CAB also formed salt bridges with Zn++ of all tested MMPs. In addition, salt bridge interactions occurred with glutamate amino acids of MMP-1, 8, 9, 10, 12, 14, 17, 19, 21, 23, 24, and 26. Salt bridges with Zn++ or with other amino acids were not observed with

TABLE 1 Dolutegravir (DTG)- Matrix metalloproteinases (MMPs) Interactions.

MMP-1 interactions			
Ligand	Receptor	Type	Distance (Å)
Ar1	His 218	Pi stacking	3.60
NH	Glu 219	Hydrogen bond	1.98
O2	Zn 166	Metal coordination	2.01
MMP-2 interactions			
Ligand	Receptor	Type	Distance (Å)
Ar1	His 120	Pi stacking	3.59
NH	Ala 84	Hydrogen bond	2.28
O1	Zn 166	Metal coordination	2.19
O2	Zn 166	Metal coordination	2.21
MMP-3 interactions			
Ligand	Receptor	Type	Distance (Å)
Ar1	His 218	Pi stacking	3.57
Ar1	Tyr 240	Pi stacking	5.32
NH	Glu 219	Hydrogen bond	2.36
O2	Zn 479	Metal coordination	2.13
MMP-7 interactions			
Ligand	Receptor	Type	Distance (Å)
O1	Leu 176	Hydrogen bond	2.02
O1	Ala 177	Hydrogen bond	2.07
O2	Zn 269	Metal coordination	2.14
MMP-8 interactions			
Ligand	Receptor	Type	Distance (Å)
Ar1	His 217	Pi stacking	3.8
O1	Leu 180	Hydrogen bond	1.93
O1	Ala 181	Hydrogen bond	2.32
O2	Zn 469	Metal coordination	2.02
O5	Asn 170	Hydrogen bond	1.91
MMP-9 interactions			
Ligand	Receptor	Type	Distance (Å)
NH	Gly 186	Hydrogen bond	1.87
O1	Try 423	Hydrogen bond	1.96
O3	Pro 421	Hydrogen bond	2.09
O4	Zn 709	Metal coordination	2.14
O5	Leu 188	Hydrogen bond	2.80
MMP-10 interactions			
Ligand	Receptor	Type	Distance (Å)
Ar1	His 217	Pi stacking	3.42

(Continued in next column)

TABLE 1 (*Continued*) Dolutegravir (DTG)- Matrix metalloproteinases (MMPs) Interactions.

MMP-10 interactions			
Ligand	Receptor	Type	Distance (Å)
NH	Glu 218	Hydrogen bond	1.99
O1	Leu 180	Hydrogen bond	2.67
O2	Zn 478	Metal coordination	2.15
MMP-11 interactions			
Ligand	Receptor	Type	Distance (Å)
Ar1	His 215	Pi stacking	4.03
Ar1	Tyr 237	Pi Stacking	5.48
Ar1	Zn 490	Cation pi	4.63
NH	Ala 178	Hydrogen bond	1.91
O2	Zn 490	Metal coordination	2.13
MMP-12 interactions			
Ligand	Receptor	Type	Distance (Å)
Ar1	His 218	Pi stacking	3.75
NH	Glu 219	Hydrogen bond	2.22
O1	Leu 181	Hydrogen bond	2.1
O2	Zn 472	Metal coordination	2.13
MMP-13 interactions			
Ligand	Receptor	Type	Distance (Å)
Ar1	His 222	Pi stacking	3.72
O2	Zn 473	Metal coordination	2.07
MMP-14 interactions			
Ligand	Receptor	Type	Distance (Å)
Ar2	His 239	Pi stacking	3.49
O3	Ala 258	Hydrogen bond	1.87
O4	Zn 584	Metal coordination	2.12
MMP-15 interactions			
Ligand	Receptor	Type	Distance (Å)
Ar1	His 259	Pi stacking	3.4
NH	Glu 260	Hydrogen bond	2.03
O1	Leu 219	Hydrogen bond	2.22
O2	Zn 671	Metal coordination	2.06
MMP-16 interactions			
Ligand	Receptor	Type	Distance (Å)
Ar1	His 246	Pi stacking	3.34
Ar1	Tyr 268	Pi Stacking	5.43
NH	Glu 247	Hydrogen bond	2.11
O1	Leu 206	Hydrogen bond	2.07
O2	Zn 609	Metal coordination	2.05
MMP-17 interactions			
Ligand	Receptor	Type	Distance (Å)
Ar1	His 259	Pi stacking	3.89

(Continued on following page)

TABLE 1 (*Continued*) Dolutegravir (DTG)- Matrix metalloproteinases (MMPs) Interactions.

MMP-17 interactions			
Ligand	Receptor	Type	Distance (Å)
Ar1	Zn 605	Cation pi	4.72
NH	Ala 208	Hydrogen bond	1.89
O2	Zn 605	Metal coordination	2.09
MMP-19 interactions			
Ligand	Receptor	Type	Distance (Å)
O1	Zn 510	Metal coordination	2.10
O3	Ala 231	Hydrogen bond	2.03
O4	Glu 235	Hydrogen bond	2.14
MMP-20 interactions			
Ligand	Receptor	Type	Distance (Å)
Ar1	His 226	Pi stacking	3.49
NH	Glu 227	Hydrogen bond	2.06
O1	Leu 189	Hydrogen bond	2.26
O2	Zn 485	Metal coordination	2.05
MMP-21 interactions			
Ligand	Receptor	Type	Distance (Å)
Ar1	His 283	Pi stacking	3.52
NH	Glu 284	Hydrogen bond	2.00
O1	Phe 249	Hydrogen bond	2.03
O2	Zn 571	Metal coordination	2.11
O5	Gln 247	Hydrogen bond	2.60
MMP-23 interactions			
Ligand	Receptor	Type	Distance (Å)
Ar1	His 226	Pi stacking	3.59
NH	Glu 227	Hydrogen bond	2.18
O1	Leu 189	Hydrogen bond	2.23
O2	Zn 485	Metal coordination	2.09
MMP-24 interactions			
Ligand	Receptor	Type	Distance (Å)
Ar1	His 282	Pi stacking	3.44
NH	Glu 283	Hydrogen bond	2.19
O1	Leu 242	Hydrogen bond	2.20
O2	Zn 647	Metal coordination	2.09
MMP-25 interactions			
Ligand	Receptor	Type	Distance (Å)
Ar1	His 233	Pi stacking	3.43
NH	Glu 234	Hydrogen bond	2.63
O1	Leu 192	Hydrogen bond	2.06
O2	Zn 564	Metal coordination	2.02
MMP-26 interactions			
Ligand	Receptor	Type	Distance (Å)
Ar1	His 208	Pi stacking	3.41

(Continued in next column)

TABLE 1 (*Continued*) Dolutegravir (DTG)- Matrix metalloproteinases (MMPs) Interactions.

MMP-26 interactions			
Ligand	Receptor	Type	Distance (Å)
NH	Glu 209	Hydrogen bond	2.6
O1	Leu 171	Hydrogen bond	2.46
O2	Zn 263	Metal coordination	2.09
MMP-27 interactions			
Ligand	Receptor	Type	Distance (Å)
NH	Gly 177	Hydrogen bond	2.08
O1	Tyr 238	Hydrogen bond	1.79
O3	Zn 515	Metal coordination	2.22
O4	Zn 515	Metal coordination	2.27
MMP-28 interactions			
Ligand	Receptor	Type	Distance (Å)
Ar1	His 240	Pi stacking	3.87
Ar1	Zn 522	Cation pi	4.75
O2	Zn 522	Metal coordination	2.12

any of DTG-MMP interactions. Other interactions between CAB and MMPs were cation pi, pi stacking and hydrogen bonding. Cation pi interactions occurred at histidine 263 and phenylalanine 205 of MMP-15 and 16 respectively. Pi stacking interactions occurred with histidine amino acids of MMP-1, 2, 11, 12, 15, 17, 19, 21, 23, 25, and 28; phenylalanine amino acids of MMP-1 and 16; tyrosine amino acids of MMP-2, 14, and 19. Hydrogen bonding of CAB with tested MMPs was found, except MMP-17. Like DTG, CAB was found to produce hydrogen bonding with leucine, alanine, glutamate, phenylalanine, glycine, proline, asparagine, and tyrosine amino acid residues. However, other hydrogen bonding occurred at serine 239 amino acid residue of MMP-1, valine 233 amino acid residue of MMP-19, and arginine 240 amino acid residue of MMP-23. The distances of all the receptor-ligand bonds are shown in the respective CAB-MMP interaction table (Table 2). Docking simulation of CAB into individual MMP showed binding energy of −14.251, −8.588, −15.222, −12.305, −14.337, −14.222, −14.592, −10.352, −12.19, −11.798, −12.983 −9.632, −12.249, −11.666, −12.718, −12.413, −14.389, −13.109, −15.339, −11.62, −12.381, −12.614, or −10.11 kcal/mol for MMP-1 to −28, respectively (Table 4). Altogether, observed high binding energies from the docking simulation and docking interactions (Table 1; Table 4) evaluations confirmed that CAB is a broad-spectrum inhibitor, and it inhibits all MMPs activities by binding to Zn++ at the catalytic domain.

Further, docking simulation confirmed that BIC formed a metal coordination complex with Zn^{++} in the catalytic domain of all tested MMPs, validating that all INSTIs possess chemical abilities to inhibits MMPs activities by chelating Zn++ at the catalytic domain. Metal coordination of BIC with Zn++ occurred at Zn 471, 166, 479, 269, 469, 709, 478, 490, 472, 473, 584, 671, 609, 605, 510, 485, 571, 392, 647, 564, 263, 515, and 522 receptors of MMP-1,

TABLE 2 Cabotegravir (CAB)- Matrix metalloproteinases (MMPs) Interactions.

MMP-1 Interactions			
Ligand	Receptor	Type	Distance (Å)
Ar1	His 218	Pi stacking	4.9
Ar1	Phe 242	Pi stacking	5.28
O2	Ser 239	Hydrogen bond	2.28
O2	Zn 471	Salt bridge	2.14
O3	Zn 471	Metal coordination	2.08
O3	Zn 471	Salt bridge	2.08
N2	Glu 219	Salt bridge	4.91
MMP-2 Interactions			
Ligand	Receptor	Type	Distance (Å)
Ar1	His 120	Pi stacking	3.34
Ar1	Tyr 142	Pi stacking	5.07
O1	Leu 83	Hydrogen bond	1.99
O1	Ala 84	Hydrogen bond	2.40
O2	Glu 121	Hydrogen bond	1.92
O2	Zn 166	Metal coordination	2.25
O3	Zn 166	Metal coordination	2.05
O3	Zn 166	Salt bridge	2.05
MMP-3 Interactions			
Ligand	Receptor	Type	Distance (Å)
O1	Leu 181	Hydrogen bond	1.76
N1	Pro 238	Hydrogen bond	1.96
O2	Zn 479	Metal coordination	2.41
O3	Zn 479	Metal coordination	2.00
O3	Zn 479	Salt bridge	2.00
MMP-7 Interactions			
Ligand	Receptor	Type	Distance (Å)
O1	Leu 176	Hydrogen bond	2.05
O1	Ala 177	Hydrogen bond	2.1
O2	Glu 215	Hydrogen bond	2.14
O2	Zn 269	Metal coordination	2.39
O3	Zn 269	Metal coordination	2.01
O3	Zn 269	Salt bridge	2.01
MMP-8 Interactions			
Ligand	Receptor	Type	Distance (Å)
O1	Asn 170	Hydrogen bond	2.03

(Continued in next column)

TABLE 2 (*Continued*) Cabotegravir (CAB)- Matrix metalloproteinases (MMPs) Interactions.

MMP-8 Interactions			
Ligand	Receptor	Type	Distance (Å)
O3	Zn 469	Metal coordination	2.14
O3	Zn 469	Salt bridge	2.14
N2	Glu 218	Salt bridge	4.78
O4	Zn 469	Metal coordination	2.05
O5	Leu 180	Hydrogen bond	1.76
MMP-9 Interactions			
Ligand	Receptor	Type	Distance (Å)
N1	Pro 421	Hydrogen bond	2.03
O1	Leu 188	Hydrogen bond	1.95
O2	Zn 709	Metal coordination	2.24
N2	Glu 402	Salt bridge	4.73
O3	Zn 709	Metal coordination	1.98
O3	Zn 709	Salt bridge	1.98
MMP-10 Interactions			
Ligand	Receptor	Type	Distance (Å)
N1	Pro 237	Hydrogen bond	2.24
O1	Leu 180	Hydrogen bond	1.95
O2	Zn 478	Metal coordination	2.37
O3	Zn 478	Metal coordination	1.92
O3	Zn 478	Salt bridge	1.92
N2	Glu 218	Salt bridge	4.77
MMP-11 Interactions			
Ligand	Receptor	Type	Distance (Å)
Ar1	His 215	Pi stacking	3.98
O1	Leu 177	Hydrogen bond	2.2
O2	Zn 490	Metal coordination	2.08
O3	Zn 490	Metal coordination	2.10
O3	Zn 490	Salt bridge	2.10
MMP-12 Interactions			
Ligand	Receptor	Type	Distance (Å)
Ar1	His 183	Pi stacking	4.16
O3	Zn 472	Metal coordination	2.05
O3	Zn 472	Salt bridge	2.05
N2	Glu 219	Salt bridge	4.27
O4	Zn 472	Metal coordination	2.23

(Continued on following page)

TABLE 2 (*Continued*) Cabotegravir (CAB)- Matrix metalloproteinases (MMPs) Interactions.

MMP-12 Interactions			
Ligand	Receptor	Type	Distance (Å)
O5	Leu 181	Hydroen bond	1.94
MMP-13 Interactions			
Ligand	Receptor	Type	Distance (Å)
N1	Pro 242	Hydrogen bond	2.11
O1	Leu 185	Hydrogen bond	2.11
O2	Zn 473	Metal coordination	2.09
O3	Zn 473	Metal coordination	1.92
O3	Zn 473	Salt bridge	1.92
MMP-14 Interactions			
Ligand	Receptor	Type	Distance (Å)
Ar1	His 239	Pi stacking	3.76
Ar1	Tyr 261	Pi stacking	5.36
Ar2	His 239	Pi stacking	4.98
O2	Zn 584	Metal coordination	2.33
O3	Zn 584	Metal coordination	2.05
O3	Zn 584	Salt bridge	2.05
O5	Ala 202	Hydrogen bond	2.42
N1	Glu 240	Hydrogen bond	2.15
N2	Glu 240	Salt bridge	3.15
MMP-15 Interactions			
Ligand	Receptor	Type	Distance (Å)
Ar1	Tyr 223	Pi stack	4.84
O1	Ala 222	Hydrogen bond	1.94
O2	Glu 260	Hydrogen bond	2.23
O3	Zn 671	Metal coordination	1.96
O3	Zn 671	Salt bridge	1.96
N2	His 263	Cation pi	5.84
O4	Zn 671	Metal coordination	2.29
MMP-16 Interactions			
Ligand	Receptor	Type	Distance (Å)
O1	Leu 206	Hydrogen bond	2.17
O1	Ala 207	Hydrogen bond	1.84
O2	Glu 247	Hydrogen bond	1.74
O2	Zn 609	Metal coordination	2.49
Ar2	Phe 205	Pi stacking	4.25

(Continued in next column)

TABLE 2 (*Continued*) Cabotegravir (CAB)- Matrix metalloproteinases (MMPs) Interactions.

MMP-16 Interactions			
Ligand	Receptor	Type	Distance (Å)
O3	Zn 609	Metal coordination	2.03
O3	Zn 609	Salt bridge	2.03
N2	Phe 205	Cation pi	3.97
MMP-17 Interactions			
Ligand	Receptor	Type	Distance (Å)
Ar1	His 248	Pi stacking	4.3
O2	Zn 605	Metal coordination	1.98
O3	Zn 605	Salt bridge	2.14
O3	Zn 605	Metal coordination	2.14
N2	Glu 249	Salt bridge	4.98
MMP-19 Interactions			
Ligand	Receptor	Type	Distance (Å)
O2	Val 233	Hydrogen bond	1.53
Ar2	His 212	Pi stacking	3.92
Ar2	Tyr 234	Pi stacking	4.27
O3	Zn 510	Metal coordination	2.13
O3	Zn 510	Salt bridge	2.13
N2	Glu 213	Salt bridge	3.36
O4	Zn 510	Metal coordination	2.42
MMP-20 Interactions			
Ligand	Receptor	Type	Distance (Å)
O1	Leu 189	Hydrogen bond	1.86
O1	Ala 190	Hydrogen bond	2.1
O2	Glu 227	Hydrogen bond	1.94
O2	Zn 485	Metal coordination	2.37
O3	Zn 485	Metal coordination	2.15
O3	Zn 485	Salt bridge	2.15
MMP-21 Interactions			
Ligand	Receptor	Type	Distance (Å)
Ar1	His 283	Pi stacking	4.76
N1	Glu 284	Hydrogen bond	1.69
O1	Phe 249	Hydrogen bond	2.1
O2	Zn 571	Metal coordination	2.11
O3	Zn 571	Metal coordination	2.15
O3	Zn 571	Salt bridge	2.15

(Continued on following page)

TABLE 2 (*Continued*) Cabotegravir (CAB)- Matrix metalloproteinases (MMPs) Interactions.

MMP-21 Interactions			
Ligand	Receptor	Type	Distance (Å)
N2	Glu 248	Salt bridge	4.83
O5	Arg 240	Hydrogen bond	1.87
MMP-23 Interactions			
Ligand	Receptor	Type	Distance (Å)
Ar1	His 211	Pi stacking	4.19
O1	Leu 168	Hydrogen bond	2.01
O2	Ala 169	Hydrogen bond	2.48
O2	Glu 212	Hydrogen bond	2.25
O3	Zn 392	Metal coordination	2
O3	Zn 392	Salt bridge	2
N2	Glu 167	Salt bridge	3.36
MMP-24 Interactions			
Ligand	Receptor	Type	Distance (Å)
O1	Leu 242	Hydrogen bond	2.14
O2	Zn 647	Metal coordination	2.28
O3	Zn 647	Salt bridge	2.12
O3	Zn 647	Metal coordination	2.12
N2	Glu 283	Salt bridge	4.63
MMP-25 Interactions			
Ligand	Receptor	Type	Distance (Å)
Ar1	His 233	Pi stacking	3.52
O1	Leu 192	Hydrogen bond	1.79
O1	Ala 193	Hydrogen bond	2.02
O2	Glu 234	Hydrogen bond	1.72
O2	Zn 564	Metal coordination	2.18
O3	Zn 564	Salt bridge	2.06
O3	Zn 564	Metal coordination	2.06
MMP-26 Interactions			
Ligand	Receptor	Type	Distance (Å)
O3	Zn 263	Metal coordination	1.99
O3	Zn 263	Salt bridge	1.99
N2	Glu 209	Salt bridge	4.9
O4	Zn 263	Metal coordination	2.22

(Continued in next column)

TABLE 2 (*Continued*) Cabotegravir (CAB)- Matrix metalloproteinases (MMPs) Interactions.

MMP-26 Interactions			
Ligand	Receptor	Type	Distance (Å)
O5	Leu 171	Hydrogen bond	1.92
MMP-27 Interactions			
Ligand	Receptor	Type	Distance (Å)
O1	Gly 180	Hydrogen bond	1.99
O2	Glu 217	Hydrogen bond	1.66
O2	Zn 515	Metal coordination	2.48
O3	Zn 515	Salt bridge	2.11
O3	Zn 515	Metal coordination	2.11
MMP-28 Interactions			
Ligand	Receptor	Type	Distance (Å)
Ar1	His 240	Pi stacking	3.92
O1	Leu 205	Hydrogen bond	2.01
O1	Ala 206	Hydrogen bond	2.41
O2	Ala 206	Hydrogen bond	2.57
O2	Glu 241	Hydrogen bond	2.34
O2	Zn 522	Metal coordination	2.35
O3	Zn 522	Metal coordination	2.19
O3	Zn 522	Salt bridge	2.19

2, 3, 7, 8, 9, 10, 11, 12, 13, 14, 15, 16, 17, 19, 20, 21, 23, 24, 25, 26, 27, and 28, respectively. Like CAB, BIC also formed salt bridges with Zn++ of all tested MMPs. Along with Zn++, BIC was found to form salt bridge interactions with glutamate amino acids of all tested MMPs except MMP-2, 13, 15, 24 and 26. Cation pi interactions occurred only at phenylalanine 241 of MMP-24. Pi stacking interactions occurred with histidine amino acids of MMP-1, 9, 14, 17, 24, 26, 27, and 28; tyrosine amino acids of MMP-3, 10, 16, and 19, phenylalanine amino acids of MMP-12 and 24; tryptophan amino acid of MMP-26. Hydrogen bonding of BIC was observed with all MMPs except MMP-2, 19, 28. Like DTG and CAB, BIC was found to form hydrogen bonds with asparagine, histidine, leucine, alanine, proline, glutamate, valine, phenylalanine, glycine, and arginine amino acid residues. The distances of all the receptor-ligand bonds are shown in the respective BIC-MMP interaction table (Table 3). Docking simulation of BIC into individual MMP showed binding energy of −14.55, −10.972, −15.082, −11.385, −15.771, −13.415, −16.021, −12.143, −13.482, −12.73, −14.539, −8.877, −14.625, −12.409, −11.695, −11.923, −12.698, −12.25, −10.181, −11.716, −11.971, −12.54, and −10.823 kcal/mol for MMP-1 to −28, respectively (Table 4).

TABLE 3 Bictegravir (BIC)- Matrix metalloproteinases (MMPs) Interactions.

MMP-1 Interactions			
Ligand	Receptor	Type	Distance (Å)
Ar1	His 183	Pi stacking	4.4
O1	Asn 179	Hydrogen bond	1.99
O1	His 183	Hydrogen bond	2.64
O3	Zn 471	Metal coordination	1.99
O3	Zn 471	Salt bridge	1.99
O4	Zn 471	Metal coordination	2.2
O4	Glu 219	Salt bridge	4.4
O5	Leu 181	Hydrogen bond	2.38
MMP-2 Interactions			
Ligand	Receptor	Type	Distance (Å)
O2	Zn 166	Metal coordination	2.24
O3	Zn 166	Metal coordination	2.05
O3	Zn 166	Salt bridge	2.05
MMP-3 Interactions			
Ligand	Receptor	Type	Distance (Å)
Ar1	Tyr 185	Pi stacking	5.35
O3	Zn 479	Metal coordination	2.09
O3	Zn 479	Salt bridge	2.09
N2	Glu 219	Salt bridge	4.64
O4	Zn 479	Metal coordination	2.13
O5	Leu 181	Hydrogen bond	2.25
MMP-7 Interactions			
Ligand	Receptor	Type	Distance (Å)
O1	Ala 179	Hydrogen bond	2.06
N2	Glu 215	Salt bridge	4.86
O3	Zn 269	Metal coordination	2.04
O3	Zn 269	Salt bridge	2.04
O4	Zn 269	Metal coordination	2.07
MMP-8 Interactions			
Ligand	Receptor	Type	Distance (Å)
O1	Asn 170	Hydrogen bond	2.19
O3	Zn 469	Metal coordination	2.04
O3	Zn 469	Salt bridge	2.04
N2	Glu 218	Salt bridge	4.71

(Continued in next column)

TABLE 3 (*Continued*) Bictegravir (BIC)- Matrix metalloproteinases (MMPs) Interactions.

MMP-8 Interactions			
Ligand	Receptor	Type	Distance (Å)
O4	Zn 469	Metal coordination	2.29
O5	Leu 180	Hydrogen bond	2.3
MMP-9 Interactions			
Ligand	Receptor	Type	Distance (Å)
Ar1	His 401	Pi stacking	3.84
O2	Pro 421	Hydrogen bond	2.28
O2	Zn 709	Metal coordination	2.29
O3	Zn 709	Metal coordination	2.01
O3	Zn 709	Salt bridge	2.01
N2	Glu 402	Salt bridge	4.3
MMP-10 Interactions			
Ligand	Receptor	Type	Distance (Å)
Ar1	Tyr 184	Pi stacking	5.01
O1	Ala 183	Hydrogen bond	2.03
N2	Glu 218	Salt bridge	4.58
O3	Zn 478	Metal coordination	1.96
O3	Zn 478	Salt bridge	1.96
O4	Zn 478	Metal coordination	2.11
O5	Leu 180	Hydrogen bond	1.96
MMP-11 Interactions			
Ligand	Receptor	Type	Distance (Å)
O1	Ala 180	Hydrogen bond	1.91
O3	Zn 490	Metal coordination	2.26
O3	Zn 490	Salt bridge	2.26
N2	Glu 216	Salt bridge	4.69
O4	Zn 490	Metal coordination	2.21
O5	Leu 177	Hydrogen bond	1.9
MMP-12 Interactions			
Ligand	Receptor	Type	Distance (Å)
Ar1	Phe 171	Pi stacking	5.1
O1	His 172	Hydrogen bond	2.01
O3	Zn 472	Metal coordination	2.03
O3	Zn 472	Salt bridge	2.03

(Continued on following page)

TABLE 3 (*Continued*) Bictegravir (BIC)- Matrix metalloproteinases (MMPs) Interactions.

MMP-12 Interactions			
Ligand	Receptor	Type	Distance (Å)
N2	Glu 219	Salt bridge	4.44
O4	Zn 472	Metal coordination	2.02
O5	Leu 181	Hydrogen bond	1.91
MMP-13 Interactions			
Ligand	Receptor	Type	Distance (Å)
O1	Leu 185	Hydrogen bond	1.92
O1	Ala 186	Hydrogen bond	1.85
O2	Glu 223	Hydrogen bond	1.98
O3	Zn 473	Metal coordination	1.99
O3	Zn 473	Salt bridge	1.99
MMP-14 Interactions			
Ligand	Receptor	Type	Distance (Å)
Ar1	His 239	Pi stacking	3.69
O1	Leu 199	Hydrogen bond	2.61
O2	Zn 584	Metal coordination	2.24
O3	Zn 584	Metal coordination	2.07
O3	Zn 584	Salt bridge	2.07
N1	Glu 240	Hydrogen bond	2.64
N2	Glu 240	Salt bridge	3.61
MMP-15 Interactions			
Ligand	Receptor	Type	Distance (Å)
O1	Leu 219	Hydrogen bond	1.92
O2	Zn 671	Metal coordination	2.19
O3	Zn 671	Metal coordination	2.18
O3	Zn 671	Salt bridge	2.18
MMP-16 Interactions			
Ligand	Receptor	Type	Distance (Å)
Ar1	Tyr 210	Pi stacking	5.02
O3	Zn 609	Metal coordination	2.01
O3	Zn 609	Salt bridge	2.01
N2	Glu 247	Salt bridge	4.06

(Continued in next column)

TABLE 3 (*Continued*) Bictegravir (BIC)- Matrix metalloproteinases (MMPs) Interactions.

MMP-16 Interactions			
Ligand	Receptor	Type	Distance (Å)
O4	Zn 609	Metal coordination	2.18
O5	Leu 206	Hydrogen bond	2.05
MMP-17 Interactions			
Ligand	Receptor	Type	Distance (Å)
Ar1	His 209	Pi stacking	4.62
O3	Zn 605	Metal coordination	2.09
O3	Zn 605	Salt bridge	2.09
N2	Glu 249	Salt bridge	4.63
O4	Zn 605	Metal coordination	2.02
O5	Val 207	Hydrogen bond	2.33
MMP-19 Interactions			
Ligand	Receptor	Type	Distance (Å)
O2	Zn 510	Metal coordination	2.03
Ar2	Tyr 234	Pi stacking	4.39
O3	Zn 510	Metal coordination	2.04
O3	Zn 510	Salt bridge	2.04
N2	Glu 213	Salt bridge	3.79
MMP-20 Interactions			
Ligand	Receptor	Type	Distance (Å)
O3	Zn 485	Metal coordination	1.99
O3	Zn 485	Salt bridge	1.99
N2	Glu 227	Salt bridge	4.19
O4	Zn 485	Metal coordination	2.07
O5	Leu 189	Hydrogen bond	2.27
MMP-21 Interactions			
Ligand	Receptor	Type	Distance (Å)
N1	Glu 248	Hydrogen bond	1.93
O3	Zn 571	Metal coordination	2
O3	Zn 571	Salt bridge	2.2
N2	Glu 248	Salt bridge	3.33
N2	Glu 284	Salt bridge	4.15

(Continued on following page)

TABLE 3 (*Continued*) Bictegravir (BIC)- Matrix metalloproteinases (MMPs) Interactions.

MMP-21 Interactions			
Ligand	Receptor	Type	Distance (Å)
O4	Zn 571	Metal coordination	2.2
O5	Phe 249	Hydrogen bond	2.23
MMP-23 Interactions			
Ligand	Receptor	Type	Distance (Å)
N1	Glu 167	Hydrogen bond	1.99
O3	Zn 392	Metal coordination	2.15
O3	Zn 392	Salt bridge	2.15
N2	Glu 212	Salt bridge	4.47
O4	Zn 392	Metal coordination	2.24
O5	Leu 168	Hydrogen bond	1.87
MMP-24 Interactions			
Ligand	Receptor	Type	Distance (Å)
Ar1	His 282	Pi stacking	4.35
O1	Leu 242	Hydrogen bond	2.14
O1	Ala 243	Hydrogen bond	2.64
O2	Glu 283	Hydrogen bond	2.14
O2	Zn 647	Metal coordination	2.34
Ar2	Phe 241	Pi stacking	3.99
O3	Zn 647	Metal coordination	2.08
O3	Zn 647	Salt bridge	2.08
N2	Phe 241	Cation pi	3.62
MMP-25 Interactions			
Ligand	Receptor	Type	Distance (Å)
O3	Zn 564	Metal coordination	2.14
O3	Zn 564	Salt bridge	2.14
N2	Glu 234	Salt bridge	4.33
O4	Zn 564	Metal coordination	2.05
O5	Leu 192	Hydrogen bond	2.35
MMP-26 Interactions			
Ligand	Receptor	Type	Distance (Å)
Ar1	His 208	Pi stacking	4.05
Ar1	Trp 231	Pi stacking	5.45
O1	Gly 172	Hydrogen bond	1.94
O2	Glu 209	Hydrogen bond	1.94
O2	Zn 263	Metal coordination	2.29

(Continued in next column)

TABLE 3 (*Continued*) Bictegravir (BIC)- Matrix metalloproteinases (MMPs) Interactions.

MMP-26 Interactions			
Ligand	Receptor	Type	Distance (Å)
O3	Zn 263	Metal coordination	1.96
O3	Zn 263	Salt bridge	1.96
MMP-27 Interactions			
Ligand	Receptor	Type	Distance (Å)
Ar1	His 181	Pi stacking	3.71
O1	Arg 170	Hydrogen bond	1.95
O3	Zn 515	Metal coordination	2.14
O3	Zn 515	Salt bridge	2.14
N2	Glu 217	Salt bridge	4.14
O4	Zn 515	Metal coordination	2.28
O5	Leu 179	Hydrogen bond	2.13
MMP-28 Interactions			
Ligand	Receptor	Type	Distance (Å)
Ar1	His 240	Pi stacking	4.07
O2	Zn 522	Metal coordination	2.14
O3	Zn 522	Metal coordination	1.92
O3	Zn 522	Salt bridge	1.92
N2	Glu 241	Salt bridge	4.79

Observed high binding energies and docking interactions (Table 1; Table 4) confirmed that BIC is a broad-spectrum MMPs inhibitor.

For comparative evaluations, docking simulations were also performed using the known broad-spectrum MMPs inhibitor DOX. DOX is the only US Food and Drug Administration (FDA)-approved broad-spectrum MMPs inhibitor. These were performed against five MMPs. These included MMP-2, 8, 9, 14, and 19. These MMPs were selected as INSTIs have higher binding energies with these enzymes compared to others and each enzyme represented different class of the MMP family. DOX was found to form metal coordination with Zn++ for all tested MMPs. These metal co-ordinations occurred at Zn 166, 469, 709, 584, and 510 receptors of MMP-2, 8, 9, 14, and 19 respectively. Pi stacking interactions occurred with histidine amino acids of MMP-2 and 14. Hydrogen bonding of DOX occurred with all five MMPs tested. DOX was found to form hydrogen bonds with glutamate, alanine, aspartic acid, tyrosine, asparagine, serine, and proline amino acid residues. The distances of receptor-ligand bonds are shown in the DOX-MMP interaction table (Supplementary Table S1). Further, docking simulations of DOX into individual MMPs showed binding energies of −6.595, −7.024, −7.658, −7.114, and −6.488 kcal/mol for MMP-2, 8, 9, 14, and 19 respectively. In comparison to DOX,

TABLE 4 Binding energies for each MMP with DTG, CAB or BIC.

Structure	DTG [Energy (kcal/mol)]	CAB [Energy (kcal/mol)]	BIC [Energy (kcal/mol)]
MMP-1	−6.032	−14.251	−14.55
MMP-2	−6.450	−8.588	−10.972
MMP-3	−6.253	−15.222	−15.082
MMP-7	−7.243	−12.305	−11.385
MMP-8	−8.330	−14.337	−15.771
MMP-9	−9.430	−14.222	−13.415
MMP-10	−6.686	−14.592	−16.021
MMP-11	−6.210	−10.352	−12.143
MMP-12	−6.713	−12.19	−13.482
MMP-13	−6.461	−11.798	−12.73
MMP-14	−9.040	−12.983	−14.539
MMP-15	−5.885	−9.632	−8.877
MMP-16	−7.325	−12.249	−14.625
MMP-17	−6.810	−11.666	−12.409
MMP-19	−7.130	−12.718	−11.695
MMP-20	−6.097	−12.413	−11.923
MMP-21	−6.179	−14.389	−12.698
MMP-23	−6.213	−13.109	−12.25
MMP-24	−6.917	−15.339	−10.181
MMP-25	−6.865	−11.62	−11.716
MMP-26	−7.198	−12.381	−11.971
MMP-27	−7.427	−12.614	−12.54
MMP-28	−6.012	−10.11	−10.823

all three INSTIs (DTG, CAB and BIC) showed higher binding energies with each tested MMP. Interestingly, both, CAB and BIC, showed significantly higher energies compared to DOX and DTG, suggesting CAB or BIC may have comparatively stronger inhibition effect on MMPs (Supplementary Table S2).

The lower binding energy of DOX compared to INSTIs can be explained by its fit within the catalytic binding site. An overlay of the docked DTG, CAB, BIC and DOX on catalytic domain of MMP-9 and -14 showed that DOX (yellow color) has more solvent exposed area than DTG (magenta color), BIC (light blue color) and CAB (red color) (Figure 1). Further, solvent accessible surface area (SASA) calculations confirmed the higher solvent exposure of DOX compared to any of the INSTI (Supplementary Table S3). The higher SASA values of docking complex indicate that the DOX is interacting at lesser extent with MMP's structural binding site and has a higher affinity to form bonds with the solvent compared to INSTIs. These data confirmed that INSTIs fit the MMP binding pocket with greater efficiency than DOX.

INSTIs-induced inhibition of MMPs activities

To affirm that inhibition of MMPs activity is an INSTI class effect, gelatin zymography, a commonly used assay to study MMPs activity and their inhibitors, was performed. For gelatin zymography, cell culture of THP-1 cells was utilized. Cells were treated with phorbol-12-myristate-13-acetate (PMA) to induce differentiation of THP-1 cells into macrophage like cells and to promote MMPs secretion. Herein, PMA-stimulated THP-1 cells were treated with escalating concentrations (25, 50, 75 or 100 μM) of DTG, CAB or BIC for 24 h in serum-free culture medium. Further, to validate the outcome, DOX was utilized as an MMP inhibitor control and the same treatment conditions were employed. To determine the proteolytic activity of MMP-2 and -9 (gelatinases), equal amount of protein (3 μg) from cell culture medium was loaded on SDS-PAGE containing gelatin. Gel area digested by both MMPs was visualized using Coomassie blue stain (Figures 2A, C, E). A decrease in activity of MMP-2 and -9 was observed following treatment with all three INSTIs compared to vehicle-treated

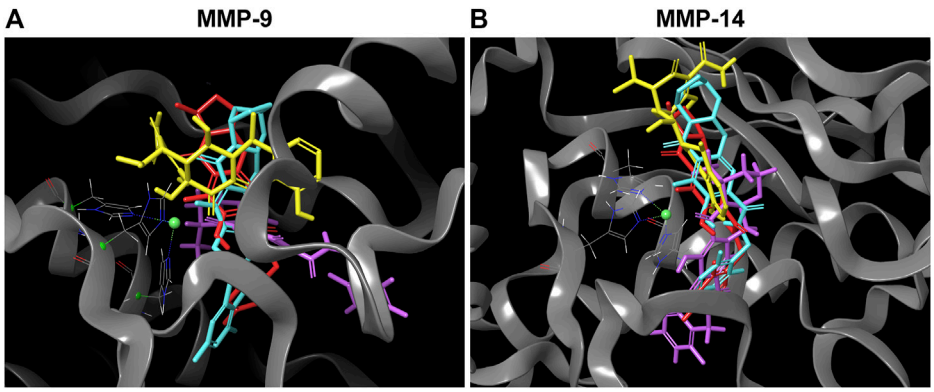

FIGURE 1
Superior affinity of DTG, CAB, BIC compared to DOX at MMPs catalytic binding site. **(A and B)** 3D representative images of overlapping molecular docking complexes of DTG, CAB, BIC, and DOX on MMP-9 or -14 catalytic domain containing Zn++ (green ball) are shown in ribbon (gray color) format. The color scheme utilized for drugs is as follows: DTG - Magenta; CAB - Red; BIC - Light blue; and DOX - Yellow.

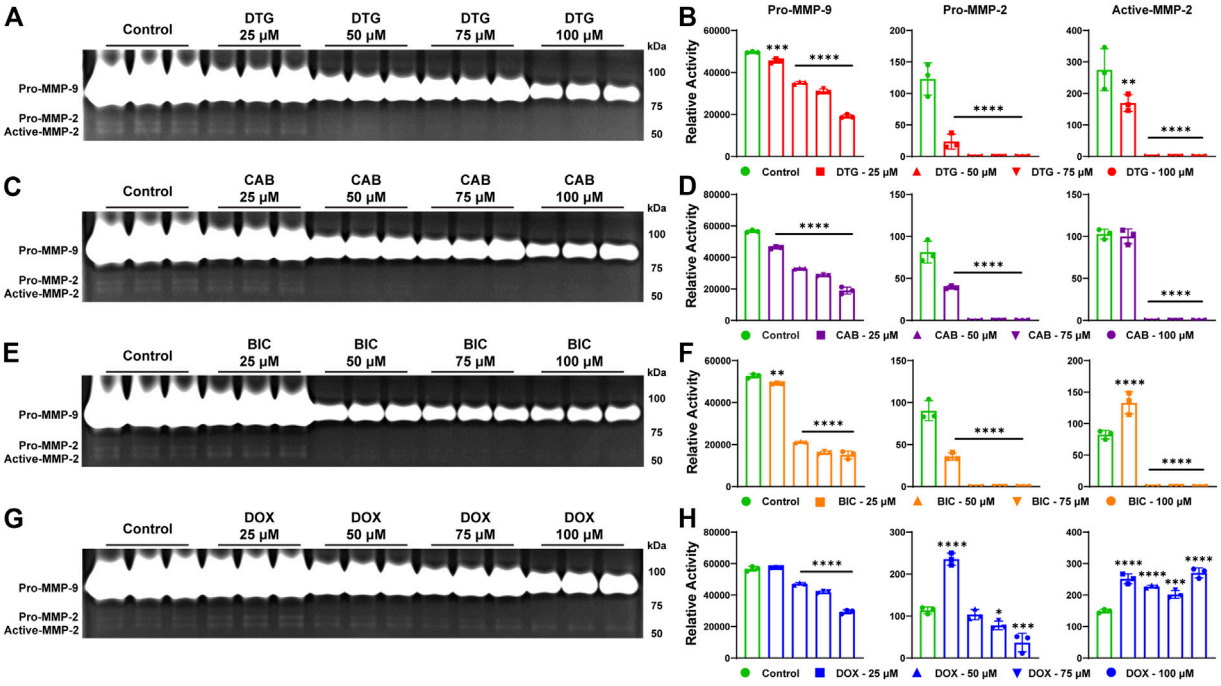

FIGURE 2
Inhibition of MMPs by INSTIs. **(A, C, E, and G)** Gelatin zymogram. Activity of MMP-2 and MMP-9 was evaluated in serum-free medium of THP-1 cells following treatment with DTG, CAB, BIC or DOX (25, 50, 75 or 100 μM). Vehicle treated cells were used as controls. **(B, D, F, and H)** Relative activity of MMP-9 or -2 was measured following treatment with DTG, CAB, BIC or DOX. A one-way ANOVA followed by Dunnett's test was used to compare activity of individual MMP between each treatment concentration of individual drug and respective control (*$p < 0.05$, **$p < 0.01$, ***$p < 0.001$, ***$p < 0.0001$). Data are expressed as the mean ± SEM, N = 3 biological replicates. Experiments were repeated independently three times with equivalent results.

controls on gelatin zymogram (Figures 2A, C, E). Relative activity of the pro forms of MMP-2 and MMP-9 was significantly decreased in a concentration-dependent manner at each tested concentration after treatment with DTG, CAB or BIC compared to controls (Figures 2B, D, F). Relative activity of the active form of MMP-2 was significantly reduced at all concentrations of DTG. However, for CAB and BIC, relative activity of the active form of MMP-2 was significantly reduced at 75 or 100 μM. Interestingly, there was a significant increase in relative activity of the active form of MMP-2 at 25 μM BIC compared to controls. Further, DOX treatment,

showed a significant decrease in relative activity of pro-form of MMP-9 in a concentration dependent manner (Figures 2G, H). However, variable inhibition of MMP-2 was observed after DOX treatment (Figures 2G, H). Relative activity of the pro form of MMP-2 was significantly increased at 25 μM DOX, but significantly decreased in a concentration-dependent manner at 75 and 100 μM concentrations. Relative activity of the active form of MMP-2 was significantly increased at all treatment concentrations of DOX. When comparing DOX and INSTIs at the same treatment concentration, DTG, CAB, and BIC showed higher MMP inhibition compared to DOX (Supplementary Figure S1A–H). Overall, gelatin zymography results confirmed that inhibition of MMPs activities is an INSTI class effect. These results demonstrated that INSTIs inhibit MMP at a higher degree than the known broad-spectrum MMP inhibitor, DOX.

Discussion

The risk of pre- or post-natal neurodevelopmental deficits due to gestational exposure to ARVs remains possible (Hill et al., 2018; Cassidy et al., 2019; Zash et al., 2019; Crowell et al., 2020; Williams et al., 2020). Works outlined in this report provide unique insights into the underlying mechanisms linked to such adverse events. Recently, clinical and pre-clinical studies reported a potential association between DTG usage at the time of conception and NTDs (Hill et al., 2018; Raesima et al., 2019; Zash et al., 2019; Kreitchmann et al., 2021) and postnatal neurological abnormalities(Crowell et al., 2020). Due to mass usage of DTG-based regimens worldwide, reports highlighted the need to find an underlying mechanism of potential DTG-related adverse neurodevelopmental outcomes. With the introduction of new potent ARVs from the INSTI class to treatment regimens, it is essential to establish if such mechanism can be linked to other ARVs from the INSTI class. Herein, we show that INSTIs including DTG, CAB, and BIC possess chemical abilities to interact with Zn++ at the catalytic domain of all twenty-three MMPs observed in humans and thus, can be classified as broad-spectrum MMPs inhibitors. Such secondary mechanism of MMPs inhibition introduces potential for adverse effects, especially during critical periods of fetal brain development.

All ARVs from the INSTI class possess metal-binding pharmacophore, MBP in their chemical structure. This chemical property enables INSTIs to interact with active metal ion (Mg++) sites in the HIV-1 integrase enzyme to block its action of insertion of the viral genome into the host cellular DNA (Smith et al., 2021). With such inherent metal chelating chemical property, INSTIs have potential to interact with other metalloenzymes that are critical for normal cellular functions such as cell proliferation, differentiation, cell signaling, protein cleavage, *etc.* MMPs are well recognized Zn++ dependent metalloenzymes (Ethell and Ethell, 2007; Page-McCaw et al., 2007; Agrawal et al., 2008; van Hinsbergh and Koolwijk, 2008; Loffek et al., 2011; Fujioka et al., 2012; Reinhard et al., 2015; Rempe et al., 2016; Small and Crawford, 2016; De Stefano and Herrero, 2017; Shinotsuka et al., 2018; Kanda et al., 2019). The active site of these enzymes is highly conserved, and comprised of three histidine residues that are bound to the catalytic zinc (Laronha and Caldeira, 2020). Dysregulation of activities of MMPs through chelation of Zn++ can cause detrimental effects on structural and functional development of the CNS. The chemical property of INSTIs to chelate divalent cations enables them to engage with Zn++ in the catalytic domain of all twenty-three human MMPs. Our comprehensive molecular docking assessments confirmed that inhibition of MMPs activity is an INSTI class effect. Notably, interaction of individual DTG, CAB or BIC with each MMP was variable with different binding energy. Thus, studies evaluating drug-induced inhibitions of individual MMPs under biological conditions is needed in the future to identify the susceptibility of individual MMP enzymes under normal and genetic polymorphism conditions.

The role of MMPs in normal neural development is of critical importance. MMPs expression is at high levels during early CNS development and decreases into adulthood (Vaillant et al., 1999; Ayoub et al., 2005; Ulrich et al., 2005; Larsen et al., 2006; Bednarek et al., 2009; Aujla and Huntley, 2014; Reinhard et al., 2015). Due to their proteolytic activities, MMPs are ubiquitously expressed during neural development and their expression has been majorly studied in hippocampus, cortex and cerebellum (Fujioka et al., 2012; Reinhard et al., 2015; Small and Crawford, 2016; Beroun et al., 2019). The principal function of MMPs is to degrade extracellular matrix components (Lukes et al., 1999). However, it is well recognized that MMPs functions are essential for the regulation of several neurodevelopmental processes including neurogenesis, neurite outgrowth, migration of newly born neurons, myelination, axonal guidance, synaptic plasticity and angiogenesis (Fujioka et al., 2012; Reinhard et al., 2015; Small and Crawford, 2016). Dysregulation of MMPs activities during critical periods of fetal brain development during gestation could significantly affect these processes, resulting in adverse neurodevelopmental outcomes (Fujioka et al., 2012; Reinhard et al., 2015; Small and Crawford, 2016). Notably, previously we observed that DTG inhibits MMPs activities in rodent embryo brain during gestation leading to neuroinflammation and neuronal injury in the CNS of mice pups during postnatal assessments (Bade et al., 2021). This study identified DTG-induced inhibition of MMPs activities as a neurotoxicity biomarker. However, the previous study was proof of concept and mainly focused on DTG, but comprehensive docking assessments for consideration of each of MMP was missing. The current study confirmed that all INSTIs possess abilities to inhibit MMPs activities. Therefore, drug-induced differences in MMP activities or MMP expression levels could serve as a biomarker for INSTI-associated neurodevelopmental impairments. In addition to pregnancy outcomes, INSTIs also have been recognized to be associated with neuropsychiatric adverse events (NPAEs) in adults (Yombi, 2018; Amusan et al., 2020; Senneker and Tseng, 2021) and clinically significant weight-gain, especially in females (NAMSAL ANRS 12313 Study Group et al., 2019; Venter et al., 2019; Bourgi et al., 2020; Caniglia et al., 2020; Sax et al., 2020). Impaired MMPs activity, expression and related cellular pathways have been identified as biomarkers in both disorders (Vandenbroucke and Libert, 2014; Jaoude and Koh, 2016; Shinotsuka et al., 2018; Beroun et al., 2019; Ruiz-Ojeda et al., 2019; Gorwood et al., 2020; Li et al., 2020). Further, due to critical functions of MMPs, their dysregulation has also served as a biomarker for several types of tumors and atherosclerosis

(Goncalves et al., 2015; Huang, 2018). Thus, this work provides a potential mechanistic biomarker for neurodevelopmental assessments following *in utero* exposure to ART regimens with an INSTI component.

Identifying the roles of the MMPs and impact of their independent or broad-spectrum inhibition in physiological or pathological conditions is complex. This has reflected in cessation of clinical trials of more than fifty broad-spectrum MMP inhibitors due to adverse events following prolonged treatment (Vandenbroucke and Libert, 2014). Thus, an understanding of the inhibitory effect of INSTIs against each MMP enzyme is essential to define the mechanism linked to neurodevelopment. The INSTIs utilized for testing in this study DTG, CAB and BIC showed strong binding energy with the catalytic domains of all twenty-three MMPs. Moreover, comparison assessments against DOX, a clinically used broad-spectrum inhibitor of MMPs, confirmed the high potency of DTG, CAB or BIC against MMPs. For example, binding energies (kcal/mol) with the catalytic domain of MMP-9 were −9.430 (DTG), −14.222 (CAB), and −13.415 (BIC) against −7.658 (DOX). These molecular docking assessment differences against MMP-9 were further apparent on the confirmatory gelatin zymography biological tests. Interestingly, CAB and BIC exhibited higher binding energies for all tested MMPs compared to DTG, suggesting that these newer INSTIs may be more potent MMPs inhibitors. Such observations will need biological validations along with determination of half maximal inhibitory concentration (IC_{50}) values of each INSTI against individual enzymes in the future.

Of the twenty-three human MMPs, few MMPs are well characterized for their role during neurodevelopment. MMP-2 and MMP-9 have been studied extensively and are shown to be essential for the neuronal development, migration, axonal guidance and synaptic plasticity (Ethell and Ethell, 2007; Page-McCaw et al., 2007; Agrawal et al., 2008; Fujioka et al., 2012; Reinhard et al., 2015; Small and Crawford, 2016; De Stefano and Herrero, 2017). Widespread expression of MMP-3 has been identified in neurons in the brain and spinal cord of rodents during critical timepoints of axonal outgrowth (Van Hove et al., 2012a). Moreover, MMP-24 is also expressed in neurons in the brain and spinal cord during development, signifying its role in neuronal development, and MMP-2 and -14 are involved in angiogenesis and in establishment and/or maintenance of the blood-brain barrier (BBB) (Girolamo et al., 2004; Lehti et al., 2005; Lehti et al., 2009; Ikonomidou, 2014; Rempe et al., 2016; Kanda et al., 2019). Knock out or knockdown models of the mentioned MMPs have proved that deficiency in these MMPs can affect neurodevelopmental processes (Oh et al., 2004; Luo, 2005; Van Hove et al., 2012b; Kanda et al., 2019). Interestingly, MMPs are expressed abundantly in neural stem cells (Frolichsthal-Schoeller et al., 1999). Inhibition of MMPs activity by synthetic inhibitors was shown to reduce proliferation and differentiation of neural stem cells (Szymczak et al., 2010; Wojcik-Stanaszek et al., 2011). Thus, identifying the impact of INSTI-induced inhibition of MMPs activities on neurodevelopment and unravelling genetic susceptibility increasing the severity of adverse effects will be critical.

Clinical and pre-clinical studies showed high levels of transplacental transfer of INSTI drugs (Schalkwijk et al., 2016; Mulligan et al., 2018; Mandelbrot et al., 2019; Waitt et al., 2019; Bollen et al., 2021; Bukkems et al., 2021). Studies of DTG have found high placental transfer of DTG from mother to fetus with median cord blood to maternal blood drug level ratios from 1.21 up to 1.29 (Schalkwijk et al., 2016; Mulligan et al., 2018; Mandelbrot et al., 2019; Waitt et al., 2019; Bollen et al., 2021). Further, DTG was also found to accumulate in the fetus with noted prolonged elimination of drug from infants after birth (Mulligan et al., 2018; Waitt et al., 2019). Although few studies have addressed placental transfer of CAB and BIC, evidence does suggest that these INSTIs also cross the placental barrier (Pencole et al., 2020; Bukkems et al., 2021; Le et al., 2022). Our previous work investigated pharmacokinetic (PK) and biodistribution (BD) of DTG during pregnancy in mice and confirmed that DTG levels are detectable in brain tissues of embryos following daily oral administration at supratherapeutic dosage (Bade et al., 2021). Our work validated clinical reports of high placental transfer of DTG and was the first to show drug levels in the fetal developing brain during gestation. Such transplacental transfer of DTG indicated that direct exposure of the embryo brain to DTG during critical periods of development could have an adverse impact on neurodevelopment. Therefore, understanding the PK and BD profiles of new INSTIs during pregnancy and their effects on neurodevelopmental processes is needed for better mechanistic assessments.

It is acknowledged that despite the occurrence of birth defects has been a concern, both the United States Department of Health and Human Services (DHHS) and World Health Organization recommend DTG as a preferred first-line ARV during pregnancy (The U.S. Department of Health and Human Services, 2015; World Health Organization (WHO), 2019a). This decision was based on risk benefit ratios offered by DTG as an ARV compared to rate of associated risk. These included fewer mother-to-child HIV-1 transmission and maternal deaths, and cost-effective (Dugdale et al., 2019; Phillips et al., 2020). Moreover, DTG's high genetic barrier to drug resistance would address the critical problem of rising pretreatment resistance (PDR) to non-nucleoside reverse transcriptase inhibitors (NNRTIs) in RLCs, especially in women (World Health Organization (WHO), 2019a; World Health Organization (WHO), 2019b). Moreover, most updated data from Tsepamo study (Botswana) reported declined rate of birth defects and was comparative between DTG and other ARVs at the time of conception in late breaking abstract at the 24th International AIDS Conference, 2022. Nonetheless, assessment of birth defects in Botswana is an ongoing study and recommended guidelines were based on higher benefits offered by DTG. Yet, risk of long-term neurodevelopmental deficits persists. Particularly, there is a research gap of known adverse events reflecting DTG-associated long-term impact on postnatal neurodevelopment. Therefore, with large number of fetuses being exposed to DTG worldwide, continuous research efforts are critical to uncover any adverse effects of DTG exposures on pre- or post-natal neurodevelopment and elucidate underlying mechanism.

Although the current study provides evidence of an INSTI class effect on the inhibition of MMPs, it was limited to laboratory cell-based assessments. Future studies are necessary in order to affirm mechanistic links between altered MMP activities and adverse developmental outcomes following *in utero* INSTI exposures. Dose dependent effects of each INSTI on MMPs activities at different stages of neurodevelopment

during gestation and early postnatal period need to be studied in animal models. This work would need to include detailed BD drug profiles within the fetal CNS and related MMPs activities. Moreover, with a metal chelating motif, INSTIs possess potential to inhibit other metalloenzymes required for fetal brain development such as Zn++ dependent a disintegrin and metalloproteinase (ADAM) family members (Jorissen et al., 2010; Vandenbroucke and Libert, 2014). Whether inhibition of these metalloenzymes, even at minimal extent, in addition to MMPs could augment the developmental adverse events needs consideration. Thus, comprehensive computational modeling against other metalloenzymes along with biological validations are critical in the future. Moreover, development of ultra-long acting nanoformulations of DTG and assessment of these as a safe drug delivery system for neuroprotective outcomes will be the focus our own future work. We hypothesize that neuroprotective effect would be the outcome of lower drug biodistribution in the embryo brain preventing MMPs inhibition. Such lower drug biodistribution in fetal brain while maintaining therapeutic drug levels in maternal blood is expected due to long-acting pharmacological properties of formulations and lower total drug administration compared to daily oral drug administration. For example, the 8-week cumulative dose of daily oral CAB (VOCABRIA) is 1,680 mg. Whereas, a 600 mg bi-monthly single intramuscular injection of LA-CAB (CABENUVA or APRETUDE) results in a 3-fold reduction in drug exposure with equivalent duration of action (US Food and Drug Administration (FDA), 2021; US Food and Drug Administration (FDA), 2021). Importantly, scientific exchange between basic science mechanistic findings and the clinical assessment of INSTI-exposed children will be required in the future to provide cross-validation of scientific findings and rigorous assessments of neurodevelopment. Overall, it is timely to elucidate any potential ARV-induced secondary effects during pregnancy, in order to provide effective care for women and their fetuses. This study confirms that INSTIs are broad-spectrum MMPs inhibitors. As balanced regulation of MMP activities are crucial for neurodevelopment, the enzyme's inhibition could underlie INSTI-related adverse neurodevelopmental outcomes.

Data availability statement

The original contributions presented in the study are included in the article/Supplementary Material, further inquiries can be directed to the corresponding author.

Author contributions

EF: performed experiments, collected, analyzed and interpreted data sets, co-wrote, edited and reviewed the manuscript; NP: performed molecular docking experiments, collected, analyzed data sets, YL: provided overall project and technical guidance and edited the manuscript; BE: provided overall project and technical guidance and edited the manuscript; HG: provided overall project and technical guidance, edited and reviewed the manuscript; AB: conceived project, devised central hypothesis and the project's scientific approach, analyzed and interpreted data, co-wrote, edited and reviewed the manuscript and provided funding acquisition. All authors critically evaluated and approved the final manuscript prior to submission.

Funding

This study is supported by NIH grants R21HD106842, R21MH128123, R01AI145542, and R01AI158160.

Acknowledgments

Authors thank the technical support from UNMC Computational Chemistry Core facility.

Conflict of interest

HG and BE are Co-founders of Exavir Therapeutics, Inc., a biotechnology company focused on the development of long-acting antiretroviral medicines and HIV-1 cure strategies.

The remaining authors declare that the research was conducted in the absence of any commercial or financial relationships that could be construed as a potential conflict of interest.

Publisher's note

Supplementary material

The Supplementary Material for this article can be found online at: https://www.frontiersin.org/articles/10.3389/ftox.2023.1113032/full#supplementary-material

References

Agrawal, S. M., Lau, L., and Yong, V. W. (2008). MMPs in the central nervous system: Where the good guys go bad. *Semin. Cell Dev. Biol.* 19 (1), 42–51. doi:10.1016/j.semcdb.2007.06.003

Amusan, P., Power, C., Gill, M. J., Gomez, D., Johnson, E., Rubin, L. H., et al. (2020). Lifetime antiretroviral exposure and neurocognitive impairment in HIV. *J. Neurovirol* 26 (5), 743–753. doi:10.1007/s13365-020-00870-z

Aujla, P. K., and Huntley, G. W. (2014). Early postnatal expression and localization of matrix metalloproteinases-2 and -9 during establishment of rat hippocampal synaptic circuitry. *J. Comp. Neurol.* 522 (6), 1249–1263. doi:10.1002/cne.23468

Ayoub, A. E., Cai, T. Q., Kaplan, R. A., and Luo, J. (2005). Developmental expression of matrix metalloproteinases 2 and 9 and their potential role in the histogenesis of the cerebellar cortex. *J. Comp. Neurol.* 481 (4), 403–415. doi:10.1002/cne.20375

Bade, A. N. M. J., Liu, Y., Edagwa, B. J., and Gendelman, H. E. (2021). Dolutegravir inhibition of matrix metalloproteinases affects mouse neurodevelopment. *Mol. Neurobiol.* 58, 5703–5721. doi:10.1007/s12035-021-02508-5

Bednarek, N., Clement, Y., Lelievre, V., Olivier, P., Loron, G., Garnotel, R., et al. (2009). Ontogeny of MMPs and TIMPs in the murine neocortex. *Pediatr. Res.* 65 (3), 296–300. doi:10.1203/PDR.0b013e3181973aee

Beroun, A., Mitra, S., Michaluk, P., Pijet, B., Stefaniuk, M., and Kaczmarek, L. (2019). MMPs in learning and memory and neuropsychiatric disorders. *Cell Mol. Life Sci.* 76 (16), 3207–3228. doi:10.1007/s00018-019-03180-8

Bollen, P., Freriksen, J., Konopnicki, D., Weizsacker, K., Hidalgo Tenorio, C., Molto, J., et al. (2021). The effect of pregnancy on the pharmacokinetics of total and unbound dolutegravir and its main metabolite in women living with human immunodeficiency virus. *Clin. Infect. Dis.* 72 (1), 121–127. doi:10.1093/cid/ciaa006

Bourgi, K., Rebeiro, P. F., Turner, M., Castilho, J. L., Hulgan, T., Raffanti, S. P., et al. (2020). Greater weight gain in treatment-naive persons starting dolutegravir-based antiretroviral therapy. *Clin. Infect. Dis.* 70 (7), 1267–1274. doi:10.1093/cid/ciz407

Bukkems, V. E., Hidalgo-Tenorio, C., Garcia, C., van Hulzen, A. G. W., Richel, O., Burger, D. M., et al. (2021). First pharmacokinetic data of bictegravir in pregnant women living with HIV. *AIDS* 35 (14), 2405–2406. doi:10.1097/QAD.0000000000003032

Cabrera, R. M., Souder, J. P., Steele, J. W., Yeo, L., Tukeman, G., Gorelick, D. A., et al. (2019). The antagonism of folate receptor by dolutegravir: Developmental toxicity reduction by supplemental folic acid. *AIDS* 33 (13), 1967–1976. doi:10.1097/QAD.0000000000002289

Caniglia, E. C., Shapiro, R., Diseko, M., Wylie, B. J., Zera, C., Davey, S., et al. (2020). Weight gain during pregnancy among women initiating dolutegravir in Botswana. *EClinicalMedicine* 29-30, 100615. doi:10.1016/j.eclinm.2020.100615

Cassidy, A. R., Williams, P. L., Leidner, J., Mayondi, G., Ajibola, G., Makhema, J., et al. (2019). *In utero* efavirenz exposure and neurodevelopmental outcomes in HIV-exposed uninfected children in Botswana. *Pediatr. Infect. Dis. J.* 38 (8), 828–834. doi:10.1097/INF.0000000000002332

Chandiwana, N. C., Chersich, M., Venter, W. F., Akpomiemie, G., Hill, A., Simmons, B., et al. (2020). Unexpected interactions between dolutegravir and folate: Randomised trial evidence from south Africa. *AIDS* 35 (2), 205–211. doi:10.1097/QAD.0000000000002741

Crowell, C. S., Williams, P. L., Yildirim, C., Van Dyke, R. B., Smith, R., Chadwick, E. G., et al. (2020). Safety of *in-utero* antiretroviral exposure: Neurologic outcomes in children who are HIV-exposed but uninfected. *AIDS* 34 (9), 1377–1387. doi:10.1097/QAD.0000000000002550

De Stefano, M. E., and Herrero, M. T. (2017). The multifaceted role of metalloproteinases in physiological and pathological conditions in embryonic and adult brains. *Prog. Neurobiol.* 155, 36–56. doi:10.1016/j.pneurobio.2016.08.002

Department of Health and Human Services (DHHS) (2022). *Panel on antiretroviral guidelines for adults and adolescents. Guidelines for the use of antiretroviral agents in adults and adolescents living with HIV*. Available at: https://clinicalinfo.hiv.gov/sites/default/files/guidelines/documents/AdultandAdolescentGL.pdf.

Dorward, J., Lessells, R., Drain, P. K., Naidoo, K., de Oliveira, T., Pillay, Y., et al. (2018). Dolutegravir for first-line antiretroviral therapy in low-income and middle-income countries: Uncertainties and opportunities for implementation and research. *Lancet HIV* 5, e400–e404. doi:10.1016/S2352-3018(18)30093-6

Dugdale, C. M., Ciaranello, A. L., Bekker, L. G., Stern, M. E., Myer, L., Wood, R., et al. (2019). Risks and benefits of dolutegravir- and efavirenz-based strategies for South African women with HIV of child-bearing potential: A modeling study. *Ann. Intern Med.* 170 (9), 614–625. doi:10.7326/M18-3358

Ethell, I. M., and Ethell, D. W. (2007). Matrix metalloproteinases in brain development and remodeling: Synaptic functions and targets. *J. Neurosci. Res.* 85 (13), 2813–2823. doi:10.1002/jnr.21273

Frolichsthal-Schoeller, P., Vescovi, A. L., Krekoski, C. A., Murphy, G., Edwards, D. R., and Forsyth, P. (1999). Expression and modulation of matrix metalloproteinase-2 and tissue inhibitors of metalloproteinases in human embryonic CNS stem cells. *Neuroreport* 10 (2), 345–351. doi:10.1097/00001756-199902050-00025

Fujioka, H., Dairyo, Y., Yasunaga, K., and Emoto, K. (2012). Neural functions of matrix metalloproteinases: Plasticity, neurogenesis, and disease. *Biochem. Res. Int.* 2012, 789083. doi:10.1155/2012/789083

Gilmore, J. C., Hoque, M. T., Dai, W., Mohan, H., Dunk, C., Serghides, L., et al. (2022). Interaction between dolutegravir and folate transporters and receptor in human and rodent placenta. *EBioMedicine* 75, 103771. doi:10.1016/j.ebiom.2021.103771

Girolamo, F., Virgintino, D., Errede, M., Capobianco, C., Bernardini, N., Bertossi, M., et al. (2004). Involvement of metalloprotease-2 in the development of human brain microvessels. *Histochem Cell Biol.* 122 (3), 261–270. doi:10.1007/s00418-004-0705-x

Goncalves, I., Bengtsson, E., Colhoun, H. M., Shore, A. C., Palombo, C., Natali, A., et al. (2015). Elevated plasma levels of MMP-12 are associated with atherosclerotic burden and symptomatic cardiovascular disease in subjects with type 2 diabetes. *Arterioscler. Thromb. Vasc. Biol.* 35 (7), 1723–1731. doi:10.1161/ATVBAHA.115.305631

Gorwood, J., Bourgeois, C., Pourcher, V., Pourcher, G., Charlotte, F., Mantecon, M., et al. (2020). The integrase inhibitors dolutegravir and raltegravir exert pro-adipogenic and profibrotic effects and induce insulin resistance in human/simian adipose tissue and human adipocytes. *Clin. Infect. Dis.* 71, e549–e560. doi:10.1093/cid/ciaa259

Harder, E., Damm, W., Maple, J., Wu, C., Reboul, M., Xiang, J. Y., et al. (2016). OPLS3: A force field providing broad coverage of drug-like Small molecules and proteins. *J. Chem. Theory Comput.* 12 (1), 281–296. doi:10.1021/acs.jctc.5b00864

Hill, A., Clayden, P., Thorne, C., Christie, R., and Zash, R. (2018). Safety and pharmacokinetics of dolutegravir in HIV-positive pregnant women: A systematic review. *J. Virus Erad.* 4 (2), 66–71. doi:10.1016/s2055-6640(20)30247-8

Huang, H. (2018). Matrix metalloproteinase-9 (MMP-9) as a cancer biomarker and MMP-9 biosensors: Recent advances. *Sensors (Basel)* 18 (10), 3249. doi:10.3390/s18103249

Ikonomidou, C. (2014). Matrix metalloproteinases and epileptogenesis. *Mol. Cell Pediatr.* 1 (1), 6. doi:10.1186/s40348-014-0006-y

Jaoude, J., and Koh, Y. (2016). Matrix metalloproteinases in exercise and obesity. *Vasc. Health Risk Manag.* 12, 287–295. doi:10.2147/VHRM.S103877

Jorissen, E., Prox, J., Bernreuther, C., Weber, S., Schwanbeck, R., Serneels, L., et al. (2010). The disintegrin/metalloproteinase ADAM10 is essential for the establishment of the brain cortex. *J. Neurosci.* 30 (14), 4833–4844. doi:10.1523/JNEUROSCI.5221-09.2010

Kanda, H., Shimamura, R., Koizumi-Kitajima, M., and Okano, H. (2019). Degradation of extracellular matrix by matrix metalloproteinase 2 is essential for the establishment of the blood-brain barrier in Drosophila. *iScience* 16, 218–229. doi:10.1016/j.isci.2019.05.027

Kreitchmann, R., Oliveira, F. R., and Sprinz, E. (2021). Two cases of neural tube defects with dolutegravir use at conception in south Brazil. *Braz J. Infect. Dis.* 25 (2), 101572. doi:10.1016/j.bjid.2021.101572

Krieger, E., and Vriend, G. (2014). YASARA View - molecular graphics for all devices - from smartphones to workstations. *Bioinformatics* 30 (20), 2981–2982. doi:10.1093/bioinformatics/btu426

Laronha, H., and Caldeira, J. (2020). Structure and function of human matrix metalloproteinases. *Cells* 9 (5), 1076. doi:10.3390/cells9051076

Larsen, P. H., DaSilva, A. G., Conant, K., and Yong, V. W. (2006). Myelin formation during development of the CNS is delayed in matrix metalloproteinase-9 and -12 null mice. *J. Neurosci.* 26 (8), 2207–2214. doi:10.1523/JNEUROSCI.1880-05.2006

Le, M. P., Ferre, V. M., Mazy, F., Bourgeois-Moine, A., Damond, F., Matheron, S., et al. (2022). Bictegravir pharmacokinetics in a late-presenting HIV-1-infected pregnant woman: A case report. *J. Antimicrob. Chemother.* 77 (3), 851–853. doi:10.1093/jac/dkab424

Lehti, K., Allen, E., Birkedal-Hansen, H., Holmbeck, K., Miyake, Y., Chun, T. H., et al. (2005). An MT1-MMP-PDGF receptor-beta axis regulates mural cell investment of the microvasculature. *Genes Dev.* 19 (8), 979–991. doi:10.1101/gad.1294605

Lehti, K., Rose, N. F., Valavaara, S., Weiss, S. J., and Keski-Oja, J. (2009). MT1-MMP promotes vascular smooth muscle dedifferentiation through LRP1 processing. *J. Cell Sci.* 122 (1), 126–135. doi:10.1242/jcs.035279

Li, X., Zhao, Y., Chen, C., Yang, L., Lee, H. H., Wang, Z., et al. (2020). Critical role of matrix metalloproteinase 14 in adipose tissue remodeling during obesity. *Mol. Cell Biol.* 40 (8), e00564-19. doi:10.1128/MCB.00564-19

Loffek, S., Schilling, O., and Franzke, C. W. (2011). Series "matrix metalloproteinases in lung health and disease": Biological role of matrix metalloproteinases: A critical balance. *Eur. Respir. J.* 38 (1), 191–208. doi:10.1183/09031936.00146510

Lukes, A., Mun-Bryce, S., Lukes, M., and Rosenberg, G. A. (1999). Extracellular matrix degradation by metalloproteinases and central nervous system diseases. *Mol. Neurobiol.* 19 (3), 267–284. doi:10.1007/BF02821717

Luo, J. (2005). The role of matrix metalloproteinases in the morphogenesis of the cerebellar cortex. *Cerebellum* 4 (4), 239–245. doi:10.1080/14734220500247646

Mandelbrot, L., Ceccaldi, P. F., Duro, D., Le, M., Pencole, L., and Peytavin, G. (2019). Placental transfer and tissue accumulation of dolutegravir in the *ex vivo* human cotyledon perfusion model. *PLoS One* 14 (8), e0220323. doi:10.1371/journal.pone.0220323

Mohan, H., Lenis, M. G., Laurette, E. Y., Tejada, O., Sanghvi, T., Leung, K. Y., et al. (2020). Dolutegravir in pregnant mice is associated with increased rates of fetal defects at therapeutic but not at supratherapeutic levels. *EBioMedicine* 63, 103167. doi:10.1016/j.ebiom.2020.103167

Mulligan, N., Best, B. M., Wang, J., Capparelli, E. V., Stek, A., Barr, E., et al. (2018). Dolutegravir pharmacokinetics in pregnant and postpartum women living with HIV. *AIDS* 32 (6), 729–737. doi:10.1097/QAD.0000000000001755

NAMSAL ANRS 12313 Study Group; Kouanfack, C., Mpoudi-Etame, M., Omgba Bassega, P., Eymard-Duvernay, S., Leroy, S., Boyer, S., et al. (2019). Dolutegravir-based or low-dose efavirenz-based regimen for the treatment of HIV-1. *N. Engl. J. Med.* 381 (9), 816–826. doi:10.1056/nejmoa1904340

Oh, J., Takahashi, R., Adachi, E., Kondo, S., Kuratomi, S., Noma, A., et al. (2004). Mutations in two matrix metalloproteinase genes, MMP-2 and MT1-MMP, are synthetic lethal in mice. *Oncogene* 23 (29), 5041–5048. doi:10.1038/sj.onc.1207688

Page-McCaw, A., Ewald, A. J., and Werb, Z. (2007). Matrix metalloproteinases and the regulation of tissue remodelling. *Nat. Rev. Mol. Cell Biol.* 8 (3), 221–233. doi:10.1038/nrm2125

Pencole, L., Le, M. P., Bouchet-Crivat, F., Duro, D., Peytavin, G., and Mandelbrot, L. (2020). Placental transfer of the integrase strand inhibitors cabotegravir and bictegravir in the *ex-vivo* human cotyledon perfusion model. *AIDS* 34 (14), 2145–2149. doi:10.1097/QAD.0000000000002637

Peters, H., Francis, K., Sconza, R., Horn, A., Peckham, C. S., Tookey, P. A., et al. (2017). UK mother-to-child HIV transmission rates continue to decline: 2012-2014. *Clin. Infect. Dis.* 64 (4), 527–528. doi:10.1093/cid/ciw791

Phillips, A. N., Bansi-Matharu, L., Venter, F., Havlir, D., Pozniak, A., Kuritzkes, D. R., et al. (2020). Updated assessment of risks and benefits of dolutegravir versus efavirenz in new antiretroviral treatment initiators in sub-saharan africa: Modelling to inform treatment guidelines. *Lancet HIV* 7 (3), e193–e200. doi:10.1016/S2352-3018(19)30400-X

Raesima, M. M., Ogbuabo, C. M., Thomas, V., Forhan, S. E., Gokatweng, G., Dintwa, E., et al. (2019). Dolutegravir use at conception - additional surveillance data from Botswana. *N. Engl. J. Med.* 381 (9), 885–887. doi:10.1056/NEJMc1908155

Ramokolo, V., Goga, A. E., Slogrove, A. L., and Powis, K. M. (2019). Unmasking the vulnerabilities of uninfected children exposed to HIV. *BMJ* 366, l4479. doi:10.1136/bmj.l4479

Rasi, V., Peters, H., Sconza, R., Francis, K., Bukasa, L., Thorne, C., et al. (2022). Trends in antiretroviral use in pregnancy in the UK and Ireland. *HIV Med.* 23 (4), 397–405. doi:10.1111/hiv.13243

Reinhard, S. M., Razak, K., and Ethell, I. M. (2015). A delicate balance: Role of MMP-9 in brain development and pathophysiology of neurodevelopmental disorders. *Front. Cell Neurosci.* 9, 280. doi:10.3389/fncel.2015.00280

Rempe, R. G., Hartz, A. M. S., and Bauer, B. (2016). Matrix metalloproteinases in the brain and blood-brain barrier: Versatile breakers and makers. *J. Cereb. Blood Flow. Metab.* 36 (9), 1481–1507. doi:10.1177/0271678X16655551

Ruiz-Ojeda, F. J., Mendez-Gutierrez, A., Aguilera, C. M., and Plaza-Diaz, J. (2019). Extracellular matrix remodeling of adipose tissue in obesity and metabolic diseases. *Int. J. Mol. Sci.* 20 (19), 4888. doi:10.3390/ijms20194888

Sax, P. E., Erlandson, K. M., Lake, J. E., McComsey, G. A., Orkin, C., Esser, S., et al. (2020). Weight gain following initiation of antiretroviral therapy: Risk factors in randomized comparative clinical trials. *Clin. Infect. Dis.* 71 (6), 1379–1389. doi:10.1093/cid/ciz999

Schalkwijk, S., Greupink, R., Colbers, A. P., Wouterse, A. C., Verweij, V. G., van Drongelen, J., et al. (2016). Placental transfer of the HIV integrase inhibitor dolutegravir in an *ex vivo* human cotyledon perfusion model. *J. Antimicrob. Chemother.* 71 (2), 480–483. doi:10.1093/jac/dkv358

Schnoll, J. G., Temsamrit, B., Zhang, D., Song, H., Ming, G. L., and Christian, K. M. (2019). Evaluating neurodevelopmental consequences of perinatal exposure to antiretroviral drugs: Current challenges and new approaches. *J. Neuroimmune Pharmacol.* 16, 113–129. doi:10.1007/s11481-019-09880-z

Senneker, T., and Tseng, A. (2021). An update on neuropsychiatric adverse effects with second-generation integrase inhibitors and nonnucleoside reverse transcriptase inhibitors. *Curr. Opin. HIV AIDS* 16 (6), 309–320. doi:10.1097/COH.0000000000000705

Shinotsuka, N., Yamaguchi, Y., Nakazato, K., Matsumoto, Y., Mochizuki, A., and Miura, M. (2018). Caspases and matrix metalloproteases facilitate collective behavior of non-neural ectoderm after hindbrain neuropore closure. *BMC Dev. Biol.* 18 (1), 17. doi:10.1186/s12861-018-0175-3

Small, C. D., and Crawford, B. D. (2016). Matrix metalloproteinases in neural development: A phylogenetically diverse perspective. *Neural Regen. Res.* 11 (3), 357–362. doi:10.4103/1673-5374.179030

Smith, S. J., Zhao, X. Z., Passos, D. O., Lyumkis, D., Burke, T. R., Jr., and Hughes, S. H. (2021). Integrase strand transfer inhibitors are effective anti-HIV drugs. *Viruses* 13 (2), 205. doi:10.3390/v13020205

Szymczak, P., Wojcik-Stanaszek, L., Sypecka, J., Sokolowska, A., and Zalewska, T. (2010). Effect of matrix metalloproteinases inhibition on the proliferation and differentiation of HUCB-NSCs cultured in the presence of adhesive substrates. *Acta Neurobiol. Exp. (Wars)* 70 (4), 325–336.

The Centers for Disease Control and Prevention (CDC) (2018). *HIV and pregnant women, infants, and children*. Available at: https://www.cdc.gov/hiv/group/gender/pregnantwomen/index.html.

The Joint United Nations Programme on HIV/AIDS (UNAIDS) (2021). *Global HIV & AIDS statistics fact sheet— 2021*.

The Joint United Nations Programme on HIV/AIDS (UNAIDS) (2021). *Start free, stay free, AIDS free final report on 2020 targets*. Available at: https://www.unaids.org/en/resources/documents/2021/start-free-stay-free-aids-free-final-report-on-2020-targets.

The Lancet, H. (2020). End resistance to dolutegravir roll-out. *Lancet HIV* 7 (9), e593. doi:10.1016/S2352-3018(20)30231-9

The U.S. Department of Health and Human Services (2015). *Recommendations for the use of antiretroviral drugs in pregnant women with HIV infection and interventions to reduce perinatal HIV transmission in the United States*. Available at: https://clinicalinfo.hiv.gov/sites/default/files/guidelines/documents/Perinatal_GL.pdf.

Ulrich, R., Gerhauser, I., Seeliger, F., Baumgartner, W., and Alldinger, S. (2005). Matrix metalloproteinases and their inhibitors in the developing mouse brain and spinal cord: A reverse transcription quantitative polymerase chain reaction study. *Dev. Neurosci.* 27 (6), 408–418. doi:10.1159/000088455

US Food and Drug Administration (FDA) (2021). *FDA approves first injectable treatment for HIV pre-exposure prevention*. Available at: https://www.fda.gov/news-events/press-announcements/fda-approves-first-injectable-treatment-hiv-pre-exposure-prevention.

US Food and Drug Administration (FDA) (2021). *FDA approves cabenuva and vocabria for the treatment of HIV-1 infection*. Available at: https://www.fda.gov/drugs/human-immunodeficiency-virus-hiv/fda-approves-cabenuva-and-vocabria-treatment-hiv-1-infection.

Van Hove, I., Verslegers, M., Buyens, T., Delorme, N., Lemmens, K., Stroobants, S., et al. (2012). An aberrant cerebellar development in mice lacking matrix metalloproteinase-3. *Mol. Neurobiol.* 45 (1), 17–29. doi:10.1007/s12035-011-8215-z

Vaillant, C., Didier-Bazes, M., Hutter, A., Belin, M. F., and Thomasset, N. (1999). Spatiotemporal expression patterns of metalloproteinases and their inhibitors in the postnatal developing rat cerebellum. *J. Neurosci.* 19 (12), 4994–5004. doi:10.1523/JNEUROSCI.19-12-04994.1999

van Hinsbergh, V. W., and Koolwijk, P. (2008). Endothelial sprouting and angiogenesis: Matrix metalloproteinases in the lead. *Cardiovasc Res.* 78 (2), 203–212. doi:10.1093/cvr/cvm102

Van Hove, I., Lemmens, K., Van de Velde, S., Verslegers, M., and Moons, L. (2012). Matrix metalloproteinase-3 in the central nervous system: A look on the bright side. *J. Neurochem.* 123 (2), 203–216. doi:10.1111/j.1471-4159.2012.07900.x

Vandenbroucke, R. E., and Libert, C. (2014). Is there new hope for therapeutic matrix metalloproteinase inhibition? *Nat. Rev. Drug Discov.* 13 (12), 904–927. doi:10.1038/nrd4390

Venter, W. D. F., Moorhouse, M., Sokhela, S., Fairlie, L., Mashabane, N., Masenya, M., et al. (2019). Dolutegravir plus two different prodrugs of tenofovir to treat HIV. *N. Engl. J. Med.* 381 (9), 803–815. doi:10.1056/NEJMoa1902824

Waitt, C., Orrell, C., Walimbwa, S., Singh, Y., Kintu, K., Simmons, B., et al. (2019). Safety and pharmacokinetics of dolutegravir in pregnant mothers with HIV infection and their neonates: A randomised trial (DolPHIN-1 study). *PLoS Med.* 16 (9), e1002895. doi:10.1371/journal.pmed.1002895

Williams, P. L., Yildirim, C., Chadwick, E. G., Van Dyke, R. B., Smith, R., Correia, K. F., et al. (2020). Association of maternal antiretroviral use with microcephaly in children who are HIV-exposed but uninfected (SMARTT): A prospective cohort study. *Lancet HIV* 7 (1), e49–e58. doi:10.1016/S2352-3018(19)30340-6

Wojcik-Stanaszek, L., Sypecka, J., Szymczak, P., Ziemka-Nalecz, M., Khrestchatisky, M., Rivera, S., et al. (2011). The potential role of metalloproteinases in neurogenesis in the gerbil hippocampus following global forebrain ischemia. *PLoS One* 6 (7), e22465. doi:10.1371/journal.pone.0022465

World Health Organization (WHO) (2016). *Consolidated guidelines on the use of antiretroviral drugs for treating and preventing HIV infection: Recommendations for a public health approach*. Second edition. Available at: https://www.who.int/hiv/pub/arv/chapter4.pdf?ua=1.

World Health Organization (WHO) (2018). *Dolutegravir (DTG) and the fixed dose combination (FDC) of tenofovir/lamivudine/dolutegravir (TLD): Briefing note*. Available at: http://www.who.int/hiv/pub/arv/DTG-TLD-arv_briefing_2018.pdf.

World Health Organization (WHO) (2019). *HIV drug resistance report 2019*.

World Health Organization (WHO) (2019). *Update of recommendations on first- and second-line antiretroviral regimens*. Available at: https://apps.who.int/iris/bitstream/handle/10665/325892/WHO-CDS-HIV-19.15-eng.pdf.

Yombi, J. C. (2018). Dolutegravir neuropsychiatric adverse events: Specific drug effect or class effect. *AIDS Rev.* 20 (1), 14–26.

Zash, R., Holmes, L., Diseko, M., Jacobson, D. L., Brummel, S., Mayondi, G., et al. (2019). Neural-tube defects and antiretroviral treatment regimens in Botswana. *N. Engl. J. Med.* 381 (9), 827–840. doi:10.1056/NEJMoa1905230

frontiers | Frontiers in Toxicology

TYPE Original Research
PUBLISHED 28 February 2023
DOI 10.3389/ftox.2023.1081753

OPEN ACCESS

EDITED BY
Iseult Lynch,
University of Birmingham,
United Kingdom

REVIEWED BY
Jonathan Shannahan,
Purdue University, United States
Marco P. Monopoli,
Royal College of Surgeons in Ireland,
Ireland

*CORRESPONDENCE
Kathryn R. Riley,
kriley1@swarthmore.edu

SPECIALTY SECTION
This article was submitted
to Nanotoxicology,
a section of the journal
Frontiers in Toxicology

RECEIVED 27 October 2022
ACCEPTED 17 February 2023
PUBLISHED 28 February 2023

CITATION
Park H-Y, Chung C, Eiken MK, Baumgartner KV, Fahy KM, Leung KQ, Bouzos E, Asuri P, Wheeler KE and Riley KR (2023), Silver nanoparticle interactions with glycated and non-glycated human serum albumin mediate toxicity.
Front.Toxicol. 5:1081753.
doi: 10.3389/ftox.2023.1081753

Silver nanoparticle interactions with glycated and non-glycated human serum albumin mediate toxicity

Hee-Yon Park[1], Christopher Chung[1], Madeline K. Eiken[2], Karl V. Baumgartner[2], Kira M. Fahy[2], Kaitlyn Q. Leung[2], Evangelia Bouzos[3], Prashanth Asuri[3], Korin E. Wheeler[2] and Kathryn R. Riley[1]*

[1]Department of Chemistry and Biochemistry, Swarthmore College, Swarthmore, PA, United States, [2]Department of Chemistry and Biochemistry, Santa Clara University, Santa Clara, CA, United States, [3]Department of Bioengineering, Santa Clara University, Santa Clara, CA, United States

Introduction: Biomolecules bind to and transform nanoparticles, mediating their fate in biological systems. Despite over a decade of research into the protein corona, the role of protein modifications in mediating their interaction with nanomaterials remains poorly understood. In this study, we evaluated how glycation of the most abundant blood protein, human serum albumin (HSA), influences the formation of the protein corona on 40 nm silver nanoparticles (AgNPs) and the toxicity of AgNPs to the HepG2 human liver cell line.

Methods: The effects of glycation on AgNP-HSA interactions were quantified using circular dichroism spectroscopy to monitor protein structural changes, dynamic light scattering to assess AgNP colloidal stability, zeta potential measurements to measure AgNP surface charge, and UV-vis spectroscopy and capillary electrophoresis (CE) to evaluate protein binding affinity and kinetics. The effect of the protein corona and HSA glycation on the toxicity of AgNPs to HepG2 cells was measured using the WST cell viability assay and AgNP dissolution was measured using linear sweep stripping voltammetry.

Results and Discussion: Results from UV-vis and CE analyses suggest that glycation of HSA had little impact on the formation of the AgNP protein corona with protein-AgNP association constants of ≈2x10^7 M^{-1} for both HSA and glycated HSA (gHSA). The formation of the protein corona itself (regardless of whether it was formed from HSA or glycated HSA) caused an approximate 2-fold decrease in cell viability compared to the no protein AgNP control. While the toxicity of AgNPs to cells is often attributed to dissolved Ag(I), dissolution studies showed that the protein coated AgNPs underwent less dissolution than the no protein control, suggesting that the protein corona facilitated a nanoparticle-specific mechanism of toxicity. Overall, this study highlights the importance of protein coronas in mediating AgNP interactions with HepG2 cells and the need for future work to discern how protein coronas and protein modifications (like glycation) may alter AgNP reactivity to cellular organisms.

KEYWORDS

nanotoxicity, protein corona, silver nanoparticles, glycation, post-translational modification (PMT)

1 Introduction

The medicinal use of nanoparticles has expanded in the last few decades, including diagnostic, imaging, and therapeutic applications. This growth is driven by the increasing control of the chemical and physical properties of nanoparticles (NPs). In parallel, a mechanistic understanding of cellular and organismal response to NPs has developed. At the molecular level, NPs entering a biological system adsorb a population of biomolecules, including proteins, lipids, sugars, or DNA. This biomolecular coating is dominated by an abundance of proteins, forming a protein corona (PC) (Lynch et al., 2007; Zhang et al., 2018; Griffith et al., 2020; Lima et al., 2020). The PC significantly alters NP physicochemical properties, including surface charge and agglomeration state, as well as biological fate, biodistribution, and toxicity (Walczyk et al., 2010; Fleischer and Payne, 2014; Caracciolo et al., 2017; Shannahan, 2017; Nierenberg et al., 2018; Lima et al., 2020). Although often cited as a barrier to development of nanomedicines, the PC can also be used to increase sensitivity and therapeutic efficacy of NPs (Caracciolo et al., 2017; Corbo et al., 2017; García Vence et al., 2020).

Formation of the PC is mediated by the properties of the NP, as well as the properties of the solution and population of biomolecules within the solution. Biochemical features of the latter may vary across populations and individuals, depending upon physiological conditions and disease states. There is also significant evidence of spatiotemporal changes to the composition of the corona as biomolecules undergo dynamic association and dissociation with the NP surface and with each other over time and as the NP is transported through a biological organism (Cai et al., 2022; Cox et al., 2018; Dell'Orco et al., 2010; Weiss et al., 2019). Thus, PCs formed in serum, around otherwise identical NPs, vary significantly depending upon whether a patient is pregnant, has a cold, or has diabetes, among other medical conditions (Hajipour et al., 2014; Corbo et al., 2017; García Vence et al., 2020; Ju et al., 2020). This personalized PC, in turn, not only dictates the abundance and populations of proteins in the corona, but also results in variations in the zeta-potential of the protein coated NP and its interaction with cells (Hajipour et al., 2014; Ju et al., 2020). Therefore, the personalized PC can be used to extrapolate and identify biomarkers for disease, while serving to improve the safety and efficacy of nanomedicines.

Among the biophysical features of proteins that change across individuals are post-translational modifications (PTMs). Despite the abundance and significance of PTMs, their role at the nano-bio interface remains relatively unexplored. Glycation and glycosylation are among the most abundant PTMs. Glycosylation, which refers to the enzyme-mediated addition of glycans, plays a variety of structural and functional roles—from molecular recognition and cellular signaling to protein trafficking and enzymatic regulation (Varki and Gagneux, 2015). Glycation, on the other hand, refers to the non-enzymatic addition of monosaccharides to proteins. Changes in glycosylation and glycation profiles are associated with a variety of diseases, including cancer and diabetes (Varki and Gagneux, 2015). For example, HbA1c, a common indicator test for diabetes, examines glucose bound to hemoglobin due to glycation and serves as an indicator of long-term blood glucose levels. In parallel, the glycation of another common blood protein, human serum albumin (HSA), can be used similarly. Interestingly, glycation contributes to changes in HSA structure and function, depending on the nature and amount of glycation (Qiu et al., 2021).

While impacts of protein glycation have not been specifically interrogated within PC studies, a few studies have assessed the role of glycosylation on PC formation and NP cellular interactions. Such studies are often motivated by the understanding that glycosylation can mediate cellular uptake of drugs (Cai et al., 2018; Ghazaryan et al., 2019). In the context of PC studies, glycosylation alters the population of proteins in the PC and alters adhesion of NPs to cell membranes (Wan et al., 2015; Ghazaryan et al., 2019; Clemente et al., 2022). More recently, the PC was used to identify enrichment of glycoproteins and identify disease biomarkers (Trinh et al., 2022). In a more focused study of just one commonly glycosylated blood protein, transferrin, significant variations in binding strength were observed with glycosylation, as well as protein structural changes upon interaction with gold NPs (Barbir et al., 2021). With an understanding of the impact of glycans on NP interactions and PC formation, the safety and efficacy of NP-enabled drugs and diagnostics will increase, enabling precision medicine and personalized medicines (Hajipour et al., 2014; Corbo et al., 2017; García Vence et al., 2020).

Due to their antimicrobial properties, silver nanoparticles (AgNPs) are used in a variety of medical conditions, including bandages for long-term wound healing for diabetic wounds (Choudhury et al., 2020). In disease states such as poorly managed diabetes, high blood sugar drives glycation of common blood proteins and may influence PC formation and AgNP behavior. Thus, we aimed to assess the role of glycation on the interaction of the most abundant blood protein, HSA, with AgNPs, and evaluate subsequent impacts on cellular toxicity. In our study, we chose 40 nm AgNPs, which is within the size range of AgNP sizes commonly used in wound dressings (Sussman et al., 2015; Paladini and Pollini, 2019; Krishnan et al., 2020). HSA is glycated under a variety of conditions (Varki and Gagneux, 2017) and has been consistently identified as a component of the AgNP-PC formed from human serum and plasma (del Pilar Chantada-Vázquez et al., 2019; Gorshkov et al., 2019; Lai et al., 2017; Shannahan, 2017). We hypothesized that glycation of HSA would alter interactions with AgNPs, due to changes in the accessible functional groups on HSA, as well as other changes in structure upon glycation. In turn, we also speculated that these structural changes would alter HSA-coated AgNP cellular impacts, as glycation of HSA been shown to alter absorption, distribution, efficacy and excretion of other drugs (Qiu et al., 2021). We expand upon previous studies of HSA and AgNP interactions to first evaluate the role of HSA glycation in AgNP and HSA structural stability and biophysical properties, including AgNP agglomeration, oxidation, and charge state. To evaluate the impacts of AgNPs on protein interactions and structure, binding affinities and protein structures are also compared. Second, we place these biophysical results in the context of downstream impacts by monitoring the toxicity of HSA and gHSA coated AgNPs in a live human liver cell line. Finally, we evaluate the effect of the HSA and gHSA PCs on AgNP dissolution as a first step towards understanding the mechanism by which PCs alter AgNP toxicity.

2 Materials and methods

2.1 Materials

Sodium citrate monobasic, sodium chloride, Trizma base, glycine, hydrochloric acid, 70% nitric acid, HSA, and glycated HSA (gHSA) were from Sigma-Aldrich (St. Louis, MO). The degree of glycation of gHSA was 3 mol hexose (as fructosamine) per mol albumin and the purity was 94% according to the manufacturer's certificate of analysis. BioPure citrate stabilized AgNPs were purchased from nanoComposix (San Diego, CA). AgNPs had a nominal diameter of 40 nm and were supplied at a concentration of 4.8 nM in 2 mM citrate solution.

Unless otherwise noted, all solutions were prepared in Millipore water (18.2 MΩ·cm at 25°C) and all samples were prepared in a buffer consisting of 5 mM citrate—5 mM NaCl buffer at pH 6.5 (herein, citrate buffer). The pH of the buffer was adjusted through dropwise addition of 0.1 M and 1.0 M NaOH. Stock solutions of HSA and gHSA were prepared to a concentration of 5 μM in Millipore water. Stocks were aliquoted and frozen at −20°C for later use.

Human hepatoma (HepG2) cells were obtained from ATCC (Manassas, VA); Dulbecco's modified Eagle medium (DMEM) from Mediatech (Manassas, VA); fetal bovine serum and penicillin—streptomycin from Invitrogen (Carlsbad, CA); sodium pyruvate and MEM non-essential amino acids from Life Technologies (Carlsbad, CA); trypsin/EDTA from CellGro (Manassas, VA); and WST cell proliferation assay kit from Dojindo Molecular Technologies (Rockville, MD).

2.2 Preparation of AgNPs-HSA and AgNPs-gHSA

The various techniques used across this study have different sample concentration requirements, so the concentration of AgNPs, HSA, and gHSA were varied to improve the signal-to-noise for each experiment. Specifically, for dynamic light scattering (DLS), zeta potential, UV-vis spectroscopy, and dissolution studies the concentration ratio was maintained as approximately 7×10^4:1 protein:AgNPs, which was achieved by incubating 24 pM. AgNPs with 1.5 μM HSA or gHSA. For cell viability studies the concentration ratio was also approximately 7×10^4:1 protein:AgNPs, which was achieved by incubating 10 pM. AgNPs with 0.70 μM protein or by incubating 100 pM. AgNPs with 7.0 μM protein. Langmuir adsorption isotherms were performed using a concentration ratio of 2×10^4:1 protein:AgNPs, which was achieved by incubating 24 pM. AgNPs with varying concentrations of protein (25–500 nM). The decrease in the protein:AgNP ratio was necessary to achieve optimal binding conditions for quantitative analysis. For CE, the AgNP concentration was increased to improve detection sensitivity while the protein concentration was decreased to maintain the separation efficiency, resulting in a lower molar ratio than used in the other experiments. CE studies were performed using a concentration ratio of 6×10^2:1 protein:AgNPs, which was achieved by incubating 24 pM. AgNPs with varying concentrations of protein (50–150 nM). Finally, for circular dichroism (CD) studies, the protein concentration was increased to improve detection sensitivity while the AgNP concentration was decreased to minimize interference due to light scattering from the NPs, which also resulted in a lower molar ratio than used in the other experiments. CD studies were performed using a concentration ratio of 3×10^2:1 protein:AgNPs, which was achieved by incubating 3.0 nM AgNPs with 0.94 μM protein.

2.3 AgNP characterization

AgNPs were characterized using dynamic light scattering (DLS) to measure the hydrodynamic diameter, polydispersity index (PDI) and zeta potential. Measurements were recorded with a Malvern Zetasizer Nano-ZS instrument (Malvern, PA). All samples were prepared with a citrate buffer that was twice filtered with a 0.2 μm nylon syringe filter. Triplicate samples of AgNPs were prepared to a final concentration of 24 pM and contained 0 or 1.5 μM HSA or gHSA. Samples were incubated in the dark at room temperature for 24 or 72 h prior to analysis. DLS measurements were recorded using 173° backscatter mode after temperature equilibration for 2 min at 25°C. For each replicate sample, 11 sub-runs were recorded per measurement and 5 measurements were recorded and averaged. Reported values represent the average and standard deviation of three preparative replicates of AgNPs, AgNPs-HSA, and AgNPs-gHSA. Zeta potential measurements were recorded in the same way, but the number of sub-runs per measurement was set to automatic and constrained between 10–100. A Pd dip cell was used to measure zeta potential and values were determined using the Smoluchowski equation.

2.4 UV-vis spectroscopy

UV-vis experiments were performed using a Cary UV-vis spectrophotometer (Agilent Technologies, Inc.). AgNPs were prepared to a final concentration of 24 pM. in citrate buffer and were titrated with HSA or gHSA in the concentration range 0–500 nM. All samples were prepared in triplicate and incubated for 24 h in the dark at room temperature. All samples were analyzed in a semi-micro quartz cuvette with a 1 cm pathlength. Absorbance spectra were recorded from 400—450 nm at 60 nm·min^{-1}. The shift in the localized surface plasmon resonance (LSPR) band was used to determine the association constant, K_a, for the formation of the AgNP-protein complex according to (Boulos et al., 2013; Dennison et al., 2017; Boehmler et al., 2020):

$$\frac{\Delta\lambda}{\Delta\lambda_{max}} = \frac{K_a C_p}{1 + K_a C_p} \quad (1)$$

where $\Delta\lambda$ is the shift in the LSPR band relative to the sample without protein, $\Delta\lambda_{max}$ is the maximum shift in the LSPR band, and C_p is the protein concentration. Qualitative absorbance spectra of AgNPs were also recorded using the same concentration ratio of protein: AgNPs used in other studies. Specifically, 24 pM. AgNPs were incubated for 24 h in the dark at room temperature in buffer alone or in the presence of 1.5 μM HSA or gHSA. Absorbance spectra were recorded from 350 to 500 nm using a scan rate of 300 nm·min^{-1}.

2.5 Capillary electrophoresis (CE)

CE was carried out on a P/ACE MDQ Plus capillary electrophoresis system from AB SCIEX. An uncoated fused silica capillary was used with an inner diameter of 50 μm. The total length of the capillary was 60.2 cm and the length to the detector was 50.0 cm. The separation buffer consisted of 5 mM Tris—500 mM glycine with a pH of 7.8. Each day the capillary was flushed successively for 10 min with Millipore water, 10 min with 0.1 M NaOH, 10 min with Millipore water, and 20 min with separation buffer. Between each run, the capillary was flushed for 1 min with Millipore water and 2 min with separation buffer. The separation buffer and the solutions used for rinsing the capillary were filtered with a 0.2 μm nylon syringe filter prior to use. Triplicate samples of AgNPs were prepared to a final concentration of 240 pM. in the separation buffer and contained 0, 50, 100, or 150 nM HSA or gHSA. All samples were incubated in the dark at room temperature for at least 30 min prior to analysis. Samples were injected hydrodynamically at 4 psi for 5 s (≈35 nL injection volume) and a 25 kV separation voltage was applied (applied field ≈ 415 V/cm). Each replicate sample was subjected to triplicate CE analysis to obtain reliable parameters for quantitative analysis, as described below.

Non-equilibrium capillary electrophoresis of equilibrium mixtures (NECEEM) was used to characterize AgNP-protein complex formation (Berezovski and Krylov, 2002; Berezovski et al., 2003; Krylov and Berezovski, 2003; Okhonin et al., 2004; Riley et al., 2018). In accordance with NECEEM theory, electropherograms were integrated to determine the areas under the unbound AgNP peak (A_1), the AgNP-protein complex peak (A_2), and in the region of dissociation (A_3; Supplementary Figure S3). These peak areas were used to calculate the ratio of unbound to bound AgNPs, according to:

$$R = \frac{A_1}{A_2 + A_3} \tag{2}$$

Then, using the calculated value of R and the initial concentrations of protein and AgNPs, $[P]_0$ and $[AgNPs]_0$, respectively, the dissociation constant was calculated, according to:

$$K_d = \frac{[P]_0 (1 + R) - [AgNPs]_0}{1 + \frac{1}{R}} \tag{3}$$

To determine the rate constant for AgNP-protein complex dissociation, k_{off}, CE electropherograms were fit in region A_3 according to:

$$I_t = I_{t_0} e^{\left(k_{off}\left(\frac{t_{AgNP-P}}{t_{AgNP} - t_{AgNP-P}}\right)(t - t_0)\right)} \tag{4}$$

where I_t is the absorbance intensity at some point in time t and I_{t0} is the intensity of the absorbance signal at time t_0. Time t_0 represents the beginning of the exponential decay between the unbound AgNP peak at time t_{AgNP} and the AgNP-protein complex at time $t_{AgNP\text{-}P}$ (Supplementary Figure S3). Using the calculated values of K_d and k_{off}, the rate constant for AgNP-protein complex association, k_{on}, was calculated according to:

$$k_{on} = \frac{k_{off}}{K_d} \tag{5}$$

2.6 Circular dichroism (CD) spectroscopy

Samples to be analyzed by CD were prepared by diluting HSA or gHSA to a concentration of 0.94 μM in 20 mM sodium phosphate buffer at pH 7.4. Samples were analyzed in a cylindrical quartz cuvette with a 1 mm pathlength and analyzed with an Olis Rapid-Scanning monochromator. A subsequent scan was taken after the addition of AgNPs to a final concentration of 3.0 nM and for a total sample volume of 280 μL. Measurements were recorded in the wavelength range 185–260 nm and the number of increments was set to 150. Consistent with previous studies of this kind (Fleischer and Payne, 2014), spectra were acquired in millidegrees (θ_{obs}) and converted to mean residue ellipticity ($[\theta]$), according to:

$$[\theta] = \frac{MW\ [\theta]_{obs}}{10\, l\, C\, n} \tag{6}$$

The mean residue ellipticity (units of degrees $cm^2\ dmol^{-1}$) is a function of the observed signal in millidegrees, the average molecular weight of the protein (MW), path length (l in cm), protein concentration (C in g/L), and the total number of amino acids (n). The % α-helicity of the protein was determined according to (Adler et al., 1973):

$$\%\ \alpha\ helicity = \frac{-[\theta]_{MRE} - 4000}{3300 - 4000} \tag{7}$$

The percent α-helicity of a protein is a function of the mean residue ellipticity at 208 nm ($[\theta_{MRE}]$) minus the contribution from the β-form and random coil conformations at 208 nm (4000). The observed value is compared to the mean residue ellipticity of a pure α-helix protein (33000).

2.7 Cell culture and WST assay

HepG2 cells were maintained and grown in 100 mm tissue culture dishes (Greiner, Bio-One, Monroe, CA, United States) using DMEM supplemented with 10% fetal bovine serum, sodium pyruvate, MEM non-essential amino acids, and 1% penicillin-streptomycin, at 37°C in a 5% CO_2 humidified environment. The cells were grown to 70%–80% confluence (in approximately 7–10 days) and passaged using 0.25% trypsin/EDTA. For cell viability assays, cells (15,000 cells per well) were seeded in 96-well flat bottom plates and allowed to proliferate for 48 h. Cells were then washed with culture media alone (no AgNP or protein control), with culture media containing 0.70 or 7.0 μM HSA or gHSA (no AgNP control), or with culture media containing 10 pM or 100 pM of uncoated or protein-coated AgNPs (200 μL total volume per well). All samples were prepared in triplicate. Protein-coated AgNPs for the cell viability assays were prepared by reacting 100 pM AgNPs with 7.0 μM HSA or gHSA or 10 pM AgNPs with 0.7 μM HSA or gHSA for 10 min in DMEM. Control cells and cells exposed to the AgNP preparations were incubated for either 24 h or 72 h at 37°C in a humidified atmosphere containing 5% CO_2. At collection, the cells were washed with media to remove the NPs and eliminate any interference due to the NPs.

Cell viability was then measured using the commercially available WST assay according to the manufacturer's instructions.

WST solution (20 µL) was added to cells at a 1:10 dilution in DMEM (200 µL total volume per well), followed by a 2-h incubation period at 37°C in a humidified atmosphere containing 5% CO_2. Absorbance was measured at 570 nm using a Tecan Infinite 200 PRO plate reader (Tecan, Switzerland). Background absorbance due to NPs was recorded using no cell controls for all the NP preparations and subtracted from the absorbance values of the experimental samples. Cell viabilities (percent) were thereafter calculated relative to controls not treated with AgNPs or proteins.

2.8 Linear sweep stripping voltammetry (LSSV)

LSSV was carried out as previously reported (Hui et al., 2019; Boehmler et al., 2020). Briefly, a three-electrode setup consisting of a glassy carbon working electrode, Ag/AgCl reference electrode, and Pt wire counter electrode was used to carry out the analysis. Measurements were recorded using a BASi Epsilon Eclipse potentiostat and C-3 Cell Stand from BioAnalytical Systems, Inc., (West Lafayette, IN). All solutions were sparged with N_2 (*g*) for 10 min and had a final dissolved oxygen concentration of approximate 8.0 mg·L^{-1}. Each day, the working electrode was polished with 0.05 µm alumina polish and conditioned using 200 cycles of cyclic voltammetry from −0.5 to 0.35 V at 0.3 V·s^{-1}. Between experiments, all electrodes were rinsed thoroughly with Millipore water, while the working electrode was placed in a 35% nitric acid solution for 30 s, rinsed thoroughly with Millipore water, and sonicated in Millipore water for 30 s. Stripping voltammetry was carried out by deposition at −0.5 V for 30 s with stirring, followed by a 5 s quiet time, and a linear sweep from −0.5 to 0.35 V at 0.1 V·s^{-1}. A same-day matrix-matched calibration curve was prepared with Ag(I) standards in the concentration range 0–240 µg·L^{-1}.

The initial dissolution rate of AgNPs, AgNPs-HSA, and AgNPs-gHSA was measured by placing citrate buffer and the appropriate volume of protein (final concentration of 300 nM) into the electrochemical cell and sparging for 10 min. Then, the appropriate volume of AgNPs was added so that the final concentration was 4.7 pM (protein:AgNP ratio of ≈7 × 10^4:1) and LSSV was carried out every 5 min for 2 h. The experiment was repeated in triplicate and the resulting dissolution curves (plots of $[Ag(I)]_{dissolved}$ vs. time) were used to determine the dissolution rate constant, $k_{dissolution}$, according to:

$$ln\left(1 - \frac{[Ag(I)]_t}{[AgNP]_0}\right) = -k_{dissolution}t \quad (8)$$

The percentage of dissolved silver, $\%AgNPs_{dissolved}$, was determined by normalizing the $[Ag(I)]_{dissolved}$ measured at the end of the dissolution kinetics experiment (t = 2 h) to the initial silver concentration placed into solution $[Ag]_0$, according to:

$$\%\, AgNPs_{dissolved} = \frac{[Ag(I)]_{dissolved,t=2h}}{[Ag]_0} \times 100 \quad (9)$$

The dissolution of AgNPs was also monitored after 24 and 72 h incubation in buffer alone or buffer containing protein. Six samples of AgNPs, AgNPs-HSA, and AgNPs-gHSA were prepared in citrate buffer with final concentrations of 24 pM. AgNPs and 1.5 µM protein (protein:AgNP ratio of ≈7 × 10^4:1) and incubated in the dark at room temperature. After 24 h, three replicates of each sample were analyzed using LSSV to determine the percentage of dissolved Ag(I) using same-day matrix matched calibration curves. After 72 h from the initial exposure, the remaining three replicates of each sample were analyzed in the same manner.

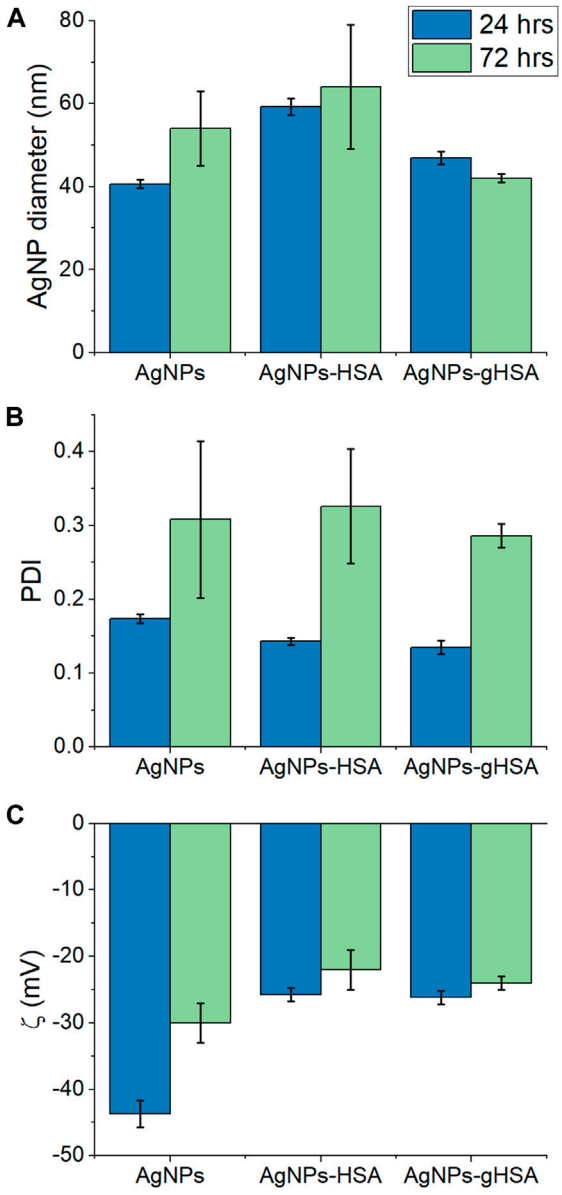

FIGURE 1
(A) Hydrodynamic diameter **(B)** PDI, and **(C)** zeta potential of AgNPs after 24 and 72 h incubation in buffer alone or buffer containing HSA or gHSA. AgNPs were prepared to a final concentration of 24 pM and the proteins to a final concentration of 1.5 µM. All solutions were prepared in 5 mM citrate—5 mM NaCl buffer (pH 6.5).

3 Results

3.1 Characterization of AgNP-protein complex formation

The formation of AgNP-protein complexes was confirmed qualitatively by measuring the hydrodynamic diameter, PDI, and zeta potential of AgNPs alone, in the presence of HSA, or in the presence of gHSA. Samples were analyzed at time points of 24 and 72 h following incubation to assess the stability of the AgNPs over time. After 24 h, an increase in the hydrodynamic diameter of AgNPs was observed in the presence of both HSA and gHSA relative to the no protein control (Figure 1A; Supplementary Figure S1; Supplementary Table S1). However, the magnitude of this increase differed between the two proteins, with the addition of HSA resulting in a larger increase in AgNP diameter (≈20 nm) and the addition of gHSA resulting in a more modest increase (≈7 nm). Differences in the thickness of the HSA and gHSA PCs formed on the AgNP surface could be a result of differences in the protein structure and/or orientation on the surface (*vide infra*). After 72 h, an increase in the diameter of AgNPs was observed suggesting slight aggregation of the particles over time. No significant differences were noted for the protein-coated AgNPs after 72 h, suggesting that the coronas was relatively stable and prevented significant aggregation of the AgNPs (Figure 1A; Supplementary Figure S1; Supplementary Table S1).

After 24 h incubation, the increase in AgNP diameter upon addition of HSA or gHSA was accompanied by either no change or a slight decrease in the PDI, providing further evidence that the formation of the AgNP-PCs provided some steric stabilization of the colloidal suspension (Figure 1B; Supplementary Table S1). Based on the decrease in PDI values, the degree of steric stabilization conferred by the proteins was more significant for gHSA than for HSA (Supplementary Table S1). After 72 h, the PDI value for all AgNPs increased, suggesting changes in the homogeneity of the samples over time and the potential for particle-particle or protein-protein aggregation. The formation of the AgNP-protein complex was further demonstrated by a decrease in the AgNP zeta potential (toward more positive potential) after 24 h incubation with HSA or gHSA (Figure 1C; Supplementary Table S1). After 72 h incubation, the zeta potential significantly decreased for the sample of AgNPs alone, further supporting the likelihood that the uncoated AgNPs had begun to aggregate. The zeta potentials for the protein-coated AgNPs showed only a subtle decrease in magnitude, further supporting the stability conferred by the protein coating. Overall, only subtle differences were observed between the AgNP-HSA and AgNP-gHSA coronas and more significant changes were observed between uncoated and protein-coated AgNPs.

The formation of AgNP-protein complexes was also confirmed quantitatively using UV-vis spectroscopy and CE to measure association and rate constants for complex formation. The 40 nm AgNPs exhibited a prominent LSPR band at approximately 420 nm that shifted to longer wavelength in the presence of HSA and gHSA (Supplementary Figure S2). Langmuir adsorption isotherms were constructed to determine the association constant, K_a, for AgNP-protein complex formation (Figure 2). The K_a values for HSA and gHSA were 2.3 (±0.2) × 10^7 M^{-1} and 2.4 (±0.1) × 10^7 M^{-1} ($n = 3$, $R^2 > 0.97$), respectively, suggesting that both proteins had similar affinity for the AgNP surface (Table 1).

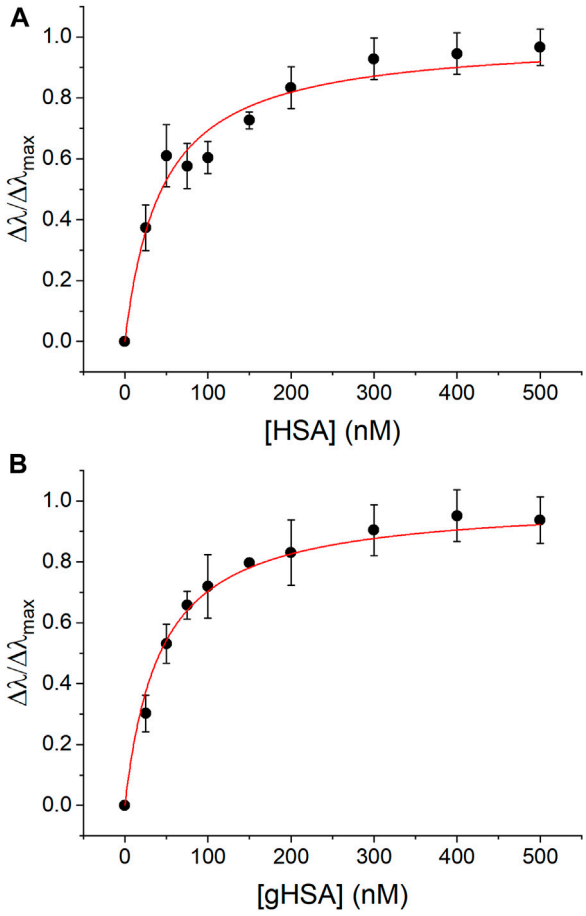

FIGURE 2
UV-vis Langmuir adsorption isotherms for complex formation between AgNPs and **(A)** HSA and **(B)** gHSA. The experimental data was fit using Eq. 1 ($R^2 > 0.97$). AgNPs were prepared to a concentration of 24 pM and the protein concentrations were as indicated. All solutions were prepared in 5 mM citrate—5 mM NaCl buffer (pH 6.5).

The formation of AgNP-protein complexes was further quantified using CE and NECEEM analysis. While NECEEM theory was initially developed to measure DNA-protein complexes, it has recently been demonstrated as an effective tool to measure the NP-PC (Riley et al., 2018). According to NECEEM theory, injection of the equilibrium mixture (containing unbound AgNPs, unbound protein, and AgNP-protein complexes) onto the capillary and application of the separation voltage will lead to a non-equilibrium condition, whereby each component of the mixture will migrate according to their unique electrophoretic mobilities. As a result, when the AgNP-protein complexes dissociate and the unbound AgNPs and protein migrate away from one another in the capillary, they are no longer proximate and cannot reestablish the AgNP-protein complex (i.e., a non-equilibrium condition) (Berezovski and Krylov, 2002; Berezovski et al., 2003; Krylov and Berezovski, 2003; Okhonin et al., 2004; Riley et al., 2018). By directly monitoring the dissociation of AgNP-protein complexes, both the dissociation constant (K_d) and the on/off rate constants (k_{on}/k_{off}) can be determined in a single experimental run (Berezovski and Krylov, 2002).

TABLE 1 Characterization of AgNP-HSA and AgNP-gHSA complex formation.

Protein	K_a (×10^7 M^{-1})		k_{off}[b] (s^{-1})	k_{on}[b] (x10^5 M^{-1}·s^{-1})
	UV-vis[a]	CE[b]		
HSA	2.3 ± 0.2	2.5 ± 1.0	0.041 ± 0.008	1.1 ± 0.5
gHSA	2.4 ± 0.1	2.2 ± 1.1	0.062 ± 0.024	1.3 ± 0.8

[a]Experimental conditions were as reported in Figure 2 and values were calculated using Eq. 1. Values are the average and standard deviation of 3 trials.
[b]Experimental conditions were as reported in Figure 3 and values were calculated using Eqs 2–5. Values are the average and standard deviation of 9 trials (three replicate experiments performed at each of three protein concentrations).

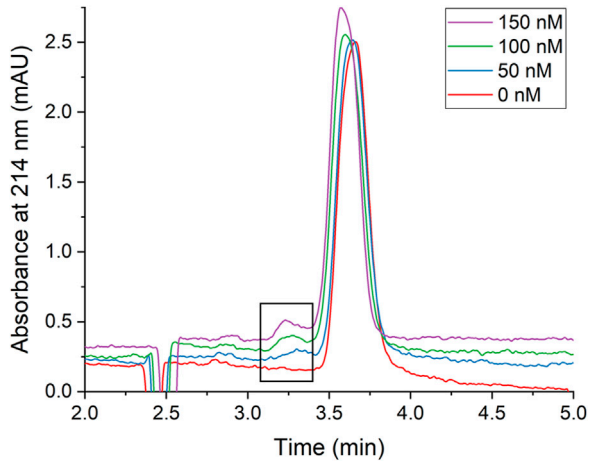

FIGURE 3
Representative CE electropherograms of AgNPs in the presence of increasing concentrations of HSA. The boxed region highlights the AgNP-HSA complex peak which increases with increasing [HSA]. Electropherograms are vertically offset for clarity. AgNPs were prepared to a concentration of 240 pM and the protein concentrations were as indicated. All solutions were prepared in 5 mM Tris—500 mM Gly buffer (pH 7.8).

In this work, only the AgNPs generated an absorbance signal in the electropherogram because the concentration and volume of protein injected onto the capillary was too low to be detected. In the absence of protein, a single peak at approximately 3.7 min was observed and attributed to the AgNPs (Figure 3, red trace). With the addition of HSA, a new peak was observed at approximately 3.3 min and was attributed to the AgNP-HSA complex due to an observed increase in absorbance intensity of the peak with increasing protein concentration (Figure 3). Electropherograms for NECEEM analysis of AgNPs-gHSA complexes exhibited similar features (Supplementary Figure S4). By applying quantitative NECEEM analysis (Eqs 2, 3; Supplementary Figure S3), the K_d values of AgNP-HSA and AgNP-gHSA complexes were obtained and then converted to K_a values for ease of comparison. The values obtained by NECEEM were consistent with those obtained using UV-vis spectroscopy within error, confirming that HSA and gHSA have similar affinity for the AgNP surface (Table 1). NECEEM analysis of the dissociation kinetics was also carried out (Eqs 4, 5; Supplementary Figure S3), and likewise, no significant differences were noted between the k_{on} and k_{off} values determined for the AgNP-HSA and AgNP-gHSA complexes. Generally, the values obtained suggest fast adsorption and slow desorption of the proteins from the AgNP surface (Table 1).

Finally, changes to protein structure upon PC formation were probed using CD spectroscopy (Figure 4A; Table 2). A comparison of the two proteins in the absence of AgNPs revealed slight differences in the protein secondary structure, with gHSA exhibiting slightly greater α-helicity than HSA (Figure 4A; Table 2). Others have noted changes in HSA structure upon glycation, where the degree and exact nature of those changes depend upon the type of monosaccharide, concentration, and length of exposure (Nakajou et al., 2003; Qiu et al., 2021). Upon the addition of AgNPs to each protein solution, the α-helical character of the protein decreased, as measured by changes in the ellipticity at 208 and 220 nm and the calculated % α-helicity (Figure 4B; Table 2). While CD suffers from low sensitivity and an inability to distinguish free from surface-adsorbed protein, it can provide qualitative and semi-quantitative analysis of changes in protein secondary structure, which may be attributed to the formation of NP-protein complexes. Generally, changes in protein ellipticity can be taken as further evidence of the formation of the NP-PC. Our results demonstrate that the reduction of α-helicity upon interaction with AgNPs was slightly larger for HSA than for gHSA, which suggests possible differences in the surface interaction of HSA and gHSA due to protein glycation.

3.2 Cell viability studies

Studying the effect of protein coating on cell viability is important because NPs used in the body will inevitably be coated with a PC when they come in contact with biological fluids (e.g., blood) or culture medium. Such a protein coating has been shown to influence targeting abilities, cellular uptake, and immunotoxicity of NPs (Monteiro-Riviere et al., 2013; Nierenberg et al., 2018). Thus, we hypothesized that the HSA and gHSA PCs would each alter cell toxicity, but that there would be no significant differences between their impact since biophysical analyses suggested that the coronas had remarkably similar properties under the chosen experimental conditions. To evaluate this hypothesis, we investigated the role of protein coatings on the toxicity of AgNPs to human cells. We chose liver hepatocellular carcinoma (HepG2) cells as our cell model, as they are widely used in the literature to determine toxicity. The liver has also shown to be a target organ for several NPs, making liver cells biologically relevant for toxicity studies (Balasubramanian et al., 2010; Lankveld et al., 2010; Khosravi-Katuli et al., 2017; Wu and Tang, 2018).

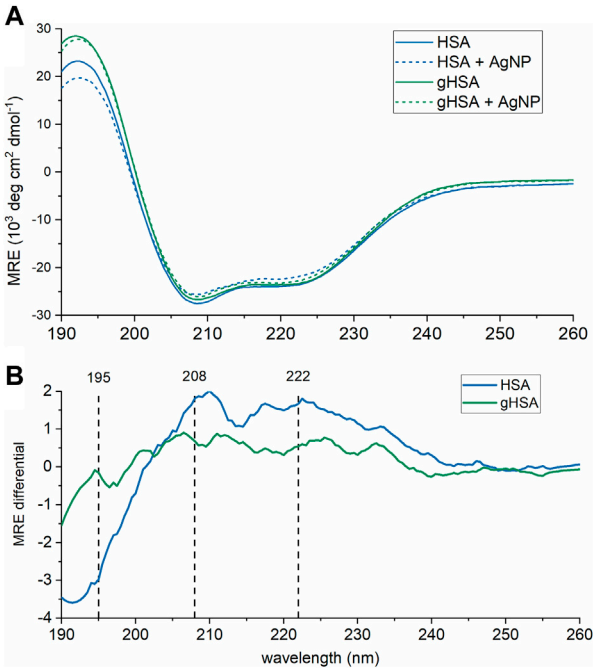

FIGURE 4
CD spectra of HSA and gHSA (blue and green, respectively) alone (solid lines) and with AgNPs (dashed). Spectra, in units of mean residue ellipticity (MRE), are the average of 3 consecutive scans. **(A)** Raw CD spectra. **(B)** CD difference spectra calculated by subtracting the spectrum of HSA (blue) or gHSA (green) from that in the presence of AgNPs. The black vertical lines correspond to the spectral peaks at 195, 208, and 222 nm. The protein concentration was 0.94 μM and the AgNP concentration was 3.0 nM. All solutions were prepared in 5 mM sodium phosphate buffer (pH 7.4).

TABLE 2 Percent α-helicity for HSA and gHSA alone and in the presence of AgNPs[a].

Sample	% α-helicity	
	Alone	With AgNPs
HSA	53	46
gHSA	67	64

[a]Percent α-helicity was calculated using Eqs 6, 7.

HepG2 cells were incubated with varying concentrations of AgNPs under three conditions: AgNPs exposed to HSA, gHSA, and no protein (uncoated AgNPs). Control studies included incubation of HepG2 cells in culture media alone or with culture media containing different concentrations of HSA or gHSA. After 24 or 72 h incubation, a WST assay was performed to evaluate cell viability. As expected, relative to cells incubated in cell culture media alone, no toxicity was observed for cells exposed to just HSA or gHSA with no AgNPs (Supplementary Table S2). The toxicity due to the addition of AgNPs was concentration dependent with higher levels of toxicity observed at higher AgNP concentrations. Interestingly, the results revealed increased toxicity for both HSA-coated and gHSA-coated AgNPs relative to uncoated AgNPs (Figure 5; Supplementary Table S3).

3.3 Towards a mechanistic understanding of protein mediated AgNP toxicity

As a first step towards investigating the mechanism by which the HSA and gHSA PCs decrease HepG2 cell viability, LSSV was used to measure AgNP dissolution in the absence and presence of both proteins. For all LSSV analyses, same-day matrix-matched calibration curves were obtained, which was important to account for any impact of the proteins on the electrochemical signal. All calibration curves had sub-micromolar LODs (typically around 0.10–0.30 μM) under all experimental conditions evaluated (Supplementary Tables S4, S5) suggesting that the protein did not unduly effect LSSV analyses.

First, the initial rate of dissolution was measured for AgNPs alone or in the presence of HSA or gHSA over the first 2 h following incubation. The dissolution rate constant, $k_{dissolution}$, of AgNPs alone was 1.6×10^{-4} min^{-1} indicating rapid dissolution of AgNPs after dilution in buffer (Supplementary Figure S5; Supplementary Table S4). In contrast, AgNPs added to buffer containing either HSA or gHSA exhibited slow dissolution and a nearly constant concentration of Ag(I) over the 2 h analysis period, so dissolution rate constants were unable to be measured (Supplementary Figure S5; Supplementary Table S4). At the conclusion of the 2 h AgNP dissolution experiment, the faster dissolution kinetics of AgNPs in the no protein condition led to a 2-fold increase in the percentage of dissolved Ag(I) relative to AgNPs in the presence of HSA and gHSA (Supplementary Figure S5; Supplementary Table S4).

Analysis of AgNP dissolution behaviors was extended by measuring the percentage of dissolved Ag(I) after 24 and 72 h incubation in buffer alone, or in buffer containing HSA and gHSA. These time points were chosen to exactly mimic the conditions used for the cell viability assay. Under all experimental conditions a slight increase in the percentage of dissolved Ag(I) was observed after 72 h incubation relative to 24 h (Figure 6; Supplementary Table S5). This increase was most significant for the AgNPs incubated in buffer only, consistent with kinetic dissolution experiments that showed the AgNPs alone undergo much faster dissolution. Relative to the AgNPs alone, AgNPs incubated with HSA or gHSA exhibited a statistically significant decrease in the percentage of dissolved Ag(I) at both 24 and 72 h following incubation (Figure 6; Supplementary Table S5). Specifically, the dissolution of AgNPs in the presence of protein was ≈5-fold lower than the no protein control after 24 h and ≈6-fold lower after 72 h.

4 Discussion

Biophysical analyses demonstrated subtle differences in the HSA and gHSA PCs, including the thickness of the corona measured using DLS (Figure 1A) and changes in the protein secondary structure upon interaction with AgNPs measured using CD spectroscopy (Figure 4). Inherent differences in the chemical composition and secondary structure of HSA and gHSA due to glycation may alter the orientation of the proteins on the AgNP surface, which may contribute to the observed differences in the corona thickness in DLS analyses. In a previous study, the thickness of the PC formed on quantum dots varied between unmodified HSA

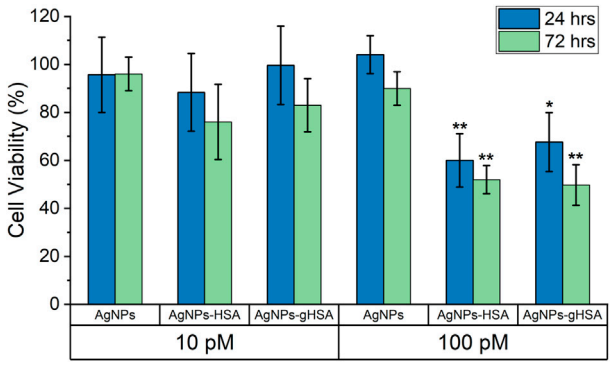

FIGURE 5
Percent cell viability of HepG2 cells, as determined by WST assay, after 24 and 72 h exposure to 10 pM and 100 pM AgNPs, AgNPs-HSA, or AgNPs-gHSA. Cell viability data was corrected by subtracting background absorbance due to AgNPs and normalized against HepG2 cells incubated in culture media alone (no protein and no AgNPs). Error bars represent the standard deviation of three samples and statistical significance was independently evaluated for each protein condition relative to the no protein control using a two-tailed *t*-test evaluated at the 95% (*) or 99% (**) confidence interval.

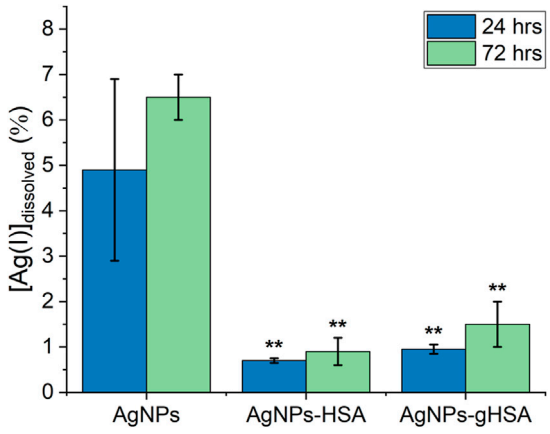

FIGURE 6
Percent dissolution of AgNPs after 24 and 72 h incubation in buffer alone or buffer containing HSA or gHSA. Dissolution was measured by LSSV and the percentage of dissolved Ag(I) was quantified using Eq. 9. AgNPs were prepared to a final concentration of 24 pM and the proteins to a final concentration of 1.5 μM. All solutions were prepared in 5 mM citrate—5 mM NaCl buffer (pH 6.5). Statistical significance was independently evaluated for each protein condition relative to the no protein control using a two-tailed *t*-test evaluated at the 99% (**) confidence interval.

and HSA modified either through succinylation or amination due to differences in protein orientation on the surface (Treuel et al., 2014). Further, the subtle increase in α-helicity upon glycation of HSA measured using CD spectroscopy has been previously observed and is presumed to be due to slight structural changes conferred by the glycation of specific amino acid residues (Coussons et al., 1997; Barzegar et al., 2007). Consistent with previous results, a decrease in α-helicity of HSA and gHSA upon interaction with AgNPs suggests slight unfolding of the protein as it adsorbs to the NP surface, presumably due to favorable interactions (e.g., hydrophobic) between specific regions of the protein and the NP surface (Shang et al., 2007; Bardhan et al., 2009; Pan et al., 2012; Fleischer and Payne, 2014). For example, lysine residues are commonly glycated in HSA (Anguizola et al., 2013), which can lead to changes in protein structure that cause further changes in NP-protein interactions. Our results demonstrate that the reduction of α-helicity upon interaction with AgNPs was slightly larger for HSA than for gHSA, which is consistent with previous studies of transferrin interactions with citrate-coated AgNPs (Barbir et al., 2021), and further suggests possible differences in the surface interaction of HSA and gHSA due to protein glycation.

Quantitative UV-vis and CE studies (Figures 2, 3) showed no distinguishable differences between the equilibrium and rate constants for the formation of AgNP-HSA and AgNP-gHSA complexes. AgNP-protein association constants (K_a values) obtained in this work are also similar to those reported in the literature for BSA and 40 nm citrate-stabilized AgNPs (Dasgupta et al., 2016; Boehmler et al., 2020). Ultimately, under our experimental conditions, biophysical characterization indicates no significant differences in the formation of the AgNP-HSA and AgNP-gHSA complexes, but distinct changes in AgNP physical properties upon corona formation compared to protein-free conditions. Specifically, the formation of the HSA and gHSA PCs resulted in increased colloidal stability of the AgNPs as evidenced by less significant changes in AgNP diameter and zeta potential over time (Figures 1A, C). The stabilization of AgNPs due to the formation of the PC is consistent with a previous study that showed that the analogous protein bovine serum albumin (BSA) can stabilize AgNPs even in solution conditions that promote AgNP aggregation (Levak et al., 2017). Our overall observations are also consistent with a previous study conducted with SiO_2 NPs, where only subtle changes in NP diameter, PDI, and zeta potential were observed between PCs with and without glycosylation, and more significant changes were observed between the NPs with and without protein (Wan et al., 2015).

The HSA and gHSA PCs also altered the reactivity of the AgNPs to HepG2 cells. Specifically, after 72 h exposure to protein-coated AgNPs, HepG2 cells showed an approximately 2-fold decrease in cell viability compared to uncoated AgNPs. These results indicate no observable differences in toxicity between AgNPs coated with HSA compared to gHSA, for the experimental conditions and endpoints evaluated herein, a conclusion consistent with the biophysical experiments. Notably, there are limited studies on the role of PC glycation in toxicity. For example, Wan et al. (2015) demonstrated increased cell membrane adhesion and uptake in macrophages upon removal of glycans from the human plasma PC on silica NPs. More recent studies with different NPs show that glycation can vary nanocarrier cellular uptake in different directions, depending on the protein (Ghazaryan et al., 2019). Given the differences across studies, including corona composition, NP types, and cell types, it is difficult to draw any meaningful connections. Further, both studies are limited to evaluation of the role of glycation in hard corona formation. Glycation of the PC may also influence soft corona formation and other toxicity related endpoints, which deserve further attention.

The observed increase in toxicity with a PC is consistent with a recent paper that shows an increase in toxicity for citrate-coated

AgNPs when coated with serum proteins (Barbalinardo et al., 2018). This is not a consistently reported finding, as other studies have demonstrated that the PC may decrease cellular uptake of AgNPs and their toxicity (Monteiro-Riviere et al., 2013; Shannahan et al., 2015). The observed differences in toxic responses may be due to myriad of factors, including nanoparticle size and concentration, exposure times, different cell types, and choice of toxicity assays (Sohaebuddin et al., 2010; Kroll et al., 2011). Additional studies are necessary to further evaluate the source(s) of the differences, as well as the role of PC on the response of AgNPs to human cells. The oxidative dissolution of AgNPs to release bioactive Ag(I) is the primary contributor to AgNP antimicrobial properties. Ag(I) dissolved from AgNPs can interfere with transport proteins and enzymes in the respiratory chain reaction, compromise the proton-motive force, and interfere with phosphate uptake (Schreurs and Rosenberg, 1982; Dibrov et al., 2002; Holt and Bard, 2005; Lok et al., 2006). However, there is strong evidence that AgNPs also contribute to toxicity (Navarro et al., 2008; Li et al., 2017), which can proceed through direct disruption of the cell membrane and/or the generation of reactive oxygen species (ROS), which disrupt protein structures and interfere with DNA replication (Sondi and Salopek-Sondi, 2004; Choi et al., 2008; Smetana et al., 2008; Monteiro-Riviere et al., 2013; Barbalinardo et al., 2018; Nierenberg et al., 2018). Thus, to elucidate whether the decreased cell viability observed for protein-coated AgNPs was due to protein-induced enhancement in the dissolved Ag(I) concentration we measured the dissolution of AgNPs in the absence and presence of HSA or gHSA. After 2 h incubation, the AgNP only control underwent 2-fold greater dissolution than the protein-coated AgNPs, which increased to a factor of 5-fold greater dissolution after 24 h and 6-fold greater dissolution after 72 h (Supplementary Figure S5; Figure 6). Other reports in the literature highlight the concentration-dependence of protein-mediated AgNP dissolution. At low protein concentrations, where the AgNP surface is unsaturated or there is only monolayer surface coverage, proteins can enhance dissolution through a nucleophilic mechanism (Martin et al., 2014; Liu et al., 2018; Boehmler et al., 2020). At higher protein concentrations (like the ones used in this study), where the AgNP surface is fully saturated and a stable corona is formed, the surface-bound proteins form a protective coating that inhibits dissolution (Martin et al., 2014; Tai et al., 2014; Shannahan et al., 2015; Liu et al., 2018). Taken together, the protein-coated AgNPs were more toxic to HepG2 cells compared to the no protein control, even as the dissolution of protein-coated AgNPs was decreased relative to the no protein control. These results suggest that a NP- and PC-specific mechanism rather than a dissolution mechanism is likely responsible for the increased toxicity measured for protein-coated AgNPs. In fact, since the completion of this work, a recent study in the literature showed the colocalization of 20 nm and 100 nm citrate-stabilized AgNPs and the mitochondria of HepG2 cells, leading to greater mitochondrial damage and apoptosis relative to exposure to Ag(I) alone (Wang et al., 2022). This supports our hypothesis that a NP-specific mechanism is responsible for the observed toxicity of AgNPs to HepG2 cells. The present study extends this work by demonstrating that the HSA and gHSA coronas potentiate AgNP toxicity.

Previously reported biophysical studies using model lipid membranes can provide insights to the mechanism of NP- and PC-specific toxicity of NPs to cells. Previous studies demonstrated that very small (<5 nm) AgNPs can be trapped within liposomes and increase the fluidity of model lipid bilayers (Park et al., 2005; Bothun, 2008). Similarly, another study showed that 40 nm AgNPs coated with HSA can lead to increased bilayer fluidity (Chen et al., 2012), while a separate study showed that the interaction of HSA-coated AgNPs with model membranes is strongly dependent on solution pH (Wang et al., 2016). Few studies have examined protein-mediated interactions between AgNPs and model membranes with the level of detail needed to elucidate a full mechanism. However, more sophisticated experimental techniques have been developed to investigate NP-membrane interactions with AuNPs and can serve as a model for future work with AgNPs. Using model lipid membranes, researchers showed that AuNPs caused membrane disruption through lipid extraction. This process was strongly influenced by the particle capping agents, with more positively charged particles leading to greater lipid extraction from the membrane (Olenick et al., 2018; Zhang et al., 2018). Another study demonstrated the complexity of nano-bio interactions, whereby the AuNP surface properties influenced the composition of the PC, and the corona, in turn, impacted the interactions of the AuNPs with model membranes (Melby et al., 2017). Further adding to this complexity is the possibility that AuNPs can form PCs through extraction of peripheral membrane proteins (Melby et al., 2018), and the likelihood that a combination of all of these processes (and those yet to be studied) contribute to toxicity mechanisms *in vivo*.

5 Conclusion

This study serves as a first step to interrogating the role of protein modification, like glycation, in mediating PC formation and AgNP toxicity. We have provided robust, qualitative and quantitative characterization of the AgNP-HSA and AgNP-gHSA PCs. We have further demonstrated that, under our experimental conditions, glycation of HSA does not significantly alter the formation of the AgNP-PC or its impact on AgNP dissolution and toxicity to HepG2 cells. Instead, we have shown that both HSA- and gHSA-coated AgNPs are more toxic to HepG2 cells than uncoated AgNPs, and that the mechanism of toxicity cannot be simply explained by AgNP dissolution. Indeed, we observe decreased AgNP dissolution upon formation of the HSA and gHSA coronas at the same time that we observe increased cell toxicity, suggesting a NP- and PC-induced mechanism of toxicity. While glycation of HSA did not appear to have a significant impact in our study, the incorporation of protein modifications into the study of the PC is ultimately an important first step toward understanding the complete AgNP biocorona that includes proteins, metabolites, and lipids (Chetwynd and Lynch, 2020). Our study further highlights the need for continued experimentation and development of biophysical and analytical methods to elucidate the mechanism of protein-mediated AgNP toxicity.

Data availability statement

The raw data supporting the conclusion of this article will be made available by the authors, without undue reservation.

Author contributions

H-YP—Writing and Experiments, including DLS, electrochemistry, and UV-vis; CC—Experiments, including UV-vis and CE; ME and KB—Writing and Experiments, including toxicity studies; KF and KL—Experiments, including UV-vis and CD; EB—Experiments, including toxicity studies; KW, PA, KR—Conceptualization, Methodology, Experiments, Writing, and editing.

Funding

This research was supported by the National Institutes of Health awarded to KW under award number R15ES025929.

Acknowledgments

KF, KB, and ME acknowledge the support of the Jean Dreyfus Lectureship for Undergraduate Institutions, the Hayes Scholar program, and the Clare Boothe Luce Scholar program, respectively.

Conflict of interest

The authors declare that the research was conducted in the absence of any commercial or financial relationships that could be construed as a potential conflict of interest.

Publisher's note

Supplementary material

The Supplementary Material for this article can be found online at: https://www.frontiersin.org/articles/10.3389/ftox.2023.1081753/full#supplementary-material

References

Adler, A. J., Greenfield, N. J., and Fasman, G. D. (1973). Circular dichroism and optical rotatory dispersion of proteins and polypeptides. *Methods Enzymol.* 27, 675–735. doi:10.1016/s0076-6879(73)27030-1

Anguizola, J., Matsuda, R., Barnaby, O. S., Joseph, K. S., Wa, C., DeBolt, E., et al. (2013). Review: Glycation of human serum albumin. *Clin. Chim. Acta Int. J. Clin. Chem.* 0, 64–76. doi:10.1016/j.cca.2013.07.013

Balasubramanian, S. K., Jittiwat, J., Manikandan, J., Ong, C.-N., Yu, L. E., and Ong, W.-Y. (2010). Biodistribution of gold nanoparticles and gene expression changes in the liver and spleen after intravenous administration in rats. *Biomaterials* 31, 2034–2042. doi:10.1016/j.biomaterials.2009.11.079

Barbalinardo, M., Caicci, F., Cavallini, M., and Gentili, D. (2018). Protein corona mediated uptake and cytotoxicity of silver nanoparticles in mouse embryonic fibroblast. *Small Weinh. Bergstr. Ger.* 14, e1801219. doi:10.1002/smll.201801219

Barbir, R., Jiménez, R. R., Martín-Rapún, R., Strasser, V., Domazet Jurašin, D., Dabelić, S., et al. (2021). Interaction of differently sized, shaped, and functionalized silver and gold nanoparticles with glycosylated versus nonglycosylated transferrin. *ACS Appl. Mat. Interfaces* 13, 27533–27547. doi:10.1021/acsami.1c04063

Bardhan, M., Mandal, G., and Ganguly, T. (2009). Steady state, time resolved, and circular dichroism spectroscopic studies to reveal the nature of interactions of zinc oxide nanoparticles with transport protein bovine serum albumin and to monitor the possible protein conformational changes. *J. Appl. Phys.* 106, 034701. doi:10.1063/1.3190483

Barzegar, A., Moosavi-Movahedi, A., Sattarahmady, N., Hosseinpour-Faizi, M., Aminbakhsh, M., Ahmad, F., et al. (2007). Spectroscopic studies of the effects of glycation of human serum albumin on L-trp binding. *Protein Pept. Lett.* 14, 13–18. doi:10.2174/092986607779117191

Berezovski, M., and Krylov, S. N. (2002). Nonequilibrium capillary electrophoresis of equilibrium mixtures – A single experiment reveals equilibrium and kinetic parameters of Protein–DNA interactions. *J. Am. Chem. Soc.* 124, 13674–13675. doi:10.1021/ja028212e

Berezovski, M., Nutiu, R., Li, Y., and Krylov, S. N. (2003). Affinity analysis of a Protein–Aptamer complex using nonequilibrium capillary electrophoresis of equilibrium mixtures. *Anal. Chem.* 75, 1382–1386. doi:10.1021/ac026214b

Boehmler, D. J., O'Dell, Z. J., Chung, C., and Riley, K. R. (2020). Bovine serum albumin enhances silver nanoparticle dissolution kinetics in a size- and concentration-dependent manner. *Langmuir* 36, 1053–1061. doi:10.1021/acs.langmuir.9b03251

Bothun, G. D. (2008). Hydrophobic silver nanoparticles trapped in lipid bilayers: Size distribution, bilayer phase behavior, and optical properties. *J. Nanobiotechnology* 6, 13. doi:10.1186/1477-3155-6-13

Boulos, S. P., Davis, T. A., Yang, J. A., Lohse, S. E., Alkilany, A. M., Holland, L. A., et al. (2013). Nanoparticle–protein interactions: A thermodynamic and kinetic study of the adsorption of bovine serum albumin to gold nanoparticle surfaces. *Langmuir* 29, 14984–14996. doi:10.1021/la402920f

Cai, L., Gu, Z., Zhong, J., Wen, D., Chen, G., He, L., et al. (2018). Advances in glycosylation-mediated cancer-targeted drug delivery. *Drug Discov. Today* 23, 1126–1138. doi:10.1016/j.drudis.2018.02.009

Cai, R., Ren, J., Guo, M., Wei, T., Liu, Y., Xie, C., et al. (2022). Dynamic intracellular exchange of nanomaterials' protein corona perturbs proteostasis and remodels cell metabolism. *Proc. Natl. Acad. Sci.* 119, e2200363119. doi:10.1073/pnas.2200363119

Caracciolo, G., Farokhzad, O. C., and Mahmoudi, M. (2017). Biological identity of nanoparticles *in vivo*: Clinical implications of the protein corona. *Trends Biotechnol.* 35, 257–264. doi:10.1016/j.tibtech.2016.08.011

Chen, R., Choudhary, P., Schurr, R. N., Bhattacharya, P., Brown, J. M., and Chun Ke, P. (2012). Interaction of lipid vesicle with silver nanoparticle-serum albumin protein corona. *Appl. Phys. Lett.* 100, 013703–137034. doi:10.1063/1.3672035

Chetwynd, A. J., and Lynch, I. (2020). The rise of the nanomaterial metabolite corona, and emergence of the complete corona. *Environ. Sci. Nano* 7, 1041–1060. doi:10.1039/C9EN00938H

Choi, O., Deng, K. K., Kim, N.-J., Ross, L., Surampalli, R. Y., and Hu, Z. (2008). The inhibitory effects of silver nanoparticles, silver ions, and silver chloride colloids on microbial growth. *Water Res.* 42, 3066–3074. doi:10.1016/j.watres.2008.02.021

Choudhury, H., Pandey, M., Lim, Y. Q., Low, C. Y., Lee, C. T., Marilyn, T. C. L., et al. (2020). Silver nanoparticles: Advanced and promising technology in diabetic wound therapy. *Mat. Sci. Eng. C* 112, 110925. doi:10.1016/j.msec.2020.110925

Clemente, E., Martinez-Moro, M., Trinh, D. N., Soliman, M. G., Spencer, D. I. R., Gardner, R. A., et al. (2022). Probing the glycans accessibility in the nanoparticle biomolecular corona. *J. Colloid Interface Sci.* 613, 563–574. doi:10.1016/j.jcis.2021.11.140

Corbo, C., Molinaro, R., Tabatabaei, M., Farokhzad, O. C., and Mahmoudi, M. (2017). Personalized protein corona on nanoparticles and its clinical implications. *Biomater. Sci.* 5, 378–387. doi:10.1039/c6bm00921b

Coussons, P. J., Jacoby, J., McKay, A., Kelly, S. M., Price, N. C., and Hunt, J. V. (1997). Glucose modification of human serum albumin: A structural study. *Free Radic. Biol. Med.* 22, 1217–1227. doi:10.1016/S0891-5849(96)00557-6

Cox, A., Andreozzi, P., Dal Magro, R., Fiordaliso, F., Corbelli, A., Talamini, L., et al. (2018). Evolution of nanoparticle protein corona across the blood–brain barrier. *ACS Nano* 12, 7292–7300. doi:10.1021/acsnano.8b03500

Dasgupta, N., Ranjan, S., Patra, D., Srivastava, P., Kumar, A., and Ramalingam, C. (2016). Bovine serum albumin interacts with silver nanoparticles with a "side-on" or "end on" conformation. *Chem. Biol. Interact.* 253, 100–111. doi:10.1016/j.cbi.2016.05.018

del Pilar Chantada-Vázquez, M., López, A. C., Bravo, S. B., Vázquez-Estévez, S., Acea-Nebril, B., and Núñez, C. (2019). Proteomic analysis of the bio-corona formed on the surface of (Au, Ag, Pt)-nanoparticles in human serum. *Colloids Surf. B Biointerfaces* 177, 141–148. doi:10.1016/j.colsurfb.2019.01.056

Dell'Orco, D., Lundqvist, M., Oslakovic, C., Cedervall, T., and Linse, S. (2010). Modeling the time evolution of the nanoparticle-protein corona in a body fluid. *PLOS ONE* 5, e10949. doi:10.1371/journal.pone.0010949

Dennison, J. M., Zupancic, J. M., Lin, W., Dwyer, J. H., and Murphy, C. J. (2017). Protein adsorption to charged gold nanospheres as a function of protein deformability. *Langmuir* 33, 7751–7761. doi:10.1021/acs.langmuir.7b01909

Dibrov, P., Dzioba, J., Gosink, K. K., and Häse, C. C. (2002). Chemiosmotic mechanism of antimicrobial activity of Ag(+) in *Vibrio cholerae*. *Antimicrob. Agents Chemother.* 46, 2668–2670. doi:10.1128/aac.46.8.2668-2670.2002

Fleischer, C. C., and Payne, C. K. (2014). Secondary structure of corona proteins determines the cell surface receptors used by nanoparticles. *J. Phys. Chem. B* 118, 14017–14026. doi:10.1021/jp502624n

García Vence, M., Chantada-Vázquez, M., del, P., Vázquez-Estévez, S., Manuel Cameselle-Teijeiro, J., Bravo, S. B., et al. (2020). Potential clinical applications of the personalized, disease-specific protein corona on nanoparticles. *Clin. Chim. Acta* 501, 102–111. doi:10.1016/j.cca.2019.10.027

Ghazaryan, A., Landfester, K., and Mailänder, V. (2019). Protein deglycosylation can drastically affect the cellular uptake. *Nanoscale* 11, 10727–10737. doi:10.1039/C8NR08305C

Gorshkov, V., Bubis, J. A., Solovyeva, E. M., Gorshkov, M. V., and Kjeldsen, F. (2019). Protein corona formed on silver nanoparticles in blood plasma is highly selective and resistant to physicochemical changes of the solution. *Environ. Sci. Nano* 6, 1089–1098. doi:10.1039/C8EN01054D

Griffith, D. M., Jayaram, D. T., Spencer, D. M., Pisetsky, D. S., and Payne, C. K. (2020). DNA-nanoparticle interactions: Formation of a DNA corona and its effects on a protein corona. *Biointerphases* 15, 051006. doi:10.1116/6.0000439

Hajipour, M. J., Laurent, S., Aghaie, A., Rezaee, F., and Mahmoudi, M. (2014). Personalized protein coronas: A "key" factor at the nanobiointerface. *Biomater. Sci.* 2, 1210–1221. doi:10.1039/C4BM00131A

Holt, K. B., and Bard, A. J. (2005). Interaction of silver(I) ions with the respiratory chain of *Escherichia coli*: An electrochemical and scanning electrochemical microscopy study of the antimicrobial mechanism of micromolar Ag+. *Biochemistry* 44, 13214–13223. doi:10.1021/bi0508542

Hui, J., O'Dell, Z. J., Rao, A., and Riley, K. R. (2019). *In situ* quantification of silver nanoparticle dissolution kinetics in simulated sweat using linear sweep stripping voltammetry. *Environ. Sci. Technol.* 53, 13117–13125. doi:10.1021/acs.est.9b04151

Ju, Y., Kelly, H. G., Dagley, L. F., Reynaldi, A., Schlub, T. E., Spall, S. K., et al. (2020). Person-specific biomolecular coronas modulate nanoparticle interactions with immune cells in human blood. *ACS Nano* 14, 15723–15737. doi:10.1021/acsnano.0c06679

Khosravi-Katuli, K., Prato, E., Lofrano, G., Guida, M., Vale, G., and Libralato, G. (2017). Effects of nanoparticles in species of aquaculture interest. *Environ. Sci. Pollut. Res. Int.* 24, 17326–17346. doi:10.1007/s11356-017-9360-3

Krishnan, P. D., Banas, D., Durai, R. D., Kabanov, D., Hosnedlova, B., Kepinska, M., et al. (2020). Silver nanomaterials for wound dressing applications. *Pharmaceutics* 12, 821. doi:10.3390/pharmaceutics12090821

Kroll, A., Dierker, C., Rommel, C., Hahn, D., Wohlleben, W., Schulze-Isfort, C., et al. (2011). Cytotoxicity screening of 23 engineered nanomaterials using a test matrix of ten cell lines and three different assays. *Part. Fibre Toxicol.* 8, 9. doi:10.1186/1743-8977-8-9

Krylov, S. N., and Berezovski, M. (2003). Non-equilibrium capillary electrophoresis of equilibrium mixtures - appreciation of kinetics in capillary electrophoresis. *Analyst* 128, 571–575. doi:10.1039/b212913b

Lai, W., Wang, Q., Li, L., Hu, Z., Chen, J., and Fang, Q. (2017). Interaction of gold and silver nanoparticles with human plasma: Analysis of protein corona reveals specific binding patterns. *Colloids Surf. B Biointerfaces* 152, 317–325. doi:10.1016/j.colsurfb.2017.01.037

Lankveld, D. P. K., Oomen, A. G., Krystek, P., Neigh, A., Troost – de Jong, A., Noorlander, C. W., et al. (2010). The kinetics of the tissue distribution of silver nanoparticles of different sizes. *Biomaterials* 31, 8350–8361. doi:10.1016/j.biomaterials.2010.07.045

Levak, M., Burić, P., Dutour Sikirić, M., Domazet Jurašin, D., Mikac, N., Bačić, N., et al. (2017). Effect of protein corona on silver nanoparticle stabilization and ion release kinetics in artificial seawater. *Environ. Sci. Technol.* 51, 1259–1266. doi:10.1021/acs.est.6b03161

Li, Y., Qin, T., Ingle, T., Yan, J., He, W., Yin, J.-J., et al. (2017). Differential genotoxicity mechanisms of silver nanoparticles and silver ions. *Arch. Toxicol.* 91, 509–519. doi:10.1007/s00204-016-1730-y

Lima, T., Bernfur, K., Vilanova, M., and Cedervall, T. (2020). Understanding the lipid and protein corona formation on different sized polymeric nanoparticles. *Sci. Rep.* 10, 1129–9. doi:10.1038/s41598-020-57943-6

Liu, C., Leng, W., and Vikesland, P. J. (2018). Controlled evaluation of the impacts of surface coatings on silver nanoparticle dissolution rates. *Environ. Sci. Technol.* 52, 2726–2734. doi:10.1021/acs.est.7b05622

Lok, C.-N., Ho, C.-M., Chen, R., He, Q.-Y., Yu, W.-Y., Sun, H., et al. (2006). Proteomic analysis of the mode of antibacterial action of silver nanoparticles. *J. Proteome Res.* 5, 916–924. doi:10.1021/pr0504079

Lynch, I., Cedervall, T., Lundqvist, M., Cabaleiro-Lago, C., Linse, S., and Dawson, K. A. (2007). The nanoparticle–protein complex as a biological entity; a complex fluids and surface science challenge for the 21st century. *Adv. Colloid Interface Sci.* 135, 167–174. doi:10.1016/j.cis.2007.04.021

Martin, M. N., Allen, A. J., MacCuspie, R. I., and Hackley, V. A. (2014). Dissolution, agglomerate morphology, and stability limits of protein-coated silver nanoparticles. *Langmuir* 30, 11442–11452. doi:10.1021/la502973z

Melby, E. S., Allen, C., Foreman-Ortiz, I. U., Caudill, E. R., Kuech, T. R., Vartanian, A. M., et al. (2018). Peripheral membrane proteins facilitate nanoparticle binding at lipid bilayer interfaces. *Langmuir* 34, 10793–10805. doi:10.1021/acs.langmuir.8b02060

Melby, E. S., Lohse, S. E., Park, J. E., Vartanian, A. M., Putans, R. A., Abbott, H. B., et al. (2017). Cascading effects of nanoparticle coatings: Surface functionalization dictates the assemblage of complexed proteins and subsequent interaction with model cell membranes. *ACS Nano* 11, 5489–5499. doi:10.1021/acsnano.7b00231

Monteiro-Riviere, N. A., Samberg, M. E., Oldenburg, S. J., and Riviere, J. E. (2013). Protein binding modulates the cellular uptake of silver nanoparticles into human cells: Implications for *in vitro* to *in vivo* extrapolations? *Toxicol. Lett.* 220, 286–293. doi:10.1016/j.toxlet.2013.04.022

Nakajou, K., Watanabe, H., Kragh-Hansen, U., Maruyama, T., and Otagiri, M. (2003). The effect of glycation on the structure, function and biological fate of human serum albumin as revealed by recombinant mutants. *Biochim. Biophys. Acta BBA - Gen. Subj.* 1623, 88–97. doi:10.1016/j.bbagen.2003.08.001

Navarro, E., Piccapietra, F., Wagner, B., Marconi, F., Kaegi, R., Odzak, N., et al. (2008). Toxicity of silver nanoparticles to Chlamydomonas reinhardtii. *Environ. Sci. Technol.* 42, 8959–8964. doi:10.1021/es801785m

Nierenberg, D., Khaled, A. R., and Flores, O. (2018). Formation of a protein corona influences the biological identity of nanomaterials. *Rep. Pract. Oncol. Radiother. J. Gt. Cancer Cent. Poznan Pol. Soc. Radiat. Oncol.* 23, 300–308. doi:10.1016/j.rpor.2018.05.005

Okhonin, V., Krylova, S. M., and Krylov, S. N. (2004). Nonequilibrium capillary electrophoresis of equilibrium mixtures, mathematical model. *Anal. Chem.* 76, 1507–1512. doi:10.1021/ac035259p

Olenick, L. L., Troiano, J. M., Vartanian, A., Melby, E. S., Mensch, A. C., Zhang, L., et al. (2018). Lipid corona formation from nanoparticle interactions with bilayers. *Chem* 4, 2709–2723. doi:10.1016/j.chempr.2018.09.018

Paladini, F., and Pollini, M. (2019). Antimicrobial silver nanoparticles for wound healing application: Progress and future trends. *Materials* 12, 2540. doi:10.3390/ma12162540

Pan, H., Qin, M., Meng, W., Cao, Y., and Wang, W. (2012). How do proteins unfold upon adsorption on nanoparticle surfaces? *Langmuir* 28, 12779–12787. doi:10.1021/la302258k

Park, S.-H., Oh, S.-G., Mun, J.-Y., and Han, S.-S. (2005). Effects of silver nanoparticles on the fluidity of bilayer in phospholipid liposome. *Colloids Surf. B Biointerfaces* 44, 117–122. doi:10.1016/j.colsurfb.2005.06.002

Qiu, H.-Y., Hou, N.-N., Shi, J.-F., Liu, Y.-P., Kan, C.-X., Han, F., et al. (2021). Comprehensive overview of human serum albumin glycation in diabetes mellitus. *World J. Diabetes* 12, 1057–1069. doi:10.4239/wjd.v12.i7.1057

Riley, K. R., Sims, C. M., Wood, I. T., Vanderah, D. J., and Walker, M. L. (2018). Short-chained oligo(ethylene oxide)-functionalized gold nanoparticles: Realization of significant protein resistance. *Anal. Bioanal. Chem.* 410, 145–154. doi:10.1007/s00216-017-0704-0

Schreurs, W. J., and Rosenberg, H. (1982). Effect of silver ions on transport and retention of phosphate by *Escherichia coli*. *J. Bacteriol.* 152, 7–13. doi:10.1128/jb.152.1.7-13.1982

Shang, L., Wang, Y., Jiang, J., and Dong, S. (2007). pH-dependent protein conformational changes in albumin:gold nanoparticle bioconjugates: A spectroscopic study. *Langmuir* 23, 2714–2721. doi:10.1021/la062064e

Shannahan, J. H., Podila, R., Aldossari, A. A., Emerson, H., Powell, B. A., Ke, P. C., et al. (2015). formation of a protein corona on silver nanoparticles mediates cellular toxicity via scavenger receptors. *Toxicol. Sci.* 143, 136–146. doi:10.1093/toxsci/kfu217

Shannahan, J. (2017). The biocorona: A challenge for the biomedical application of nanoparticles. *Nanotechnol. Rev.* 6, 345–353. doi:10.1515/ntrev-2016-0098

Smetana, A. B., Klabunde, K. J., Marchin, G. R., and Sorensen, C. M. (2008). Biocidal activity of nanocrystalline silver powders and particles. *Langmuir ACS J. Surf. Colloids* 24, 7457–7464. doi:10.1021/la800091y

Sohaebuddin, S. K., Thevenot, P. T., Baker, D., Eaton, J. W., and Tang, L. (2010). Nanomaterial cytotoxicity is composition, size, and cell type dependent. *Part. Fibre Toxicol.* 7, 22. doi:10.1186/1743-8977-7-22

Sondi, I., and Salopek-Sondi, B. (2004). Silver nanoparticles as antimicrobial agent: A case study on *E. coli* as a model for gram-negative bacteria. *J. Colloid Interface Sci.* 275, 177–182. doi:10.1016/j.jcis.2004.02.012

Sussman, E. M., Jayanti, P., Dair, B. J., and Casey, B. J. (2015). Assessment of total silver and silver nanoparticle extraction from medical devices. *Food Chem. Toxicol.* 85, 10–19. doi:10.1016/j.fct.2015.08.013

Tai, J.-T., Lai, C.-S., Ho, H.-C., Yeh, Y.-S., Wang, H.-F., Ho, R.-M., et al. (2014). Protein–silver nanoparticle interactions to colloidal stability in acidic environments. *Langmuir* 30, 12755–12764. doi:10.1021/la5033465

Treuel, L., Brandholt, S., Maffre, P., Wiegele, S., Shang, L., and Nienhaus, G. U. (2014). Impact of protein modification on the protein corona on nanoparticles and nanoparticle–cell interactions. *ACS Nano* 8, 503–513. doi:10.1021/nn405019v

Trinh, D. N., Gardner, R. A., Franciosi, A. N., McCarthy, C., Keane, M. P., Soliman, M. G., et al. (2022). Nanoparticle biomolecular corona-based enrichment of plasma glycoproteins for N-glycan profiling and application in biomarker discovery. *ACS Nano* 16, 5463–5475. doi:10.1021/acsnano.1c09564

Varki, A., and Gagneux, P. (2015). "Biological functions of glycans," in *Essentials of glycobiology*. Editors A. Varki, R. D. Cummings, J. D. Esko, P. Stanley, G. W. Hart, M. Aebi, et al. (Cold Spring Harbor (NY): Cold Spring Harbor Laboratory Press).

Varki, A., and Gagneux, P. (2017). "Biological functions of glycans," in *Essentials of glycobiology*. Editors A. Varki, R. D. Cummings, J. D. Esko, P. Stanley, G. W. Hart, M. Aebi, et al. (Cold Spring Harbor (NY): Cold Spring Harbor Laboratory Press), 77–88.

Walczyk, D., Bombelli, F. B., Monopoli, M. P., Lynch, I., and Dawson, K. A. (2010). What the cell "sees" in bionanoscience. *J. Am. Chem. Soc.* 132, 5761–5768. doi:10.1021/ja910675v

Wan, S., Kelly, P. M., Mahon, E., Stöckmann, H., Rudd, P. M., Caruso, F., et al. (2015). The "sweet" side of the protein corona: Effects of glycosylation on nanoparticle–cell interactions. *ACS Nano* 9, 2157–2166. doi:10.1021/nn506060q

Wang, F., Chen, Z., Wang, Y., Ma, C., Bi, L., Song, M., et al. (2022). Silver nanoparticles induce apoptosis in HepG2 cells through particle-specific effects on mitochondria. *Environ. Sci. Technol.* 56, 5706–5713. doi:10.1021/acs.est.1c08246

Wang, Q., Lim, M., Liu, X., Wang, Z., and Chen, K. L. (2016). Influence of solution chemistry and soft protein coronas on the interactions of silver nanoparticles with model biological membranes. *Environ. Sci. Technol.* 50, 2301–2309. doi:10.1021/acs.est.5b04694

Weiss, A. C. G., Krüger, K., Besford, Q. A., Schlenk, M., Kempe, K., Förster, S., et al. (2019). *In situ* characterization of protein corona formation on silica microparticles using confocal laser scanning microscopy combined with microfluidics. *ACS Appl. Mat. Interfaces* 11, 2459–2469. doi:10.1021/acsami.8b14307

Wu, T., and Tang, M. (2018). Review of the effects of manufactured nanoparticles on mammalian target organs. *J. Appl. Toxicol.* 38, 25–40. doi:10.1002/jat.3499

Zhang, X., Pandiakumar, A. K., Hamers, R. J., and Murphy, C. J. (2018). Quantification of lipid corona formation on colloidal nanoparticles from lipid vesicles. *Anal. Chem.* 90, 14387–14394. doi:10.1021/acs.analchem.8b03911

frontiers | Frontiers in Toxicology

TYPE Original Research
PUBLISHED 06 March 2023
DOI 10.3389/ftox.2023.1096173

OPEN ACCESS

EDITED BY
Saber Hussain,
Wright State University, United States

REVIEWED BY
Colette Miller,
United States Environmental Protection Agency (EPA), United States
Jennifer Anne Thompson,
University of Calgary, Canada

*CORRESPONDENCE
Timothy R. Nurkiewicz,
tnurkiewicz@hsc.wvu.edu

†These authors share senior authorship

SPECIALTY SECTION
This article was submitted to Nanotoxicology, a section of the journal Frontiers in Toxicology

RECEIVED 11 November 2022
ACCEPTED 16 February 2023
PUBLISHED 06 March 2023

CITATION
Griffith JA, Dunn A, DeVallance E, Schafner KJ, Engles KJ, Batchelor TP, Goldsmith WT, Wix K, Hussain S, Bowdridge EC and Nurkiewicz TR (2023), Maternal nano-titanium dioxide inhalation alters fetoplacental outcomes in a sexually dimorphic manner. *Frontiers Toxicol.* 5:1096173. doi: 10.3389/ftox.2023.1096173

Maternal nano-titanium dioxide inhalation alters fetoplacental outcomes in a sexually dimorphic manner

Julie A. Griffith[1,2], Allison Dunn[1], Evan DeVallance[1,2], Kallie J. Schafner[1,2], Kevin J. Engles[1], Thomas P. Batchelor[1,2], William T. Goldsmith[1,2], Kimberley Wix[1,2], Salik Hussain[1,2], Elizabeth C. Bowdridge[1,2†] and Timothy R. Nurkiewicz[1,2†*]

[1]Department of Physiology, Pharmacology, and Toxicology, West Virginia University School of Medicine, Morgantown, WV, United States, [2]Center for Inhalation Toxicology, West Virginia University School of Medicine, Morgantown, WV, United States

The placenta plays a critical role in nutrient-waste exchange between the maternal and fetal circulations, thus functioning as an interface that profoundly impacts fetal growth and development. The placenta has long been considered an asexual organ, but, due to its embryonic origin it shares the same sex as the fetus. Exposures to toxicant such as diesel exhaust, have been shown to result in sexually dimorphic outcomes like decreased placental mass in exposed females. Therefore, we hypothesize that maternal nano-TiO_2 inhalation exposure during gestation alters placental hemodynamics in a sexually dimorphic manner. Pregnant Sprague-Dawley rats were exposed from gestational day 10–19 to nano-TiO_2 aerosols (12.17 ± 1.69 mg/m^3) or filtered air (sham-control). Dams were euthanized on GD20, and fetal tissue was collected based on fetal sex: whole placentas, placental junctional zone (JZ), and placental labyrinth zone (LZ). Fetal mass, placental mass, and placental zone percent areas were assessed for sex-based differences. Exposed fetal females were significantly smaller compared to their exposed male counterparts (2.65 ± 0.03 g vs 2.78 ± 0.04 g). Nano-TiO_2 exposed fetal females had a significantly decreased percent junctional zone area compared to the sham-control females (24.37 ± 1.30% vs 30.39 ± 1.54%). The percent labyrinth zone area was significantly increased for nano-TiO_2 females compared to sham-control females (75.63 ± 1.30% vs 69.61 ± 1.54%). Placental flow and hemodynamics were assessed with a variety of vasoactive substances. It was found that nano-TiO_2 exposed fetal females only had a significant decrease in outflow pressure in the presence of the thromboxane (TXA_2) mimetic, U46619, compared to sham-control fetal females (3.97 ± 1.30 mm Hg vs 9.10 ± 1.07 mm Hg) and nano-TiO_2 fetal males (9.96 ± 0.66 mm Hg). Maternal nano-TiO_2 inhalation exposure has a greater effect on fetal female mass, placental zone mass and area, and adversely impacts placental vasoreactivity. This may influence the female growth and development later in life, future studies need to further study the impact of maternal nano-TiO_2 inhalation exposure on zone specific mechanisms.

KEYWORDS

titanium dioxide, thromboxane (TXA_2), prostacyclin, sexual dimoprhism, placental flow

1 Introduction

Adverse intrauterine environments have been shown to influence fetal development in a sex-dependent way, as was classically shown in work examining the Dutch famine at the end of WWII (Gabory et al., 2013). Undernutrition in mid to late gestation caused a sex-based difference, with increased placental thickness in female fetuses compared to males (Roseboom et al., 2011). It was speculated this may be the female placenta's attempt to compensate for reduced growth by deeper spiral artery invasion (Roseboom et al., 2011). Diseases, such as preeclampsia (PE), can also result in hindered fetal development in a sexually dimorphic manner. It has been suggested that the normal growth of males in PE pregnancies is due to an adaptation in peripheral microvascular tone by the maternal circulation to maintain fetal-placental blood flow, despite disrupted hemodynamics and placental insufficiency (Stark et al., 2006). Female fetuses from a PE pregnancy do not demonstrate altered microvascular function, due to a lack of compensatory peripheral vascular responses, have reduced uteroplacental blood flow, and thusly decreased placental hemodynamics that ultimately decrease fetal female growth and development (Stark et al., 2009). In addition to nutritional or vascular derived disease states affecting fetal growth and development, environmental exposures during gestation may also result in compromised fetal health.

Exposure to certain toxicants can modify placental and fetal growth in a sexually dimorphic manner (Miller et al., 2020). A rat model of inhaled ozone found that fetal females from this study demonstrated adaptive mechanisms to increase nutrient availability to support fetal development, while males did not (Miller et al., 2020). In pregnant mice exposed to diesel exhaust, female offspring in the exposed group had decreased placental mass and crown-to-rump length (Behlen et al., 2021). Exposed fetal females demonstrated increased placental decidua area, lacunae areas, and lipid metabolism signaling (Behlen et al., 2021). While not an inhalation exposure, arsenic exposure *via* drinking water in humans also produces a sexually dimorphic effect, with female placentas having increased levels of the aquaglyceroporin transporter (Winterbottom et al., 2017). This transporter may lead to increased movement of arsenic across the female placenta and elicit the expression of a subset of genes that are female-specific in response to arsenic exposure (Winterbottom et al., 2017). Maternal inhalation of nano-titanium dioxide, a nanomaterial used in building materials and water/air filters (Bowdridge et al., 2019), during gestation has caused decreased female pup mass (Griffith et al., 2022) and decreased male: female sex ratios in early and mid-gestation (Garner et al., 2022b). This exposure paradigm our laboratory has utilized for nano-titanium dioxide (nano-TiO_2) inhalation exposure is a model for pregnant women working in an occupational setting would experience. This encompasses the time periods when women may not realize they are pregnant through late gestation (Griffith et al., 2022). These studies indicate that maternal environmental exposures affect offspring in a sexually dimorphic manner that appears to be paradigm specific. Adaptations in vascular reactivity, to estrogen stimulatory compounds such as prostacyclin (Sobrino et al., 2010), may be part of the sexual dimorphic responses seen in detrimental *in utero* environments such as improper nutrition, disease, or toxicant exposure.

Prostacyclin (PGI_2) and thromboxane (TXA_2), potent vasodilator and vasoconstrictor, respectively, are vital in establishing vascular resistance systemically, and are especially critical to the uterine microcirculation and placental vasculature. In normotensive human pregnancies, umbilical arteries and chorionic plate arteries had decreased PGI_2 induced-vasodilatory capability (Chaudhuri et al., 1993). A study using human placenta chorionic plate vessels determined the TXA_2 mimetic, U46619, increased perfusion pressure in normotensive fetal placental circulation *in vitro* (Read et al., 1999). A rat gestational hypoxia model demonstrated that vasoactivity can change in both the uterine circulation and umbilical vein (Aljunaidy et al., 2016). Our lab has demonstrated that maternal nano-titanium dioxide (nano-TiO_2) inhalation alters the uterine microcirculation and results in increased sensitivity to the vasoconstrictive actions of U46619 (Griffith et al., 2022). Maternal inhalation of nano-TiO_2 also reduced vasodilation in response to the stable PGI_2 analog, carbaprostacyclin (Griffith et al., 2022). In conjunction with this, we have also found that maternal nano-TiO_2 inhalation during gestation results in litter decreased fetal mass (Bowdridge et al., 2019), increased placental mass (Bowdridge et al., 2019), and decreased male: female ratio in early and mid-gestational exposures (Garner et al., 2022b). Further studies expanded on the fetal mass and determined that maternal nano-TiO_2 inhalation during gestation specifically decreased female pup mass (Griffith et al., 2022). This has led us to hypothesize herein that maternal nano-TiO_2 inhalation exposure during gestation alters placental hemodynamics and therefore influences fetal health outcomes in a sexually dimorphic manner.

2 Materials and methods

2.1 Animal model

Timed pregnant Sprague-Dawley (SD; delivered on GD 5–10) rats were purchased from Hilltop Laboratories (Scottdale, PA) and single-housed in an American Association for Accreditation of Laboratory Animal Care (AAALAC) approved facility at West Virginia University (WVU) Health Sciences Center. Rats were housed in a maintained environment: temperature (20–26°C), relative humidity (30–70%), and light-dark cycle (12:12 h). Rats were acclimated for 48–72 h, then randomly assigned to either sham-control (N = 13) or nano-TiO_2 (N = 14) exposure groups. Rat cages were lined with standard bedding (0.25-inch corncob) and had *ad libitum* access to standard chow (2918X; Envigo, Indianapolis, IN) and water throughout the acclimation and exposure periods.

On GD 20, rats were weighed and then anesthetized with isoflurane gas (5% induction, 2–3.5% maintenance), placed on a warm heating pad, and maintained at a rectal temperature of 37°C. Rats were euthanized *via* thoracotomy and heart removal and then distribution of fetuses within the uterine horns and fetal sex was recorded. Fetal tissue was weighed and grouped according to fetal sex: whole placentas, placental junctional zone, and placental

labyrinth zone. All procedures were approved by the WVU Institutional Animal Care and Use Committee.

2.2 Nanomaterial

Nano-TiO_2 powder was obtained from Evonik (P25 Aeroxide TiO_2, Parsippany, NJ) and is composed of a mixture of anatase (80%) and rutile (20%) TiO_2. Particle characteristics have previously been determined, including primary particle size (21 nm), specific surface area (48.08 m^2/g), and Zeta potential (-56.6 mV) (Yi et al., 2013; Stapleton et al., 2018).

2.3 Inhalation exposure and aerosol characterization

A high-pressure acoustical generator (HPAG, IEStechno, Morgantown, WV) created nano-TiO_2 aerosols. Output from the generator was fed into a Venturi pump (JS-60M, Vaccon, Medway, MA) to further de-agglomerate particles. The nano-TiO_2 aerosol mix enters a whole-body exposure chamber and a personal DataRAM (pDR-1500; Thermo Environmental Instruments Inc., Franklin, MA) samples the air to determine aerosol mass concentration in real-time. Software feedback loops automatically adjust the acoustic energy needed to maintain a stable mass aerosol concentration throughout the exposure. Gravimetric aerosol sampling measurements were conducted with Teflon filters concurrently with the DataRAM measurements to obtain calibration factors. Gravimetric measurements were taken during each exposure to calculate the mass concentration measurement. Real-time aerosol size distributions were measured in the exposure chamber at a target mass concentration of 12 mg/m^3 *via*: 1) a high-resolution electrical low-pressure impactor (ELPI+; Dekati, Tampere, Finland); 2) a scanning particle mobility sizer (SMPS 3938; TSI Inc., St. Paul, MN); 3) an aerodynamic particle sizer (APS 3321; TSI Inc., St. Paul, MN); and 4) a micro-orifice uniform deposit impactor (MOUDI 115R, MSP Corp, Shoreview, MN). Bedding material was soaked to maintain proper humidity (20–70%). Similar temperature and humidity conditions were maintained in exposure chambers utilized only for sham-control animals, which were exposed to HEPA-filtered air only.

Inhalation exposures were performed for 6 non-consecutive days from GD 10–19 to prevent pregnancy loss. A target concentration of 12 mg/m^3 was used for late gestation inhalation exposure (Stapleton et al., 2013; Stapleton et al., 2018). For estimation of lung deposition (dose) with nano-TiO_2 aerosols, equation D = F•V•C•T was used where F is the deposition fraction (10%), V is the minute ventilation (208.3 cc), C is mass concentration (mg/m^3), and T equals the exposure duration (minutes) (Nurkiewicz et al., 2008; Stapleton et al., 2013). The exposure paradigm (12 mg/m^3, 6 h/exposure, 6 days) produced a calculated cumulative lung deposition of 525 ± 16 μg (Bowdridge et al., 2022; Griffith et al., 2022) with the last exposure occurring on GD19 24-h prior tissue collection. The calculations represent total lung deposition and do not account for lung clearance (MPPD Software v 2.11, Arlington, VA).

2.4 Pressure myography with isolated placentas

Once dams were euthanized and pups per horn count was recorded, the uterus was surgically excised and placed into a dissection dish containing physiological salt solution (PSS, in mmol/L: 129.8 NaCl, 5.4 KCl, 0.5 NaH_2PO_4, 0.83 $MgSO_4$, 19.0 $NaHCO_3$, 1.8 $CaCl_2$, 5.5 glucose). The uterus was incised longitudinally, and amnionic sacs were opened to allow for quick identification of fetal sex. Fetal sex and position within the horn was recorded, then the first male and female nearest the cervix were removed with the placenta still attached. The placenta/pup units were placed into dissection dishes with PSS maintained at 4°C and were utilized for placental hemodynamic assessment (Garner et al., 2022a).

The umbilical artery and vein were separated from the umbilical cord. Once the amnionic sac and vitelline vessels were removed, the umbilical vessels were cut as close to the pup as possible (Garner et al., 2022a). The placenta was then closed at the site of implantation with 6–0 silk sutures (AD Surgical, Sunnyvale, CA) and placentas were transferred to an isolated vessel chamber (Living Systems Instrumentation, Burlington, VT) containing 10 ml of oxygenated (21% O_2/5% CO_2) 37°C PSS. The umbilical artery was attached to the inflow glass pipette tip and the umbilical vein was attached to the outflow pipette tip (Garner et al., 2022a) using 6–0 silk sutures. Placentas were then pressurized from 0 to 20 mm Hg in 5 mm Hg increments.

Outflow pressure and flow rate were assessed following addition of vasoactive drugs to assess vascular hemodynamics. Endothelium-dependent responses were assessed by acetylcholine (ACh, 1×10^{-4} M), application of s-nitroso-N-acetyl-DL-penicillamine (SNAP, 1×10^{-4} M) assessed endothelium-independent responses, addition of phenylephrine (PE, 1×10^{-4} M) assessed α_1-adrenergic vasoconstriction, addition of carbaprostacyclin (1×10^{-10} M) assessed cyclooxygenase metabolite vasodilation, and application of U46619 (1×10^{-4} M) assessed cyclooxygenase metabolite vasoconstriction. Drugs were added to the bath individually to assess outflow pressure and flow rate response. Washes were done between each drug to ensure clearance. Once all drug response were assessed PSS was removed and replaced with Ca^{2+}-free PSS to assess passive maximum outflow pressure and flow rate.

2.5 Placental histology

Male and female placentas were collected from sham-control (N = 5 per sex) and nano-TiO_2 (N = 5 per sex) exposed dams. Placentas were perfused with 4% paraformaldehyde and fixed *ex situ* with 4% paraformaldehyde at 4°C overnight. Placental tissue was then cleared with phosphate buffer solution (PBS) and transferred PBS overnight. Tissue was then rapidly frozen *via* isopentane and liquid nitrogen and stored at -80°C. Using a cryostat at -20°C, placentas were sectioned at 10 μm thickness. Sections from the center of the placenta, which provided the largest cross-sectional area, were placed on subbed slides, and stained with hematoxylin and eosin (H&E) following provided protocol instructions (Vector Laboratories, Burlingame, CA). Tissue sections were incubated with

hematoxylin for 1 min and eosin for 5 min. Slides were imaged at 10x and analyzed using ImageJ (Xu et al., 2020). Total placental area and percent total area of the junctional and labyrinth zones were determined using an average of measures from three sections per pup.

2.6 Immunohistochemical staining of placentas

Male and female placentas from sham-control (N = 5 per sex) and nano-TiO_2 (N = 5 per sex) dams were collected on GD20. Placentas were perfused and then placed into a 4% paraformaldehyde fixative overnight at 4°C and then transferred to PBS for the following night (Bowdridge et al., 2019). Tissue was then flash frozen and stored at -80°C until sectioned (Bowdridge et al., 2019). Placentas were sectioned at 10 μm through the center of the placenta. Three sections per pup were analyzed. Sections were washed 4 × 5 min with 0.1 M PBS to remove cryoprotectant. Sections were then incubated for 10 min with 1% H_2O_2 and washed 4 × 5 min with 0.1 M PBS. Sections were incubated for 1 h at room temperature with 0.1 M PBS, 0.4% Triton-X100 (Sigma-Aldrich, St. Louis, MO, United States of America) and 20% normal goat serum (NGS; Jackson ImmunoResearch Laboratories, Inc., West Grove, PA, United States of America). Sections were then incubated with mouse monoclonal anti-Pan cytokeratin antibody (1: 250, F3418; Sigma-Aldrich) (Nteeba et al., 2020) for 24 h at 4°C. Slides were washed 5 × 5 min, and then incubated in mouse monoclonal anti-rat CD163 (1:500, MCA342R; Bio-Rad Laboratories, Hercules, CA, United States of America) (Rosario et al., 2009) for 24 h at four°C. The final day, slides were washed with 0.1 M PBS 3 × 5 min. Then incubated with Alexa555 goat anti-mouse IgG1 (1:200; A21127; Thermo Fisher Scientific Inc., Waltham, MA, United States of America) for 1 h. Slides were washed 4 × 5 min and covered with a coverslip using ProLong Diamond Antifade Mountant with DAPI (Thermo Fisher). Slides were stored in the dark at 4°C until analysis.

2.7 statistics

Dam characteristics, such as age, mass, and litter size, were assessed by unpaired *t*-test with Welch's correction. The remainder of the dam characteristics were assessed by two-way analysis of variance (ANOVA). Fetal mass characteristics and total area of placental zones were analyzed *via* a two-way mixed-effects ANOVA. A two-way mixed effects model was used for assessing point-to-point differences in dose response curves to vascular agonists and increased pressure curves. If statistical significance occurred, then a Tukey *post hoc* test was used for all ANOVA analysis. All data are reported as mean ± SEM, unless otherwise stated. Significance was set at $p \leq 0.05$.

3 Results

3.1 Nanoparticle aerosol characteristics

Average real-time aerosol mass concentration over the course of exposures was 12.17 mg/m^3 with a standard deviation of 1.69 (Figure 1A). SMPS and APS measured the aerosol mobility diameter, which had a count median diameter (CMD) of 118 nm and a geometric standard deviation (GSD) of 2.10 (Figure 1B). ELPI assessment of the aerosol aerodynamic diameter showed, a mass median aerodynamic diameter (MMAD) of 164 nm with a geometric standard deviation of 1.89 (Figure 1C). A Nano Micro-Orifice Uniform Deposit Impactor (MOUDI 115R, MSP Corp, Shoreview, MN) was utilized to measure mass size distribution, which had a mass median aerodynamic diameter (MMAD) of 0.92 μm and a GSD of 2.47 (Figure 1D). The morphology of the nano-TiO_2 agglomerates has been previously characterized extensively with electron microscopy (Abukabda et al., 2019; Bowdridge et al., 2019).

3.2 Pregnant rat and litter characteristics

Dams displayed no significant differences in age, litter size, or fetal sex on GD20 between groups (Table 1). There was a significant decrease in dam mass on GD20 in nano-TiO_2 exposed dams (N = 14) compared to sham-control (N = 13; Table 1).

Fetal pup and placental zone mass after nano-TiO_2 inhalation exposure during gestation were assessed according to fetal sex to determine any sexually dimorphic outcomes (Figure 2). Maternal nano-TiO_2 inhalation exposure significantly decreased fetal female wet mass (2.65 ± 0.03 g) compared to the nano-TiO_2 fetal males (2.78 ± 0.04 g; Figure 2A). The nano-TiO_2 exposed fetal female mass decreased compared to the sham-control fetal female mass (2.74 ± 0.03 g). The placenta is composed of two core regions, the junctional zone (JZ) and the labyrinth zone (LZ). The JZ (Figure 2B) presented sex-based differences in mass and an effect of exposure seen only in the females. Sham-control fetal females (0.23 ± 0.01 g) had significantly larger JZ compared to sham-control fetal males (0.20 ± 0.01 g). Nano-TiO_2 exposed fetal female JZ wet mass (0.18 ± 0.01 g) was significantly decreased compared to sham-control fetal females (0.23 ± 0.01 g) and nano-TiO_2 exposed fetal males (0.20 ± 0.04 g). The wet LZ mass (Figure 2C) of nano-TiO_2 fetal females (0.30 ± 0.01 g) was significantly smaller compared to nano-TiO_2 fetal males (0.34 ± 0.01 g). This indicates that maternal nano-TiO_2 inhalation exposure during gestation has a greater effect on fetal female pup and placenta mass.

Dry mass was also measured to discern if wet mass differences were driven by water content. Dry fetal mass (Figure 2D) was significantly decreased in nano-TiO_2 fetal females (0.33 ± 0.01 g) compared to the nano-TiO_2 male counterparts (0.35 ± 0.01 g). The dry sham-control fetal males (0.36 ± 0.01 g) tended to be larger than the dry fetal sham-control females (0.34 ± 0.01 g). Dry JZ mass (Figure 2E) was also significantly decreased in nano-TiO_2 fetal females (0.028 ± 0.001 g) compared to nano-TiO_2 fetal males (0.033 ± 0.001 g). There were no significant differences in dry LZ mass across treatment groups (Figure 2F). This provides evidence that nano-TiO_2 exposure during gestation causes structural mass changes, not based on water content.

3.3 Sexually dimorphic placental hemodynamics

Placental outflow pressure for sham-control fetal males (n = 5–6), sham-control fetal females (n = 4–6), nano-TiO_2 fetal males (n = 5–7), and nano-TiO_2 fetal females (n = 5–7) was measured to assess vascular resistance within the perfused tissue. Placentas were

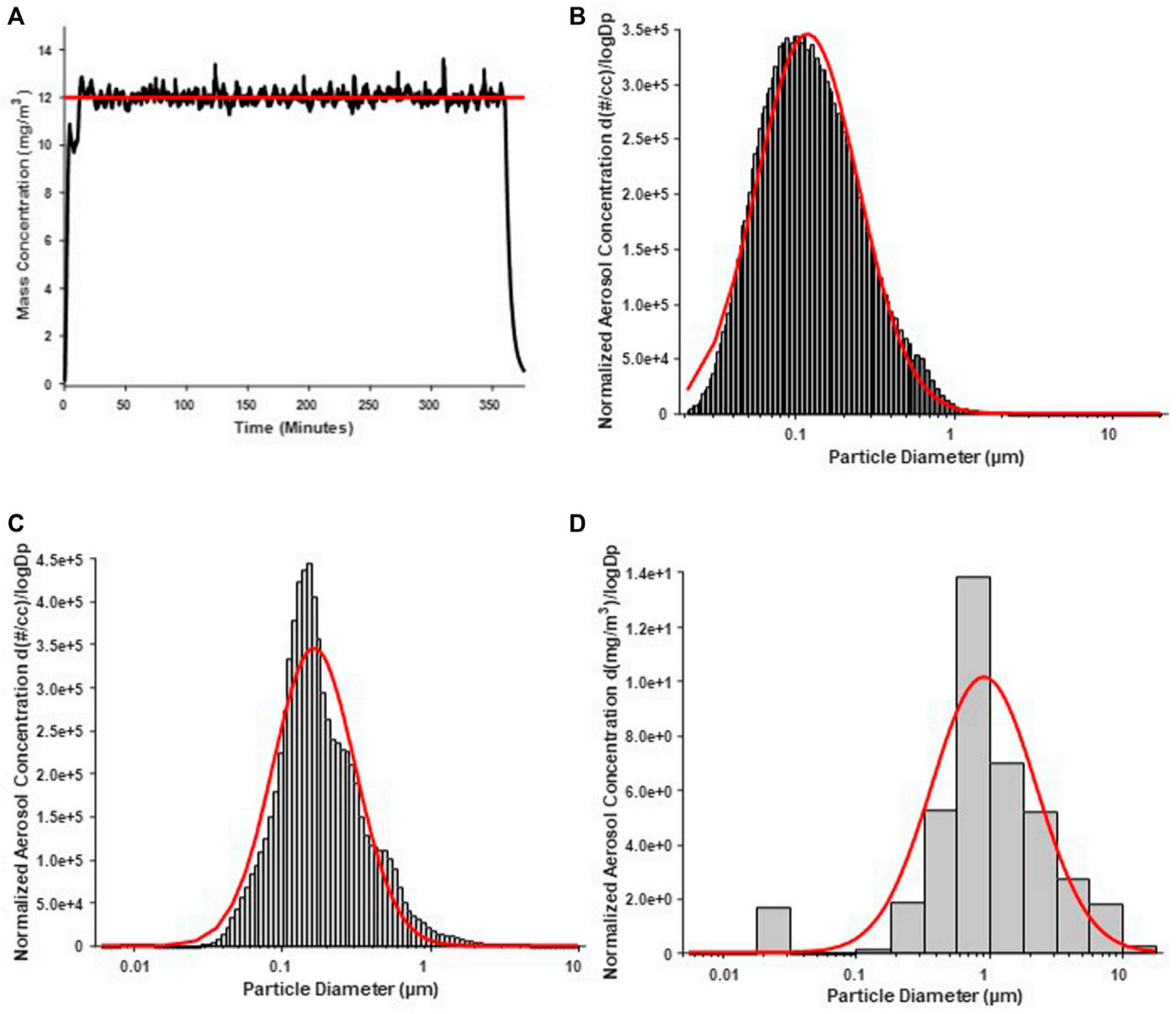

FIGURE 1
Nano-TiO_2 aerosol real-time characterizations. Aerosol characterization was monitored and verified during the exposure periods. Red lines indicate size distribution curves for a log normal fit of the size data. **(A)** Program software-controlled aerosol mass concentration over the 6-h exposure paradigm. Real-time nano-TiO_2 aerosol mass concentration (black line) was maintained near the desired 12 mg/m^3, the target average concentration (red line). **(B)** Aerosol aerodynamic diameter was assessed by scanning mobility particle sizer (SMPS; light gray) and an aerodynamic particle sizer (APS; dark gray). The particle diameter, determined by SMPS and APS, had a CMD of 118 nm and a geometric standard deviation of 2.10. **(C)** Aerosol aerodynamic diameter was also assessed by a high-resolution electrical low-pressure impactor (ELPI) which had a CMD of 164 nm and geometric standard deviation of 1.89. **(D)** A nano micro-orifice uniform deposit impactor (MOUDI) was used to evaluate aerosol mass size distribution and indicated a mass median aerodynamic diameter (MMAD) of 0.918 µm and a geometric standard deviation of 2.47.

TABLE 1 Dam and litter characteristics include dam age (days), mass (grams), litter size, pup distribution across horns, fetal sex distribution, and resorptions distributions across horns. N is the number of dams. Data are mean ± SEM. *, $p \leq 0.05$ vs sham-control.

Exposure	N	Dam age (d)	Dam mass (g)	Litter size (pup number)	Fetal horn distribution (pup number)		Sex distribution (pup number)		Resorptions distribution (number of sites)	
					Left	Right	Male	Female	Left	Right
Sham-control	13	70.2 ± 2.2	358.4 ± 9.3	13.2 ± 0.6	6.7 ± 0.4	6.5 ± 0.6	6.5 ± 0.3	6.2 ± 0.5	0.9 ± 0.09	0.55 ± 0.21
Nano-TiO_2	14	71.9 ± 1.6	**330.8 ± 4.7** *	12.6 ± 0.6	7.0 ± 0.5	5.6 ± 0.6	6.0 ± 0.4	5.4 ± 0.2	0.08 ± 0.08	0.23 ± 0.17

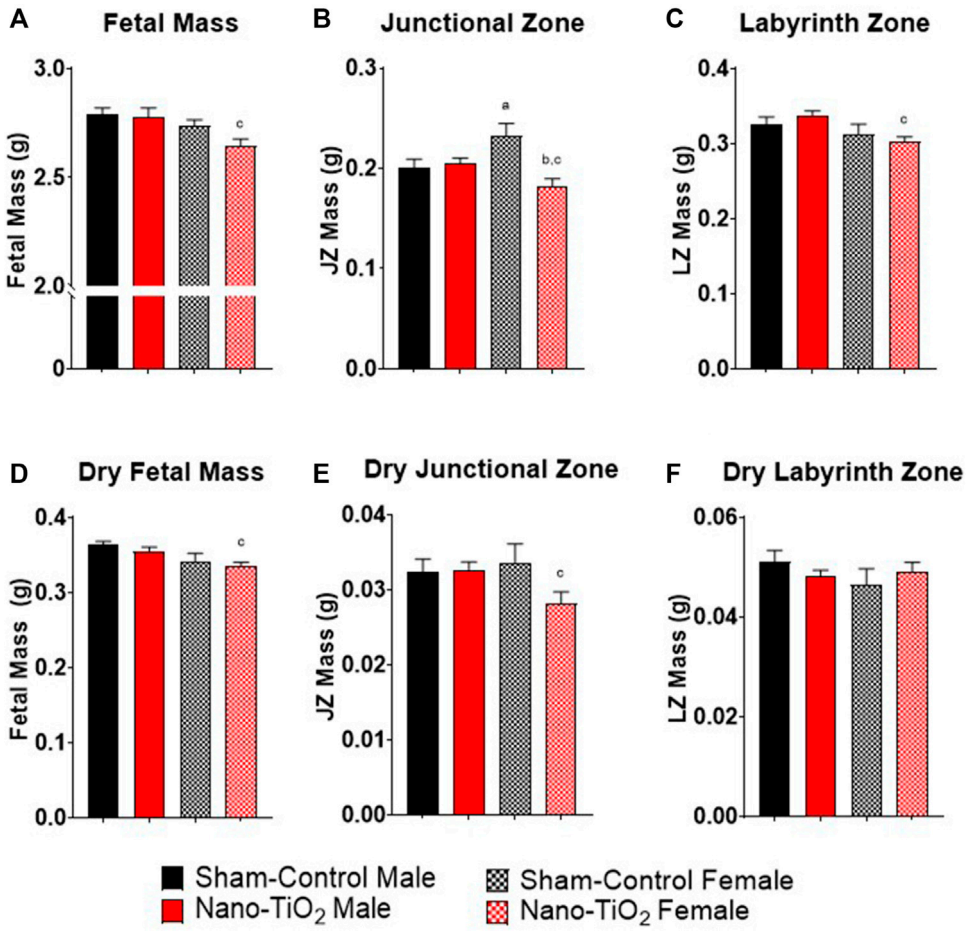

FIGURE 2
Fetal Pup and Placental Zone Mass. Fetal and placental mass were recorded based on fetal sex on GD 20 (N = 13, sham-control fetal male and female, and N = 14, nano-TiO_2 fetal male and female). **(A)** Wet fetal mass. **(B)** Wet junctional zone mass. **(C)** Wet labyrinth zone mass. **(D)** Dry fetal mass. **(E)** Dry junctional zone mass. **(F)** Dry labyrinth zone mass. a, $p \leq 0.05$ vs sham-control fetal male. b, $p \leq 0.05$ vs sham-control fetal female. c, $p \leq 0.05$ vs nano-TiO_2 fetal male.

incubated in the presence of PSS, ACh, carbaprostacyclin, and thromboxane and outflow pressure was assessed (Figures 3, 4). Responses were also determined following exposure to SNAP, PE, and Ca^{2+}-free PSS (Supplementary Figure S1).

Placental responses to physiological saline solution (PSS) were assessed to test baseline outflow pressure (Figures 3A, B), which was not significantly different amongst treatments. Placental outflow pressure response to the endothelium-dependent vasodilator, ACh (Figures 3C, D) were not significantly different amongst treatments. Responses to carbaprostacyclin, a cyclooxygenase vasodilator (Figures 4A, B), were also not significantly different between groups. The thromboxane mimetic, U46619 (Figures 4C, D), resulted in sham-control fetal females to have increased outflow compared to sham-control fetal males at 15 mm Hg inflow pressure (9.10 ± 1.07 mm Hg vs 5.11 ± 1.02 mm Hg). Placentas of nano-TiO_2 exposed fetal females had significantly decreased outflow pressure (3.97 ± 1.30 mm Hg) compared to sham-control fetal females (9.10 ± 1.07 mm Hg) and nano-TiO_2 exposed fetal male placentas (9.96 ± 0.66 mm Hg). Nano-TiO_2 exposed fetal male placentas also had significantly increased outflow compared to sham-control fetal males (9.96 ± 0.66 vs 5.11 ± 1.02 mm Hg, respectively). There were no significant differences between groups for outflow pressures when incubated with PE, SNAP, or Ca^{2+}-free PSS (Supplementary Figure S1A–C). This indicates that maternal nano-TiO_2 inhalation exposure during gestation results in modified placental hemodynamics that are specific to thromboxane.

Placental flow rates were also assessed for each group to determine hemodynamic responses to inflow pressure and vasoactive drugs. There were no significant differences for placenta flow rates across groups when incubated with PSS, ACh, PGI_2 analog, carbaprostacyclin, and the TXA_2 mimetic, U46619 (Figures 5A–D and Figures 6A–D). Placenta flow rates did not demonstrate significant differences between groups when incubated with PE, SNAP, or Ca^{2+}-free PSS (Supplementary Figure S2A–C).

3.4 Placental histology & immunohistochemistry

Placentas were collected for each group (sham-control males and females (n = 5/sex); nano-TiO_2 males and females (n = 5/sex))

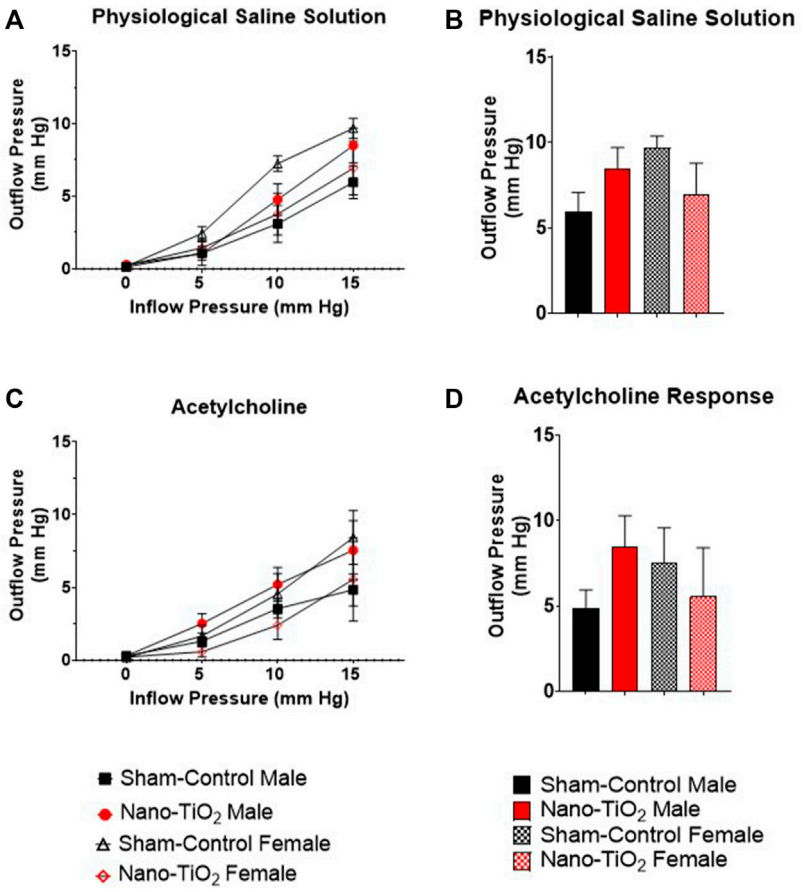

FIGURE 3
Placental Outflow Hemodynamics. Outflow pressure readings were recorded in conjunction with increased inflow input. **(A)** Outflow pressure in the presence of physiological saline solution (PSS). **(B)** Maximum outflow response in the presence of PSS. **(C)** Outflow pressure in the presence of the endothelium-dependent vasodilator, ACh. **(D)** Maximum outflow response in the presence of ACh. Sham-control fetal male, n = 5-6, nano-TiO_2 fetal male, n = 5-7, sham-control fetal female, n = 4-5, and nano-TiO_2 fetal female, n = 5-6.

to assess differences in placental JZ and LZ area and anatomy between fetal sex and exposure paradigm. A representative image of the placenta histology is shown in Figure 7A. Total placenta area was assessed, in which there was a significant increase in area size for sham-control female compared to sham-control male (84,130 ± 3834 AU vs 69,956 ± 3660 AU; Figure 7B). Nano-TiO_2 female area was also significantly increased compared to nano-TiO_2 male total placenta area (89,697 ± 6141 AU vs 76,558 ± 4272 AU; Figure 7B). The percent JZ area was significantly decreased for nano-TiO_2 males (26.15 ± 1.59%) compared to sham-control males (30.93 ± 1.37%; Figure 7C). Nano-TiO_2 females also had a significantly decreased JZ area compared to sham-control females (24.37 ± 1.30% vs 30.39 ± 1.54%; Figure 7C). There was no significant difference between fetal sex within their exposure group (Figure 7C). Total LZ area is highlighted in Figure 7D. Nano-TiO_2 males had a significant increase in LZ area compared to sham-control males (73.85 ± 1.59% vs 69.07 ± 1.37%). Nano-TiO_2 females (75.63 ± 1.30%) had a significant increase of LZ area compared to sham-control females (69.61 ± 1.54%; Figure 7D). There was not a significant difference for fetal sex within their exposures. This indicates that not only does maternal nano-TiO_2 inhalation exposure during gestation change placental mass, but results in placental area changes as well.

Additionally, a subset of placentas was used to quantify Hofbauer cell (CD163; macrophages specific to gestation) and trophoblast cell (anti-Pan cytokeration; placental lineage cells), along with their co-localization. A representative image is provided in Figure 8A. Hofbauer cell pixel intensity for the total placenta is depicted in Figure 8B. There was a significant increase in fluorescent intensity for nano-TiO_2 females compared to sham-control females (93.41 ± 3.05 AU vs 52.80 ± 6.67 AU; Figure 8B). Trophoblast cell fluorescent intensity was significantly decreased in sham-control female (57.12 ± 3.84 AU) compared to sham-control males (80.17 ± 7.90 AU) and compared to nano-TiO_2 females (81.18 ± 6.53 AU; Figure 8C) in the total placenta. Colocalization of Hofbauer and trophoblast cells is depicted in Figure 8D. Co-localization was significantly increased in nano-TiO_2 females compared to sham-control females (23,387 ± 3,172 AU vs 11,293 ± 1,896 AU). Maternal nano-TiO_2 inhalation exposure during gestation results in modified cellular composition of the placentas.

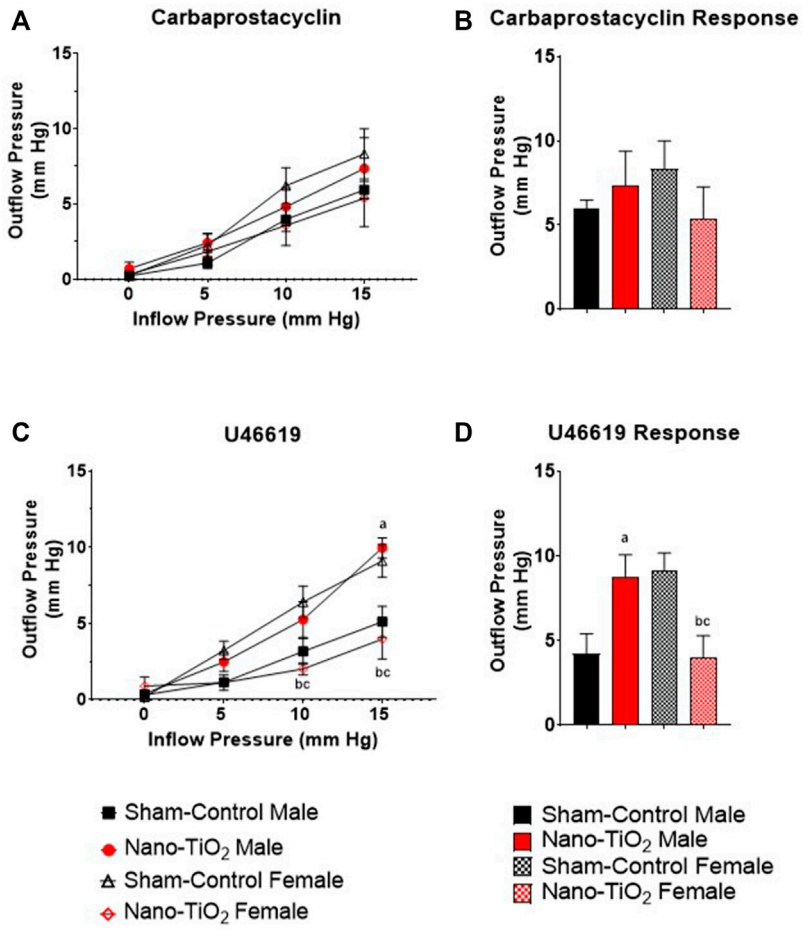

FIGURE 4
Placental Cyclooxygenase Metabolites Outflow Hemodynamics. Outflow pressure readings were recorded with increased inflow input. **(A)** Placental outflow pressure in the presence of carbaprostacyclin, a stable PGI_2 agonist. **(B)** Maximum outflow response to carbaprostacyclin. **(C)** Outflow pressure with U46619, the TXA_2 mimetic. **(D)** Maximum outflow pressure response in the presence of U46619. Sham-control fetal male, n = 5-6, nano-TiO_2 fetal male, n = 5-7, sham-control fetal female, n = 4-5, and nano-TiO_2 fetal female, n = 5–6. a, $p \leq 0.05$ vs sham-control fetal male. b, $p \leq 0.05$ vs sham-control fetal female. c, $p \leq 0.05$ vs nano-TiO_2 fetal male.

Immunohistochemistry staining was also evaluated based on JZ and LZ fluorescent intensity and colocalization, which is shown in Figure 9. Hofbauer cells significantly decrease in nano-TiO_2 females compared to nano-TiO_2 males (66.47 ± 5.08 AU vs 103.1 ± 5.75 AU). Nano-TiO_2 males tended to have increased CD163 intensity compared to sham-control males (78.65 ± 5.91 AU; $p = 0.06$; Figure 9A). Pan-cytokeratin intensity for JZ was significantly increased in sham-control males compared to females (67.24 ± 5.21 AU vs 44.43 ± 2.59 AU; Figure 9B) and nano-TiO_2 female (67.38 ± 9.43) tended to have increased compared to sham-control females ($p = 0.07$). Colocalization of CD163 and pan-cytokeratin was assessed in the JZ, in which there was no significant difference (Figure 9C).

Within the LZ, there was a significant decrease for CD163 intensity of sham-control females compared to males (62.00 ± 12.80 AU vs 94.74 ± 15.00 AU; Figure 9D). Nano-TiO_2 females (116.1 ± 7.869) had significantly increased CD163 intensity compared to sham-control females (62.00 ± 12.80) and nano-TiO_2 males (75.61 ± 6.58 AU). LZ pan-cytokeratin fluorescence was significantly decreased for sham-control female compared to males (64.65 ± 7.47 AU vs 91.55 ± 10.23 AU; Figure 9E) and nano-TiO_2 females (95.19 ± 7.19 AU) tended to have increased staining compared to sham-control females ($p = 0.08$). Within the LZ, there was a significant decrease of colocalization for sham-control female (3,415 ± 819.8 AU) compared to sham-control male (6,513 ± 719.8 AU) and nano-TiO_2 female (18,706 ± 2,802 AU; Figure 9F). There was also a significant increase for colocalization for nano-TiO_2 female compared to nano-TiO_2 male (18,706 ± 2,802 vs 11,631 ± 11,577). The placenta zones of the exposed fetuses are also impacted with changes in their cellular composition, and thus may change their functionality.

4 Discussion

The primary aim of this project was to determine if maternal nano-TiO_2 inhalation exposure during gestation alters placental vascular reactivity and fetal growth in a sexually dimorphic

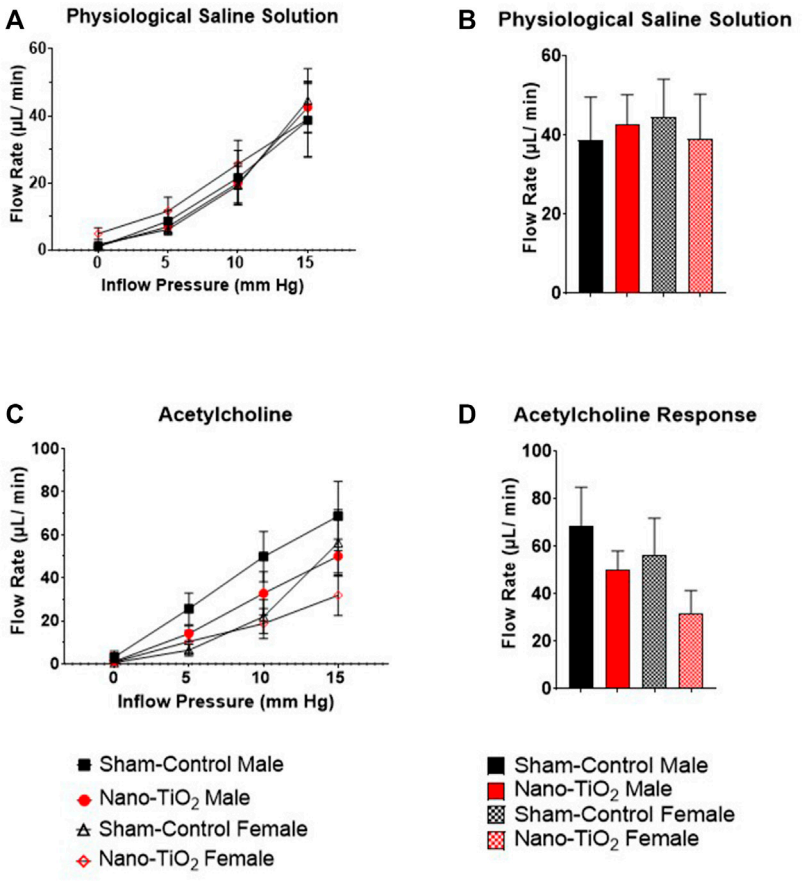

FIGURE 5
Placental flow rate hemodynamics. Flow rate was calculated and recorded throughout experiment as inflow pressure was increased stepwise manner. **(A)** Flow rate in PSS bathe. **(B)** Maximum flow rate response in PSS. **(C)** Flow rate of placentas in the presence of the ACh, an endothelium-dependent vasodilator. **(D)** Maximum flow rate response across increased pressure. Sham-control fetal male, n = 5-6, nano-TiO_2 fetal male, n = 5-7, sham-control fetal female, n = 4-5, and nano-TiO_2 fetal female, n = 5-6.

manner. Herein, we demonstrated that maternal nano-TiO_2 gestational inhalation exposure produces placental dysfunction in a sex-dependent manner. While female fetuses have the greatest impact, with decreased placental size and area, fetal growth, and placental hemodynamic capabilities, these are likely adaptations to preserve fetal life. Our laboratory has also previously demonstrated decreased male to female ratio in early and mid-gestation inhalation exposures (Garner et al., 2022b). Males are more susceptible to fetal loss due to external maternal stress during gestation (Kraemer, 2000). Additionally, maternal disease (like Diabetes Mellitus) may affect male fetal congenital development and perinatal outcomes (Evers et al., 2009; García-Patterson et al., 2011). It appears that females are more adaptable in hostile environments to ensure they survive gestation, but these adaptations may be to their detriment later in life.

In utero perturbations can result in fetal intrauterine growth restriction (IUGR), which is a risk factor for many adult diseases such as cardiovascular disease (CVD), diabetes, dyslipidemia, hypertension, metabolic syndrome, or renal diseases later in life (Menendez-Castro et al., 2018). Insults that result in a hostile gestational environments that cause diseases later in life is part of the Barker hypothesis, widely referred to as the developmental origins of health and disease (DOHaD) (Barker, 1990; Barker and Martyn, 1992). In this study, we observed a significant decrease in fetal mass for the nano-TiO_2 exposed fetal females compared to nano-TiO_2 males (Figure 2A) which was anticipated as this has been previously shown (Griffith et al., 2022). Modification of blood flow or nutrient exchange to the fetus can have different impacts on the progression of fetal growth between sexes. In a gestational guinea pig model, it was found that early-onset hypoxia caused both male and female mass to decrease, but late-onset hypoxia caused only female mass to decrease compared to sex-matched controls (Thompson et al., 2020). Hypoxic models are important as they indicate modifications in blood flow and vascular resistance changes to increased oxygen delivery to critical organs (Heinonen et al., 2016). Intrauterine growth restriction (IUGR), as seen in our study and guinea pig hypoxia study (Thompson et al., 2020), has a strong association with impaired fetal blood flow (Laurin et al., 1987), thus leaving fetuses to attempt to adapt to this hostile gestational environment. Fetal growth can be impacted by toxicant exposures, in a sexually dimorphic manner and these perturbations can be exasperated by direct toxic effects on the placenta.

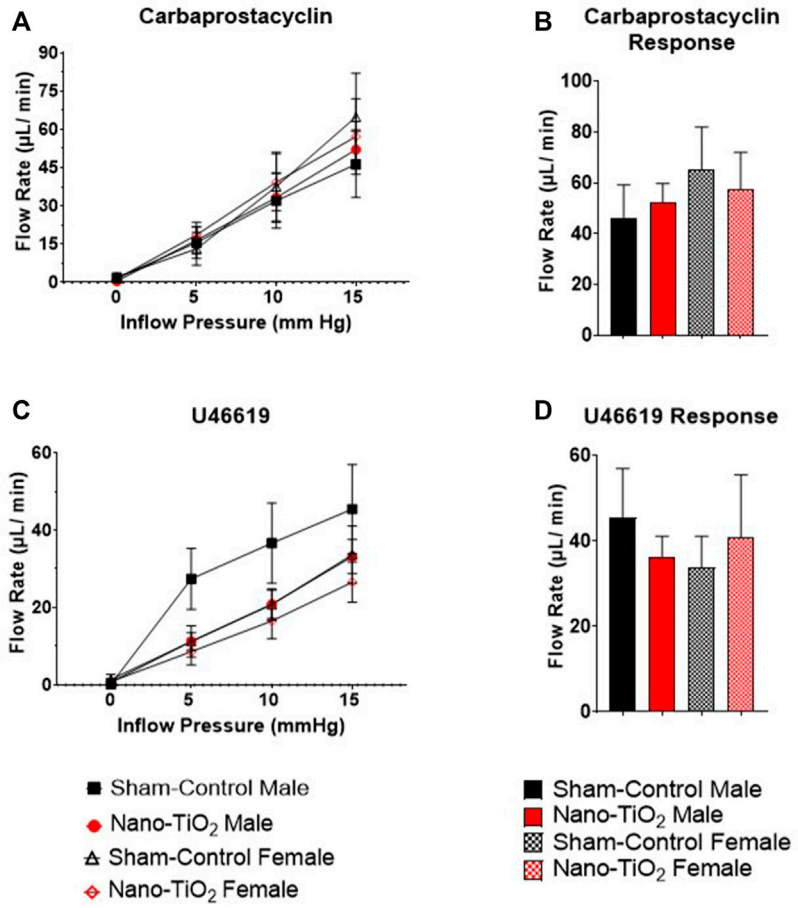

FIGURE 6
Placental Cyclooxygenase Metabolites flow rate hemodynamics. Flow rate was calculated and recorded during inflow pressure increases in a stepwise manner. **(A)** Placenta flow rate in the presence of carbaprostacyclin, a stable PGI_2 agonist, across increased inflow pressure. **(B)** Maximum flow rate in response to carbaprostacyclin. **(C)** Placenta flow rate with U46619, a TXA_2 mimetic, added to the bathe. **(D)** Maximum flow rate response to U46619. Sham-control fetal male, n = 5-6, nano-TiO_2 fetal male, n = 5-7, sham-control fetal female, n = 4-5, and nano-TiO_2 fetal female, n = 5-6.

Toxicant exposures can affect total placental mass, placenta zone mass and area of placental zones. Herein, placental zone mass (Figures 2B, C) and placenta zone areas (Figures 7C, D) changes occurred after nano-TiO_2 exposure during gestation. Placental perturbations were most pronounced in the nano-TiO_2 exposed females, which had decreased JZ and LZ mass, decreased JZ area, and increased LZ area. Decreased JZ mass and area could lead to modifications in hormone production and increased LZ area results in modifications to placental nutrient-waste exchange capabilities in a sex-dependent manner (Gårdebjer et al., 2014). Studies of diet restriction, in mice have demonstrated decreased fetal mass (Belkacemi et al., 2009; Coan et al., 2010; Connor et al., 2020), decreased JZ and LZ mass (Belkacemi et al., 2009), and decreased JZ volume (Coan et al., 2010) or area (Schulz et al., 2012; Connor et al., 2020). Undernutrition in mice has also been reported to increase LZ area or volume (Coan et al., 2010; Schulz et al., 2012) and make up a larger proportion of the placenta. These studies came to similar conclusions, that while the overall placenta mass was decreased, the increased LZ area is an attempt to compensate for nutrient restriction and preserve fetal growth (Coan et al., 2010; Schulz et al., 2012). Changes in the mass and area of the JZ and LZ are important to fetal development, however the cellular composition of these zones is equally as important. These changes could be due to cell proliferation or hypertrophy and can result in functional changes in the fetoplacental unit.

A hostile *in utero* environment during gestation may cause the placenta to go through modifications in zone size, mass, area, and volume, as discussed above, but it may also result in cellular composition changes preserve fetal life. Indeed, we observed changes in the cellular composition of placentas in our exposure model. Further, these changes occur in a sexually dimorphic manner in the whole placenta (Figures 8B, C) and in the placenta zones (Figures 9A–E, H). A reduced uteroplacental perfusion pressure (RUPP) mouse model for PE during pregnancy found that RUPP surgery on E14.5 resulted in altered proliferation and differentiation LZ trophoblast makers (Natale et al., 2018). At E16.5, there was an increase in trophoblast and endothelial proliferation markers within the LZ of RUPP placentas (Natale et al., 2018). The JZ of RUPP placentas had a constant trophoblast giant cell (TGC) population, shrinking spongiotrophoblast relative to placenta size, unlike controls which decreased their TGC population over gestation (Natale et al., 2018). It was proposed in this study that the

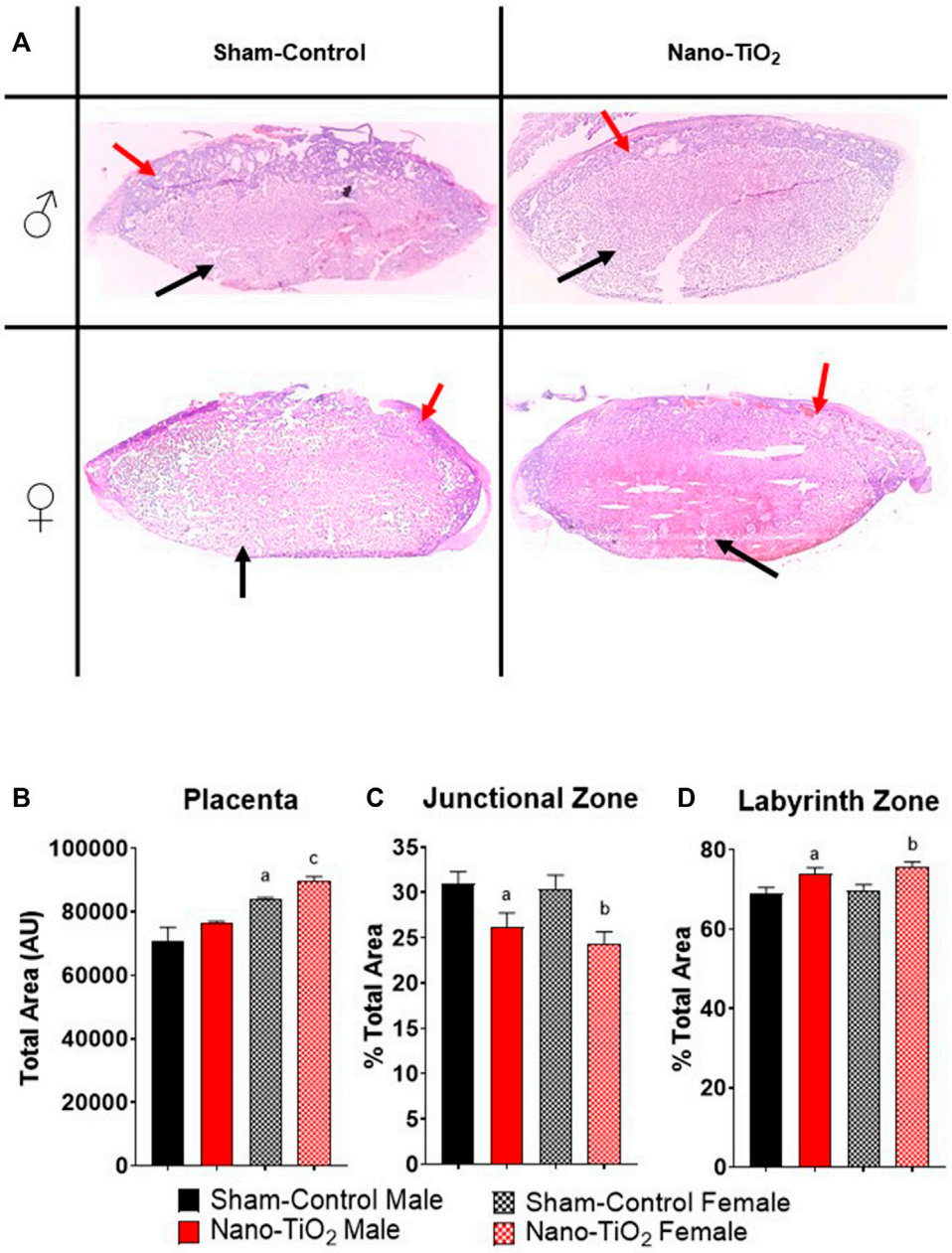

FIGURE 7
Placental Histology. Total placental zone areas were assessed after H&E staining to determine anatomical and structural differences after maternal nano-TiO_2 inhalation exposure. **(A)** Representative images of placenta histology are depicted for each group. **(B)** Total area of the placenta. **(C)** Percent total area of the junctional zone (JZ). **(D)** Percent total area of the labyrinth zone (LZ). Sham-control males (n = 5), sham-control females (n = 5), nano-TiO_2 males (n = 5), and nano-TiO_2 females (n = 5). a, $p \leq 0.05$ vs sham-control fetal male. b, $p \leq 0.05$ vs sham-control fetal female. c, $p \leq 0.05$ vs nano-TiO_2 fetal male.

altered trophoblast proliferation was due to hypoxic conditions, which has been demonstrated to trigger trophoblast proliferation *in vitro* (Caniggia et al., 2000; Natale et al., 2018). This is important because increased trophoblast proliferation, may indicate increased fetal blood space area (Natale et al., 2018), to help increase nutrient-waste exchange. The Hofbauer cell marker, CD163, has been shown to preferentially localize near fetal vessels and trophoblasts and are found within the placenta throughout the majority of gestation (Swieboda et al., 2020). Hofbauer cells are still not fully understood, but their function has been shown to be perturbed in diseases like chronic villitis or villitis of unknown etiology (VUE), in which proliferation of Hofbauer cells is seen (Reyes and Golos, 2018). In these disease states, the Hofbauer cells exhibit more inflammatory phenotypes, which is actually thought to cause more placental damage (Reyes and Golos, 2018). In this model, it is likely the trophoblast cells are increasing within the LZ, much like the Hofbauer cells, and both are functioning to compensate for the nutrient restriction and aid to preserve fetal life and growth. Our lab

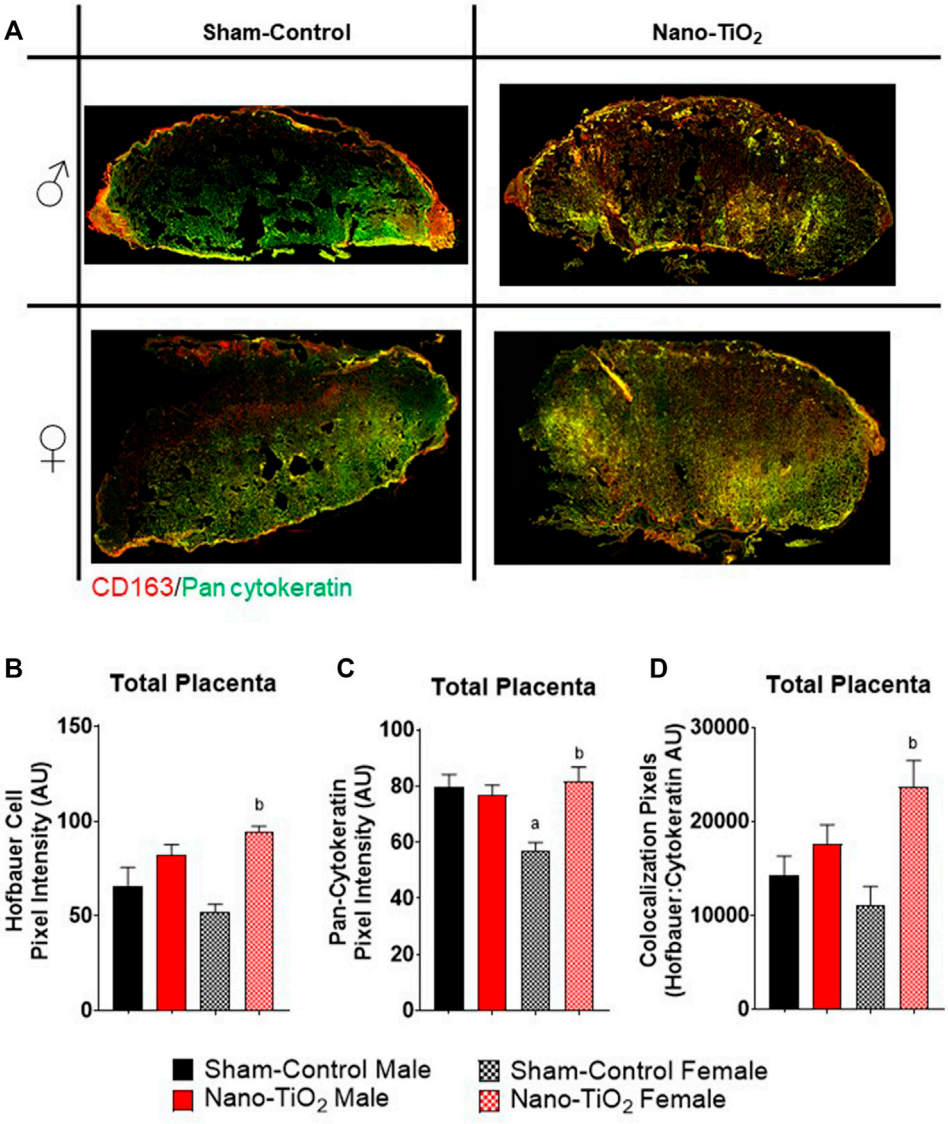

FIGURE 8
Whole Placental Immunohistochemistry. Total placental fluorescence intensity and colocalization of anti-CD163 and anti-pan cytokeratin was assessed after maternal nano-TiO_2 inhalation exposure. **(A)** Representative placental images for each group. **(B)** Total placental Hofbauer cell pixel intensity. **(C)** Total placental pan-cytokeratin pixel intensity. **(D)** Total placental colocalization of Hofbauer: Pan-cytokeratin. Sham-control males (n = 5), sham-control females (n = 5), nano-TiO_2 males (n = 5), and nano-TiO_2 females (n = 5). a, $p \leq 0.05$ vs sham-control fetal male. b, $p \leq 0.05$ vs sham-control fetal female.

has previously reported that gestational nano-TiO_2 inhalation exposure alters maternal uterine radial arteriole vascular reactivity (Bowdridge et al., 2019; Garner et al., 2022b; Griffith et al., 2022). Therefore, it is likely that the changes in fetal female JZ and LZ placenta mass and area are changing in response to the toxicant exposure and the upstream alterations that are occurring on the maternal side of the vasculature to preserve fetal life and growth.

Adaptations within the placental structure and cellular composition are not the only way that fetal life preservation can be achieved in perturbed uterine environments. The maternal side of the vasculature, such as the uterine radial arterioles, have been shown to have reduced vasoreactivity in the presence of vasoactive compounds like prostacyclin or thromboxane (Griffith et al., 2022). Additionally, the placentas from nano-TiO_2 exposed dams have increased reactive oxygen species production rate (Bowdridge et al., 2022). Increased reactive oxygen species, like H_2O_2, has been shown to increase TXB_2, the stable TXA_2 metabolite, production in hypertensive rat mesenteric arterioles (Gao and Lee, 2001). This study demonstrates that nano-TiO_2 exposed placentas also have modified placenta outflow in the presence of thromboxane agonist, U46619 (Figures 4C, D). Exposed fetal female placentas have decreased outflow pressure in the presence of U46619 compared to sham-control females and nano-TiO_2 fetal males. Understanding the importance of this requires understanding the fetoplacental unit and the flow of nutrient-waste exchange by the umbilical cord (Figure 10). The umbilical vein (outflow from the placenta)

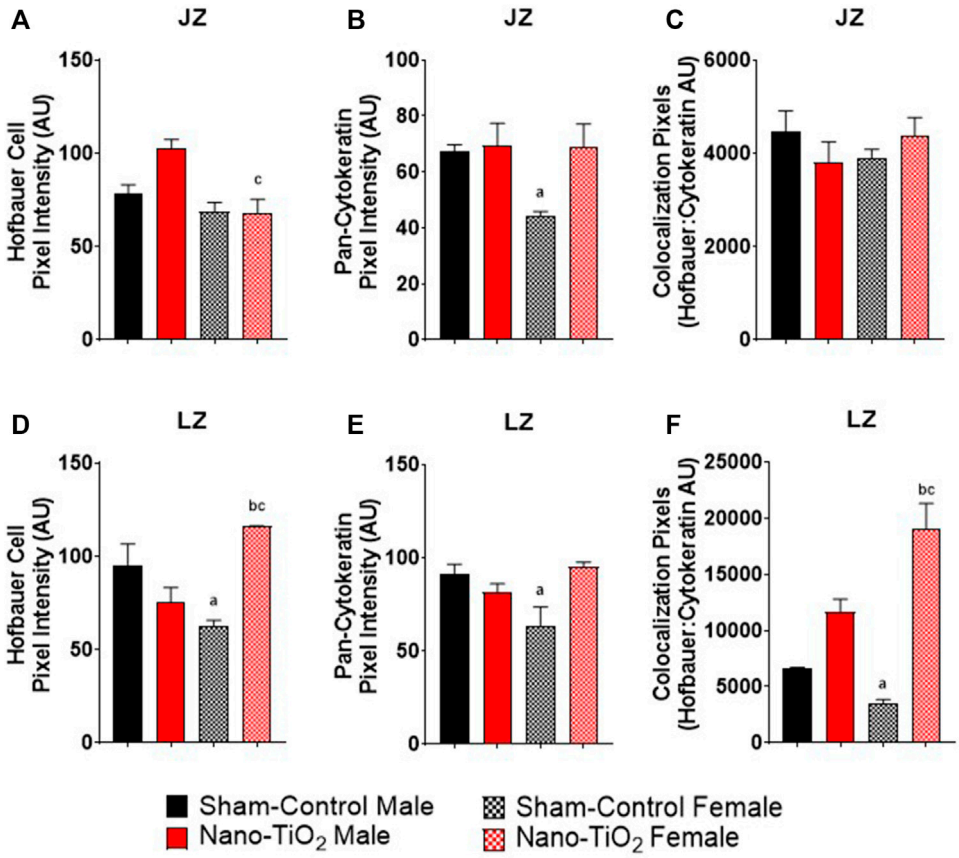

FIGURE 9
Placental Zone Immunohistochemistry. Placental fluorescence intensity and colocalization of anti-CD163 and anti-pan cytokeratin in each placenta zone. **(A)** Junctional zone (JZ) pixel intensity of anti-CD163 (Hofbauer cell). **(B)** JZ pixel intensity for pan-cytokeratin. **(C)** JZ colocalization for CD163: pan-cytokeratin. **(D)** Labyrinth zone (LZ) pixel intensity for Hofbauer cells. **(E)** LZ pixel intensity for pan-cytokeratin. **(F)** LZ colocalization for CD163: pan-cytokeratin. Sham-control males (n = 5), sham-control females (n = 5), nano-TiO_2 males (n = 5), and nano-TiO_2 females (n = 5). a, $p \leq 0.05$ vs sham-control fetal male. b, $p \leq 0.05$ vs sham-control fetal female. c, $p \leq 0.05$ vs nano-TiO_2 fetal male.

carries the nutrient-rich oxygenated blood to the fetus while the umbilical artery (inflow toward the placenta) carries deoxygenated, nutrient-deprived blood to the placenta (Wang and Zhao, 2010). With this in mind, ultrasound and doppler flow measurements visualize and record measurements of umbilical artery, in which greater flow from the fetus to the placenta reflects a healthier fetus, that utilizes more nutrients for increased metabolic processes, growth, and development (Wang and Zhao, 2010). In conjunction with this, reduced umbilical vein blood flow is associated with low fetal birthweight (Wang and Zhao, 2010). In this model, the exposed female placentas demonstrate a decreased outflow pressure in the presence of a highly vasoconstrictive compound, U46619. The decreased outflow pressure reflects elevated placenta resistance in the presence of U46619. It is possible that these placentas have adapted to decrease their responsiveness to TXA_2 to preserve fetal growth and ultimately prevent fetal death. Females are smaller at GD 20 (Griffith et al., 2022) (Figure 2A) and this same pattern of diminished growth persists up to 8-week (data not published). Additionally, adult females (~10–11 weeks of age) exposed to nano-TiO_2 *in utero* will also have smaller pups at GD 20 (Bowdridge et al., 2022) and have decreased plasma estrogen levels, which could be due to the decreased JZ area and mass seen in this study. In studies of mouse maternal nano-TiO_2 inhalation exposure during gestation we found that fetal hearts had decreased cardiac output and increased LV mass (Kunovac et al., 2019). Young adult mice from this same exposure paradigm demonstrated decreased systolic radial displacement (Hathaway et al., 2017), decreased ejection fraction and fractional shortening (Kunovac et al., 2019). This indicates that maternal exposure to nano-TiO_2 inhalation during gestation may cause fetal cardiac dysfunction that reaches into adulthood. As such, the fetal females from exposed dams are impacted to a greater extent, as shown by decreased fetal mass, decreased JZ area and mass, increased LZ area, and decreased outflow pressure in the presence of TXA_2 mimetic. These adaptations may be compensatory mechanisms in impacted females that support gestational survival, growth, and reproduction later in life.

In conclusion, this project sought to determine if maternal nano-TiO_2 inhalation exposure during gestation alters fetal growth, placental size, trophoblast invasion, and placental vasoactivity in a sexually dimorphic manner. Our exposure paradigm provides evidence that maternal nano-TiO_2 inhalation exposure had a greater, and lasting,

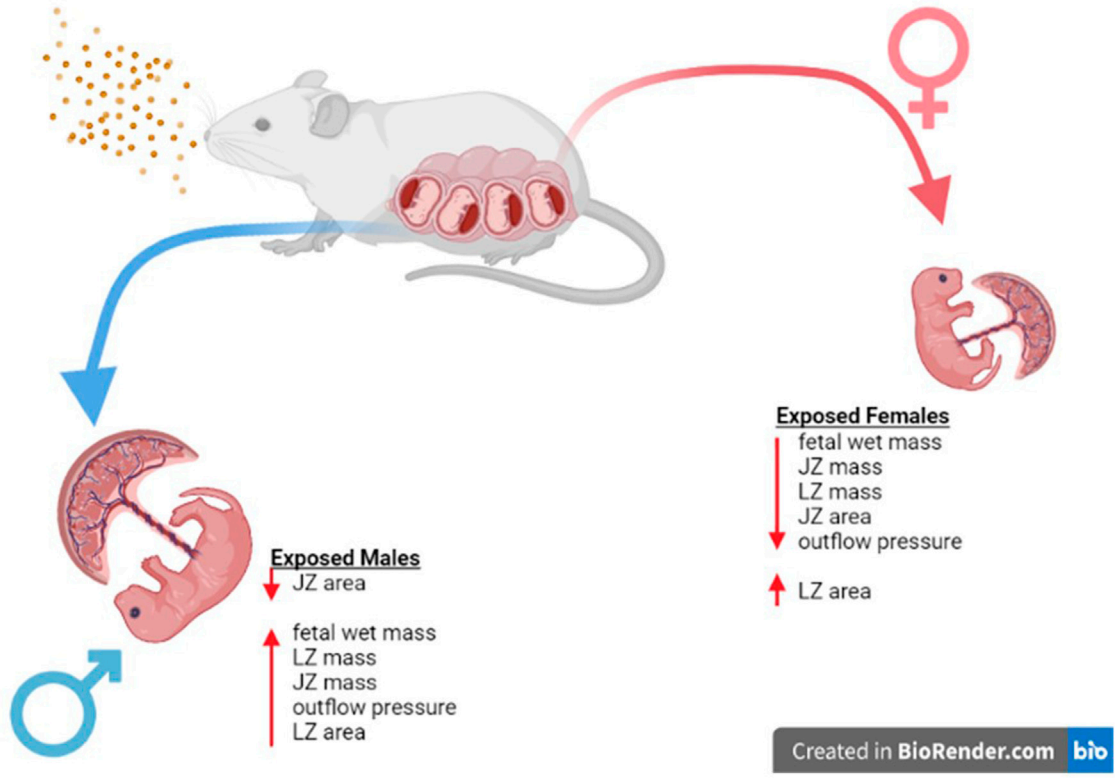

FIGURE 10
Sex Based Placental Outcomes Summary. Maternal nano-TiO_2 exposure during gestation results in sexually dimorphic outcomes in the placental and fetal tissue at GD 20. Females undergo more placental changes including decreases in mass (JZ and LZ) and area (JZ) when compared to males. These resulting changes may be responsible for the decreased fetal mass seen in females compared to their male counterparts at GD 20, and these changes have been shown to result in health deficits for the females into adulthood (Bowdridge et al., 2022).

impact on fetal females regarding mass, placental zone mass, zone area, as well as placental vasoactivity. The modifications reported may be physiological adaptations for the fetal females to guarantee survival after maternal nano-TiO_2 inhalation exposure, but at what cost? Future studies should investigate the impact of maternal nano-TiO_2 inhalation exposure on zone specific mechanisms: H_2O_2 levels, production of TXA_2 and PGI_2, and this interaction in a sexually dimorphic manner. This would clarify if H_2O_2 and redox metabolites are driving these changes seen based on fetal sex.

Data availability statement

The original contributions presented in the study are included in the article/Supplementary Material, further inquiries can be directed to the corresponding author.

Ethics statement

The animal study was reviewed and approved by West Virginia University Institutional Animal Care and Use Committee.

Author contributions

Study design, JG, EB, and TN. Data collection: JG, AD, ED, KS, KW, TB, and EB. Data analysis and interpretation, JG, AD and EB. Animal exposures, JG, AD, KE, TB, WG, KW, and EB. Manuscript draft, JG. Critical revisions and final decision to submit, all authors.

Funding

This work was supported by the following NIH sources: WV-CTSI U54 GM104942-05; K01 10029010 (ECB), P20GM103434 (WV-INBRE), R01 ES031253 (SH), R01 ES015022 (TRN), T32 AG 52375 (JAG), P20 GM103434 (WV-INBRE), T32 ES032920 (JAG).

Acknowledgments

The authors are grateful to Stan Hileman for his review comments on this article.

Conflict of interest

The authors declare that the research was conducted in the absence of any commercial or financial relationships that could be construed as a potential conflict of interest.

Publisher's note

All claims expressed in this article are solely those of the authors and do not necessarily represent those of their affiliated organizations, or those of the publisher, the editors and the reviewers. Any product that may be evaluated in this article, or claim that may be made by its manufacturer, is not guaranteed or endorsed by the publisher.

Supplementary material

The Supplementary Material for this article can be found online at: https://www.frontiersin.org/articles/10.3389/ftox.2023.1096173/full#supplementary-material

References

Abukabda, A. B., Bowdridge, E. C., McBride, C. R., Batchelor, T. P., Goldsmith, W. T., Garner, K. L., et al. (2019). Maternal titanium dioxide nanomaterial inhalation exposure compromises placental hemodynamics. *Toxicol. Appl. Pharmacol.* 367, 51–61. doi:10.1016/j.taap.2019.01.024

Aljunaidy, M. M., Morton, J. S., Cooke, C.-L., and Davidge, S. T. (2016). Maternal vascular responses to hypoxia in a rat model of intrauterine growth restriction. *Am. J. Physiol.-Regul. Integr. Comp. Physiol.* 311, R1068–R1075. doi:10.1152/ajpregu.00119.2016

Barker, D. J., and Martyn, C. N. (1992). The maternal and fetal origins of cardiovascular disease. *J. Epidemiol. Community Health* 46, 8–11. doi:10.1136/jech.46.1.8

Barker, D. J. (1990). The fetal and infant origins of adult disease. *BMJ* 301, 1111. doi:10.1136/bmj.301.6761.1111

Behlen, J. C., Lau, C. H., Li, Y., Dhagat, P., Stanley, J. A., Rodrigues Hoffman, A., et al. (2021). Gestational exposure to ultrafine particles reveals sex- and dose-specific changes in offspring birth outcomes, placental morphology, and gene networks. *Toxicol. Sci.* 184, 204–213. doi:10.1093/toxsci/kfab118

Belkacemi, L., Chen, C. H., Ross, M. G., and Desai, M. (2009). Increased placental apoptosis in maternal food restricted gestations: Role of the fas pathway. *Placenta* 30, 739–751. doi:10.1016/j.placenta.2009.06.003

Bowdridge, E. C., Abukabda, A. B., Engles, K. J., McBride, C. R., Batchelor, T. P., Goldsmith, W. T., et al. (2019). Maternal engineered nanomaterial inhalation during gestation disrupts vascular kisspeptin reactivity. *Toxicol. Sci. Off. J. Soc. Toxicol.* 169, 524–533. doi:10.1093/toxsci/kfz064

Bowdridge, E. C., DeVallance, E., Garner, K. L., Griffith, J. A., Schafner, K., Seaman, M., et al. (2022). Nano-titanium dioxide inhalation exposure during gestation drives redox dysregulation and vascular dysfunction across generations. *Part. Fibre Toxicol.* 19, 18. doi:10.1186/s12989-022-00457-y

Caniggia, I., Mostachfi, H., Winter, J., Gassmann, M., Lye, S. J., Kuliszewski, M., et al. (2000). Hypoxia-inducible factor-1 mediates the biological effects of oxygen on human trophoblast differentiation through TGFβ_3. *J. Clin. Invest.* 105, 577–587. doi:10.1172/JCI8316

Chaudhuri, G., Cuevas, J., Buga, G. M., and Ignarro, L. J. (1993). NO is more important than PGI2 in maintaining low vascular tone in feto-placental vessels. *Am. J. Physiol.* 265, H2036–H2043. doi:10.1152/ajpheart.1993.265.6.H2036

Coan, P. M., Vaughan, O. R., Sekita, Y., Finn, S. L., Burton, G. J., Constancia, M., et al. (2010). Adaptations in placental phenotype support fetal growth during undernutrition of pregnant mice. *J. Physiol.* 588, 527–538. doi:10.1113/jphysiol.2009.181214

Connor, K. L., Kibschull, M., Matysiak-Zablocki, E., Nguyen, T. T.-T. N., Matthews, S. G., Lye, S. J., et al. (2020). Maternal malnutrition impacts placental morphology and transporter expression: An origin for poor offspring growth. *J. Nutr. Biochem.* 78, 108329. doi:10.1016/j.jnutbio.2019.108329

Evers, I. M., de Valk, H. W., and Visser, G. H. A. (2009). Male predominance of congenital malformations in infants of women with type 1 diabetes. *Diabetes Care* 32, 1194–1195. doi:10.2337/dc09-0367

Gabory, A., Roseboom, T. J., Moore, T., Moore, L. G., and Junien, C. (2013). Placental contribution to the origins of sexual dimorphism in health and diseases: Sex chromosomes and epigenetics. *Biol. Sex. Differ.* 4, 5. doi:10.1186/2042-6410-4-5

Gao, Y. J., and Lee, R. M. K. W. (2001). Hydrogen peroxide induces a greater contraction in mesenteric arteries of spontaneously hypertensive rats through thromboxane A2 production. *Br. J. Pharmacol.* 134, 1639–1646. doi:10.1038/sj.bjp.0704420

García-Patterson, A., Aulinas, A., Sojo, L., Ginovart, G., Adelantado, J. M., de Leiva, A., et al. (2011). Poorer perinatal outcome in male newborns of women with pregestational diabetes mellitus. *Diabet. Med. J. Br. Diabet. Assoc.* 28, 436–439. doi:10.1111/j.1464-5491.2011.03227.x

Gårdebjer, E. M., Cuffe, J. S. M., Pantaleon, M., Wlodek, M. E., and Moritz, K. M. (2014). Periconceptional alcohol consumption causes fetal growth restriction and increases glycogen accumulation in the late gestation rat placenta. *Placenta* 35, 50–57. doi:10.1016/j.placenta.2013.10.008

Garner, K. L., Bowdridge, E. C., DeVallance, E., Griffith, J. A., Kelley, E. E., and Nurkiewicz, T. R. (2022a). Using the isolated rat placenta to assess fetoplacental hemodynamics. *Front. Toxicol.* 4, 814071. doi:10.3389/ftox.2022.814071

Garner, K. L., Bowdridge, E. C., Griffith, J. A., DeVallance, E., Seman, M. G., Engels, K. J., et al. (2022b). Maternal nanomaterial inhalation exposure: Critical gestational period in the uterine microcirculation is angiotensin II dependent. *Cardiovasc. Toxicol.* 22, 167–180. doi:10.1007/s12012-021-09712-8

Griffith, J. A., Garner, K. L., Bowdridge, E. C., DeVallance, E., Schafner, K. J., Engles, K. J., et al. (2022). Nanomaterial inhalation during pregnancy alters systemic vascular function in a cyclooxygenase-dependent manner. *Toxicol. Sci. Off. J. Soc. Toxicol. Kfac055.* 188, 219–233. doi:10.1093/toxsci/kfac055

Hathaway, Q. A., Nichols, C. E., Shepherd, D. L., Stapleton, P. A., McLaughlin, S. L., Stricker, J. C., et al. (2017). Maternal-engineered nanomaterial exposure disrupts progeny cardiac function and bioenergetics. *Am. J. Physiol.-Heart Circ. Physiol.* 312, H446–H458. doi:10.1152/ajpheart.00634.2016

Heinonen, I. H. A., Boushel, R., and Kalliokoski, K. K. (2016). The circulatory and metabolic responses to hypoxia in humans – with special reference to adipose tissue physiology and obesity. *Front. Endocrinol.* 7, 116. doi:10.3389/fendo.2016.00116

Kraemer, S. (2000). The fragile male. *BMJ* 321, 1609–1612. doi:10.1136/bmj.321.7276.1609

Kunovac, A., Hathaway, Q. A., Pinti, M. V., Goldsmith, W. T., Durr, A. J., Fink, G. K., et al. (2019). ROS promote epigenetic remodeling and cardiac dysfunction in offspring following maternal engineered nanomaterial (ENM) exposure. *Part. Fibre Toxicol.* 16, 24. doi:10.1186/s12989-019-0310-8

Laurin, J., Lingman, G., Marsál, K., and Persson, P. H. (1987). Fetal blood flow in pregnancies complicated by intrauterine growth retardation. *Obstet. Gynecol.* 69, 895–902.

Menendez-Castro, C., Rascher, W., and Hartner, A. (2018). Intrauterine growth restriction - impact on cardiovascular diseases later in life. *Mol. Cell. Pediatr.* 5, 4. doi:10.1186/s40348-018-0082-5

Miller, C. N., Dye, J. A., Henriquez, A. R., Stewart, E. J., Lavrich, K. S., Carswell, G. K., et al. (2020). Ozone-induced fetal growth restriction in rats is associated with sexually dimorphic placental and fetal metabolic adaptation. *Mol. Metab.* 42, 101094. doi:10.1016/j.molmet.2020.101094

Natale, B. V., Mehta, P., Vu, P., Schweitzer, C., Gustin, K., Kotadia, R., et al. (2018). Reduced Uteroplacental Perfusion Pressure (RUPP) causes altered trophoblast differentiation and pericyte reduction in the mouse placenta labyrinth. *Sci. Rep.* 8, 17162. doi:10.1038/s41598-018-35606-x

Nteeba, J., Varberg, K. M., Scott, R. L., Simon, M. E., Iqbal, K., and Soares, M. J. (2020). Poorly controlled diabetes mellitus alters placental structure, efficiency, and plasticity. *BMJ Open Diabetes Res. Care* 8, e001243. doi:10.1136/bmjdrc-2020-001243

Nurkiewicz, T. R., Porter, D. W., Hubbs, A. F., Cumpston, J. L., Chen, B. T., Frazer, D. G., et al. (2008). Nanoparticle inhalation augments particle-dependent systemic microvascular dysfunction. *Part. Fibre Toxicol.* 5, 1. doi:10.1186/1743-8977-5-1

Read, M. A., Leitch, I. M., Giles, W. B., Bisits, A. M., Boura, A. L., and Walters, W. A. (1999). U46619-mediated vasoconstriction of the fetal placental vasculature *in vitro* in normal and hypertensive pregnancies. *J. Hypertens.* 17, 389–396. doi:10.1097/00004872-199917030-00012

Reyes, L., and Golos, T. G. (2018). Hofbauer cells: Their role in healthy and complicated pregnancy. *Front. Immunol.* 9, 2628. doi:10.3389/fimmu.2018.02628

Rosario, G. X., Ain, R., Konno, T., and Soares, M. J. (2009). Intrauterine fate of invasive trophoblast cells. *Placenta* 30, 457–463. doi:10.1016/j.placenta.2009.02.008

Roseboom, T. J., Painter, R. C., de Rooij, S. R., van Abeelen, A. F. M., Veenendaal, M. V. E., Osmond, C., et al. (2011). Effects of famine on placental size and efficiency. *Placenta* 32, 395–399. doi:10.1016/j.placenta.2011.03.001

Schulz, L. C., Schlitt, J. M., Caesar, G., and Pennington, K. A. (2012). Leptin and the placental response to maternal food restriction during early pregnancy in mice. *Biol. Reprod.* 87, 120. doi:10.1095/biolreprod.112.103218

Sobrino, A., Oviedo, P. J., Novella, S., Laguna-Fernandez, A., Bueno, C., García-Pérez, M. A., et al. (2010). Estradiol selectively stimulates endothelial prostacyclin production through estrogen receptor-{alpha}. *J. Mol. Endocrinol.* 44, 237–246. doi:10.1677/JME-09-0112

Stapleton, P. A., Minarchick, V. C., Yi, J., Engels, K., McBride, C. R., and Nurkiewicz, T. R. (2013). Maternal engineered nanomaterial exposure and fetal microvascular function: Does the barker hypothesis apply? *Am. J. Obstet. Gynecol.* 209, 227.e1–227.11. doi:10.1016/j.ajog.2013.04.036

Stapleton, P. A., McBride, C. R., Yi, J., Abukabda, A. B., and Nurkiewicz, T. R. (2018). Estrous cycle-dependent modulation of *in vivo* microvascular dysfunction after nanomaterial inhalation. *Reprod. Toxicol. Elmsford N.* 78, 20–28. doi:10.1016/j.reprotox.2018.03.001

Stark, M. J., Dierkx, L., Clifton, V. L., and Wright, I. M. R. (2006). Alterations in the maternal peripheral microvascular response in pregnancies complicated by preeclampsia and the impact of fetal sex. *J. Soc. Gynecol. Investig.* 13, 573–578. doi:10.1016/j.jsgi.2006.06.006

Stark, M. J., Clifton, V. L., and Wright, I. M. R. (2009). Neonates born to mothers with preeclampsia exhibit sex-specific alterations in microvascular function. *Pediatr. Res.* 65, 292–295. doi:10.1203/PDR.0b013e318193edf1

Swieboda, D., Johnson, E. L., Beaver, J., Haddad, L., Enninga, E. A. L., Hathcock, M., et al. (2020). Baby's first macrophage: Temporal regulation of hofbauer cell phenotype influences ligand-mediated innate immune responses across gestation. *J. Immunol.* 204, 2380–2391. doi:10.4049/jimmunol.1901185

Thompson, L. P., Turan, S., and Aberdeen, G. W. (2020). Sex differences and the effects of intrauterine hypoxia on growth and *in vivo* heart function of fetal Guinea pigs. *Am. J. Physiol.-Regul. Integr. Comp. Physiol.* 319, R243–R254. doi:10.1152/ajpregu.00249.2019

Wang, Y., and Zhao, S. (2010). *Placental blood circulation, vascular biology of the placenta*. Morgan & Claypool Life Sciences.

Winterbottom, E. F., Koestler, D. C., Fei, D. L., Wika, E., Capobianco, A. J., Marsit, C. J., et al. (2017). The aquaglyceroporin AQP9 contributes to the sex-specific effects of *in utero* arsenic exposure on placental gene expression. *Environ. Health* 16, 59. doi:10.1186/s12940-017-0267-8

Xu, B., Chen, X., Ding, Y., Chen, C., Liu, T., and Zhang, H. (2020). Abnormal angiogenesis of placenta in progranulin-deficient mice. *Mol. Med. Rep.* 22, 3482–3492. doi:10.3892/mmr.2020.11438

Yi, J., Chen, B. T., Schwegler-Berry, D., Frazer, D., Castranova, V., McBride, C., et al. (2013). Whole-body nanoparticle aerosol inhalation exposures. *J. Vis. Exp.*, e50263. doi:10.3791/50263

frontiers | Frontiers in Toxicology

TYPE Review
PUBLISHED 14 April 2023
DOI 10.3389/ftox.2023.1178482

OPEN ACCESS

EDITED BY
Sijie Lin,
Tongji University, China

REVIEWED BY
Yue Jiang,
Tongji University, China
Guotao Peng,
Tongji University, China

*CORRESPONDENCE
Zhiling Guo,
z.guo@bham.ac.uk
Iseult Lynch,
i.lynch@bham.ac.uk

RECEIVED 02 March 2023
ACCEPTED 06 April 2023
PUBLISHED 14 April 2023

CITATION
Reilly K, Ellis L-JA, Davoudi HH, Supian S, Maia MT, Silva GH, Guo Z, Martinez DST and Lynch I (2023), Daphnia as a model organism to probe biological responses to nanomaterials—from individual to population effects via adverse outcome pathways.
Front. Toxicol. 5:1178482.
doi: 10.3389/ftox.2023.1178482

Daphnia as a model organism to probe biological responses to nanomaterials—from individual to population effects via adverse outcome pathways

Katie Reilly[1], Laura-Jayne A. Ellis[1], Hossein Hayat Davoudi[1], Suffeiya Supian[1], Marcella T. Maia[2], Gabriela H. Silva[2], Zhiling Guo[1]*, Diego Stéfani T. Martinez[2] and Iseult Lynch[1]*

[1]School of Geography, Earth and Environmental Sciences, University of Birmingham, Birmingham, United Kingdom, [2]Brazilian Nanotechnology National Laboratory (LNNano), Brazilian Center for Research in Energy and Materials (CNPEM), Campinas, Brazil

The importance of the cladoceran *Daphnia* as a model organism for ecotoxicity testing has been well-established since the 1980s. *Daphnia* have been increasingly used in standardised testing of chemicals as they are well characterised and show sensitivity to pollutants, making them an essential indicator species for environmental stress. The mapping of the genomes of *D. pulex* in 2012 and *D. magna* in 2017 further consolidated their utility for ecotoxicity testing, including demonstrating the responsiveness of the *Daphnia* genome to environmental stressors. The short lifecycle and parthenogenetic reproduction make *Daphnia* useful for assessment of developmental toxicity and adaption to stress. The emergence of nanomaterials (NMs) and their safety assessment has introduced some challenges to the use of standard toxicity tests which were developed for soluble chemicals. NMs have enormous reactive surface areas resulting in dynamic interactions with dissolved organic carbon, proteins and other biomolecules in their surroundings leading to a myriad of physical, chemical, biological, and macromolecular transformations of the NMs and thus changes in their bioavailability to, and impacts on, daphnids. However, NM safety assessments are also driving innovations in our approaches to toxicity testing, for both chemicals and other emerging contaminants such as microplastics (MPs). These advances include establishing more realistic environmental exposures via medium composition tuning including pre-conditioning by the organisms to provide relevant biomolecules as background, development of microfluidics approaches to mimic environmental flow conditions typical in streams, utilisation of field daphnids cultured in the lab to assess adaption and impacts of pre-exposure to pollution gradients, and of course development of mechanistic insights to connect the first encounter with NMs or MPs to an adverse

Abbreviations: AOPs, adverse outcome pathways; CAT, catalase; CB, carbon black; CNT, carbon nanotube; DEB, Dynamic Energy Budgets; EPS, extracellular polymeric substances; FAIR, Findable, Accessible, Interoperable, Re-usable; GPx, glutathione peroxidase; GST, glutathione-s-transferase; KEs, key events; MDA, malondialdehyde; MIE, molecular initiating event; MOA, mechanism/mode of action; MP(s), microplastic(s); NM, nanomaterial(s); NOM, natural organic matter; QD, quantum dot; ROS, reactive oxygen species; SOD, Superoxide dismutase; TEM, Transmission electron microscopy; TK-TD, Toxicokinetic-Toxicodynamic.

outcome, via the key events in an adverse outcome pathway. Insights into these developments are presented below to inspire further advances and utilisation of these important organisms as part of an overall environmental risk assessment of NMs and MPs impacts, including in mixture exposure scenarios.

KEYWORDS

ecotoxicity, high throughput, microfluidics, nanosafety assessment, standardised testing, nanomaterials (A)

1 Introduction

The zooplankton cladoceran *Daphnia* has captivated biologists for centuries because of its importance in aquatic ecosystems, and its flexibility to cope with, and respond to, environmental stressors. *Daphnia* are a well-established and widely used model organism for freshwater toxicity testing as they are well characterised, have a rapid parthenogenetic reproductive cycle and show sensitivity to a range of environmental xenobiotics. *Daphnia* are also a non-sentient species, meaning that their use in toxicity testing is considered acceptable as a strategy for the reduction, replacement and refinement (NC3Rs) of traditional animal testing, making them an optimal model in ecotoxicology (Colbourne et al., 2022; NC3Rs, 2022). A broad set of behavioural and morphological changes can be observed in *Daphnia* when exposed to environmental stimuli, which forms the foundation of the defined and standardised protocols for chemical toxicity testing, such as the OECD 202 (Acute toxicity) and 211 (Reproduction) tests and the EPA testing of chemicals (OECD, 2004; OECD, 2012; Maxwell et al., 2014). Endpoints evaluated encompass responses such as immobilisation and lethality, which are measured in the acute immobilisation tests in the OECD 202 assay. Changes in life history traits during the chronic test (OECD 211) are also measured, including reproductive changes (such as an increase or decrease in the number of neonates per adult daphnid, or a delay between broods), and growth trends. Further to the standard test end points, phenotypic changes can be observed such as additional spines on the helmet, variability in lipid deposits and behavioural changes such as swimming activity (Colbourne et al., 2011; Chevalier et al., 2015; Karatzas et al., 2020; Tkaczyk et al., 2021). Due to the historic use of *Daphnia* for chemical testing, they are also an optimal model organism for testing challenging and emerging toxicants such as nanomaterials (NMs) and microplastics (MPs) (Nasser and Lynch, 2019; Zimmermann et al., 2020).

NMs, as described by the European Commission, have at least one dimension less than 100 nm (European Commission. Joint Research Centre, 2020). NMs exist in the environment from a range of sources, including naturally occurring (e.g., volcanic ash), incidental particles formed as a result of human activities (e.g., combustion particles, secondary MPs) or can be engineered/manufactured by industry at the nanoscale to exploit specific properties (Jeevanandam et al., 2018). During synthesis, NMs are normally coated with ligands to control their size and limit their agglomeration (Buesser and Pratsinis, 2012). They are distinguished from other non-nanoscale materials by their unique physico-chemical properties (Haase and Lynch, 2018). Being small in size, NMs have a larger surface areas per unit mass than bigger particles, which makes them highly reactive and more dynamic in environmental systems, giving them the ability to interact with different molecules and biological systems (Rosenkranz et al., 2009; Markiewicz et al., 2018; Nasser et al., 2020) which can transform their original identity (Lowry et al., 2012; Spurgeon et al., 2020).

MPs are a significant environmental concern due to their ubiquitous presence, increased biological interactions (compared to macroscale plastic) and difficulties in sampling. Although the size classification of microplastic is often discussed within the literature, the most frequently used definition of MPs is the National Oceanic and Atmospheric Administration (NOAA) definition of less than 5 mm (NOAA, 2023), but discussions within the research community are underway to re-evaluate this in line with the advanced analytical methods now being developed and implemented (Hartmann et al., 2019). MP are also often reported by morphology, categorised as beads or spheres, fibres and fibre bundles, pellets, film, foam or fragments and are introduced into the environment as either primary or secondary plastic (Rochman et al., 2019).

In theory, the considerations applied to NMs for ecotoxicity testing can also be applied to MPs, as the physical interactions and surface conditioning of MPs will also occur in their local environments. Although a relatively emerging field, *Daphnia* have already been used for a range of MP toxicity studies to date, to elucidate the potential impacts that MPs induce in freshwater environments (Nasser and Lynch, 2016; Schür et al., 2020; Zimmermann et al., 2020; Kelpsiene et al., 2022).

Nanomaterials and microplastics are challenging toxicants to assess due to their physical nature and the surface area of the particles, which makes them an interesting lens from which to review the development in the field of ecotoxicology. *Daphnia* are a fantastic model for toxicity assessment due to their filter feeding mechanism which means that particle uptake is highly likely, and their transparent bodies then enables a range of optical methods to be applied and developed to quantify the uptake of the physical toxicants, which in turn leads to novel approaches compared to those available for assessment of toxicity of the soluble chemicals that have historically been assessed (Nasser and Lynch, 2019). The particle surface also poses an interesting aspect of the ecotoxicological assessment; the surface of the particles is dynamic and will be affected by the local environment including by biomolecules released by the *Daphnia*, leading to a more changeable and complex relationship between the toxicant and model organism than that for soluble chemicals (Wheeler et al., 2021; Reilly et al., 2022). These dynamic surface-driven properties, which are shared between microplastics and nanomaterials, have enabled interesting developments across the field of ecotoxicology, leading to the development of techniques for assessing *in situ* transformations and eco-corona evolution. Technological

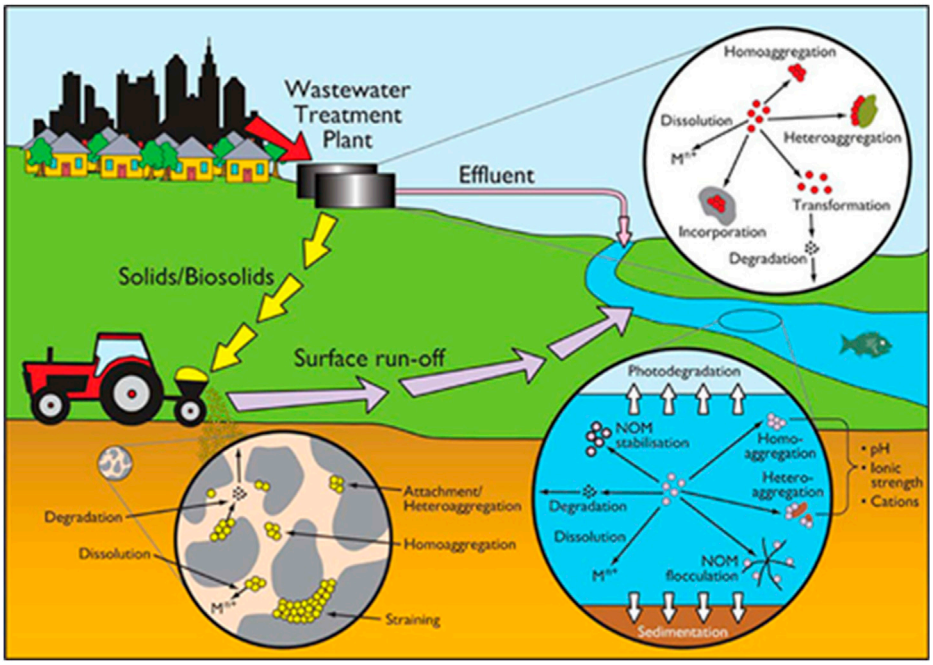

FIGURE 1
Transformation processes of NMs in the environment. Reproduced from (Batley et al., 2013) with permission from ACS Publications.

advances such as lab on a chip (Section 7) and conceptual frameworks for identification of key (molecular) events that contribute to adverse outcome pathways (Section 6) provide exciting avenues for further research and development (Mortensen et al., 2022).

2 Nanomaterial transformations in the environment and the role of *Daphnia*

When NMs are released into the environment, they interact with many environmental components and go through various dynamic transformation processes which can change their physico-chemical properties (Abbas et al., 2020; Malakar et al., 2021; Wheeler et al., 2021), and significantly impact their toxicity, reactivity, fate and transport in both environmental and biological systems (Ellis and Lynch, 2020; Wheeler et al., 2021; Reilly et al., 2022). Transformation processes such as adsorption of molecules/ions and macromolecules, agglomeration, oxidation/reduction (redox) reactions, sulfidation and dissolution all occur in biological and environmental systems and can greatly affect the behaviour of NMs (Lowry et al., 2012; Spurgeon et al., 2020). The physicochemical transformation of NMs under different environmental conditions are driven by several variables such as ionic strength, kinetics, pH, stability, synthesis method, valency, capping agent, and cation type (Mitrano et al., 2015; Louie et al., 2016; Goswami et al., 2017). To understand how NMs behave in ecosystems and to determine their toxicity and fate, we must first understand the life cycle and mechanism of NMs transformation processes upon their release into environmental compartments and their interaction with the surrounding environmental components (Figure 1).

2.1 Chemical transformations

Dissolution is a key chemical transformation process driven by the release of water-soluble molecules or ions from NMs. The equilibrium solubility (amount of dissolved matter) and the kinetics of particle dissolution (rate of solubility) of NMs will affect their toxicity, behaviour and environmental fate. In general, NMs that readily dissolve were more toxic than poorly soluble NMs, as once bioaccumulated in organisms they undergo rapid dissolution, leading to oxidative stress from the release of reactive oxygen species (ROS) via a so-called trojan horse mechanism. Sulfidation is a major transformation process for many metal NMs, particularly when enhanced concentrations of sulfide are present, such as the ones found in sub-oxic or anoxic sediments or in some parts of wastewater treatment plants (Lead et al., 2018). Sulfidation can reduce solubility, and change particle size and surface charge of NMs and in most studies, the sulfidation of NMs reduces their toxicity (Devi et al., 2015; Starnes et al., 2015). Photochemically induced reactions are another main driver of NM transformation, including photolysis, photo-oxidation and photo-catalysis, with sunlight playing an important role in the dissolution of NMs (Goswami et al., 2017; Kansara et al., 2022; Xu et al., 2023).

2.2 Physical transformations

The physical transformation of NMs leads to alterations in their stability when interacting with environmental components, due to changes in the local ionic strength and pH or due to interactions with sediments and NOM, and are affected by other physical

parameters such as sunlight exposure and temperature (Kansara et al., 2022). Agglomeration and sedimentation/deposition are the main physical transformation processes that NMs undergo once released into the environment (Abbas et al., 2020). Agglomerates are particle clusters held together by electrostatic reactions or chemical bonds, they cluster together due to the attractive forces between particles, and this can occur during use, production, storage or upon release of NMs into the environment (Hartmann et al., 2014). The surface area to volume ratio, and thus NMs reactivity, is reduced by the agglomeration process, which will affect their toxicity, transport in porous media, reactivity, sedimentation and uptake by organisms (Lowry et al., 2012). Lead et al. (2018) demonstrated in their review that although many studies showed that agglomeration usually reduces the bioavailability of NMs, however, in some cases it can enhance bioaccumulation by increasing the ingestion rate or by making the particles size more accessible (Martinez et al., 2022). Abbas et al. (2020) also highlighted that at realistic environmental concentrations, homoagglomeration (single NMs only) was proven to be quantitatively unimportant, suggesting that heteroagglomeration (mixture of NMs/particle types) could be more important due to the higher environmental concentrations of natural colloids such as clay. Agglomeration leads to a reduction in NMs number concentration in water or soil suspensions favouring the deposition of agglomerated large particles (Abbas et al., 2020). Larger, denser, particles tend to settle faster than smaller particles and therefore gravitational settling will reduce NM migration (Hartmann et al., 2014; Yin et al., 2015; Giorgi et al., 2021).

2.3 Biological and macromolecular NM transformations

The major biologically mediated transformation processes that NMs undergo upon their release into natural environments are eco/bio-corona interactions and biodegradation (Abbas et al., 2020). Biomolecules are readily adsorbed onto NM surfaces in ecosystems, and NMs that are taken up by biological organisms can be transformed upon their interaction with biomolecules (Lowry et al., 2012; Xu et al., 2023). Additionally, metal ions can be transformed into NMs due to the presence of functional groups and reductive enzymes, for example, metal ions can be transformed into their corresponding NMs by a reducing agent, such as ascorbic acid ($C_6H_8O_6$), which occurs naturally (Abbas et al., 2020).

The process of biodegradation is driven by the ability of microorganisms to decompose an organic substance. The interaction of NMs with microbes, extracellular polymeric substances (EPS) and extracellular enzymes determines their relative significance and rate of the biodegradation processes. Biodegradation of NMs core components and surface coatings is a possible transformation pathway of NMs in surrounding environments, particularly for carbon-based NMs including fullerene and carbon nanotubes (CNTs) (Abbas et al., 2020). The biodegradation of organic surface coatings is relevant to all types of manufactured NMs and to MPs, and the gut microbiota of aquatic organisms are likely to play a key role (Nasser et al., 2020). Biomodification is an additional process that can affect the fate and toxicity of NMs, which includes processes that are indirectly mediated by organisms after NMs are taken up by the organisms (Kelpsiene et al., 2022).

In natural environments organisms such as *Daphnia* produce and secrete a variety of tissue extracts that contain biomolecules (e.g., proteins and polysaccharides). These secreted biomolecules can form coronas on NMs and MPs as the biomolecules adsorb onto the surface of the particles. These coronas are dynamic in nature, and result from the adsorption of different types of available proteins, metabolites and polysaccharides, which also exchange between bound and free forms (Westmeier et al., 2016; Grintzalis et al., 2019; Kelpsiene et al., 2022). Environmental and biological constitutes that have a molecular weights spanning from 10 to 2,000,000 Da adsorb onto NMs surfaces forming the eco-corona, and affecting the stability, identity, uptake and toxicity of NMs towards *Daphnia* (Nasser et al., 2020). The adsorbed proteins can also facilitate NMs entry into cells through the receptor-mediated endocytosis process (Lowry et al., 2012). Furthermore, identifying proteins present on the surface of NMs can provide important insights into their biological interactions, including uptake and which mechanistic pathways are induced by NM exposures as part of an ecotoxicity assessment (Ellis and Lynch, 2020; Wheeler et al., 2021). Naturally occurring biomolecules (e.g., natural organic matter (NOM), humic substances) also play a major and similar role when interacting with NMs. Therefore, the fate and behaviour of NMs is highly dependent on understanding the characteristics of these macromolecular processes. Interactions with NOM and macromolecules can increase NMs persistence in aquatic systems (Wang et al., 2016).

2.4 Environmental testing conditions—bridging the gap between field and laboratory

Current guidelines for NMs ecotoxicology tests do not prioritise the use environmentally transformed NMs in environmentally representative waters, for example, natural waters that are complex matrices containing natural organic matter and other biopolymers, the concentrations and compositions of which go through various environmental changes which can impact the physiochemical properties and toxicity of the NMs they interact with. Estimates for NM toxicity based on simplified salt only media thus under or over-estimate the impacts of NMs by not testing the appropriate NMs forms (Selck et al., 2016; Ouyang et al., 2022). To allow for comparisons between toxicity studies, the Organisation for Cooperation and Development (OECD) promotes the use of a fully defined testing medium for exposures in ecotoxicity testing. As with many biological elements, there is a narrow concentration range between deficiency and toxicity of key elements which needs to be carefully considered, as the testing medium needs to be suitable for the test species (i.e., both algae and *Daphnia* during chronic testing). Medium composition can also impact the toxicant in question, for example, when testing metal toxicity, it is important to ensure there are no chelating agents, such as EDTA, present that would react with the metals and therefore change the metal bioavailability during the exposure. Media such as the OECD 'M4' and 'M7' can be modified by removing the EDTA, or an alternative medium can be used that contains no chelating agents (OECD, 2004).

The OECD 202 and 211 tests (along with most current test guidelines) were designed for testing of chemical toxicants, and as such, modification of medium for emerging pollutants such as NMs and MPs, with their large reactive surfaces, and more environmentally realistic testing scenarios is needed (Giusti et al., 2019; Ellis et al., 2020a; Nasser et al., 2020). This includes the potential addition of NOM, which is the decaying plant and animal matter present in natural waters and soils, and has been described as containing varying fractions of humic acids, fulvic acids, polymeric substances and a hydrophilic fraction, and which has been widely reported to have strong absorption to colloidal materials (Afshinnia et al., 2018; Tayyebi Sabet Khomami et al., 2020), or the use of medium conditioned by pre-filtration through *Daphnia* guts (or other relevant organisms used for toxicity testing, including oysters, worms, etc.) which is often termed "conditioned medium," for example, (Nasser and Lynch, 2016). Although the addition of NOM is not recommended by the OECD due to its heterogenous nature, NOM can act as a stabiliser for NMs within the testing medium, preventing agglomeration of the NMs and therefore maintaining the bioavailable fraction. On the other hand, NOM can sorb chemicals in test solutions which can ultimately affect the fate and bioavailability of the toxicants within the test solutions by decreasing the concentration in the dissolved phase and changing the exposure pathway. The addition or exclusion of NOM is therefore test dependent and should be considered during the toxicity test design stage.

Given the role of standardised tests in ranking the toxicity of chemicals, including NMs and MPs, as well as the use of data from *Daphnia* toxicity assays for environmental modelling and establishment of threshold levels for pollutants, a deeper understanding of the inherent variability in the test systems is needed. Similarly, the standardised test media has been developed to optimise the test population health, which does not take into consideration any deficiencies in species health or fitness that occur due to natural environmental variation and adaption to the environment. Utilisation of laboratory cultured daphnids, whose conditions are optimised for health and fitness and where there is no competition for food and no predation, could mean that we underestimate the potential toxicity of chemicals to real environmental populations, especially when looking at sublethal toxicity markers such as growth and reproduction due to the lack of variability in other parameters such as temperature and food availability. However, examples emerging in the literature are showing that the "as engineered pristine" NM have fewer toxic consequences in environmentally realistic medium compared to the standard culture media used in standard toxicity testing (Schultz et al., 2018; Ellis and Lynch, 2020; Schultz et al., 2020). Thus, standardised *Daphnia* tests following the OECD protocols overestimate NMs toxicity, which can be resolved through using environmentally transformed NMs in representative natural water compositions (Nasser and Lynch, 2019; Ellis and Lynch, 2020; Nasser et al., 2020). Conversely, wild daphnids from the field are believed by aquatic toxicologists to have a higher resistance towards pollution compared to *Daphnia* that have been cultured in the laboratory over long periods (Abdullahi et al., 2022; Eastwood et al., 2022). This is due to the exposure of wild *Daphnia* to a much wider range of natural stressors than their lab-cultured equivalents where conditions are closely controlled, leading the wild daphnids to have resistance towards pollutants, decrease of water quality and competition for a limited of food supply, resulting in a greater overall "fitness" and ability to survive in changing environments (Barata et al., 2000). Taking this into consideration, a precautionary approach should be applied when applying lab observations to field studies and *vice versa*.

According to Brans et al. (2018), human-induced and natural stressors induce changes in energy metabolism and stress physiology in populations of a wide array of species. Urbanization is a pervasive process with 476,000 ha of arable land are lost annually by the expansion of urban areas (World Resources Institute, 1996; Grimm et al., 2008). Urbanization alters both biotic and abiotic ecosystem properties within and surrounding the urban centre (Miles et al., 2019; Ruas et al., 2022). Differential selection of stress-coping mechanisms results from stressful environments like those found in cities. For instance, city ponds are exposed to the urban heat island effect and receive polluted run-off, with the result that several stressors may act together and affect the life traits of organisms inhabiting these ecosystems, which might acquire genetic differentiation for physiological traits enabling them to cope better with higher overall stress levels (Pavlaki et al., 2014). Evidence from 62 *Daphnia* genotypes from replicated urban and rural populations in garden ponds revealed that urban *Daphnia* have significantly higher concentrations of total body fat, proteins and sugars than their rural counterparts (Brans et al., 2018) highlighting that environmental conditions contribute to *Daphnia* fitness. This can be further explored through study of acclimation, also called adaptation, resistance, or tolerance, which has been defined as the ability of organisms to cope with stress, either natural such as temperature changes, salinity variation, oxygen level fluctuations, and plant toxins or chemicals arising from anthropogenic inputs of many different classes of contaminants into the environment (Biagianti-Risbourg et al., 2013; Akbar et al., 2022). The capacity of physiological adaptation or acclimation toward a stressor is related to the stress syndrome. Physiological acclimation to toxicant conditions also depletes energy reserve levels (Biagianti-Risbourg et al., 2013). For example, in *Daphnia* organisms pre-exposed to zinc (and having acquired a tolerance toward this metal) did not mobilize their energy reserves further following a laboratory exposure to zinc (0.1 and 1.0 μM) compared with non-exposed animals (Canli, 2005).

Therefore, the culturing history of the *Daphnia*, or other test species, in addition to the environmental conditioning of the NMs or MPs in the exposure medium can have a significant impact on the toxicity response and the overall impact on the ecosystem, and this should be considered at the test design stage to determine the adequate levels of comparability and environmental relevance of the exposure.

3 The development of *Daphnia* as a model organism: lifecycle, reproduction and multigenerational approaches

One of the most important issues to address in toxicological testing is how exposure, whether it be acute or chronic, impacts the organism and the subsequent effects to their offspring. When environmental conditions deteriorate, for example, due to an

TABLE 1 Recommended conditions for optimal culture growth of *Daphnia* as outlined in the OECD test guideline for acute toxicity (OECD 202).

Factor	Optimal range
pH	6–9
Temperature	18–22°C
Dissolved oxygen	>6 mg/L, ideally at saturation
Water Hardness	140–250 mg $CaCO_3$/L
Light/dark cycle	16 light/8 dark

influx of environmental pollution or predator stress, daphnids can develop different phenotypes and can switch from clonal to sexual reproduction (Colbourne et al., 2011; Eastwood et al., 2022).

Under favourable environmental conditions (e.g., within the optimal range shown in Table 1), *Daphnia* reproduce parthenogenetically (clonally). Parthenogenesis is a type of asexual reproduction in which the offspring develops from unfertilized eggs. Female *Daphnia* produce genetically identical daughter clones, which are released from the brood pouch as neonates (Ebert, 2005). The reproduction process continues while the environmental conditions continue to support their growth. *Daphnia* can change to sexual reproduction under stressful conditions, such as overcrowding, low food, toxicant exposures or variations in abiotic factors such as temperature and pH (Alekseev and Lampert, 2001; Abdullahi et al., 2022). This results in the development of ephippia, or resting eggs, that can remain dormant in the sediment for long periods of time (years) and may hatch when conditions improve (Eastwood et al., 2022).

As a consequence of NMs induced stress, the genetic processes are altered, which can be easily monitored by identification of epigenetic (heritable from one generation to the next) changes in subsequent generations. These changes are due to modifications of the histone proteins of chromatin and DNA methylation, which results in altered gene expression (Feil and Fraga, 2012). This makes *Daphnia* an ideal model organism for studying the effects of NM toxicity, as epigenetic developmental programs can be used to monitor the effects in the offspring as hereditary traits (Asselman et al., 2017). Having the ability to monitor the offspring after NM parental exposure provides invaluable information regarding the molecular events that occur for survival, growth, reproduction, and adaptation to change (Abdullahi et al., 2022).

An advantage of using multiple generations that follow a germline after parental exposure, is that the genes expressed at an early stage of exposure might not be the same genes as those directly associated with phenotypic effects over a chronic exposure time scale. Therefore, capturing the phenotypical events in the offspring will also identify the longer-term causable effects (van Straalen and Feder, 2012). Multigenerational studies also help to demonstrate how maternal effects of exposure to what is considered a sub lethal concentration, results in a trade-off between growth, reproduction, and survivorship over all generations, which ultimately defines the natural selection of the strongest surviving daphnids.

Several multigenerational studies using *Daphnia*, in the presence of either chemical or NM exposure have each reported an increased toxic effect in the immediate post-parental exposure generations compared to the exposed parental generation (Arndt et al., 2014; Jeong et al., 2016; Kim H. Y. et al., 2017; Ellis et al., 2020b). A study investigating the species difference between *D. magna*, *pulex* and *galeata* over five generations exposed to silver nanoparticles demonstrated that NM exposure had the most negative effects on the first generations, with notable changes between increased toxicity and tolerance in the subsequent generations (Völker et al., 2013). The altered toxicity in the latter generations provides evidence that the ecological risk and safety assessments underestimate NM toxicity using only single generation acute and chronic tests. Ellis et al. (2020b) also identified that the transgenerational responses of multiple germlines showed a direct link with maternal exposure time to 'sub-lethal' effect concentrations of NMs (identified from standard OECD acute toxicity tests which chronically presented as lethal) including increased survival and production of males for sexual reproduction in the subsequent germlines (Ellis et al., 2020b). Multigenerational studies using only pristine engineered NMs have manifested adverse toxicological outcomes in multiple generations post maternal exposure to *Daphnia* that could not have been predicted from the single standard 1-generation reproductive studies (Ellis et al., 2020b; Ellis and Lynch, 2020; Karatzas et al., 2020). Collectively, the research demonstrates the importance of updating standard toxicity testing to reflect scientific advances and increase trust in regulation by monitoring the effects in the transgenerational germlines (Jeong et al., 2016; Ellis et al., 2020b; Nederstigt et al., 2022).

4 Feeding behaviour of daphnids and bioaccumulation potential of NM

Daphnia are filter-feeders that have the ability to ingest particulates of up to 50 µm in size through mechanical sieving mechanisms (Geller and Müller, 1981). *Daphnia* mainly feed on phytoplankton, such as green algae (considered as a high-quality food, such as *Scenedesmus* sp.), bacteria and organic detritus (considered as a low-quality food). However, their non-selectivity in the uptake process increases the bioaccumulation of environmentally unfriendly materials along the higher trophic levels (Schwarzenberger and Fink, 2018). Therefore, *Daphnia* are likely recipients of contaminants, including NMs and MPs and, as primary consumers, they are vital for energy transfer in the food chain (Martinez et al., 2022; Yin et al., 2023).

4.1 Nano-intestinal interactions and gut chemistry

The gut luminal chemistry is of particular interest to comprehend the fate and adverse effects of NMs on the organism after NM ingestion. The pH (6.8–7.2), ionic strength (e.g., Na^+, Ca^{2+}, and Mg^{2+}), the presence of NOM, the cuticle chemistry, and redox chemistry are factors that interfere in the absorption of particulates in the gut, and they act as barriers in NMs exposure during uptake from the gut into the tissue (Van Der Zande et al., 2020). From the external environment to the gut, NMs are likely to acquire an eco-corona which is generally

TABLE 2 Effects of exposure of *D. magna* to NMs on the activity and/or expression of antioxidant and digestive enzymes.

NMs	Dose (mg L^{-1})	Co-exposure with	Exposure time (days)	Antioxidant enzymes		Digestive enzymes		EC_{50}/LC_{50} (mg L^{-1})	References
				With effect	No effect	With effect	No effect		
TiO_2	0, 1, 5, 10	-	2	↑CAT, GST, GPX	SOD	-	-	Non-toxic	Kim et al. (2010)
TiO_2[b]	1	-	2	↑CAT	SOD	↓esterase	cellulase, trypsin, amylase	-	Fouqueray et al. (2012)
			21	-	CAT, SOD	↓trypsin, amylase, esterase	cellulase	-	
	1.10^{-2}	-	2	-	CAT, SOD	↓amylase	cellulase, trypsin, esterase	-	
			21	-	SOD, CAT	↓amylase, esterase	cellulase, trypsin	-	
C_{60}	0, 5, 20	-	1	↑SOD	-	↓trypsin, amylase, cellulase, b-galactosidase	-	-	Lv et al. (2017)
			2	↑SOD	-	-	-	-	
			3	↓SOD	-	-	-	14.9 ± 1.2/ 16.3 ± 0.8	
MPA -Au	1	-	1	↑GST	CAT	-	-	Non-toxic[c]	Qiu et al. (2015)
			21	↓CAT	GST			Non-toxic	
PAH -Au	5.10^{-3}	-	1	-	GST, CAT	-	-	-	
			21	-	GST, CAT			Toxic	
MPA -Au	5.10^{-2}	-	1	-	GST, CAT	-	-	Non-toxic[c]	Dominguez et al. (2015)
	1.10^{-2}			↑CAT	GST				
PAH -Au	5.10^{-2}	-	1	↑GST	CAT	-	-	Toxic[c]	
	1.10^{-2}			↑CAT	GST				
TiO_2	2	Cu^{2+}	3	↑↓CAT, SOD, ↓Na^+/K^+ ATPase	-	-	-	-	Fan et al. (2012)
QDs-indolicidin	1.5[a]	-	3, 9	↓SOD, CAT, ↑GST	-	-	-	Non-toxic	Falanga et al. (2018)
			15, 24	↑GST, CAT	SOD				
ZnO	1.10^{-1}	-	1, 3, 7, 14	↓SOD, GST, CAT	-	-	-	1.04[c]/-	Chen et al. (2017)
C_{60}[b]	0.5–2	-	21	-	-	↓amylase, trypsin, lipase	-	-	Tao et al. (2016)
TiO_2	1	Cu^{2+}	2	↓SOD	Na^+/K^+ ATPase	-	-	-	Liu et al. (2015)
ZnO	0.8, 1.1	-	3	↓ GST	-	-	-	-	Mwaanga et al. (2014)
CuO	0.8, 1.1	-	3	↓ GST	-	--	-	-	

[a]Concentration unit: nM.
[b]NMs, ingested from dietary route.
[c]48 h of exposure.
↑ increase of enzyme activity/gene expression related, while ↓ implies decrease.

expected to reduce their toxicity (Ekvall et al., 2021), although if the acquired corona results in some particle agglomeration the particles may become a more attractive food source and thus be taken up to a greater extent resulting in increased toxicity (Nasser and Lynch, 2016). Depending on their location in the intestine, NMs can acquire an unique eco-corona profile (Chetwynd et al., 2020; Cui et al., 2020), and undergo different transformations, for example, a pH-dependent dissolution (Cao et al., 2022). Due to the particularities of NMs, they are normally dispersed in the luminal liquid, rather than dissolved, and a wide diversity of macromolecules (solid-phase food, exudates, digestive enzymes, and proteins) present in or from the external environment can also be considered as additional colloidal components that can contribute to its dispersibility or not (Nasser et al., 2020; Van Der Zande et al., 2020). The composition of the digestive tract and the interaction forces between NMs and gut lumen matrix determine NMs bioavailability, potentiating or mitigating NM toxicity to daphnids (Cui et al., 2020). Consequently, the physicochemical characteristics of NMs and natural biological constituents must be studied in terms of their colloidal chemistry to determine their colloidal behaviour and impacts on daphnids' physiology (Christenson, 1984).

4.2 Enzymes as biochemical markers of nanotoxicity

The median effective concentration leading to immobility (EC_{50}) or lethality (LC_{50}) are the OECD standardised endpoints considered in acute toxicity assessment (OECD, 2004), while body burden, reproductive, and growth rate are the end points for the chronic assessment (OECD, 2012). However, these apical endpoints are less sensitive than the biochemical ones (De Coen and Janssen, 1997). To enable a better understanding of the adverse outcomes on food metabolism and stress response, we need to identify suitable biomarkers for ecotoxicity (Schwarzenberger and Fink, 2018). Biochemical markers can work as early indicators (sub-lethal toxicological effects) of perturbance on organisms metabolism, resulting in alterations in enzyme activity or expression, and can be identified using enzyme assays (Galhano et al., 2020; Galhano et al., 2022), or a range of omics techniques (Taylor et al., 2018; Zhang et al., 2018; Bhagat et al., 2022), respectively. Here, we summarise the main findings reported for two major enzymes classes (digestive and antioxidant) from *Daphnia* nanoecotoxicology studies (Table 2).

4.2.1 Digestive enzymes (food metabolism)

In addition to the mechanisms involved in the digestive process mentioned earlier, digestive enzymes play an important role in the metabolism of ingested food, breaking down food particles and increasing the efficiency of digestion. Overall, several enzymes are secreted to metabolize proteins such as trypsin and chymotrypsin, sugars such as cellulase, α-amylase and β-galactosidase; and lipids such as esterase (Lv et al., 2017). When exposed to NMs and/or pollutants, their activity is changed to maintain the homeostasis of organism's metabolism. However, depending on the dosage level which they are exposed, these compounds can affect digestive physiology and food metabolism in *Daphnia* (Qi et al., 2022). NMs were shown to target mainly intestine epithelium and peritrophic membrane (Mattsson et al., 2016). Recent evidence depicted that NMs can penetrate cell membrane without disrupting it, and be endocytosed (Santo et al., 2014). NMs physicochemical characteristics (e.g., shape, size, and surface chemistry) are determinant to the chemical transformations they undergo in the digestive tract of daphnids and later elicited biological responses (Liu et al., 2019).

An inhibition on the activity of amylase and esterase in the treatment with a low and higher concentration of TiO_2 NMs in acute toxicity assessment was observed, and this effect was even more evident during a chronic assay. Exposure to the NMs has shown to affect the nutrition, growth, and reproductive processes in daphnids (Fouqueray et al., 2012) and this was demonstrated by a dose-dependent decrease in the enzymes' activity after exposure to fullerene (C_{60}) (Lv et al., 2017). In another work, the activity of enzymes was monitored over days, which confirmed a reduction of their activity in *D. magna* (Tao et al., 2016). In *D. pulex*, zinc oxide NMs (ZnO NMs), bulk (ZnO), and ionic species (Zn^{2+}) dysregulated the expression of genes related to chymotrypsin, carboxypeptidases, and serine protease enzymes (Lin et al., 2019). Disruption of intestinal structure of daphnids after interaction with stressors commonly impacts on energy acquisition and causes high metabolic costs, via reduction of the available energy reserves (carbohydrates, lipids, and proteins), to keep the basal metabolism. The adsorption of NMs to active sites or surface of trypsin enzyme was suggested as a possible mechanism to inactivate digestive macromolecules by a comparable experimental and theoretical study (Zhang et al., 2014).

4.2.2 Antioxidant enzymes (oxidative stress)

Daphnids initially respond to the intake of foreign materials (NMs and contaminants) by producing ROS, which results in oxidative stress. Prolonged exposure to these stressors can lead to lipid peroxidation, protein inactivation, and DNA damage. Antioxidant enzymes modulate their activity to reduce the damage caused. Superoxide dismutase (SOD) is the first defence line in detoxification that produces the substrate for catalase (CAT) to metabolize. Then, CAT, glutathione-s-transferase (GST), and glutathione peroxidase (GPx) remove harmful metabolites generated from this process transforming them into less toxic compounds, such as water and oxygen (Galhano et al., 2022). Proteins associated with oxidative stress response can be found in the NM eco-corona, giving insights into the mechanistic pathways associated with NM toxicity (Nasser and Lynch, 2016; Fadare et al., 2019; Ellis and Lynch, 2020).

Similarly, *Daphnia* exposed to C_{60} (fullerenes) increased SOD activity after 48 h, and decreased after 72 h, indicating oxidative stress damage and possibly the beginning of lipid peroxidation since simultaneously a dramatic increase of malondialdehyde (MDA) was obtained (Lv et al., 2017). Increasing dose of TiO_2 NMs exposed to daphnids augmented the activity of CAT, GST, and GPx but no effect was observed for SOD (Kim et al., 2010). CAT response was similar to those observed for GST and GPx, but in long-term exposure to the NMs, their activity recovered due to acclimation (Fouqueray et al., 2012). In contrast, ZnO NMs increasingly inhibited the activity of enzymes as exposure duration increased. Similarly, the genes corresponding to SOD and GST were upregulated initially and later downregulated, while MDA content increased over time, indicating that the detoxification

was overwhelmed and possibly led to GST inactivation (Mwaanga et al., 2014; Chen et al., 2017). Exposure to quantum dots (QDs) functionalized with indolicidin (an antimicrobial peptide) also affected enzyme efficiency, but SOD adapted to the stress condition, while CAT was greatly induced after 15 days and GST activity slightly increased during period of exposure (Falanga et al., 2018).

The role of surface chemistry on enzyme activity was investigated using gold NMs (AuNMs). Negatively charged AuNMs (MPA-AuNMs) caused a significant increase in *gst* expression, related to GST, while no effect was noted from positively charged (PAH-AuNMs) after 24 h (Qiu et al., 2015). However, in another work, exposure to PAH-AuNMs, induced *gst* expression compared to MPA-AuNMs (Dominguez et al., 2015). Both studies considered that the toxicity may be associated with the AuNMs colloidal behaviour, because PAH-AuNMs were more stably dispersed in the test medium than the MPA-AuNMs, they were more bioavailable to be absorbed and cause damage to the daphnid gut. PAH-AuNMs was slightly toxic even at a low exposure dose (5 $\mu g\ L^{-1}$) and increased significantly at 10 and 50 $\mu g\ L^{-1}$ (Bozich et al., 2014). The contrasting responses in these studies may have resulted from the distinct exposure conditions (i.e., the concentration used).

Combining NMs with inorganic or organic contaminants is an attractive approach to investigate the oxidative damage triggered in a real-world-like scenario (Galhano et al., 2022). For example, exposure to TiO_2 NMs in a range of concentration (from 10 to 100 $\mu g\ L^{-1}$) of copper (Cu^{2+}) resulted in induction of CAT, reaching a maximum of 10 and 20 $\mu g\ L^{-1}$ in the presence and absence of the NMs respectively. Inhibition of CAT occurred as the dose of Cu^{2+} increased (Fan et al., 2012). Similar behaviour was described for SOD, but no statistical difference was found between the exposure in the presence and absence of TiO_2 NMs, meaning that the presence of NMs had no additional effect on the activity of this enzyme. However, an inhibitory effect was observed in Na+/K+ ATPase transporter in mixture conditions compared to the condition without TiO_2 NMs. With respect to the mortality rate, the co-exposure of TiO_2 NMs with Cu^{2+} increased the toxicity compared to the treatment which organisms were exposed to Cu^{2+} only (Fan et al., 2012). In another study, TiO_2 NMs with varied percentage of free {001}facets combined with Cu^{2+} reduced SOD activity, but just a slight decrease was observed in Na+/K+ ATPase activity and no change in this transporter activity in the single exposure condition to the NM (Liu et al., 2015). In Mwaanga et al. (2014) work, NOM was added to the test medium and reduced the inhibitory effect of ZnO and CuO NMs on GST activity, possibly, by diminishing the accessibility of NMs to adsorb GST.

Galhano et al. (2020) integrated an individual and subcellular level approach to effectively assess the toxicity of TiO_2 NMs (12.5–100 $\mu g\ L^{-1}$ Ti) or AgNPs (25–125 $\mu g\ L^{-1}$ Ag), under environmentally relevant conditions, i.e., transformed NMs. The authors observed significant alterations in the activity of GST and CAT mainly after exposure to AgNPs dispersed in wastewater compared to test water. Later, Galhano et al. (2022) evidenced that only in the case of AgNPs dispersed in the wastewate and effluent was SOD activity decreased. The differences in the enzymatic activity of antioxidant enzymes under the conditions of exposure were indicated as resulting from the difference in the physicochemical characteristics of the TiO_2 NMs under the different exposure conditions (7.8 and 4,761.4 $\mu g\ L^{-1}$ Ti in water, 6.3 $\mu g\ L^{-1}$ Ti in wastewater-borne, 17.3 and 5,467.5 $\mu g\ L^{-1}$ Ti in effluent) and AgNPs (81.7 and 105.4 $\mu g\ L^{-1}$ Ag in water, 30.3 $\mu g\ L^{-1}$ Ag in wastewater-borne, 56.4 and 80.5 $\mu g\ L^{-1}$ Ag in effluent), the complexity of the matrices and the aging of the effluents used (Galhano et al., 2022). Stable agglomeration of TiO_2 NMs may have reduced their bioavailability. Interestingly, the author also observed a toxicity coming from the background effluent that proved to be relevant and should be considered in further studies (Galhano et al., 2022).

4.3 Challenges and perspectives for enzyme activity studies in *Daphnia*

Most studies on nanobio-interfacial interactions in the gut have been carried out on animal models, and cultures of intestinal cells from invertebrates are not yet available, representing a great challenge for the advancement of research on the underlying mechanisms of absorption and bioavailability of NMs in invertebrates. The small size of daphnids and sample contamination (e.g., mucus and carapace) are the main limiting factors that influence data collection (Mattsson et al., 2016; Van Der Zande et al., 2020). Besides investigating nano-intestinal epithelial cells interaction, understanding NMs interactions with *Daphnia* gut microbiota are necessary, since ingested NMs and other stressors change the composition and functioning of microorganisms that inhabit the gut (Akbar et al., 2020; Cui et al., 2020). The alteration of life history traits have also been shown to mediate the toxicity response (Li et al., 2019), however, the understanding of life history and gut microbiome influence NM and MP toxicity are still in their infancy (Li et al., 2019; Akbar et al., 2020; Varg et al., 2022).

Despite biochemical markers being promising tools for early aquatic toxicity assessment (Michalaki et al., 2022), the biochemical and physiological responses generally do not correlate and sometimes there is no consistency in the results. Therefore, it is essential to push the scientific community to harmonise experimental procedures to produce reliable data, following the Findable, Accessible, Interoperable, and Reusable (FAIR) principles (Wilkinson et al., 2016), which will later allow linking physiological responses with molecular patterns and (sub) organismal responses and facilitate computational modelling and predictive (nano) toxicology. This will allow computational modelling of current data, identification of biomarkers that predict adverse outcomes and decision making for regulatory purposes (Taylor et al., 2018).

4.4 Bioaccumulation of NMs in aquatic food webs and quantification of particle uptake

Uptake and bioavailability studies are significant for studying the behaviour of NMs in natural environments and for linking the biological effects to the environmental chemistry of NMs (Lead et al., 2018). In addition to microorganisms, crustaceans

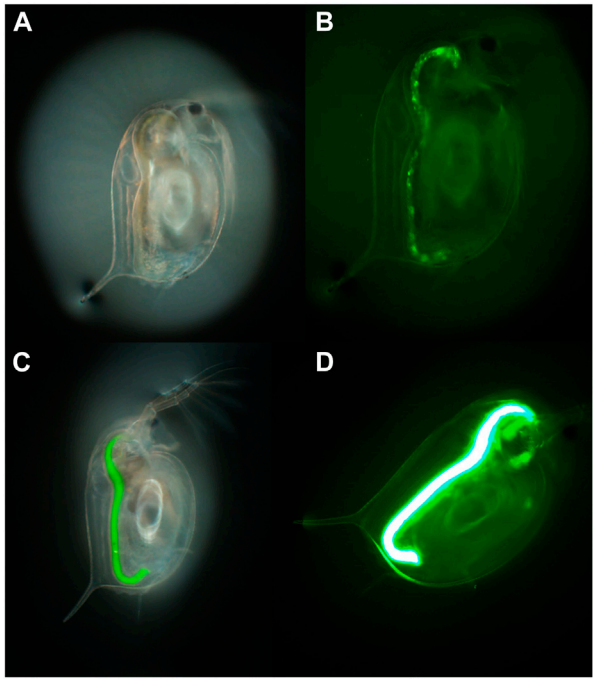

FIGURE 2
An example of the use of fluorescence to determine uptake of 1–5 µm polyethylene MP particles by *D. magna* visualised in two daphnids exposed to different concentrations of the MPs (50 and 500 mg/L, respectively) for 24 h. **(A,C)** brightfield, and **(B,D)** fluorescence imaging of the first and second daphnids, respectively. Taken with an Olympus optical microscope with a Green Fluorescent Protein (GFP) filter cube and dichroic mirror and a DP74 colour camera and viewed using CellSens software (×70 magnification).

such as *Daphnia* are involved in the degradation of organic matter and nutrient recycling, working as shredders in natural ecosystems and acting as pivotal components of the food web (Ebert, 2005). Further to already being an established model species for regulatory testing, *Daphnia* are an advantageous model for NM and MP toxicity testing due to their clear body which allows visualisation of the uptake and potential retention of NMs and MP within the *Daphnia* gut. Fluorescently labelled industrial beads have been widely used to undertake initial toxicity assessments of MPs, which uses the fluorescence as a proxy for the MPs to theoretically determine uptake, translocation, and potential storage in the organism's tissue (Figure 2) (Rosenkranz et al., 2009). However, the potential for dye to leach from the beads can confound the results, as dyes can be retained in the lipid deposits and other tissues within the *Daphnia* leading to incorrect tracing of the MPs and to misreporting of translocation of MPs in cases where this has not occurred (Schür et al., 2019). For example, Nile red is often used as a stain to identify MP in environmental samples, but this dye is also widely used for lipid staining within *Daphnia* which can lead to overestimation of internalised MPs concentrations and retention. Furthermore, the change in internal biological conditions (such as pH) can affect the fluorescent signalling from the dye which can significantly impact the results or could further impact the dye leaching from the particles (Triebskorn et al., 2019; Davis et al., 2020).

Quantifying the internalised concentration of particles during exposures can vary depending on the material type but is very useful data to collect as the internalised concentration can be used to more accurately determine a dose response relationship. Internalised concentration, or body load, is needed for Toxicokinetic-Toxicodynamic (TK-TD) modelling such as Dynamic Energy Budgets (DEB) which can link several aspects of life history trait observations to potential changes in the population distribution. Some of the more widely used methods for visualisation of particle accumulation and damage are transmission electron microscopy (TEM) to determine the uptake, potential translocation and retention of particles within organisms tissues as per the example shown in Figure 3 (Ellis and Lynch, 2020) and ICP-MS analysis for quantification of metal, or metal doped, particles in tissue (Schmiedgruber et al., 2019; Ellis and Lynch, 2020).

5 *Daphnia* genome and key NMs toxicity pathways

Direct investigations of how NMs are associated with adverse outcomes and disease in humans are very limited (Lima et al., 2022), mainly due to the issues around how chemicals including NMs are regulated under existing chemical frameworks and the ethical limitations of testing directly on humans (Hansen, 2017; Oksel Karakus et al., 2021). Due to the shared mammalian biology, information safeguarding human health relies on the toxicological information from invertebrate (mice and rat models) *in vivo* studies to protect human health (Festing and Wilkinson, 2007; Franco, 2013), as well as fish and algae, which have been traditionally used to set regulatory limits to safeguard environmental health (Brunner et al., 2009; Kaltenhäuser et al., 2017).

The principles of the 3Rs (Replacement, Reduction and Refinement) were developed over 50 years ago providing a framework for performing more humane animal research (https://nc3rs.org.uk) (Burden et al., 2017; Sneddon et al., 2017). Advancement of animal genome research over the last 20 years has led to significant understanding of the relationship between simple organisms and their changing environment (van Straalen and Feder, 2012; Stracke and Hejnol, 2023). Moreover, the advancement in evolutionary developmental biology and ecological functional genomics, has identified a possibility to reduce the use of animal experimentation using simple model organisms including invertebrates, due to the large amount of the genome that is conserved across species. Genomics is used to identify genetic variation under natural selection (Mitchell-Olds and Feder, 2003; Leinonen et al., 2013; Grummer et al., 2019) in model test organisms, which are accessible to both laboratory and field studies along defined environmental gradients (Spanier et al., 2017). Furthermore, comparative studies into the evolution and conservation of genes and genomes, provides significant information on genetic diversity and similarities among major groups of organisms from simple organisms to larger invertebrates (Ros-Rocher et al., 2021).

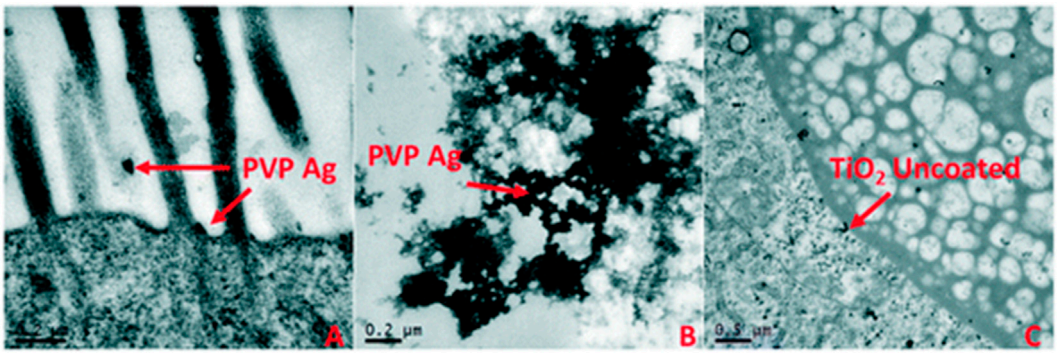

FIGURE 3
An example of the use of TEM images to determine the accumulation of NM in *Daphnia* guts and potential translocation. Uptake and localisation of **(A)** freshly dispersed PVP-coated Ag NMs in HH combo medium showing microvilli interactions, **(B)** freshly dispersed PVP-coated Ag NMs in HH combo found in the gut lumen space; and **(C)** freshly dispersed uncoated TiO_2 NMs in HH combo, showing evidence of NM translocation in the bush border. Reproduced from (Ellis and Lynch, 2020) with permission from the Royal Society of Chemistry.

5.1 *Daphnia* genome

Characterisation of *Daphnia* genomes enables the progress of molecular ecotoxicology for evaluating pollutants and NMs impacts, by analysing molecular pathways related to their defence mechanism response (Lee et al., 2019). The complete genome sequence of *D. pulex* (Colbourne et al., 2011) and *D. magna* have been elucidated but the search for key gene families related to stressors exposure is ongoing through screening of likely molecular biomarkers (Orsini et al., 2016). Identification of genomic expression profiles enables understanding of how genes are regulated under different ecological conditions and how these expressions are linked to phenotypic change (Rozenberg et al., 2015; Hales et al., 2017; Ros-Rocher et al., 2021). Phenotypical variation is understood to be largely due to gene and environment interactions that were shaped by evolution, or by environmental stress that predictably disrupt the normal functioning of genes (Hodgins-Davis and Townsend, 2009; Moyerbrailean et al., 2016; Alexander-Dann et al., 2018).

The expression profile (when compared to a non-treated control organism) of all genes that are expressed in response to a particular initiating event, is called a "molecular phenotype." The transcription of the "molecular phenotype" is based on the evolutionary history of populations (Ravindran et al., 2019). Hence, the transcriptional responses of *Daphnia* to environmentally exposed NMs are a rich source of both phenotypic and genotypic information about the mechanisms of adaptation. This approach aligns human- and eco-toxicology towards a more general understanding of how exposure to NMs disrupts biological processes that otherwise ensure animal (including human) health. Evidence is growing on the feasibility of classifying the effect of NMs on humans, based on gene expression monitoring using distantly related environmentally relevant model organisms such as *Daphnia* (Amorim et al., 2023). Therefore, we can use comparative genomics to confirm that model organisms retain a greater number of ancestral gene families that are highly conserved and are shared with humans which are also closely linked to human diseases (Marwal and Gaur, 2020; Colbourne et al., 2022). Consequently, a chemical hazard assessment framework built upon key events may be informative for a greater diversity of species, by exploring the use of the homology between ecological model test species and humans to understand original molecular interactions and responses to emerging pollutants such as MPs and NMs.

5.2 Conserved biochemical pathways as a basis for understanding NM toxicity

The challenging ecological environments in which the multiple species of *Daphnia* inhabit, make *Daphnia*, an optimal genomic model for monitoring stress and adaptive changes (Vandegehuchte et al., 2010; Vandenbrouck et al., 2010; Colbourne et al., 2011) to their reproductive nature (as discussed in section 4). Understanding the genomic traits in *Daphnia* has already given great insight into developmental plasticity, causing altered morphology and behaviour in response to environmental stress (Akbar et al., 2022; Sha and Hansson, 2022) and adaptation to environmental toxicity (van Straalen and Feder, 2012). Therefore, due to their high degree of phenotypic plasticity, physiology and ecological importance (Lee et al., 2019), understanding the mechanism of action (MOA) as a result of daphnids exposure to NMs, is critical for the prediction of the selectivity and sensitivity in other species. Furthermore, this understanding will lead to the development of adverse outcome pathways (AOPs), by understanding what NMs concentrations cause harm (Russo et al., 2018), which can then be imposed onto standardized toxicological tests and risk assessments.

Access to the *Daphnia* genome sequence has enabled researchers to study specific gene changes in response to a multitude of environmental influences, and to discover the MOAs of several chemicals (Garcia-Reyero et al., 2009; Garcia-Reyero and Perkins, 2011; Giraudo et al., 2017) rendering gene transcription profiling one of the most powerful tools in developmental biology. The advancement of high-throughput RNA-sequencing (RNA-seq) provides whole transcriptome profiling, which allows the unbiased detection of novel transcripts in a sample at a given time (Giraudo et al., 2017).

Over the past decade, developmental work using phylogenetic mapping relationships and amino acid homology have identified

that genomic regions under natural selection show evolutionary relationships among conserved genes from different species (van Straalen and Feder, 2012). Although there are major differences between vertebrates and invertebrates, there is a growing body of evidence that distantly related species share many ancestral genes by common descent that serve the same biochemical pathways (Rogozin et al., 2014). The homology between genes (similarity in genes due to shared ancestry between species) are analysed using Gene Ontology (http://geneontology.org/), gene orthologs database (https://www.orthodb.org/), or pathway enrichment tools (such as DAVID, GSEA or Reactome). This analysis catalogues genes shared among species by descent across the animal kingdom to infer functional conservation, which helps to highlight highly conserved key genes involved in stress response pathways. Therefore, the homology-based approach identifies genes "in common" from model species and aligns them with similar orthologues to gene family members across large evolutionary distances (Spanier et al., 2017; Adrian-Kalchhauser et al., 2020). Comparative genomics studies have confirmed that crustaceans retain a greater number of ancestral gene families that are shared with humans than insects (such as *Drosophila*), including genes responsible for growth, reproduction, and maintenance (Rogozin et al., 2014; Colbourne et al., 2022). Indeed, *Daphnia* retain a disproportionately large number of ancestral gene families that are linked to human diseases, despite more than 780 million years since present day crustaceans and mammals last shared a common ancestor (Colbourne et al., 2022).

Several studies have presented preliminary links, using qualitative gene expression profiling and *Daphnia*, between NM exposure-related harm and human disease (Asselman et al., 2013; Aksakal and Arslan, 2019; Ellis et al., 2020b). Such research uses gene expression to help bridge the gap between distantly related species by understanding how exposure to pollutants disrupts key conserved biological processes (Mav et al., 2018). The most common homologous genes observed in these studies have been those associated with metal detoxification, oxidative stress, energy production, DNA repair (Poynton et al., 2007) and general maintenance (Asselman et al., 2013; Qiu et al., 2015), which all served as biomarkers that are shared between species. The results from these studies collectively recognise that genes associated with growth, reproduction, homeostasis, xenobiotic detoxification, and metabolism, all provide mechanistic insights into NM-organism interactions and represent pathways encoding for cellular functions that are known to be induced by NM exposure studies.

Although further research is needed, comparing common genes and the biochemical pathways that link the differential transcriptomes, shared by common descent among species, offers meaningful insights into the connections between model test species and environmental health exposure, which can help to establish areas for development in NM risk assessment.

6 Adverse outcome pathways—gaps in terms of ecotoxicity and NMs

Relating molecular responses to phenotypic effects is crucial in environmental risk assessment. A promising approach is the AOP framework, which describes key steps of toxic mechanisms resulting in adverse effects in animals and populations (Ankley et al., 2010; Mortensen et al., 2022). AOP starts with a molecular initiating event (MIE) that can be triggered by various environmental contaminants. These MIEs are linked to a series of key events (KEs) that can result in an adverse outcome via different signalling pathways with different levels of biological organisation, e.g., molecular, cellular, tissue, organ, organism, and population (Villeneuve et al., 2014; Rugard et al., 2020). These interlinked pathways can be assembled into AOPs and serve as a foundation for the development of a mechanistic understanding of toxicity and disease. Therefore, AOPs play an essential role in the ecological risk assessment of environmental contaminants (Ankley et al., 2010; Khan et al., 2020).

To date, the majority of AOP-building effort has been focussed in human health and mammalian studies, but the application of AOPs for model organisms such as *Daphnia* is increasingly being investigated (Song et al., 2020). While in principle AOPs are chemical-agnostic, and focussed more on mechanisms, such as endocrine disruption or ion-channel blocking, for example, work is underway to establish NMs-specific AOPs, focussing on key aspects such as NMs-biomolecule interactions, NM-membrane interactions, and NMs-induced disruption of enzyme activity, for example, Jagiello et al. found that only 8 of 331 available AOPs in the AOP-Wiki are specific for NMs (namely, AOP numbers 144, 173, 207, 208, 209, 210, 241, and 319), meaning that only 2.4% of all AOPs in the AOP-Wiki have (as of 2022) been assessed or considered for their direct relevance to NMs, and thus there is a need to evaluate whether remaining AOPs might be applicable fully or partially to NMs (Jagiello et al., 2022).

NMs induced formation of ROS is one of the most significant reasons for adverse effects from NMs. Likewise, oxidative stress is well known to contribute to pollutant-induced cell damage and toxicity (Balážová et al., 2020). ROS can target multiple cellular components, including mitochondria, membrane lipids, DNA, structural proteins, and enzymes, resulting in different adverse outcome. NM exposure to *Daphnia* has caused NM accumulation in the gut, which led to accumulated ROS (Kim et al., 2010; Nasser et al., 2020), decreased growth (Karimi et al., 2018; Ellis et al., 2020b), and decreased fertility and reproduction (Mendonça et al., 2011; Olkova, 2022). When Cu (II) was absorbed on TiO_2, the oxidative stress increased, and intestinal damage was found (Liu et al., 2015). It has been reported that CNT exposure can cause ingestion of CNTs, leading to impacted gut and poor food assimilation, which in turn, may lead to poor nutrition and cause adverse effects to growth, moulting, and eventually reproduction (Arndt et al., 2014). Thus, it is likely that gut accumulation of NMs can lead, via oxidative stress, reduced growth and thus reduced fertility, to reduced reproductive success and population decline. Within the RiskGONE, NanoSolveIT and CompSafeNano projects we are documenting the key events in this proposed AOP for discussion with the AOP community.

NMs accumulation in the gut of *Daphnia* can cause blockage of gut, leading to reduced feeding, followed by decreased supply of oxygen and triggering of antioxidant pathways (e.g., decreased SOD, upregulation of NOX5, increased ROS), which result in decreased moulting and thus the decreased growth, fertility, and reproduction (Sasaki et al., 2019). ROS production induced oocyte apoptosis-associated reproduction decline has been reported previously, whereby increased ROS damages cellular components, leading to

energy (ATP) shortage, DNA breaks, telomere shortening, spindle instability, chromosomal abnormalities, dysregulation of autophagy and proteasome system, which may contribute to the reduced developmental competence compared to normal oocytes (Sasaki et al., 2019). In addition, excessive ROS formation can induce increased DNA damage, apoptosis, follicular atresia, and decreased oogenesis, reducing fecundity (Chatterjee and Bhattacharjee, 2016). Therefore, excessive ROS production can lead to oocyte apoptosis-associated reproduction decline. Calorific reduction related to NMs accumulation in the gut (as discussed in Section 4) may also trigger a cascade of signalling pathway alteration, including inhibition of FAR gene expression, activation of DMRT and DMRT genes and sex determination genes (doublesex1), and changes in chitin and ceramide metabolism, which subsequently lead to decreased carapace shedding, *Daphnia* maturation, sex communication, and induced male production.

We propose that all these KEs are triggered by the MIE of physical blockage of the gut. Absorption of NMs onto the surface of aquatic organism is a key step in determining their bioavailability. Absorption of AuNMs on the carapace and appendages of *D. magna* and the resulting mechanical disruption of the feeding appendages was observed after AuNM exposure (Botha et al., 2016). TiO_2 NMs were taken up mainly by endocytosis, resulting in their accumulation in abdominal areas and the gut of *D. magna* (Tan et al., 2017). Elimination of NMs is reportedly difficult; the excretion rate constant of AgNMs in daphnids was much lower than that of Ag ions (Zhao and Wang, 2010). The main elimination routes for AgNMs in *Daphnia* were excretion (63%) and faecal production (Zhao and Wang, 2010). The monodispersed NMs can easily get deep inside the organisms and are harder to be excreted compared with aglomerated NMs.

The application of omics technologies can be of great value for elucidating how contaminants cause adverse effects in an organism. For example, proteomics provides a systematic qualitative and quantitative mapping of the whole proteome in cells and tissues and enables identification of differentially expressed proteins (DEPs) as biomarkers for AOPs. In addition, transcriptomics (single organism), metabolomics, and lipidomics can also be used for future studies for identifying the AOPs (Ankley et al., 2010; Vinken, 2019).

7 Innovative approaches to assessing NMs toxicity using *Daphnia* microfluidics

Microfluidics and lab-on-a-chip are promising technologies to address many of the limitations in toxicity assays. With these innovative approaches the manipulation of small volumes of liquids/fluids under a network of miniaturized channels allows them to 1) mimic the microenvironment conditions, 2) enables easy manipulation of cells and organisms to measure biological specimens and biomolecular targets, and 3) facilitates automatic extraction of relevant data in a fast and easy way. Additionally, these devices can be combined with sensors, cameras, computers, and smartphones becoming a powerful toolbox in toxicological sciences. Initially, lab-on-a-chip devices were applied in toxicity studies to miniaturize and refine *in vitro* assays. These devices reduce and automate manual handling procedures, miniaturize testing, decrease the required amount of reagent and chemicals for testing and improve performance due to the real-time monitoring capability. Microfluidics technology creates the potential for multiplexed analysis, single-cell, and gradient cytotoxicity assessments. Furthermore, this technology combines sensors and digital cameras for cytotoxicity studies with real-time data collection, allowing the monitoring of many cellular parameters, such as mortality, cell-substrate adhesion, electrophysiology, cell division and kinetics responses of cytotoxicity in a label-free manner (Garcia-Hernando et al., 2020; Wlodkowic and Jansen, 2022).

Despite the evolution of microfluidics devices and lab-on-a-chip technologies in the biomedical field, its potential in ecotoxicology has emerged just recently. Ecotoxicology testing using *in vivo* assays is, in general, labour intensive, whereby the manipulation of organisms is mainly manual, which may increase data variability and decrease reproducibility. In this way, microfluidics automation of organisms sorting, collection and positioning and chemical addition and dilution, combined with powerful data collection and analysis tools offer a significant upgrade to ecotoxicological tests (Campana and Wlodkowic, 2018a; Abreu et al., 2022). However, there are also some limitations for its development, such as organism size, which is an important parameter to the development of micro/millifluidic devices, currently limited to organisms < mm in size (Campana and Wlodkowic, 2018b). Consequently, a limited number of studies combine micro/millifluidics with ecotoxicology, and most address unicellular organisms such as bacteria, algae or protozoa. Such devices can detect growth, cell viability, bioluminescence, movement, and electrochemical changes to understand the mechanisms of toxicity for those model organisms (Kim J. et al., 2017; Zhang et al., 2017; Altintas et al., 2018). For multicellular organisms, some ecotoxicity studies were reported, for example, with: rotifers (*Brachionus calyciflorus*) (Cartlidge and Wlodkowic, 2018), Crustacea (*Artemia* sp.) (Huang et al., 2015), *Allorchestes copressa* (Cartlidge et al., 2017) and *Daphnia magna* (Huang et al., 2017; Tabatabaei Anaraki et al., 2018), nematode (*Caenorhabditis elegans*) (Kim J. et al., 2017; Zhang et al., 2021; Aubry et al., 2022) and fish (*Danio rerio*) models (Yang et al., 2016; Khalili and Rezai, 2019).

Traditional ecotoxicology assays evaluate the survival, reproduction, or growth rate at a specific time point (hours/days) and estimate the chemical median lethality (LC_{50}) or effective concentrations (EC_{50}). Exploring microfluidics technology, it is possible to refine the analysed toxicological parameters and assess different preliminary responses and/or obtain real-time mortality rates. For example, behavioural parameters are often more sensitive than physiological, developmental or reproductive endpoints (Melvin and Wilson, 2013). Therefore, microfluidics technology can increase data analysis and collection by caging test specimens in miniaturized devices allowing the observation of mobility and/or swimming alteration (Bai et al., 2018). Another limitation for classical assays is the caging and manipulation of organisms for imaging, or measurements that need the animal to stay still, such as optical imaging, size and heartbeat measurements. For example, for *C. elegans* model microfluidic devices allowed immobilization by the restriction in thin microfluidic channels (Chokshi et al., 2009; Kim

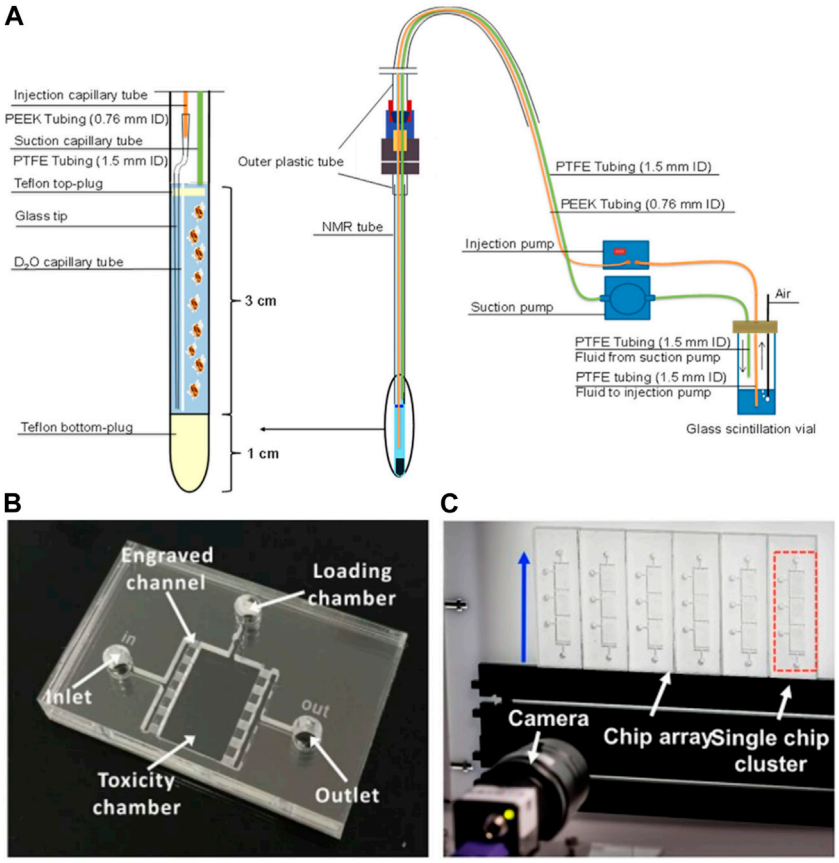

FIGURE 4
(A) Low-volume flow system for *D. magna in vivo* NMR (Tabatabaei Anaraki et al., 2018); **(B)** microfluidic chip for *D. magna* toxicity testing (Huang et al., 2015); **(C)** Photograph of the system setup consisting of a millifluidic chip-based array, fluid actuation and optical detection modules (Huang et al., 2017). Reproduced with permission from SCRIP and SPIE, respectively.

J. et al., 2017). Microfabricated devices for precise and controllable rotation of organisms, for analysis of specific body parts, imaging or injection of substances, were already fabricated for *C. elegans* (Pan et al., 2021) and zebrafish models (Zhang et al., 2017).

As for *Daphnia*, there is a complete open avenue for innovation using microfluidics and lab-on-chip technologies because there are just three reports in the literature (Figure 4). Tabatabaei Anaraki et al. (2018), developed a low-volume flow system that allows *D. magna in vivo* analysis under nuclear magnetic resonance (NMR) testing using a 5 mm NMR tube; inside the tube are two capillary tubes for injection and suction of fluids (sample, media and/or algae injection), allowing the exposure of the living organism to low volumes of chemicals for *in vivo* metabolomic studies (Tabatabaei Anaraki et al., 2018). Huang et al. (2015), automated the Daphtox kit-F with a microfluidic technology by developing a microchip, consisting of a toxicity chamber with a fluid inlet and outlet and loading chamber, for caging *D. magna*. The system was connected with a high-definition time resolved video data analysis to monitor *Daphnia* behaviour when exposed to $CuCl_2$ as a model toxicant (Huang et al., 2015). The was further improved (Huang et al., 2017) to include an array of 24 cuboid test chambers, grouped in eight clusters of three chambers, each chamber having its own specimen loading port and interconnected chambers in a cluster have a shared inlet and outlet for media and sample injection. The device was connected with a time-resolved video microscopy and software to track and analyse *D. magna* locomotory responses towards pollutants (i.e., $CuCl_2$, potassium dichromate, xanthine alkaloids (caffeine), ethanol and dimethyl sulfoxide) (Huang et al., 2017). Interestingly, these results showed that the milli-fluidic device (Daphtox II) presented an EC_{50} equivalent to the conventional multi-well plate acute toxicity assay but can assess multiple behavioural endpoints and provide a more sensitive test with higher automation than the conventional multi-well test.

Despite the enormous benefits that can be achieved by microfluidics applications in nanotoxicity assessment, there are still few studies addressing this subject. With the *Daphnia* model, to the best of our knowledge, there are only two toxicity studies with chemicals (Huang et al., 2015; Huang et al., 2017) and no reports involving NMs, daphnids and microfluidics at the moment. This knowledge gap has been initially addressed by Seitz et al. (2013) when studying the toxicity of TiO_2 NMs towards *D. magna* (Seitz et al., 2013), who showed that in semi-static experiments the initial concentration of TiO_2 decreased approximately 95% while in flow-through the concentration of TiO_2 remained constant in the water column throughout the test duration, with a concurrent decrease in particle agglomeration and sedimentation, as determined by

Dynamic Light Scattering. The flow-through conditions also showed lower toxicity of TiO_2 NMs suggesting that agglomeration may play an important role in the toxicity profile of NMs (see Section 2.1). In addition, the NM sample is usually limited and expensive, and microfluidics devices can be useful not only in this sense (saving sample and producing less residues) but also in improving test conditions, increasing flow control, decreasing evaporation, controlling media oxygenation, temperature, etc. The fabrication of devices may require specific laboratory facilities and can be laborious, limiting mass production of devices for application in ecotoxicology currently (Campana and Wlodkowic, 2018a). However, this technology can obtain measurements and information that traditional assays are not able such as toxicity dynamics events, *in situ* analysis and real-time monitoring. Additionally, all the data generated can be automatically collected using specific software analysis and computational tools, supporting the implementation of big data and machine learning methods in nanoecotoxicology, especially, when considering *Daphnia* as a key organism model in nanosafety regulation.

8 Key recommendations and future directions

Daphnia have been well established as an important model organism for ecotoxicity testing due to their role in the ecosystem, rapid parthenogenetic reproduction, their responsiveness to xenobiotics and environmental stressors and the range of endpoints available to access for toxicity testing. In addition, their use in toxicity testing is compliant with the principles of reduction, replacement, and refinement (NC3Rs) of traditional animal testing makes them an ideal model organism to explore and develop methods for to evaluate emerging contaminants and concerns. Their historic use in chemical testing made them an ideal species to evaluate NM and MP toxicity in freshwater ecosystems, and as highlighted several advances have already been established in the field of NM and MP ecotoxicity assessments. The importance of characterisation of particles has been well established for NM, and lessons and best practice can be taken into MP research to further advance this field, including methods to quantify uptake and techniques to characterise particle surface which are have been identified as important aspects of ecotoxicity studies.

When evaluating the use of *Daphnia* as an ecotoxicology model to determine biological and environmental impacts of NMs and MPs, several developments in terms of both methodology and understanding emerged that offer enormous promise for the future. Highlights include the complete sequencing and elucidating the *Daphnia* genome which, when paired with the parthenogenetic reproductive pathways in *Daphnia,* enables detailed genetic responses to be determined and subsequent changes to offspring to be ascertained (Section 5). Although further research is required, the capacity to compare common genes and pathways across species, by comparing genes shared by common descent among species, and the biochemical pathways that link differential transcriptomes offers meaningful insights into the relationship between model species and environmental health exposure, which can help to identify areas for development in NM risk assessment and support the development of New Approach Methodologies and Next-Generation Risk assessment approaches that rely far less on mammalian *in vivo* testing (Ellis and Lynch, 2020). In addition to transcriptomics of single organisms, application of omics techniques can further support the development of AOPs for *Daphnia* populations and whole ecosystems in response to exposure to NM and MPs, the use of proteomics, metabolomics, lipidomics can help to link the responses to MIEs (Section 6).

Additionally, new methodologies such as microfluidic and lab-on-chip technologies have been identified as areas ripe for development in NMs ecotoxicology. The use of microfluidics can enable real time monitoring of physico-chemical properties of the NM in addition to the toxicity response of the organism. The potential for NM to agglomerate and sediment in test systems can be overcome by the optimised flow conditions that can be established in the microfluidic systems compared to the tradition static test system set up (Section 8). Furthermore, data collection during this application is automatic, enabling machine learning methods and big data computations approached to evaluate the changes and response in due course, utilising harmonised and curated datasets produced according to the FAIR data principles (Wilkinson et al., 2016). While developments of *in silico* models for NMs toxicity to *Daphnia* have been limited to date, and focus primarily on predicting acute toxicity (Varsou et al., 2021), exciting progress in terms of models for assessing impacts from mixtures of different types of NMs (Zhang et al., 2022) and on use of machine learning from images of daphnids exposure to NMs and assessment of changes in tail length, lipid deposits and other phenotypical characteristics from paired multi-generational studies comparing continuous versus parent-only NMs exposure (Karatzas et al., 2020) suggest that computational modelling is a very promising direction for the future.

There are also key areas that have been highlighted where adaptation or further development of approaches and methodologies would be beneficial to strengthen the capacity to evaluate the biological and environmental effects of NMs and MPs. Firstly, through ongoing efforts to adapt test guideline and toxicity study designs to take into consideration the surface characterisation and changes of NM and MPs that result from the exposure medium/conditions and the local environment. This has been demonstrated to have significant impacts on the chemical and biological signalling of the particles that can influence the subsequent interaction. Furthermore, the testing of particles that have been 'aged' in the biological/environmental test medium can lead to substantial changes to the observed toxicity response in both acute and chronic exposure. A balance between comparable/reproducible results and environmentally realistic exposure scenarios would address these challenges going forwards (Section 2), and a strong focus on knowledge transfer for NMs to MPs researchers is essential in order to prevent re-invention of knowledge.

Whilst developing the complexity of the testing conditions for particles, increasing the scale of exposure timeframes can also lead to significant changes to the observed toxicity. Multigenerational assessments to date have highlighted that the offspring of the exposed parents most often have increased sensitivity (and therefore observed toxicity) compared to the initially exposed parent. This suggests that there could be significant detrimental impacts to natural populations based on the assumption that the

toxicity response of all daphnids would be within the range observed in initial acute (48-h short term exposures) and even chronic (21-day reproductive exposures) test windows when not considering the impact of subsequent generations (Section 3). Application of machine learning approaches might enable assessment of the impact of different media compositions and thus different underlying *Daphnia* fitness conditions, as well as the role of additional stressors, such as competition for food or climate change.

As particle uptake does not follow the octanal-water partition coefficient (log Kow) principles, the qualification of uptake of NMs and MPs is an important aspect of ecotoxicity studies to determine an accurate dose-response relationship, and to enable Toxicokinetic-Toxicodynamic (TK-TD) modelling which can link life history traits observed as a result of exposure to changes in the population dynamics in the ecosystem. There are several methods currently available, including TEM imaging, ICP-MS quantification of metal and metal doped particles and the use of fluorescence for stained particles, however the method used depends on the material of the particle (Section 4). However, there are limitations to the use of fluorescence, such as the leaching of fluorescence dye or the impedance of these methods based on the NM properties which can cause interference with assay read-outs including autofluorescence. As a result, further work into accurate methods for determining the internalised concentration of particles would be beneficial to make this a valuable source of data for machine learning.

Author contributions

KR and IL conceptualised the paper; KR, L-JAE, HHD, SS, MTM, GHS, ZG, DSTM, and IL wrote sections of the manuscript; KR, L-JAE, DSTM, and IL edited the final draft of the manuscript; DSTM and IL secured funding. All authors read and approved the submitted version.

Funding

This work was financially supported by the EU H2020 projects NanoCommons (731032), NanoSolveIT (Grant Agreement no. 814572) and RiskGONE (Grant Agreement no. 814425). SS acknowledges funding for her PhD studies from Malaysian Government MARA (Majlis Amanah Rakyat). DM. thanks the Sao Paulo Research Foundation (FAPESP) for the visiting research fellowship at GEES/UoB (2018/25140-3) and the National Council for Scientific and Technological Development (CNPq) for the productivity research fellowship and the FAPESP-UoB research grant.

Conflict of interest

The authors declare that the research was conducted in the absence of any commercial or financial relationships that could be construed as a potential conflict of interest.

Publisher's note

References

Abbas, Q., Yousaf, B., AminaAli, M. U., Mujtaba Munir, M. A., El-Naggar, A., et al. (2020). Transformation pathways and fate of engineered nanoparticles (ENPs) in distinct interactive environmental compartments: A review. *Environ. Int.* 138, 105646. doi:10.1016/j.envint.2020.105646

Abdullahi, M., Zhou, J., Dandhapani, V., Chaturvedi, A., and Orsini, L. (2022). Historical exposure to chemicals reduces tolerance to novel chemical stress in Daphnia (waterflea). *Mol. Ecol.* 31 (11), 3098–3111. doi:10.1111/mec.16451

Abreu, S. N., Jesus, F., Domingues, I., Baptista, F., Pereira, J. L., Serpa, D., et al. (2022). Automated counting of daphnid neonates, Artemia nauplii, and zebrafish eggs: A proof of concept. *Environ. Toxicol. Chem.* 41 (6), 1451–1458. doi:10.1002/etc.5323

Adrian-Kalchhauser, I., Sultan, S. E., Shama, L. N. S., Spence-Jones, H., Tiso, S., Keller Valsecchi, C. I., et al. (2020). Understanding "non-genetic" inheritance: Insights from molecular-evolutionary crosstalk. *Trends Ecol. Evol.* 35 (12), 1078–1089. doi:10.1016/j.tree.2020.08.011

Afshinnia, K., Marrone, B., and Baalousha, M. (2018). Potential impact of natural organic ligands on the colloidal stability of silver nanoparticles. *Sci. Total Environ.* 625, 1518–1526. doi:10.1016/j.scitotenv.2017.12.299

Akbar, S., Gu, L., Sun, Y., Zhang, L., Lyu, K., Huang, Y., et al. (2022). Understanding host-microbiome-environment interactions: Insights from Daphnia as a model organism. *Sci. Total Environ.* 808, 152093. doi:10.1016/j.scitotenv.2021.152093

Akbar, S., Gu, L., Sun, Y., Zhou, Q., Zhang, L., Lyu, K., et al. (2020). Changes in the life history traits of Daphnia magna are associated with the gut microbiota composition shaped by diet and antibiotics. *Sci. Total Environ.* 705, 135827. doi:10.1016/j.scitotenv.2019.135827

Aksakal, F. I., and Arslan, H. (2019). Detoxification and reproductive system-related gene expression following exposure to Cu(OH)2 nanopesticide in water flea (Daphnia magna Straus 1820). *Environ. Sci. Pollut. Res. Int.* 27 (6), 6103–6111. doi:10.1007/s11356-019-07414-x

Alekseev, V., and Lampert, W. (2001). Maternal control of resting-egg production in Daphnia. *Nature* 414 (6866), 899–901. doi:10.1038/414899a

Alexander-Dann, B., Pruteanu, L. L., Oerton, E., Sharma, N., Berindan-Neagoe, I., Módos, D., et al. (2018). Developments in toxicogenomics: Understanding and predicting compound-induced toxicity from gene expression data. *Mol. omics* 14 (4), 218–236. doi:10.1039/c8mo00042e

Altintas, Z., Akgun, M., Kokturk, G., and Uludag, Y. (2018). A fully automated microfluidic-based electrochemical sensor for real-time bacteria detection. *Biosens. Bioelectron.* 100, 541–548. doi:10.1016/j.bios.2017.09.046

Amorim, M. J. B., Peijnenburg, W., Greco, D., Saarimäki, L., Dumit, V., Bahl, A., et al. (2023). Systems toxicology to advance human and environmental hazard assessment: A roadmap for advanced materials. *Nano Today* 48, 101735. doi:10.1016/j.nantod.2022.101735

Ankley, G. T., Bennett, R. S., Erickson, R. J., Hoff, D. J., Hornung, M. W., Johnson, R. D., et al. (2010). Adverse outcome pathways: A conceptual framework to support ecotoxicology research and risk assessment. *Environ. Toxicol. Chem.* 29 (3), 730–741. doi:10.1002/etc.34

Arndt, D. A., Chen, J., Moua, M., and Klaper, R. D. (2014). Multigeneration impacts on Daphnia magna of carbon nanomaterials with differing core structures and functionalizations. *Environ. Toxicol. Chem.* 33 (3), 541–547. doi:10.1002/etc.2439

Asselman, J., De Coninck, D. I., Beert, E., Janssen, C. R., Orsini, L., Pfrender, M. E., et al. (2017). Bisulfite sequencing with Daphnia highlights a role for epigenetics in regulating stress response to microcystis through preferential differential methylation of serine and threonine amino acids. *Environ. Sci. Technol.* 51 (2), 924–931. doi:10.1021/acs.est.6b03870

Asselman, J., Shaw, J. R., Glaholt, S. P., Colbourne, J. K., and De Schamphelaere, K. A. C. (2013). Transcription patterns of genes encoding four metallothionein homologs in

Daphnia pulex exposed to copper and cadmium are time- and homolog-dependent. *Aquat. Toxicol.* 142 (143), 422–430. doi:10.1016/j.aquatox.2013.09.010

Aubry, G., Milisavljevic, M., and Lu, H. (2022). Automated and dynamic control of chemical content in droplets for scalable screens of small animals. *Small* 18 (17), 2200319. doi:10.1002/smll.202200319

Bai, Y., Gao, M., Wen, L., He, C., Chen, Y., Liu, C., et al. (2018). Applications of microfluidics in quantitative biology. *Biotechnol. J.* 13 (5), 1700170. doi:10.1002/biot.201700170

Balážová, Ľ., Baláž, M., and Babula, P. (2020). Zinc oxide nanoparticles damage tobacco BY-2 cells by oxidative stress followed by processes of autophagy and programmed cell death. *Nanomaterials* 10 (6), 1066. doi:10.3390/nano10061066

Barata, C., Baird, D. J., Amat, F., and Soares, A. M. V. M. (2000). Comparing population response to contaminants between laboratory and field: An approach using Daphnia magna ephippial egg banks. *Funct. Ecol.* 14 (4), 513–523. doi:10.1046/j.1365-2435.2000.00445.x

Batley, G. E., Kirby, J. K., and McLaughlin, M. J. (2013). Fate and risks of nanomaterials in aquatic and terrestrial environments. *Accounts Chem. Res.* 46 (3), 854–862. doi:10.1021/ar2003368

Bhagat, J., Zang, L., Nishimura, N., and Shimada, Y. (2022). Application of omics approaches for assessing microplastic and nanoplastic toxicity in fish and seafood species. *Trends Anal. Chem.* 154, 116674. doi:10.1016/j.trac.2022.116674

Biagianti-Risbourg, S., Paris-Palacios, S., and Mouneyrac, C. (2013). "Pollution acclimation, adaptation, resistance, and tolerance in ecotoxicology," in *Encyclopedia of aquatic ecotoxicology*. Editors J.-F. Férard and C. Blaise (Dordrecht: Springer Netherlands), 883–892. doi:10.1007/978-94-007-5704-2_81

Botha, T. L., Boodhia, K., and Wepener, V. (2016). Adsorption, uptake and distribution of gold nanoparticles in Daphnia magna following long term exposure. *Aquat. Toxicol.* 170, 104–111. doi:10.1016/j.aquatox.2015.11.022

Bozich, J. S., Lohse, S. E., Torelli, M. D., Murphy, C. J., Hamers, R. J., and Klaper, R. D. (2014). Surface chemistry, charge and ligand type impact the toxicity of gold nanoparticles to Daphnia magna. *Environ. Sci. Nano* 1 (3), 260–270. doi:10.1039/c4en00006d

Brans, K. I., Stoks, R., and De Meester, L. (2018). Urbanization drives genetic differentiation in physiology and structures the evolution of pace-of-life syndromes in the water flea Daphnia magna. *Proc. R. Soc. B, Biol. Sci.* 285, 20180169. doi:10.1098/rspb.2018.0169

Brunner, E. J., Jones, P. J. S., Friel, S., and Bartley, M. (2009). Fish, human health and marine ecosystem health: Policies in collision. *Int. J. Epidemiol.* 38 (1), 93–100. doi:10.1093/ije/dyn157

Buesser, B., and Pratsinis, S. E. (2012). Design of nanomaterial synthesis by aerosol processes. *Annu. Rev. Chem. Biomol. Eng.* 3, 103–127. doi:10.1146/annurev-chembioeng-062011-080930

Burden, N., Aschberger, K., Chaudhry, Q., Clift, M. J. D., Fowler, P., Johnston, H., et al. (2017). Aligning nanotoxicology with the 3Rs: What is needed to realise the short, medium and long-term opportunities? *Regul. Toxicol. Pharmacol.* 91, 257–266. doi:10.1016/j.yrtph.2017.10.021

Campana, O., and Wlodkowic, D. (2018a). Ecotoxicology goes on a chip: Embracing miniaturized bioanalysis in aquatic risk assessment. *Environ. Sci. Technol.* 52 (3), 932–946. doi:10.1021/acs.est.7b03370

Campana, O., and Wlodkowic, D. (2018b). The undiscovered country: Ecotoxicology meets microfluidics. *Sensors actuators. B* 257, 692–704. doi:10.1016/j.snb.2017.11.002

Canli, M. (2005). Dietary and water-borne Zn exposures affect energy reserves and subsequent Zn tolerance of Daphnia magna. *Comp. Biochem. physiology. Toxicol. Pharmacol.* 141 (1), 110–116. doi:10.1016/j.cca.2005.05.007

Cao, J., Yang, Q., Jiang, J., Dalu, T., Kadushkin, A., Singh, J., et al. (2022). Coronas of micro/nano plastics: A key determinant in their risk assessments. *Part. Fibre Toxicol.* 19 (1), 55. doi:10.1186/s12989-022-00492-9

Cartlidge, R., Nugegoda, D., and Wlodkowic, D. (2017). Millifluidic Lab-on-a-Chip technology for automated toxicity tests using the marine amphipod Allorchestes compressa. *Sensors actuators. B, Chem.* 239, 660–670. doi:10.1016/j.snb.2016.08.058

Cartlidge, R., and Wlodkowic, D. (2018). Caging of planktonic rotifers in microfluidic environment for sub-lethal aquatic toxicity tests. *Biomicrofluidics* 12 (4), 044111. doi:10.1063/1.5042779

Chatterjee, N., and Bhattacharjee, B. (2016). Revelation of ZnS nanoparticles induces follicular atresia and apoptosis in the ovarian preovulatory follicles in the catfish mystus tengara (Hamilton, 1822). *Scientifica* 2016, e3927340. doi:10.1155/2016/3927340

Chen, Y., Wu, F., Li, W., Luan, T., and Lin, L. (2017). Comparison on the effects of water-borne and dietary-borne accumulated ZnO nanoparticles on Daphnia magna. *Chemosphere* 189, 94–103. doi:10.1016/j.chemosphere.2017.08.132

Chetwynd, A. J., Zhang, W., Thorn, J. A., Lynch, I., and Ramautar, R. (2020). The nanomaterial metabolite corona determined using a quantitative metabolomics approach: A pilot study. *Small* 16 (21), 2000295. doi:10.1002/smll.202000295

Chevalier, J., Harscoët, E., Keller, M., Pandard, P., Cachot, J., and Grote, M. (2015). Exploration of *Daphnia* behavioral effect profiles induced by a broad range of toxicants with different modes of action: Effects of different toxicants on *Daphnia* behavior. *Environ. Toxicol. Chem.* 34 (8), 1760–1769. doi:10.1002/etc.2979

Chokshi, T. V., Ben-Yakar, A., and Chronis, N. (2009). CO2 and compressive immobilization of *C. elegans* on-chip. *Lab a chip* 9 (1), 151–157. doi:10.1039/b807345g

Christenson, H. K. (1984). DLVO (Derjaguin–Landau–Verwey–Overbeek) theory and solvation forces between mica surfaces in polar and hydrogen-bonding liquids. *J. Chem. Soc. Faraday Trans. 1* 80 (7), 1933. doi:10.1039/f19848001933

Colbourne, J. K., Pfrender, M. E., Gilbert, D., Thomas, W. K., Tucker, A., Oakley, T. H., et al. (2011). The ecoresponsive genome of *Daphnia pulex*. *Science* 331 (6017), 555–561. doi:10.1126/science.1197761

Colbourne, J. K., Shaw, J. R., Sostare, E., Rivetti, C., Derelle, R., Barnett, R., et al. (2022). Toxicity by descent: A comparative approach for chemical hazard assessment. *Environ. Adv.* 9, 100287. doi:10.1016/j.envadv.2022.100287

Cui, X., Bao, L., Wang, X., and Chen, C. (2020). The nano–intestine interaction: Understanding the location-oriented effects of engineered nanomaterials in the intestine. *Small* 16 (21), e1907665. doi:10.1002/smll.201907665

Davis, A., Nasser, F., Lead, J. R., and Shi, Z. (2020). Development and application of a ratiometric nanosensor for measuring pH inside the gastrointestinal tract of zooplankton. *Environ. Sci. Nano* 7 (6), 1652–1660. doi:10.1039/C9EN01300H

De Coen, W. M., and Janssen, C. R. (1997). The use of biomarkers in Daphnia magna toxicity testing II. Digestive enzyme activity in Daphnia magna exposed to sublethal concentrations of cadmium, chromium and mercury. *Chemosphere* 35 (5), 1053–1067. doi:10.1016/S0045-6535(97)00172-0

Devi, G. P., Ahmed, K. B. A., Varsha, M. K. N. S., Shrijha, B. S., Lal, K. K. S., Anbazhagan, V., et al. (2015). Sulfidation of silver nanoparticle reduces its toxicity in zebrafish. *Aquat. Toxicol.* 158, 149–156. doi:10.1016/j.aquatox.2014.11.007

Dominguez, G. A., Lohse, S. E., Torelli, M. D., Murphy, C. J., Hamers, R. J., Orr, G., et al. (2015). Effects of charge and surface ligand properties of nanoparticles on oxidative stress and gene expression within the gut of Daphnia magna. *Aquat. Toxicol.* 162, 1–9. doi:10.1016/j.aquatox.2015.02.015

Eastwood, N., Stubbings, W. A., Abou-Elwafa Abdallah, M. A., Durance, I., Paavola, J., Dallimer, M., et al. (2022). The time machine framework: Monitoring and prediction of biodiversity loss. *Trends Ecol. Evol.* 37 (2), 138–146. doi:10.1016/j.tree.2021.09.008

Ebert, D. (2005). *Ecology, epidemiology, and evolution of parasitism in Daphnia*, 126.

Ekvall, M. T., Hedberg, J., Odnevall Wallinder, I., Malmendal, A., Hansson, L. A., and Cedervall, T. (2021). Adsorption of bio-organic eco-corona molecules reduces the toxic response to metallic nanoparticles in Daphnia magna. *Sci. Rep.* 11 (1), 10784. doi:10.1038/s41598-021-90053-5

Ellis, L.-J. A., Kissane, S., and Lynch, I. (2020b). Maternal responses and adaptive changes to environmental stress via chronic nanomaterial exposure: Differences in inter and transgenerational interclonal broods of Daphnia magna. *Int. J. Mol. Sci.* 22 (1), 15. doi:10.3390/ijms22010015

Ellis, L.-J. A., and Lynch, I. (2020). Mechanistic insights into toxicity pathways induced by nanomaterials in *Daphnia magna* from analysis of the composition of the acquired protein corona. *Environ. Sci. Nano* 7 (11), 3343–3359. doi:10.1039/D0EN00625D

Ellis, L.-J. A., Valsami-Jones, E., and Lynch, I. (2020a). Exposure medium and particle ageing moderate the toxicological effects of nanomaterials to *Daphnia magna* over multiple generations: A case for standard test review? *Environ. Sci. Nano* 7 (4), 1136–1149. doi:10.1039/D0EN00049C

European Commission. Joint Research Centre (2020). The NanoDefine methods manual: 2020. LU: Publications office. Available at: https://data.europa.eu/doi/10.2760/79490 (Accessed: September 12, 2022).

Fadare, O. O., Wan, B., Guo, L. H., Xin, Y., Qin, W., and Yang, Y. (2019). Humic acid alleviates the toxicity of polystyrene nanoplastic particles to *Daphnia magna*. *Environ. Sci. Nano* 6 (5), 1466–1477. doi:10.1039/C8EN01457D

Falanga, A., Mercurio, F. A., Siciliano, A., Lombardi, L., Galdiero, S., Guida, M., et al. (2018). Metabolomic and oxidative effects of quantum dots-indolicidin on three generations of Daphnia magna. *Aquat. Toxicol.* 198, 158–164. doi:10.1016/j.aquatox.2018.03.001

Fan, W. H., Cui, M. M., Shi, Z. W., Tan, C., and Yang, X. P. (2012). Enhanced oxidative stress and physiological damage in daphnia magna by copper in the presence of Nano-TiO 2. *J. Nanomater.* 2012, 1–7. doi:10.1155/2012/398720

Feil, R., and Fraga, M. F. (2012). Epigenetics and the environment: Emerging patterns and implications. *Nat. Rev. Genet.* 13 (2), 97–109. doi:10.1038/nrg3142

Festing, S., and Wilkinson, R. (2007). The ethics of animal research. Talking Point on the use of animals in scientific research. *EMBO Rep.* 8 (6), 526–530. doi:10.1038/sj.embor.7400993

Fouqueray, M., Dufils, B., Vollat, B., Chaurand, P., Botta, C., Abacci, K., et al. (2012). Effects of aged TiO2 nanomaterial from sunscreen on Daphnia magna exposed by dietary route. *Environ. Pollut.* 163, 55–61. doi:10.1016/j.envpol.2011.11.035

Franco, H. (2013). Animal experiments in biomedical research: A historical perspective. *Animals* 3 (1), 238–273. doi:10.3390/ani3010238

Galhano, V., Hartmann, S., Monteiro, M. S., Zeumer, R., Mozhayeva, D., Steinhoff, B., et al. (2020). Impact of wastewater-borne nanoparticles of silver and titanium dioxide on the swimming behaviour and biochemical markers of Daphnia magna: An integrated approach. *Aquat. Toxicol.* 220, 105404. doi:10.1016/j.aquatox.2020.105404

Galhano, V., Zeumer, R., Monteiro, M. S., Knopf, B., Meisterjahn, B., Soares, A. M. V. M., et al. (2022). Effects of wastewater-spiked nanoparticles of silver and titanium dioxide on survival, growth, reproduction and biochemical markers of Daphnia magna. *Sci. Total Environ.* 839, 156079. doi:10.1016/j.scitotenv.2022.156079

Garcia-Hernando, M., Benito-Lopez, F., and Basabe-Desmonts, L. (2020). Advances in microtechnology for improved cytotoxicity assessment. *Front. Mater.* 7. doi:10.3389/fmats.2020.582030

Garcia-Reyero, N., and Perkins, E. J. (2011). Systems biology: Leading the revolution in ecotoxicology. *Environ. Toxicol. Chem.* 30 (2), 265–273. doi:10.1002/etc.401

Garcia-Reyero, N., Poynton, H. C., Kennedy, A. J., Guan, X., Escalon, B. L., Chang, B., et al. (2009). Biomarker discovery and transcriptomic responses in Daphnia magna exposed to munitions constituents. *Environ. Sci. Technol.* 43 (11), 4188–4193. doi:10.1021/es803702a

Geller, W., and Müller, H. (1981). The filtration apparatus of Cladocera: Filter mesh-sizes and their implications on food selectivity. *Oecologia* 49 (3), 316–321. doi:10.1007/BF00347591

Giorgi, F., Macko, P., Curran, J. M., Whelan, M., Worth, A., and Patterson, E. A. (2021). Settling dynamics of nanoparticles in simple and biological media. *R. Soc. Open Sci.* 8 (11), 210068. doi:10.1098/rsos.210068

Giraudo, M., Douville, M., Cottin, G., and Houde, M. (2017). Transcriptomic, cellular and life-history responses of Daphnia magna chronically exposed to benzotriazoles: Endocrine-disrupting potential and molting effects. *PloS one* 12 (2), e0171763. doi:10.1371/journal.pone.0171763

Giusti, A., Atluri, R., Tsekovska, R., Gajewicz, A., Apostolova, M. D., Battistelli, C. L., et al. (2019). Nanomaterial grouping: Existing approaches and future recommendations. *NanoImpact* 16, 100182. doi:10.1016/j.impact.2019.100182

Goswami, L., Kim, K. H., Deep, A., Das, P., Bhattacharya, S. S., Kumar, S., et al. (2017). Engineered nano particles: Nature, behavior, and effect on the environment. *J. Environ. Manag.* 196, 297–315. doi:10.1016/j.jenvman.2017.01.011

Grimm, N. B., Foster, D., Groffman, P., Grove, J. M., Hopkinson, C. S., Nadelhoffer, K. J., et al. (2008). The changing landscape: Ecosystem responses to urbanization and pollution across climatic and societal gradients. *Front. Ecol. Environ.* 6 (5), 264–272. doi:10.1890/070147

Grintzalis, K., Lawson, T. N., Nasser, F., Lynch, I., and Viant, M. R. (2019). Metabolomic method to detect a metabolite corona on amino-functionalized polystyrene nanoparticles. *Nanotoxicology* 13 (6), 783–794. doi:10.1080/17435390.2019.1577510

Grummer, J. A., Beheregaray, L. B., Bernatchez, L., Hand, B. K., Luikart, G., Narum, S. R., et al. (2019). Aquatic landscape genomics and environmental effects on genetic variation. *Trends Ecol. Evol.* 34 (7), 641–654. doi:10.1016/j.tree.2019.02.013

Haase, A., and Lynch, I. (2018). Quality in nanosafety — towards reliable nanomaterial safety assessment. *NanoImpact* 11, 67–68. doi:10.1016/j.impact.2018.02.005

Hales, N. R., Schield, D. R., Andrew, A. L., Card, D. C., Walsh, M. R., and Castoe, T. A. (2017). Contrasting gene expression programs correspond with predator-induced phenotypic plasticity within and across generations in Daphnia. *Mol. Ecol.* 26 (19), 5003–5015. doi:10.1111/mec.14213

Hansen, S. F. (2017). React now regarding nanomaterial regulation. *Nat. Nanotechnol.* 12 (8), 714–716. doi:10.1038/nnano.2017.163

Hartmann, N. B., Hüffer, T., Thompson, R. C., Hassellöv, M., Verschoor, A., Daugaard, A. E., et al. (2019). Are we speaking the same language? Recommendations for a definition and categorization framework for plastic debris. *Environ. Sci. Technol.* 53 (3), 1039–1047. doi:10.1021/acs.est.8b05297

Hartmann, N. I. B., Skjolding, L. M., Hansen, S. F., Baun, A., Kjølholt, J., and Gottschalk, F. (2014) Environmental fate and behaviour of nanomaterials: New knowledge on important transformation processes. *Dan. Environ. Prot. Agency* doi:10.13140/2.1.1943.4240

Hodgins-Davis, A., and Townsend, J. P. (2009). Evolving gene expression: from G to E to GxE. Trends Ecol. Evol. 24 (12), 649–658. doi:10.1016/j.tree.2009.06.011

Huang, Y., Campana, O., and Wlodkowic, D. (2017). A millifluidic system for analysis of Daphnia magna locomotory responses to water-born toxicants. *Sci. Rep.* 7 (1), 17603–17612. doi:10.1038/s41598-017-17892-z

Huang, Y., Reyes Aldasoro, C. C., Persoone, G., and Wlodkowic, D. (2015). Integrated microfluidic technology for sub-lethal and behavioral marine ecotoxicity biotests. *Proc. SPIE - Int. Soc. Opt. Eng.* 9518. doi:10.1117/12.2180692

Jagiello, K., Judzinska, B., Sosnowska, A., Lynch, I., Halappanavar, S., and Puzyn, T. (2022). Using AOP-wiki to support the ecotoxicological risk assessment of nanomaterials: First steps in the development of novel adverse outcome pathways. *Environ. Sci. Nano* 9 (5), 1675–1684. doi:10.1039/D1EN01127H

Jeevanandam, J., Barhoum, A., Chan, Y. S., Dufresne, A., and Danquah, M. K. (2018). Review on nanoparticles and nanostructured materials: History, sources, toxicity and regulations. *Beilstein J. Nanotechnol.* 9 (1), 1050–1074. doi:10.3762/bjnano.9.98

Jeong, T.-Y., Yuk, M. S., Jeon, J., and Kim, S. D. (2016). Multigenerational effect of perfluorooctane sulfonate (PFOS) on the individual fitness and population growth of Daphnia magna. *Sci. Total Environ.* 569 (570), 1553–1560. doi:10.1016/j.scitotenv.2016.06.249

Kaltenhäuser, J., Kneuer, C., Marx-Stoelting, P., Niemann, L., Schubert, J., Stein, B., et al. (2017). Relevance and reliability of experimental data in human health risk assessment of pesticides. *Regul. Toxicol. Pharmacol.* 88, 227–237. doi:10.1016/j.yrtph.2017.06.010

Kansara, K., Bolan, S., Radhakrishnan, D., Palanisami, T., Al-Muhtaseb, A. H., Bolan, N., et al. (2022). A critical review on the role of abiotic factors on the transformation, environmental identity and toxicity of engineered nanomaterials in aquatic environment. *Environ. Pollut.* 296, 118726. doi:10.1016/j.envpol.2021.118726

Karatzas, P., Melagraki, G., Ellis, L. J. A., Lynch, I., Varsou, D. D., Afantitis, A., et al. (2020). Development of deep learning models for predicting the effects of exposure to engineered nanomaterials on *Daphnia magna*. *Small* 16 (36), 2001080. doi:10.1002/smll.202001080

Karimi, S., Troeung, M., Wang, R., Draper, R., and Pantano, P. (2018). Acute and chronic toxicity of metal oxide nanoparticles in chemical mechanical planarization slurries with Daphnia magna. *Environ. Sci. Nano* 5 (7), 1670–1684. doi:10.1039/C7EN01079F

Kelpsiene, E., Brandts, I., Bernfur, K., Ekvall, M. T., Lundqvist, M., Teles, M., et al. (2022). Protein binding on acutely toxic and non-toxic polystyrene nanoparticles during filtration by Daphnia magna. *Environ. Sci. Nano* 9 (7), 2500–2509. doi:10.1039/D2EN00125J

Khalili, A., and Rezai, P. (2019). Microfluidic devices for embryonic and larval zebrafish studies. *Briefings Funct. genomics* 18 (6), 419–432. doi:10.1093/bfgp/elz006

Khan, B., Ho, K. T., and Burgess, R. M. (2020). Application of biomarker tools using bivalve models toward the development of adverse outcome pathways for contaminants of emerging concern. *Environ. Toxicol. Chem.* 39 (8), 1472–1484. doi:10.1002/etc.4757

Kim, H. Y., Asselman, J., Jeong, T. Y., Yu, S., De Schamphelaere, K. A. C., and Kim, S. D. (2017). Multigenerational effects of the antibiotic tetracycline on transcriptional responses of Daphnia magna and its relationship to higher levels of biological organizations. *Environ. Sci. Technol.* 51 (21), 12898–12907. doi:10.1021/acs.est.7b05050

Kim, J., Lee, S., Cha, Y., Hong, S. J., Chung, S. K., and Park, T. H. (2017). C. elegans-on-a-chip for *in situ* and *in vivo* Ag nanoparticles uptake and toxicity assay. *Sci. Rep.* 7 (1), 40225. doi:10.1038/srep40225

Kim, K. T., Klaine, S. J., Cho, J., Kim, S. H., and Kim, S. D. (2010). Oxidative stress responses of Daphnia magna exposed to TiO2 nanoparticles according to size fraction. *Sci. Total Environ.* 408 (10), 2268–2272. doi:10.1016/j.scitotenv.2010.01.041

Lead, J. R., Batley, G. E., Alvarez, P. J. J., Croteau, M. N., Handy, R. D., McLaughlin, M. J., et al. (2018). Nanomaterials in the environment: Behavior, fate, bioavailability, and effects—an updated review. *Environ. Toxicol. Chem.* 37 (8), 2029–2063. doi:10.1002/etc.4147

Lee, B.-Y., Choi, B. S., Kim, M. S., Park, J. C., Jeong, C. B., Han, J., et al. (2019). The genome of the freshwater water flea Daphnia magna: A potential use for freshwater molecular ecotoxicology. *Aquat. Toxicol.* 210, 69–84. doi:10.1016/j.aquatox.2019.02.009

Leinonen, T., McCairns, R. J. S., O'Hara, R. B., and Merilä, J. (2013). QST -FST comparisons: Evolutionary and ecological insights from genomic heterogeneity. *Nat. Rev. Genet.* 14 (3), 179–190. doi:10.1038/nrg3395

Li, Y., Yan, N., Wong, T. Y., Wang, W. X., and Liu, H. (2019). Interaction of antibacterial silver nanoparticles and microbiota-dependent holobionts revealed by metatranscriptomic analysis. *Environ. Sci. Nano* 6 (11), 3242–3255. doi:10.1039/c9en00587k

Lima, T. S. M., Souza, W., Geaquinto, L. R. O., Sanches, P. L., Stepień, E. L., Meneses, J., et al. (2022). Nanomaterial exposure, extracellular vesicle biogenesis and adverse cellular outcomes: A scoping review. *Nanomaterials* 12 (7), 1231. doi:10.3390/nano12071231

Lin, L., Xu, M., Mu, H., Wang, W., Sun, J., He, J., et al. (2019). Quantitative proteomic analysis to understand the mechanisms of zinc oxide nanoparticle toxicity to *Daphnia pulex* (Crustacea: Daphniidae): Comparing with bulk zinc oxide and zinc salt. *Environ. Sci. Technol.* 53 (9), 5436–5444. doi:10.1021/acs.est.9b00251

Liu, L., Fan, W., Lu, H., and Xiao, W. (2015). Effects of the interaction between TiO2 with different percentages of exposed {001} facets and Cu2+ on biotoxicity in Daphnia magna. *Sci. Rep.* 5 (1), 11121. doi:10.1038/srep11121

Liu, S., Cui, M., Li, X., Thuyet, D. Q., and Fan, W. (2019). Effects of hydrophobicity of titanium dioxide nanoparticles and exposure scenarios on copper uptake and toxicity in Daphnia magna. *Water Res.* 154, 162–170. doi:10.1016/j.watres.2019.01.055

Louie, S. M., Tilton, R. D., and Lowry, G. V. (2016). Critical review: Impacts of macromolecular coatings on critical physicochemical processes controlling environmental fate of nanomaterials. *Environ. Sci. Nano* 3 (2), 283–310. doi:10.1039/C5EN00104H

Lowry, G. V., Gregory, K. B., Apte, S. C., and Lead, J. R. (2012). Transformations of nanomaterials in the environment. *Environ. Sci. Technol.*, 46(13), pp. 6893–6899. doi:10.1021/es300839e

Lv, X., Huang, B., Zhu, X., Jiang, Y., Chen, B., Tao, Y., et al. (2017). Mechanisms underlying the acute toxicity of fullerene to Daphnia magna: Energy acquisition restriction and oxidative stress. *Water Res.* 123, 696–703. doi:10.1016/j.watres.2017.07.023

Malakar, A., Kanel, S. R., Ray, C., Snow, D. D., and Nadagouda, M. N. (2021). Nanomaterials in the environment, human exposure pathway, and health effects: A review. *Sci. Total Environ.* 759, 143470. doi:10.1016/j.scitotenv.2020.143470

Markiewicz, M., Kumirska, J., Lynch, I., Matzke, M., Köser, J., Bemowsky, S., et al. (2018). Changing environments and biomolecule coronas: Consequences and challenges for the design of environmentally acceptable engineered nanoparticles. *Green Chem.* 20 (18), 4133–4168. doi:10.1039/C8GC01171K

Martinez, D. S. T., Ellis, L. J. A., Da Silva, G. H., Petry, R., Medeiros, A. M., Davoudi, H. H., et al. (2022). Daphnia magna and mixture toxicity with nanomaterials – current status and perspectives in data-driven risk prediction. *Nano Today* 43, 101430. doi:10.1016/j.nantod.2022.101430

Marwal, A., and Gaur, R. K. (2020). "Chapter 18 - molecular markers: Tool for genetic analysis," in *Animal biotechnology*. Editors A. S. Verma and A. Singh Second Edition (Boston: Academic Press), 353–372. doi:10.1016/B978-0-12-811710-1.00016-1

Mattsson, K., Adolfsson, K., Ekvall, M. T., Borgström, M. T., Linse, S., Hansson, L. A., et al. (2016). Translocation of 40 nm diameter nanowires through the intestinal epithelium of Daphnia magna. *Nanotoxicology* 10 (8), 1160–1167. doi:10.1080/17435390.2016.1189615

Mav, D., Shah, R. R., Howard, B. E., Auerbach, S. S., Bushel, P. R., Collins, J. B., et al. (2018). A hybrid gene selection approach to create the S1500+ targeted gene sets for use in high-throughput transcriptomics. *PloS one* 13 (2), e0191105. doi:10.1371/journal.pone.0191105

Maxwell, E. K., Schnitzler, C. E., Havlak, P., Putnam, N. H., Nguyen, A. D., Moreland, R. T., et al. (2014). Evolutionary profiling reveals the heterogeneous origins of classes of human disease genes: Implications for modeling disease genetics in animals. *BMC Evol. Biol.* 14 (1), 212. doi:10.1186/s12862-014-0212-1

Melvin, S. D., and Wilson, S. P. (2013). The utility of behavioral studies for aquatic toxicology testing: A meta-analysis. *Chemosphere* 93 (10), 2217–2223. doi:10.1016/j.chemosphere.2013.07.036

Mendonça, E., Diniz, M., Silva, L., Peres, I., Castro, L., Correia, J. B., et al. (2011). Effects of diamond nanoparticle exposure on the internal structure and reproduction of Daphnia magna. *J. Hazard. Mater.* 186 (1), 265–271. doi:10.1016/j.jhazmat.2010.10.115

Michalaki, A., McGivern, A. R., Poschet, G., Büttner, M., Altenburger, R., and Grintzalis, K. (2022). The effects of single and combined stressors on daphnids—enzyme markers of physiology and metabolomics validate the impact of pollution. *Toxics* 10 (10), 604. doi:10.3390/toxics10100604

Miles, L. S., Breitbart, S. T., Wagner, H. H., and Johnson, M. T. J. (2019). Urbanization shapes the ecology and evolution of plant-arthropod herbivore interactions. *Front. Ecol. Evol.* 7. Available at: https://www.frontiersin.org/articles/10.3389/fevo.2019.00310 (Accessed: March 27, 2023). doi:10.3389/fevo.2019.00310

Mitchell-Olds, T., and Feder, M. E. (2003). Evolutionary and ecological functional genomics. *Nat. Rev. Genet.* 4 (8), 651–657. doi:10.1038/nrg1128

Mitrano, D. M., Motellier, S., Clavaguera, S., and Nowack, B. (2015). Review of nanomaterial aging and transformations through the life cycle of nano-enhanced products. *Environ. Int.* 77, 132–147. doi:10.1016/j.envint.2015.01.013

Mortensen, H. M., Martens, M., Senn, J., Levey, T., Evelo, C. T., Willighagen, E. L., et al. (2022). The AOP-DB RDF: Applying FAIR principles to the semantic integration of AOP data using the research description framework. *Front. Toxicol.* 4, 803983. Available at: https://www.frontiersin.org/articles/10.3389/ftox.2022.803983 (Accessed: March 26, 2023). doi:10.3389/ftox.2022.803983

Moyerbrailean, G. A., Richards, A. L., Kurtz, D., Kalita, C. A., Davis, G. O., Harvey, C. T., et al. (2016). High-throughput allele-specific expression across 250 environmental conditions. *Genome Res.* 26 (12), 1627–1638. doi:10.1101/gr.209759.116

Mwaanga, P., Carraway, E. R., and van den Hurk, P. (2014). The induction of biochemical changes in Daphnia magna by CuO and ZnO nanoparticles. *Aquat. Toxicol.* 150, 201–209. doi:10.1016/j.aquatox.2014.03.011

Nasser, F., Constantinou, J., and Lynch, I. (2020). Nanomaterials in the environment acquire an "eco-corona" impacting their toxicity to *Daphnia magna* —A call for updating toxicity testing policies. *J. Proteomics* 20 (9), 1800412. doi:10.1002/pmic.201800412

Nasser, F., and Lynch, I. (2016). Secreted protein eco-corona mediates uptake and impacts of polystyrene nanoparticles on Daphnia magna. *J. Proteomics* 137, 45–51. doi:10.1016/j.jprot.2015.09.005

Nasser, F., and Lynch, I. (2019). Updating traditional regulatory tests for use with novel materials: Nanomaterial toxicity testing with Daphnia magna. *Saf. Sci.* 118, 497–504. doi:10.1016/j.ssci.2019.05.045

NC3Rs (2022). NC3Rs. Available at: https://www.nc3rs.org.uk/(Accessed November 16, 2022).

Nederstigt, T. A. P., Peijnenburg, W. J. G. M., Blom, R., and Vijver, M. G. (2022). Correlation analysis of single- and multigenerational endpoints in Daphnia magna toxicity tests: A case-study using TiO2 nanoparticles. *Ecotoxicol. Environ. Saf.* 241, 113792. doi:10.1016/j.ecoenv.2022.113792

NOAA (2023) Microplastics | OR&R's marine debris program. Available at: https://marinedebris.noaa.gov/what-marine-debris/microplastics (Accessed January 6, 2023).

OECD (2004). *Oecd 202: Daphnia magna acute immobilisation test*.

OECD (2012). "Oecd 211: Daphnia magna reproduction test," in *OECD guideline for the testing of chemicals 211*.

Oksel Karakus, C., Bilgi, E., and Winkler, D. A. (2021). Biomedical nanomaterials: Applications, toxicological concerns, and regulatory needs. *Nanotoxicology* 15 (3), 331–351. doi:10.1080/17435390.2020.1860265

Olkova, A. (2022). Chronic toxicity testing with Daphnia magna in three generations. *Environ. Res. Eng. Manag.* 78 (1), 31–37. doi:10.5755/j01.erem.78.1.30095

Orsini, L., Gilbert, D., Podicheti, R., Jansen, M., Brown, J. B., Solari, O. S., et al. (2016). Daphnia magna transcriptome by RNA-Seq across 12 environmental stressors:Daphnia magna transcriptome. *Nat. Sci. Data* 3, 160030. doi:10.1038/sdata.2016.30

Ouyang, S., Li, Y., Zheng, T., Wu, K., Wang, X., and Zhou, Q. (2022). Ecotoxicity of natural nanocolloids in aquatic environment. *Water* 14 (19), 2971. doi:10.3390/w14192971

Pan, P., Laver, J. D., Qin, Z., Zhou, Y., Peng, R., Zhao, L., et al. (2021). On-chip rotation of *Caenorhabditis elegans* using microfluidic vortices. *Adv. Mater. Technol.* 6, 2000575. doi:10.1002/admt.202000575

Pavlaki, M. D., Ferreira, A. L. G., Soares, A. M. V. M., and Loureiro, S. (2014). Changes of chemical chronic toxicity to Daphnia magna under different food regimes. *Ecotoxicol. Environ. Saf.* 109, 48–55. doi:10.1016/j.ecoenv.2014.07.039

Poynton, H. C., Varshavsky, J. R., Chang, B., Cavigiolio, G., Holman, P. S., Loguinov, A. V., et al. (2007). Daphnia magna ecotoxicogenomics provides mechanistic insights into metal toxicity. *Environ. Sci. Technol.* 41 (3), 1044–1050. doi:10.1021/es0615573

Qi, Q., Li, Q., Li, J., Mo, J., Tian, Y., and Guo, J. (2022). Transcriptomic analysis and transgenerational effects of ZnO nanoparticles on Daphnia magna: Endocrine-disrupting potential and energy metabolism. *Chemosphere* 290, 133362. doi:10.1016/j.chemosphere.2021.133362

Qiu, T. A., Bozich, J. S., Lohse, S. E., Vartanian, A. M., Jacob, L. M., Meyer, B. M., et al. (2015). Gene expression as an indicator of the molecular response and toxicity in the bacterium Shewanella oneidensis and the water flea Daphnia magna exposed to functionalized gold nanoparticles. *Environ. Sci. Nano* 2 (6), 615–629. doi:10.1039/c5en00037h

Ravindran, S. P., Lüneburg, J., Gottschlich, L., Tams, V., and Cordellier, M. (2019). Daphnia stressor database: Taking advantage of a decade of Daphnia "-omics" data for gene annotation. *Sci. Rep.* 9 (1), 11135. doi:10.1038/s41598-019-47226-0

Reilly, K., Davoudi, H. H., Guo, Z., and Lynch, I. (2022). "Chapter 6:the composition of the eco-corona acquired by micro- and nanoscale plastics impacts on their ecotoxicity and interactions with Co-pollutants," in *Environmental nanopollutants*, 132–155. doi:10.1039/9781839166570-00132

Rochman, C. M., Brookson, C., Bikker, J., Djuric, N., Earn, A., Bucci, K., et al. (2019). Rethinking microplastics as a diverse contaminant suite. *Environ. Toxicol. Chem.* 38 (4), 703–711. doi:10.1002/etc.4371

Rogozin, I. B., Managadze, D., Shabalina, S. A., and Koonin, E. V. (2014). Gene family level comparative analysis of gene expression in mammals validates the ortholog conjecture. *Genome Biol. Evol.* 6 (4), 754–762. doi:10.1093/gbe/evu051

Ros-Rocher, N., Pérez-Posada, A., Leger, M. M., and Ruiz-Trillo, I. (2021). The origin of animals: An ancestral reconstruction of the unicellular-to-multicellular transition. *Open Biol.* 11 (2), 200359. doi:10.1098/rsob.200359

Rosenkranz, P., Chaudhry, Q., Stone, V., and Fernandes, T. F. (2009). A comparison of nanoparticle and fine particle uptake by Daphnia magna. *Environ. Toxicol. Chem.* 28 (10), 2142–2149. doi:10.1897/08-559.1

Rozenberg, A., Parida, M., Leese, F., Weiss, L. C., Tollrian, R., and Manak, J. R. (2015). Transcriptional profiling of predator-induced phenotypic plasticity in *Daphnia pulex*. *Front. zoology* 12 (1), 18. doi:10.1186/s12983-015-0109-x

Ruas, R. d. B., Costa, L. M. S., and Bered, F. (2022). Urbanization driving changes in plant species and communities – a global view. *Glob. Ecol. Conservation* 38, e02243. doi:10.1016/j.gecco.2022.e02243

Rugard, M., Coumoul, X., Carvaillo, J. C., Barouki, R., and Audouze, K. (2020). Deciphering adverse outcome pathway network linked to bisphenol F using text mining and systems toxicology approaches. *Toxicol. Sci.* 173 (1), 32–40. doi:10.1093/toxsci/kfz214

Russo, C., Isidori, M., Deaver, J. A., and Poynton, H. C. (2018). Toxicogenomic responses of low level anticancer drug exposures in Daphnia magna. *Aquat. Toxicol.* 203, 40–50. doi:10.1016/j.aquatox.2018.07.010

Santo, N., Fascio, U., Torres, F., Guazzoni, N., Tremolada, P., Bettinetti, R., et al. (2014). Toxic effects and ultrastructural damages to Daphnia magna of two differently sized ZnO nanoparticles: Does size matter? *Water Res.* 53, 339–350. doi:10.1016/j.watres.2014.01.036

Sasaki, H., Hamatani, T., Kamijo, S., Iwai, M., Kobanawa, M., Ogawa, S., et al. (2019). Impact of oxidative stress on age-associated decline in oocyte developmental competence. *Front. Endocrinol.* 10, 811. doi:10.3389/fendo.2019.00811

Schmiedgruber, M., Hufenus, R., and Mitrano, D. M. (2019). Mechanistic understanding of microplastic fiber fate and sampling strategies: Synthesis and utility of metal doped polyester fibers. *Water Res.* 155, 423–430. doi:10.1016/j.watres.2019.02.044

Schultz, C., Adams, J., Jurkschat, K., Lofts, S., and Spurgeon, D. J. (2020). Chemical transformation and surface functionalisation affect the potential to group nanoparticles for risk assessment. *Environ. Sci. Nano* 7 (10), 3100–3107. doi:10.1039/D0EN00578A

Schultz, C., Gray, J., Verweij, R. A., Busquets-Fité, M., Puntes, V., Svendsen, C., et al. (2018). Aging reduces the toxicity of pristine but not sulphidised silver nanoparticles to soil bacteria. *Environ. Sci. Nano* 5 (11), 2618–2630. doi:10.1039/C8EN00054A

Schür, C., Rist, S., Baun, A., Mayer, P., Hartmann, N. B., and Wagner, M. (2019). When fluorescence is not a particle: The tissue translocation of microplastics in *Daphnia magna* seems an artifact. *Environ. Toxicol. Chem.* 38 (7), 1495–1503. doi:10.1002/etc.4436

Schür, C., Zipp, S., Thalau, T., and Wagner, M. (2020). Microplastics but not natural particles induce multigenerational effects in Daphnia magna. *Environ. Pollut.* 260, 113904. doi:10.1016/j.envpol.2019.113904

Schwarzenberger, A., and Fink, P. (2018). Gene expression and activity of digestive enzymes of *Daphnia pulex* in response to food quality differences. *Comp. Biochem. Physiology Part - B Biochem. Mol. Biol.* 218, 23–29. doi:10.1016/j.cbpb.2018.01.009

Seitz, F., Bundschuh, M., Rosenfeldt, R. R., and Schulz, R. (2013). Nanoparticle toxicity in Daphnia magna reproduction studies: The importance of test design. *Aquat. Toxicol.* 126, 163–168. doi:10.1016/j.aquatox.2012.10.015

Selck, H., Handy, R. D., Fernandes, T. F., Klaine, S. J., and Petersen, E. J. (2016). Nanomaterials in the aquatic environment: A European union–United States perspective on the status of ecotoxicity testing, research priorities, and challenges ahead. *Environ. Toxicol. Chem.* 35 (5), 1055–1067. doi:10.1002/etc.3385

Sha, Y., and Hansson, L. (2022). Ancestral environment determines the current reaction to ultraviolet radiation in Daphnia magna. *Evolution* 76 (8), 1821–1835. doi:10.1111/evo.14555

Sneddon, L. U., Halsey, L. G., and Bury, N. R. (2017). Considering aspects of the 3Rs principles within experimental animal biology. *J. Exp. Biol.* 220 (17), 3007–3016. doi:10.1242/jeb.147058

Song, Y., Xie, L., Lee, Y. K., Brede, D. A., Lyne, F., Kassaye, Y., et al. (2020). Integrative assessment of low-dose gamma radiation effects on Daphnia magna reproduction: Toxicity pathway assembly and AOP development. *Sci. Total Environ.* 705, 135912. doi:10.1016/j.scitotenv.2019.135912

Spanier, K. I., Jansen, M., Decaestecker, E., Hulselmans, G., Becker, D., Colbourne, J. K., et al. (2017). Conserved transcription factors steer growth-related genomic programs in Daphnia. *Genome Biol. Evol.* 9 (6), 1821–1842. doi:10.1093/gbe/evx127

Spurgeon, D. J., Lahive, E., and Schultz, C. L. (2020). Nanomaterial transformations in the environment: Effects of changing exposure forms on bioaccumulation and toxicity. *Small* 16 (36), 2000618. doi:10.1002/smll.202000618

Starnes, D. L., Unrine, J. M., Starnes, C. P., Collin, B. E., Oostveen, E. K., Ma, R., et al. (2015). Impact of sulfidation on the bioavailability and toxicity of silver nanoparticles to *Caenorhabditis elegans*. *Environ. Pollut.* 196, 239–246. doi:10.1016/j.envpol.2014.10.009

Stracke, K., and Hejnol, A. (2023). Marine animal evolutionary developmental biology—advances through technology development. *Evol. Appl.* 16 (2), 580–588. doi:10.1111/eva.13456

Tabatabaei Anaraki, M., Dutta Majumdar, R., Wagner, N., Soong, R., Kovacevic, V., Reiner, E. J., et al. (2018). Development and application of a low-volume flow system for solution-state *in vivo* NMR. *Anal. Chem.* 90 (13), 7912–7921. doi:10.1021/acs.analchem.8b00370

Tan, L.-Y., Huang, B., Xu, S., Wei, Z. B., Yang, L. Y., and Miao, A. J. (2017). Aggregation reverses the carrier effects of TiO2 nanoparticles on cadmium accumulation in the waterflea Daphnia magna. *Environ. Sci. Technol.* 51 (2), 932–939. doi:10.1021/acs.est.6b03951

Tao, X., Li, C., Zhang, B., and He, Y. (2016). Effects of aqueous stable fullerene nanocrystals (nC60) on the food conversion from Daphnia magna to *Danio rerio* in a simplified freshwater food chain. *Chemosphere* 145, 157–162. doi:10.1016/j.chemosphere.2015.11.036

Taylor, N. S., Gavin, A., and Viant, M. R. (2018). Metabolomics discovers early-response metabolic biomarkers that can predict chronic reproductive fitness in individual Daphnia magna. *Metabolites* 8 (3), 42. doi:10.3390/metabo8030042

Tayyebi Sabet Khomami, N., Philippe, A., Abu Quba, A. A., Lechtenfeld, O. J., Guigner, J. M., Heissler, S., et al. (2020). Validation of a field deployable reactor for *in situ* formation of NOM-engineered nanoparticle corona. *Environ. Sci. Nano* 7 (2), 486–500. doi:10.1039/C9EN01090D

Tkaczyk, A., Bownik, A., Dudka, J., Kowal, K., and Ślaska, B. (2021). Daphnia magna model in the toxicity assessment of pharmaceuticals: A review. *Sci. Total Environ.* 763, 143038. doi:10.1016/j.scitotenv.2020.143038

Triebskorn, R., Braunbeck, T., Grummt, T., Hanslik, L., Huppertsberg, S., Jekel, M., et al. (2019). Relevance of nano- and microplastics for freshwater ecosystems: A critical review. *Trends Anal. Chem.* 110, 375–392. doi:10.1016/j.trac.2018.11.023

Van Der Zande, M., Jemec Kokalj, A., Spurgeon, D. J., Loureiro, S., Silva, P. V., Khodaparast, Z., et al. (2020). The gut barrier and the fate of engineered nanomaterials: A view from comparative physiology. *Environ. Sci. Nano* 7 (7), 1874–1898. doi:10.1039/d0en00174k

van Straalen, N. M., and Feder, M. E. (2012). Ecological and evolutionary functional Genomics? How can it contribute to the risk assessment of chemicals? *Environ. Sci. Technol.* 46 (1), 3–9. doi:10.1021/es2034153

Vandegehuchte, M. B., Vandenbrouck, T., De Coninck, D., De Coen, W. M., and Janssen, C. R. (2010). Can metal stress induce transferable changes in gene transcription in Daphnia magna? *Aquat. Toxicol.* 97 (3), 188–195. doi:10.1016/j.aquatox.2009.07.013

Vandenbrouck, T., Jones, O. A. H., Dom, N., Griffin, J. L., and De Coen, W. (2010). Mixtures of similarly acting compounds in Daphnia magna: From gene to metabolite and beyond. *Environ. Int.* 36 (3), 254–268. doi:10.1016/j.envint.2009.12.006

Varg, J. E., Outomuro, D., Kunce, W., Kuehrer, L., Svanbäck, R., and Johansson, F. (2022). Microplastic exposure across trophic levels: Effects on the host–microbiota of freshwater organisms. *Environ. Microbiome* 17 (1), 36. doi:10.1186/s40793-022-00429-x

Varsou, D.-D., Ellis, L. J. A., Afantitis, A., Melagraki, G., and Lynch, I. (2021). Ecotoxicological read-across models for predicting acute toxicity of freshly dispersed versus medium-aged NMs to Daphnia magna. *Chemosphere* 285, 131452. doi:10.1016/j.chemosphere.2021.131452

Villeneuve, D. L., Crump, D., Garcia-Reyero, N., Hecker, M., Hutchinson, T. H., LaLone, C. A., et al. (2014). Adverse outcome pathway (AOP) development I: Strategies and principles. *Toxicol. Sci.* 142 (2), 312–320. doi:10.1093/toxsci/kfu199

Vinken, M. (2019). Omics-based input and output in the development and use of adverse outcome pathways. *Curr. Opin. Toxicol.* 18, 8–12. doi:10.1016/j.cotox.2019.02.006

Völker, C., Boedicker, C., Daubenthaler, J., Oetken, M., and Oehlmann, J. (2013). Comparative toxicity assessment of nanosilver on three Daphnia species in acute, chronic and multi-generation experiments. *PloS one* 8 (10), e75026. doi:10.1371/journal.pone.0075026

Wang, Z., Zhang, L., Zhao, J., and Xing, B. (2016). Environmental processes and toxicity of metallic nanoparticles in aquatic systems as affected by natural organic matter. *Environ. Sci. Nano* 3 (2), 240–255. doi:10.1039/C5EN00230C

Westmeier, D., Stauber, R. H., and Docter, D. (2016). The concept of bio-corona in modulating the toxicity of engineered nanomaterials (ENM). *Toxicol. Appl. Pharmacol.* 299, 53–57. doi:10.1016/j.taap.2015.11.008

Wheeler, K. E., Chetwynd, A. J., Fahy, K. M., Hong, B. S., Tochihuitl, J. A., Foster, L. A., et al. (2021). Environmental dimensions of the protein corona. *Nat. Nanotechnol.* 16 (6), 617–629. doi:10.1038/s41565-021-00924-1

Wilkinson, M. D., Dumontier, M., Aalbersberg, I. J. J., Appleton, G., Axton, M., Baak, A., et al. (2016). The FAIR Guiding Principles for scientific data management and stewardship. *Nature* 3 (1), 160018. doi:10.1038/sdata.2016.18

Wlodkowic, D., and Jansen, M. (2022). High-throughput screening paradigms in ecotoxicity testing: Emerging prospects and ongoing challenges. *Chemosphere* 307, 135929. doi:10.1016/j.chemosphere.2022.135929

World Resources Institute (1996). World Resources 1996-97. Available at: https://www.wri.org/research/world-resources-1996-97 (Accessed May 6, 2022).

Xu, T., Zheng, F., and Zhao, Y. (2023). "Chapter 6 - biophysicochemical transformations of ENMs in air," in *Physicochemical interactions of engineered nanoparticles and plants*. Editors G. D. La Rosa and J. R. Peralta-Videa (Cambridge, Massachusetts, United States: Academic Press: Nanomaterial-Plant Interactions), 143–173. doi:10.1016/B978-0-323-90558-9.00010-3

Yang, F., Gao, C., Wang, P., Zhang, G. J., and Chen, Z. (2016). Fish-on-a-chip: Microfluidics for zebrafish research. *Lab a chip* 16 (7), 1106–1125. doi:10.1039/c6lc00044d

Yin, J., Long, Y., Xiao, W., Liu, D., Tian, Q., Li, Y., et al. (2023). Ecotoxicology of microplastics in Daphnia: A review focusing on microplastic properties and multiscale attributes of Daphnia. *Ecotoxicol. Environ. Saf.* 249, 114433. doi:10.1016/j.ecoenv.2022.114433

Yin, Y., Yang, X., Zhou, X., Wang, W., Yu, S., Liu, J., et al. (2015). Water chemistry controlled aggregation and photo-transformation of silver nanoparticles in environmental waters. *J. Environ. Sci.* 34, 116–125. doi:10.1016/j.jes.2015.04.005

Zhang, F., Wang, Z., Peijnenburg, W. J. G. M., and Vijver, M. G. (2022). Review and prospects on the ecotoxicity of mixtures of nanoparticles and hybrid nanomaterials. *Environ. Sci. Technol.* 56 (22), 15238–15250. doi:10.1021/acs.est.2c03333

Zhang, G., Zhuang, S., Shang, X., Qiu, J., Gao, H., Chen, X., et al. (2017). "An integrated microfluidic system for zebrafish larva organs injection," in IECON 2017 - 43rd Annual Conference of the IEEE Industrial Electronics Society, Beijing, China, 29 October 2017 - 01 November 2017, 8563–8566. doi:10.1109/IECON.2017.8217504

Zhang, H., Cao, J., Wu, S., and Wang, Y. (2014). Mechanism of gold nanoparticles-induced trypsin inhibition: A multi-technique approach. *Mol. Biol. Rep.* 41 (8), 4911–4918. doi:10.1007/s11033-014-3357-5

Zhang, X., Chen, X., Yao, Y., Shang, X., Lu, H., Zhao, W., et al. (2021). A disc-chip based high-throughput acute toxicity detection system. *Talanta* 224, 121867. doi:10.1016/j.talanta.2020.121867

Zhang, X., Xia, P., Wang, P., Yang, J., and Baird, D. J. (2018). Omics advances in ecotoxicology. *Environ. Sci. Technol.* 52 (7), 3842–3851. doi:10.1021/acs.est.7b06494

Zhao, C.-M., and Wang, W.-X. (2010). Biokinetic uptake and efflux of silver nanoparticles in Daphnia magna. *Environ. Sci. Technol.* 44 (19), 7699–7704. doi:10.1021/es101484s

Zimmermann, L., Göttlich, S., Oehlmann, J., Wagner, M., and Völker, C. (2020). What are the drivers of microplastic toxicity? Comparing the toxicity of plastic chemicals and particles to Daphnia magna. *Environ. Pollut.* 267, 115392. doi:10.1016/j.envpol.2020.115392

frontiers | Frontiers in Toxicology

TYPE Review
PUBLISHED 24 April 2023
DOI 10.3389/ftox.2023.1154538

OPEN ACCESS

EDITED BY
Iseult Lynch,
University of Birmingham,
United Kingdom

REVIEWED BY
Oluniyi Olatunji Fadare,
Texas A&M University Corpus Christi,
United States
Chang-Bum Jeong,
Incheon National University, Republic of Korea

*CORRESPONDENCE
Stacey L. Harper,
Stacey.Harper@oregonstate.edu

RECEIVED 30 January 2023
ACCEPTED 13 April 2023
PUBLISHED 24 April 2023

CITATION
Cunningham BE, Sharpe EE, Brander SM, Landis WG and Harper SL (2023), Critical gaps in nanoplastics research and their connection to risk assessment.
Front. Toxicol. 5:1154538.
doi: 10.3389/ftox.2023.1154538

Critical gaps in nanoplastics research and their connection to risk assessment

Brittany E. Cunningham[1], Emma E. Sharpe[2], Susanne M. Brander[1,3], Wayne G. Landis[2] and Stacey L. Harper[1,4,5]*

[1]Department of Environmental and Molecular Toxicology, Oregon State University, Corvallis, OR, United States, [2]Institute of Environmental Toxicology and Chemistry, Western Washington University, Bellingham, WA, United States, [3]Department of Fisheries and Wildlife, Coastal Oregon Experiment Station, Oregon State University, Corvallis, OR, United States, [4]School of Chemical, Biological and Environmental Engineering, Oregon State University, Corvallis, OR, United States, [5]Oregon Nanoscience and Microtechnologies Institute, Corvallis, OR, United States

Reports of plastics, at higher levels than previously thought, in the water that we drink and the air that we breathe, are generating considerable interest and concern. Plastics have been recorded in almost every environment in the world with estimates on the order of trillions of microplastic pieces. Yet, this may very well be an underestimate of plastic pollution as a whole. Once microplastics (<5 mm) break down in the environment, they nominally enter the nanoscale (<1,000 nm), where they cannot be seen by the naked eye or even with the use of a typical laboratory microscope. Thus far, research has focused on plastics in the macro- (>25 mm) and micro-size ranges, which are easier to detect and identify, leaving large knowledge gaps in our understanding of nanoplastic debris. Our ability to ask and answer questions relating to the transport, fate, and potential toxicity of these particles is disadvantaged by the detection and identification limits of current technology. Furthermore, laboratory exposures have been substantially constrained to the study of commercially available nanoplastics; i.e., polystyrene spheres, which do not adequately reflect the composition of environmental plastic debris. While a great deal of plastic-focused research has been published in recent years, the pattern of the work does not answer a number of key factors vital to calculating risk that takes into account the smallest plastic particles; namely, sources, fate and transport, exposure measures, toxicity and effects. These data are critical to inform regulatory decision making and to implement adaptive management strategies that mitigate risk to human health and the environment. This paper reviews the current state-of-the-science on nanoplastic research, highlighting areas where data are needed to establish robust risk assessments that take into account plastics pollution. Where nanoplastic-specific data are not available, suggested substitutions are indicated.

KEYWORDS

microplastic, nanoplastic, risk assesment, toxicity, Bayesian network

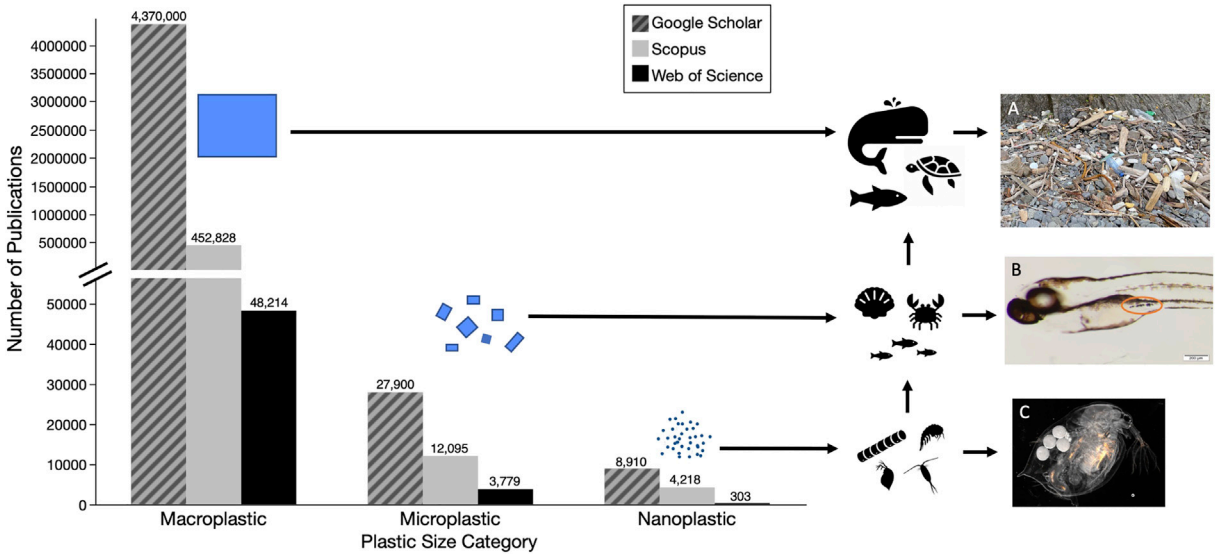

FIGURE 1
Numbers of papers on different size categories of plastic pollutants based on searches of three databases (i.e., Google Scholar—hatched grey, Scopus—grey, and Web of Science - black) **(A)** Macroplastic pollution washed up in the Katmai National Park, Alaska July 2021 **(B)** Exposed Zebrafish (1–20μm, tire particles) with ingested microplastics **(C)** Exposed *Daphnia* (40nm, fluorescent polystyrene). Detailed methods for literature search are described in Supplementary Material.

1 Introduction

Plastic pollution, synthetic organic polymers that are resistant to degradation, is a worldwide issue that, while first noted in the 1970s (Carpenter and Smith, 1972; Colton et al., 1974), did not begin to be widely studied until the 2000s (Derraik, 2002). Annual production of plastics had grown to approximately 368 million tons in 2019 (PlasticsEurope, 2020) and is predicted to increase exponentially by 2050 (Jambeck et al., 2015). In the United States, plastics are currently classified as solid waste, though some have made the case for their classification as hazardous waste, based on established physical and chemical dangers they pose to organisms as well as their persistence in the environment (Rochman et al., 2013). Plastic debris has been observed in a variety of sizes and can be generally classified as macroplastics (>25 mm), microplastics (<5 mm), and nanoplastics (<1 μm) (Gigault et al., 2018). Whereas documentation and research initially focused on easily-visible macroplastics, recent years have witnessed a shift by researchers to smaller microplastics (<100 μm). Yet, comparatively less research has been done on the occurrence and fate of nanoplastics; indeed, many early reviews conducted on plastic pollution failed to mention particles this small (Derraik, 2002; Moore, 2008; Barnes et al., 2009; Ryan et al., 2009; Wabnitz and Nichols, 2010; Sigler, 2014; Li et al., 2016; Avio et al., 2017). Figure 1 illustrates the past focus of plastic research on macro and microplastic pollutants, and highlights the paucity of research on nanoplastics in the environment.

The primary reason for this knowledge limitation is that most methods of detection and identification developed for microplastics do not work for nanoscale particles (Renner et al., 2018; Brander et al., 2020; Caputo et al., 2021). As particle size decreases, plastics become difficult––if not essentially impossible––to detect in the environment. Nanoplastics originate from primary and secondary sources: (1) primary source nanoplastics are manufactured at the nanoscale for industrial, agricultural, and biomedical uses (ASHTON et al., 2010; Cole et al., 2011; Andrady, 2015), or are generated during the manufacture of polymers (Hernandez et al., 2017); (2) secondary source nanoplastics are derived from macro- and microplastics that break down into nano-sized particles in the environment (Lambert and Wagner, 2016; González-Pleiter et al., 2019). Limited knowledge exists about the introduction and transport of nanoplastics in the environment. For example, little is known about the probability and quantity of uptake by microscopic organisms and those higher up the food chain. Overall, both the quantity and effects of plastic pollutants may be underestimated. The chemical and physical properties of plastics are also critically important in understanding the breakdown, transformations and potential environmental impacts of nanoplastics. While there is mounting research on the effects of microplastics in organisms and the environment, there remains appreciable holes in nanoplastic research and how plastic particle fate and behavior changes as it moves from the micro-to the nano-scale. Existing knowledge of microplastic exposures and impacts, as well as research on non-plastic nanomaterials can be harnessed to inform the direction of future nanoplastic studies as well as risk assessment. These knowledge gaps are the focus of subsequent sections, followed by a discussion on their connection to risk assessment.

Ecological risk assessment (ERA) has been applied to a variety of scenarios (Landis, 2021). ERA is described as a cause-effect interaction between (1) sources, (2) stressors, (3) geographical location, and (4) effects and impacts described as probability distributions (Landis and Wiegers, 1997; Wiegers et al., 1998; Landis and Wiegers, 2007). Sources are the type of location for the types of activity that introduce specific stressors to the environment. These stressors can include chemical contaminants, nutrients, non-indigenous species, emergent diseases, and plastics.

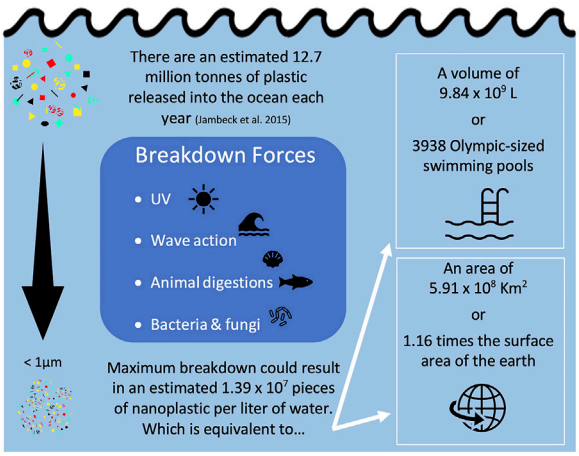

FIGURE 2
Calculation of equivalent nanoplastic particle count, volume, and surface area using a mass balance approach detailed in Supplemental spread sheet.

The stressors have the potential to change ecological systems, and can be biotic or abiotic. Location (often referred to as habitat) is the specific geographical place where the stressor and the endpoints interact. The effects describe the exposure-response relationships between the stressors and endpoints. In risk assessment, an endpoint is defined as a property of the ecosystem that is culturally valued, and is distinguished by an entity or attribute. For example, the endpoint of the spring run Chinook salmon (the entity), with the attribute as a population size at or above a management goal. If there are multiple stressors and multiple endpoints, the matrix of the probability distributions describing the effect to each endpoints is defined as the impact. Harris et al. (2017) has demonstrated that both ecological and human health endpoints can be evaluated applying the same process.

Nanoplastics can be evaluated in the same manner to estimate ecological risk. This manuscript describes and evaluates the current knowledge available to evaluate ecological risk using the described framework. The sources of nanoplastics are described and the routes of these materials to the environment. Nanoplastics can be introduced directly or the result of alteration of macro- and microplastics after introduction. The nanoplastics then exist in the environment by direct introduction or by transport processes and these are listed. There are several modes of toxicity that have been observed or hypothesized for these materials from molecular interactions to mechanical process. These interactions can lead to effects that are ecologically important, specifically those that affect survivorship, growth and reproduction that affect population and community dynamics. A carefully summary of the research and a critique of the state of the art is presented for each of these factors.

2 Detecting and estimating exposure to nanoscale plastics

Nanoplastic exposure is difficult to quantify as we still do not have clear understanding of their concentrations and characteristics in the environment. In their opinion piece, Gigault et al. (2018) attempt to define the word nanoplastic, stating that nanoplastics only come from the breakdown of larger plastics. This statement ignores the primary sources of nanoplastics which are manufactured at a nano-scale. Some examples of this include nanoplastics made for 3D printing (Stephens et al., 2013), drug delivery (Hans and Lowman, 2002), and those used to encapsulate pesticides (Meyer et al., 2015). Any source of macro/micro plastic pollution, can also eventually give rise to nanoplastics through degradation (Andrady, 2015; Lambert and Wagner, 2016). For example, degradation of the estimated 5 trillion (5.0×10^{12}) pieces of microplastic in the environment (Eriksen et al., 2014) could result in 5.0×10^{14} to 5.0×10^{15} pieces of nanoplastic, assuming all were degraded to the nano-scale. One study estimated that up to approximately 14 million tons of plastic were released into the ocean each year (Jambeck et al., 2015), which if entirely degraded to the nano-scale, would be equivalent to 1.52×10^{7} pieces of nano-sized plastics per liter of water (Figure 2). In a 2016 letter, Lenz et al. used observed environmental levels of microplastics, all larger than 5 µm, to project concentrations of nano-sized plastic particles, down to 0.05 µm, in the environment. At Lenz et al. (2016)'s smallest nano-size, the 95% confidence interval of their regression line spanned from approximately 1×10^{3}—1×10^{9} particles per L, which is in line with the degraded concentration we calculated above for Jambeck et al. (2015). No other estimates have been done yet for the concentration of nanoplastics in the environment, or the projected size-ranges that these nanoplastics would fall into.

Once in the environment, nanoplastics can come in contact with organisms and be ingested, inhaled, and/or consumed. Because of their small size, nanoplastics are more likely to pass through biological membranes (Rossi et al., 2013), meaning they can be internalized in additional ways beyond what is possible for a larger-sized particle (Kolandhasamy et al., 2018). Humans are exposed to nanoplastics through a variety of sources including in the air breathed in, the use of personal care products, and consumption of contaminated water and seafood (Yee et al., 2021). However, due to the paucity of data in this area, researchers often rely on studies of microplastic exposure to infer nanoplastic exposure. Studies have shown that both consumption and inhalation are major routes of microplastic intake for humans (Cox et al., 2019; Mohamed Nor et al., 2021). Currently, human nanoplastic exposure has not been quantified because of the lack of information available on environmental nanoplastics; studies are limited by technological limits of plastic detection and identification at the nanoscale.

For larger particles, environmental and/or organismal plastic detection is conducted visually (Moser and Lee, 1992; Eriksen et al., 2014; Van Sebille et al., 2015; Forrest and Hindell, 2018; Kotar et al., 2022). Additional methods and plastic detection and quantification include: Raman Spectroscopy, Fourier Transform Infrared Spectroscopy (FTIR), and Pyrolysis-gas chromatography coupled to mass spectrometry (Bouwmeester et al., 2015; Renner et al., 2018; Primpke et al., 2020; Cowger et al., 2021). Because the current limits of detection for plastic particles is approximately in the 1 µm range for µRaman and the 201 µm for µFTIR (Bouwmeester et al., 2015; Renner et al., 2018; De Frond et al., 2023), these methods fail to detect most nanoplastics. Therefore, existing estimates of plastic concentrations in the environment likely underestimate the true value. Currently, neither Raman nor FTIR are used to identify the

majority of nanoplastics because of the particle mass necessary for detection. However, advances are being made to expand these limits of detection. Though surface enhanced Ramen spectroscopy (Sobhani et al., 2020; Zhou et al., 2021) and pyrolysis (Ter Halle et al., 2017) have been used to identify polymers in the nano size-range, pyrolysis cannot be used for visualization and quantification of individual particles. Additionally, pyrolysis efficiency is not the same for all types of plastics (Ter Halle et al., 2017); for example, Hermabessiere et al. (2018) found that temperature had a large impact on the signal and types of products of pyrolysis for various plastics. Dynamic light scattering (DLS) and scanning electron microscopy (SEM) have also been used to confirm the presence

TABLE 1 What we can and cannot draw from microplastics and nanomaterials research to inform nanoplastics risk assessment.

	Microplastics	Nanomaterials
EXPOSURE		
Environmental Transport:	The density of microplastics and nanoplastics would be the same when broken down from the same macroplastic material. However, nanoplastics may remain suspended in the water column because their mass is so small that gravity does not affect them	Transport through the environment will depend upon the agglomeration state of the nanomaterials and nanoplastics. Both processes should be affected by salinity, pH and organic matter. Transport could be similar if the nanomaterials are similar to the density of the nanoplastics (e.g., nanocellulose)
Environmental Fate:	Fate may be similar if nanoplastics agglomerate into micron-sized agglomerates. Agglomeration is more likely in higher salinity environments	Environmental fate may be comparable if the nanomaterials and nanoplastics have similar densities (e.g., nanocellulose or lignin). The formation of an organic matter layer on the surface of nanomaterials and nanoplastics would be the same if the outermost surface chemistry is the same. Nanoplastics are persistent and do not dissolve; whereas, some nanomaterials (i.e., transition metals) readily dissolve unless coated with a protective barrier
Environmental Sampling:	Current collection techniques for microplastics do not retain nanoplastics so no environmental quantification has been done for nanoplastics	The same issues in environmental sampling for nanomaterials and nanoplastics including difficulties collecting and concentrating the samples, interference of other colloids in the system, and locating them in a complex matrix
Identification:	The same composition of materials found at the macro scale translate to compositions found at the micro scale. It is likely, but not verified, that those will also translate to composition found at the nanoscale Most micro and nanoplastics in the environment are from the breakdown of larger plastics and considered secondary particles. Lack of standard reference materials for both micro and nanoplastics. FTIR and pyrolysis-GC-MS can be used to identify the type of microplastics; however, nanoplastics do not have enough mass for these instruments/techniques to work. Shape can be determined for microplastics using a dissecting or compound microscope; whereas, nanoplastics require the use of electron microscopy to determine shape	Most engineered nanomaterials are produced at the nanoscale and are therefore considered primary particles. Whereas, only a very few types of nanoplastics (e.g., PS, PMMA) are generated as primary particles, most result from the breakdown of microplastics. Standardized reference materials are available for some classes of nanomaterials, but remain lacking for nanoplastics. Dynamic light scattering and nanoparticle tracking analysis can be used for both nanoplastics and nanomaterials. Since both instruments rely on the assumption that the particles are spherical, the vast majority of nanoplastics will violate that assumption while many engineered nanomaterials are engineered to be spheres
Quantification:	Environmental concentrations can be extrapolated across size classes. The relative concentrations of macroplastics found at the macro scale translate to the relative concentrations found at the micro scale. It is likely, but not verified, that those ratios of different types of microplastics are comparable to the ratios found at the nanoscale	Instruments used to measure the size, zeta potential and agglomeration state of nanomaterials can be applied for nanoplastics. For example, dynamic light scattering and nanoparticle tracking analysis can be used to assess nanoplastics; however, clear plastics sometimes evade detection so staining may be required prior to measurement
EFFECTS		
Who is exposed:	Larger organisms can take up micro and nanoplastics incidentally, and microplastics actively. Smaller organisms that have taken up smaller microplastics and nanoplastics may serve as another source for larger organisms through trophic transfer. Filter feeders are more likely to take up micro and nanoplastics when they are stabilized in suspension	Because of their small size, bulk forces like gravity have little effect on nanomaterials including nanoplastics. If unagglomerated, both can remain suspended in water bodies indefinitely leading to exposure of organisms the live in, or traverse, the water column. Small and large organisms can incidentally or actively ingest nanomaterials and nanoplastics
Uptake/Translocation:	The uptake and translocation potential of micro and nanoplastics will differ. While microplastics may be taken up by phagocytlosis, nanoplastics can be actively taken up by cells and translocate into inner body tissues and organs. These uptake mechanisms are size dependent and more can be gleaned from other nanomaterials *versus* microplastics	The mechanisms of uptake would be similar between nanomaterials and nanoplastics, particularly when uptake is a function of size. For example, particles around 100 nm can enter via clathrin-mediated endocytosis, while those between 50 and 80 nm can enter via caveolae-mediated endocytosis
Biodistribution:	The biodistribution of microplastics will be limited by their size where only the smaller microplastics will be small enough to enter inner tissues and organs. Nanoplastics are known to translocate to the liver after ingestion	Biodistribution should be similar among nanomaterials and nanoplastics that have similar size, shape and charge. Accumulation of nanoplastics could occur in the lysosomes as the materials are difficult to break down even in an extremely low pH environment
Toxicity:	Reactive oxygen species generation, oxidative stress, inflammation and metabolic disruption have been indicated for both micro and nanoplastics	Reactive oxygen species generation is a predominant finding for both nanomaterials and nanoplastics. Particle specific effects would be expected for both nanomaterials and nanoplastics. Inflammation, oxidative stress and metabolic disruption have also been indicated for both nanoplastics and nanomaterials

(Continued on following page)

TABLE 1 (*Continued*) **What we can and cannot draw from microplastics and nanomaterials research to inform nanoplastics risk assessment.**

	Microplastics	Nanomaterials
	UNKNOWNS	
Reference materials:	Literature is growing on the development of reference materials for the study of microplastics and the US National Institute of Standards and Technology has a MNP Metrology Project underway to establish standardized methods for size-based separations from complex matrices, chemical characterization protocols, and test materials necessary to enable quantification of micro and nanoplastics. Hawaii Pacific University offers a reference materials kit that has been shared across the micro and nanoplastics field. Reference materials are being generated for tire tread as well. Commercially available reference materials for nanoplastics remain limited to spherical polystyrene, polyethylene and polymethyl methacrylate	Many engineered nanomaterials are commercially available or can be synthesized in small batches that can be strategically designed to tweak one physicochemical property to investigate the impact of that parameter on the behavior of the nanomaterial. Nanomaterials can be precisely engineered for size, shape and surface chemistry and are available in homogeneous suspensions. Whereas, only a few nanoplastics (e.g., polystyrene, PMMA) are commercially available and they are all spherical which is not representative of what is found in the environment from the breakdown of macro and microplastics. In addition, the surface chemistries available on purchased nanoplastics include amine (+) or carboxyl (-) groups, or could be left neutral with no surface chemistry added
Dose metrics:	Microplastics dose is often reported as mg/L as that is the easiest dose metric to empirically measure. Nanoplastics dose; however, is more often reported as particle #/L. Conversion calculations have been established by Besseling et al. (2014), but are still not routinely used	For nanomaterials that dissolve, surface area is the best dose metric to apply since it determines the rate of dissolution. Most other nanomaterial toxicity studies report a mass-based dose. Since nanoplastics do not dissolve, the number of particles is typically reported although this has not been standardized. There are conversion equations to convert between mass and particle number; however, there are many assumptions that are likely violated in this conversion
Requirements for decision makers:	Policies aimed at microplastics can aid in decreasing secondary shed of nanoplastics, but would not address primary nanoplastic production	Structure-activity relationships determined for nanomaterials could likely be applied to nanoplastics with the same surface chemistry, particularly for biopolymeric nanomaterials such as lignin or cellulose
K_{ow}:	The octanol/water partition coefficient (K_{OW}) is one important consideration when asking if plastic particles are acting as vectors for other contaminants and compounds	The octanol/water partition coefficient (K_{OW}) remains a challenge to assess for both nanomaterials and nanoplastics

of nanoplastics in samples (Hernandez et al., 2017), but these operations cannot identify the chemical composition of the particles. A problem with many of these common methods of plastic detection and identification is that as the particle size of the plastic decreases, as with nanoplastics, the probability of misidentification increases (Bouwmeester et al., 2015; De Frond et al., 2023). Most recently, enrichment of environmental samples has been suggested to quantify nanoplastics in water (Cai et al., 2021) and soil (Wahl et al., 2021) samples.

3 Fate and transport of nanoplastics

3.1 Fate and transport of nanoplastics based on microplastics

Plastic particles, especially those in smaller size-ranges, have been found in almost all environmental compartments ranging from the open ocean to farmlands to polar regions (Barnes et al., 2009; Cózar et al., 2014; Van Sebille et al., 2015; Ng et al., 2018; Obbard, 2018; Ross et al., 2021). Even in remote, unpopulated areas of the world, studies have detected quantities of environmental plastics comparable to those in large cities (Allen et al., 2019; Brahney et al., 2020). Though we are beginning to gain an understanding of the transport of microplastics through the air and water, little information exists on how these same mechanisms may transport nanoplastics. Common characteristics shared between micro- and nanoplastics, such as polymer charge and density, make it reasonable to conjecture that many of the mechanisms of transport for larger plastic particles are also responsible for transport of nanoplastics (Table 1). For example, plastics are known to be transported in ocean currents (Avio et al., 2017), sewer systems (Sun et al., 2019), and in the wind (Ryan et al., 2009; Brahney et al., 2021) and atmosphere (Allen et al., 2019). However, it cannot be assumed that fate and transport will be exactly the same between plastics with different sizes or morphologies. Nanoplastic debris is known to behave differently than microplastics (Gigault et al., 2021), especially in terms of floatability (Ter Halle et al., 2017).

Because the majority of plastic research has focused on aquatic environments, we can make even fewer assumptions about the transport and fate of nanoplastics in terrestrial environments. One of the known contributors of plastic particles to soil is through the application of biosolids. Nizzetto et al. (2016b) estimated that between 48 and 330 thousand tons of microplastics contained in biosolids are added annually to farmlands in the United States. In a different study on Canadian biosolid samples, concentrations of microplastics up to 1.4×10^4 particles per kg were detected (Crossman et al., 2020). However, the plastic particles in the biosolids do not remain contained within the agricultural lands; Crossman et al. (2020) also found that over 99% of these micro-sized particles were further transported into aquatic environments. Furthermore, Geyer et al. (2022) evaluated microfiber pollution and estimated that in 1 year 1.6 kilotons of microfibers were released into terrestrial environments in California, United States alone. They also modeled the removal of microfibers from wastewater, and found that their redirection into biosolids resulted in increased application to terrestrial environments (Geyer et al., 2017; Geyer et al., 2022). Though biosolids have not yet been evaluated for concentrations of nano-sized plastics, the number of nanoplastics in farmlands may be higher considering additions of fragmented waste from other sources (Ng et al., 2018). Furthermore, earthworms have been shown to fragment microplastics into nanoplastics (Kwak and An, 2021). This emphasizes the urgency for

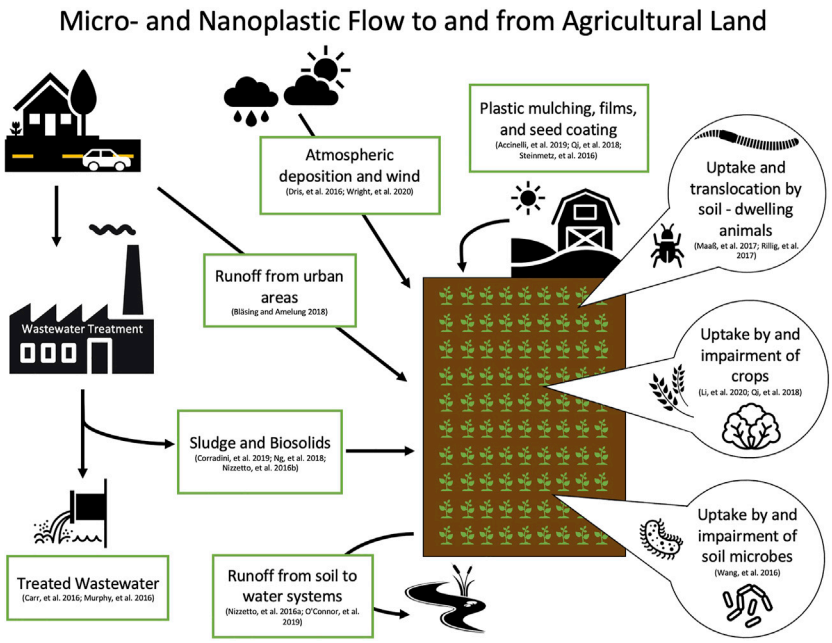

FIGURE 3
Diagram of potential sources and flow of micro- and nanoplastics to soil, and uptake by plants and soil-dwelling organisms (Accinelli et al., 2019; Bläsing and Amelung, 2018; Carr et al., 2016; Corradini et al., 2019; Dris et al., 2016; Li et al., 2020a; Murphy et al., 2016; Nizzetto et al., 2016a; O'connor et al., 2019; Qi et al., 2018; Rillig et al., 2017; Steinmetz et al., 2016; Wang et al., 2016; Wright et al., 2020).

research on nanoplastics in terrestrial environments, as farm soils in particular may act as critical pathways of plastic fragmentation and exposure to both organisms and humans (Hurley and Nizzetto, 2018) (Figure 3).

3.2 Fate and transport of nanoplastics based on non-plastic nanoparticles

Nanomaterial research can be useful in informing study of nanoplastics, particularly in relation to the suspension of nano-scale particles. As nanoparticles have different properties than their bulk counterparts (Farré et al., 2009), we cannot assume that nanoplastics will behave in the same manner as larger plastics. For example, nanoparticles are known to form agglomerates, which can affect their dispersion. The rate and strength of this agglomeration depends on the physical and chemical characteristics of the media that they are in (Gigault et al., 2018; Wu et al., 2019b; Shupe et al., 2021). At the nanoscale, Brownian motion can affect particle sedimentation (Hassan et al., 2014). Therefore, it cannot be assumed that nanoplastics will be transported and partitioned in the same manner as macro- or microplastics. While studies on non-plastic nanomaterials can inform future research on nanoplastics, we cannot simply assume that environmental characteristics and behaviors will be identical (Table 1). Nanoplastics can differ from these better studied nanomaterials in several ways including: (1) a lack of aqueous solubility (Wagner et al., 2018), (2) a lack of exterior charge (Rist and Hartmann, 2018), and/or (3) low density (Rist and Hartmann, 2018). The partitioning of nanoplastics is further complicated by the fact that their transport in differing media is partially dependent on both the particles surface modifications and transformations occurring in the environment (Dong et al., 2019).

4 Current state of nanoplastic research

4.1 Uptake and absorption

Organisms have been shown to uptake nanoplastics rapidly, although the mechanisms of nanoplastic uptake are not fully understood (Kashiwada, 2006; Casado et al., 2013; Booth et al., 2016; Pitt et al., 2018a; Brandts et al., 2020). While the majority of organisms likely ingest nanoplastic particles, either intentionally or unintentionally during feeding (Ward and Kach, 2009), other modes of uptake, such as inhalation, are possible as well (Lim et al., 2021). In fact, one study suggests that in addition to ingestion, bivalves might internalize plastic particles through adherence (Kolandhasamy et al., 2018). The chemical properties of the nanoplastics play a role in determining particle uptake and tissue distribution, which is why nanoplastics will not necessary behave in the same manner as other manufactured nanoparticles. For example, comparison of nanoparticle distribution in *Pecten maximus* exposed to polystyrene (PS) and Ag nanomaterials of similar sizes showed that the particles accumulated in different organs in the scallops (Al-Sid-Cheikh et al., 2013; Al-Sid-Cheikh et al., 2018). For plastic with surface charge modifications, charge seem to be a central component in determination of uptake and dispersion into tissue. Negatively and positively charged nanoplastics of the same type have been found to have different levels of uptake (Cole and Galloway, 2015), accumulation (Sun et al., 2020), and toxicity (Bergami et al., 2017), as well as different sites of accumulation within the organism (Bergami et al., 2016).

Nanoplastic particle size also plays a role in both rate of uptake and tissue distribution. Studies using rotifers, larval oysters, scallops, zebrafish, and *Daphnia* have found that in general smaller particles are internalized faster and disperse throughout the organism, while larger particles are taken up more slowly and tend to accumulate in the intestinal tract (Snell and Hicks, 2011; Cole and Galloway, 2015; Lu et al., 2016; Al-Sid-Cheikh et al., 2018). However, a couple of studies, also using *Daphnia*, contradict these results, citing a greater intake of larger particles than smaller particles (Rosenkranz et al., 2009; Rist et al., 2017). One reason for this discrepancy is that though these studies showed higher uptake of the larger particles, when they compared surface areas they found that values were actually higher for the intake of the smaller than the larger particles (Rosenkranz et al., 2009; Rist et al., 2017). Another reason may be related to the aggregation of certain nanoplastics. Uptake of smaller nanoplastics may have been higher in certain studies because of their increased tendency to form agglomerates resulting in an overall larger size (Ward and Kach, 2009). Nanoparticle size has also been shown to impact the location of particle accumulation within an organism (Lee et al., 2019). Another physical component that likely plays an important role in the determination of nanoplastics uptake is particle morphology or shape, though no studies have investigated this to date.

Due to the above-mentioned difficulties of locating nanoplastics, many uptake studies used commercially-available fluorescent, spherical PS nanoparticles. For example, several studies demonstrated the movement of fluorescence from the GI tract into lipid droplets in *Daphnia* (Rosenkranz et al., 2009; Brun et al., 2017; Cui et al., 2017). However, these fluorescent nanoplastics have since been demonstrated to actually leach fluorescence (Catarino et al., 2019; Schür et al., 2019). Furthermore, toxicity has been found to decrease, or even disappear, following dialysis of nanoplastics (Heinlaan et al., 2020). This information put into question the results of many of those studies and the true ability of various sizes and exposures of nanoplastics to transverse the gut. Yet, the ability of some nanoplastics to disperse into tissues has been demonstrated in studies not using fluorescent nanoplastics, suggesting that they can in-fact cross epithelial walls and cell membranes (Rossi et al., 2013). For example, nanoplastic uptake and partial depuration has been demonstrated in *Gammarus pulex* using metal-doped nano PS (Redondo-Hasselerharm et al., 2021). Overall, further uptake and distribution assessments are needed––specifically studies that use either non-fluorescent or dialyzed fluorescent nanoplastics, as well as nanoplastics of different morphology, sizes, and polymer types, to verify the true fate of these particles within an organism.

4.2 Biodistribution and effects

4.2.1 Impacts of PS nanoplastic on aquatic organisms

The effects of PS nanoplastics have been assessed using a variety of aquatic life-forms. Many studies have investigated the effects of PS nanoplastic on *Daphnia*. Exposure of *Daphnia* to nanoplastics can impact survival, growth, reproduction, and metabolic and immune functions (Besseling et al., 2014; Brun et al., 2017; Cui et al., 2017; Liu et al., 2020b; Liu et al., 2021). Additionally, differing magnitude of effect for *Daphnia pulex* exposed at different ages suggests that age may be an important factor affecting the toxicity of nanoplastic (Liu et al., 2018). Bacteria exposed to PS nanoplastic showed decreased cell growth and increased intracellular reactive oxygen species (Sun et al., 2018). Additionally, PS nanoplastic exposure was associated with decreased growth rates in green algae, *Dunaliella tertiolecta* (Sjollema et al., 2016; Bergami et al., 2017) and *Scenedesmus obliquus* (Besseling et al., 2014). Pinsino et al. (2017) report that sea urchin, *Paracentrotus lividus*, embryos exposed to nanoplastic (PS-NH_2, original particle size 50 nm, agglomerate ~143 nm) displayed developmental malformations and increased expression of stress proteins. Balbi et al. (2017) exposed mussel (*Mytilus galloprovincialis*) embryos to 50 nm cationic polystyrene (PS-NH_2) and found that embryos exposed to the plastics both developed abnormally and exhibited altered expression of genes related to shell formation (Balbi et al., 2017). In adults, exposure to nano PS had negative effects on mussel immune cells (Sendra et al., 2020a; Sendra et al., 2020b) and altered feeding behavior (Wegner et al., 2012). Furthermore, PS nanoplastic exposure has been shown to cause mortality in brine shrimp (*Artemia franciscana*) larvae (Bergami et al., 2017), and to affect feeding, behavior and physiology of adults (Bergami et al., 2016). PS nanoplastics are known to accumulated in the tissue of larval zebrafish (Pitt et al., 2018a). Neurotoxicity and oxidative damage are commonly observed effects in zebrafish nanoplastic exposures (Sarasamma et al., 2020; Sökmen et al., 2020), and nanoplastics have been found to impact zebrafish behavior even when microplastics have not (Chen et al., 2017). Though an abundance of information exists on the impacts of nanoplastic PS spheres, these particles are not representative of the full diversity of nanoplastic pollution in the environment, and their impacts cannot simply be extrapolated to nanoplastics of differing compositions.

4.2.2 Impacts of non-PS nanoplastic on aquatic organisms

Far fewer studies have investigated the effects of organismal exposure to nanoplastics other than PS. One study demonstrated that short-term exposure of a marine fish, *Dicentrarchus labrax,* to 45 nm PMMA nanoplastics effected lipid metabolism and impaired immune function (Brandts et al., 2018). For plankton, PMMA nanoplastics also inhibited growth in *Rhodomonas baltica* (Gomes et al., 2020) and caused oxidative stress in *Gymnodinium aeruginosum* (Huang et al., 2021). Additionally, exposure of cnidarian, *Hydra viridissima*, to nano PMMA resulted in mortality and malformations (Venâncio et al., 2021). Greven et al. (2016) found that exposure to polycarbonate (PC, 158.7 nm) nanoplastics had effects on the immune system of freshwater fish, *Pimephales promelas*. Additionally, *Mytilus edulis L*. exposed to high-density polyethylene (HDPE) particles exhibited an inflammatory cellular response (Von Moos et al., 2012). Further, González-Pleiter et al. (2019) assessed the effects of polyhydroxybutyrate (PHB) nanoplastics on cyanobacteria (*Anabaena*) green algae (*Chlamydomonas reinhardtii*), and *Daphnia* (*Daphnia magna*) and found an increase in ROS formation in all organisms. Clearly, non-PS nanoplastics carry unique potentials for toxicological impacts and their full impacts are not captured in nano-PS studies alone.

4.2.3 Impacts of nanoplastic on terrestrial organisms

There is a general lack of research on the effects of micro- and nanoplastic on terrestrial organisms (Gomes et al., 2022). The limited studies that do exist for these organisms show that, as with aquatic organisms, plastic exposure can be detrimental to growth and development. For example, for soil oligochaete *Enchytraeus crypticus,* exposure to PS nanoplastics resulted in a shift in their microbiome leading to a decrease in weight and reproduction (Zhu et al., 2018). Nano PE was also found to alter the gut microbiome of earthworm (*Metaphire vulgaris*) (Wang et al., 2021). Though far less studied, plants have been shown to accumulate (Sun et al., 2020) and be effected by (Li et al., 2020b) nanoplastics in soil as well. There are still relatively few publications on the toxicity of nanoplastic particles for mammals. For Wistar rats, ingestion of PS nanoplastics has been shown to have neurobehavioral consequences (Rafiee et al., 2018) and induce oxidative stress (Babaei et al., 2021). Additionally, exposure of mice to nano PS resulted in impacts to their microbiome (Szule et al., 2022).

Additionally, though toxicity of plastics for humans has not been assed at the whole-organism level, the effects of PS nanoplastics has been investigated for a variety of human cell lines, including, but not limited to, colon, lung, epithelial, and bladder (Wu et al., 2019a; Lim et al., 2019; Poma et al., 2019; Xu et al., 2019). The micro- and nanoplastics, ranging in size from 20 to over 1,000 nm, have been shown to be readily taken up by the cells and result in alterations to gene expression (Lehner et al., 2019). Much of the literature on the toxicity of nanoplastics to human cells has focused on PS spheres (Wu et al., 2019a; Lim et al., 2019; Poma et al., 2019; Xu et al., 2019). However, Magri et al. (2018) created PET nanoplastics (<100 nm) and found that they were taken up by, and translocated across the epithelium layer of an intestinal model (MAAS et al., 2017; Magrì et al., 2018). Still, little is known about how effects on human cells may differ for nanoplastics composed of materials beside PS, or in other shapes.

4.2.4 Impacts of nanoplastic morphology

The current focus on just one plastic type and shape (i.e., spherical PS) in nanoplastic ecotoxicity testing ignores hundreds of potential combinations of polymer type and particle morphology. We know that the toxicity of microplastics can vary with differing physical characteristics of the plastics; for example, Gray and Weinstein (2017) exposed grass shrimp to different sizes of spheres, fragments, and fibers, discovering a significant difference in the number of microplastic particles internalized between the different shapes. Additionally; Frydkjær et al. (2017) noted that *D. magna* egression of microplastics was slower for irregularly shaped fragments than for spheres. For zebrafish, the shape of the microplastic affects the accumulation and gut toxicity with fibers and then fragments being more toxic than beads (Qiao et al., 2019). A recent synthesis paper suggests that smaller microplastic particles cause greater toxicity (Thornton-Hampton et al., 2022). Nanoplastics also exist in a multiplicity of morphologies, a characteristic which the microplastic research tells us contributes to the toxicity of the particle. A comparison of the toxicity of nanoplastics of different shapes has not been done; however, some have assessed the impacts of nanoplastics in a fragment morphology. Both Siddiqui et al. (2022) and Cunningham et al. (2022) reported that nano tire fragments were highly toxic to aquatic organisms. This connection between morphology and toxicity is one reason that it is important to collect data on a variety of nanoplastic polymers and morphologies.

4.3 Elimination pathways and bioaccumulation

While studies have begun to document internalization of nanoplastics, very little is known about organisms' abilities to expel these materials. Research suggests that as the size of the particle decreases so too does the organism's ability to remove them from the body (Rist et al., 2017). Suspension feeding bivalves, mussels and oysters, had longer gut retention for nano-sized PS particles, than for microplastics (Ward and Kach, 2009). This trend was also observed in aquatic invertebrate, *Diaphanosoma celebensis,* as well (Yoo et al., 2021). However, within the size-category of nanoplastics, there is not a consensus on the size of particle that is egressed most quickly. There is a need for research on nanoplastic egression rates and percent retention. One limitation of existing studies is that in general, they each only compared two particles sizes, and that few of them were the same two sizes (e.g., 2 µm and 100 nm (Ward and Kach, 2009; Rist et al., 2019), 24 nm and 250 nm (Al-Sid-Cheikh et al., 2018), and 100 nm and 30 nm (Rist et al., 2017)). A comparison between only two particle sizes makes it difficult to draw conclusions about how patterns of ingestion, translocation, and egression may change as size changes. Additionally, the seemingly random sizes chosen for these exposures hampers comparison between studies.

In most cases organisms are not able to egress 100% of the nanoplastics they internalize. This may be due to the small size of nanoplastics, which increases their ability to cross biological membranes within organisms and/or to become entrapped (Rossi et al., 2013). Bhargava et al. (2018) exposed larval barnacles to nano PMMA and found that even following a single acute exposure over 3 h, the nanoplastics remained in the body of the barnacles after 7 days; they also observed accumulation of PMMA from chronic exposure (Bhargava et al., 2018). This capability to accumulate within an organism's tissue enhances the possibility for trophic transfer and biomagnification. Casado et al. (2013) studied the effects of polyethyleneimine polystyrene nanoplastics on organisms at a variety of trophic levels including: algae (*Pseudokirchneriella subcapitata*), crustaceans (*Thamnocephalus platyurus* and *D. magna*), bacteria (*Vibrio fischeri*), and rainbow trout (*Oncorhynchus mykiss*) cell lines, . but did not identify trends between toxicity and trophic level of the exposed organism. In addition, a couple of trophic transfer studies have investigated the effects of PS nanoplastics on a simple food chain made up of green algae, zooplankton (*Daphnia*), and fish (carp). Cedervall et al. (2012) found that 25 nm PS nanoplastics were taken up by the algae and transported through the *Daphnia* to the fish. The nanoplastics accumulated in the fish and resulted in disruption of lipid metabolism and alterations in fish behavior (Cedervall et al., 2012). This was supported by Mattsson et al. (2017), who also demonstrate that nanoplastics transfer up a food chain from algae to zooplankton to fish. The PS particles that the fish acquired from

their prey, crossed the blood-brain barrier and resulted in brain damage and altered fish behavior (Mattsson et al., 2017). Similarly, Chae et al. (2018) demonstrated that nano PS was transferred from alga, to *Daphnia*, to secondary-consumer fish (*Oryzias sinensis*), and finally to end-consumer fish (*Zacco temminckii*), and eventually impacted the swimming behavior of the fish. These studies suggest that nanoplastic exposure, either directly or through prey items, can result in behavioral disturbances that may have effects that ripple through the food chain. This emphasizes the need to investigate nanoplastic impacts at an ecosystem level.

4.4 Chronic and multi-generational exposures

The vast majority of studies on nanoplastic toxicity, accumulation, and transfer between organisms have been limited to acute or short-term exposures. Because most of the toxicity studies on nanoplastics use single-generation acute exposure, there remains large data gaps in the areas of chronic and multigenerational nanoplastic exposures. Chronic exposures likely more closely mirror the environmental conditions organisms experience. A few studies have investigated the chronic effects of PS nanoplastics on *Daphnia*. Zhang, et al. (2020) exposed *D. pulex* to 75 nm PS for 21 days and found a decrease in the expression of several key genes related to growth and reproduction. Additionally, they saw a change in sex ratio skewed toward an increase in male neonate (Zhang et al., 2020). Lui, et al. (2019) also exposed *D. pulex* to 75 nm PS for 21 days and reported dose- and time-dependent effects. They found that chronic exposure to the nanoplastics decreased reproductive fitness and increased expression of stress-response genes (Liu et al., 2019). Kelpsiene et al. (2020) exposed *D. magna* to positively charged (aminated) or negatively charged (carboxylated) PS nanoplastics for 103 days and observed a charge-specific decrease in survival rate. Chronic exposure to nanoplastics has also been investigated in mussel *M. galloprovincialis*, where 21-day exposure to PS resulted in genotoxicity and oxidative stress (Gonçalves et al., 2022). Additionally, 1 month exposures to PS nanoplastics have shown negative effects in adult zebrafish (Sarasamma et al., 2020). Overall, because of their short maturation time and life-span, chronic studies have focused on *Daphnia*; however, future studies will need to expand the evaluation of chronic effects of nanoplastics on a wider variety of organisms from differing trophic levels and ecosystems (e.g., freshwater, marine, terrestrial).

There is also a need to better understand the ability of nanoplastics to be passed from exposed parents to offspring, and the potential effects of this transfer on future generations. In two-generation chronic toxicity tests, Lee et al. (2013) showed that PS nanoplastic ingested by copepod (*Tigriopus japonicus*) resulted in increased mortality in the next-generation. Pitt et al. (2018b) exposed zebrafish to 42 nm PS, and found that the nanoplastics accumulated in various tissues of the F1 generation and had an effect on the larval antioxidant system. For organisms with different life histories, other methods of exposure during embryo development are possible. In *D. magna* exposed to 25 nm PS; Brun et al. (2017) reported that the nanoplastics accumulated in the lipophilic cells of embryos in the open brood pouch (Brun et al., 2017). Liu et al. (2020a) noted reproductive effects in the offspring of nanoplastic-exposed *D. pluex* parents. Additionally, Liu et al. (2020c) exposed *D. pluex* to PS nanoplastics for three generations and found alterations in gene expression. Parental exposure of *Caenorhabditis elegans* to nano PS was found to result in transgenerational toxicity (Sun et al., 2021). Though research in this area is expanding, much is left unknown about the potential for developing organisms to be exposed to nanoplastics and its effects on subsequent generations, particularly for organisms beyond *Daphnia* and exposures with non-PS nanoplastics.

5 Prioritized needs and a path forward with risk assessment

5.1 Risk assessment

There has been increased interest from the scientific community and the general public in characterizing and managing the potential risks of plastic particles, including nanoplastics, in the environment. In the terminology of the science of risk analysis, "risk" is defined as the probability of an effect on one or more specific endpoints due to a specific stressor or stressors (National Academies of Sciences and Medicine, 2016). A risk assessment determines the probability distribution of how often a specific change in the environment will affect something of value to society, such as human health, outdoor recreation, or the survival of a key species. This definition implies that there is a cause-effect chain of interactions between the input of the material into the environment and the alteration of the endpoint beyond the cultural goals of the society. The mere potential to cause an effect is not risk.

Ecological risk assessment is a process for quantitatively modeling the numerous interactions between stressors and endpoints and incorporating epistemic and other types of uncertainties (National Academies of Sciences and Medicine, 2016; Landis, 2021). Quantitative risk assessments can indicate where gaps lie in the data necessary to accurately estimate risk, therefore determining and ranking the priority of research needs. The initial steps of a risk assessment are to select ecological endpoints based on site-specific management goals and valued ecosystem services and to build a conceptual model for the relationship between stressors and endpoints. Next, spatial, toxicological, and ecological data are collected, and statistical tools and quantitative models are employed to characterize the causal relationships involved in the system and the potential to the endpoints. Finally, results from the assessment are communicated to key stakeholders and decision-makers who then make decisions about risk mitigation and management strategies (Landis et al., 2017; Coffin et al., 2022; Mehinto et al., 2022).

Here, a specific evaluation of previous risk assessments is made and the methods and results described (Sharpe, 2022). To date, these are examples of assessments for microplastics, not nanoplastics, but serve as examples. Finally, a proposed structure for a general approach to the risk assessment of nanoplastics is described. This approach is based on that developed for microplastics but with a focus on the particular issues when estimating risk due to nanoplastics.

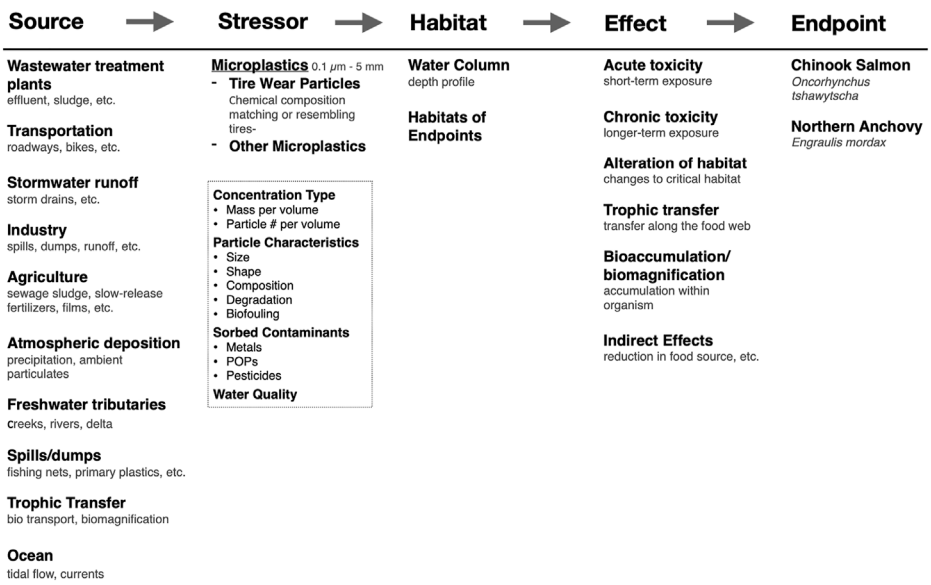

FIGURE 4
A conceptual model for an ecological risk assessment framework for microplastics and nanoplastics for the San Francisco Bay estuary. The cause-effect framework is at the top and fits the source-stressor-habitat/location-effect-endpoint/impact structure.

5.2 A proposed nanoplastic risk assessment framework

An ecological risk assessment for nanoplastics requires a framework that: 1) considers the complex nature of plastic particles and their interactions with ecological factors, other particles, and chemical contaminants, 2) integrates current data and is flexible enough to incorporate new information as it becomes available, 3) considers the uncertainty inherent in our current level of understanding of nanoplastics, and 4) complies with current practices and up-to-date techniques in the field of ecological risk assessment. The Bayesian network relative risk model (BN-RRM) meets these requirements and has been a successful framework for past risk assessments involving complex contaminants at a regional scale (Landis, 2021). The BN-RRM breaks a study site down into risk regions and then uses conditional probability tables in Bayesian networks to outline causal relationships in a system and calculate relative risk (Landis, 2021). Kaikkonen et al. (2021) discusses the capability of Bayesian networks to capture the causal relationship between environmental variables using conditional probability. They are also uniquely good at integrating different types of data and capturing uncertainty in complex systems (Kaikkonen et al., 2021). The BN-RRM can incorporate new information as it becomes available and can be used in adaptive management strategies (Landis et al., 2017). This method will be useful for a nanoplastic risk assessment where our understanding is rapidly evolving, and uncertainty is high.

The critical step in the BN-RRM is the construction of a conceptual model that outlines causal relationships between the sources, stressors, habitat of chosen endpoints, toxicity, and impacts of nanoplastics. Conceptual models used for risk assessment should be specific to a region because environmental factors, management regimes, and societally valuable endpoints can vary significantly between locations. The conceptual model for the San Francisco Bay estuary is illustrated in Figure 4. This is a regional model but can be adapted to many sites and spatial scales (Landis, 2021). Sources of micro- and nanoplastics are likely similar in other urbanized sites but may vary in the magnitude of contribution. Stressors have been broken down into microplastics, nanoplastics, and tire wear particles because of differences in sources, transport mechanisms, and toxicity. In addition, particle characteristics, sorbed contaminants, and water quality parameters are included because of their potential to act as confounding stressors to the primary stressors or endpoints. Effects may be maintained between sites, but the magnitude and measured impacts may vary based on chosen endpoints, management goals, and the presence of other site-specific stressors.

5.3 Existing plastic risk assessments

No risk assessments have been published for nanoplastics; however, several recent publications have purported to estimate risk due to microplastics. These studies are based on models that do not meet current state of the art for ecological risk assessments that is characterized by the extensive use of probability distributions, a careful and detailed description of uncertainty, and the use of sensitivity analysis to describe key variables. Everaert et al. (2018, 2020) used a non-probabilistic approach to model concentrations of microplastics in the environment to estimate the present and future global impact given various plastic waste production scenarios (Everaert et al., 2018; Everaert et al., 2020). Adam et al. (2021) and Tamis et al. (2021) used measured rather than modeled concentration of microplastics but otherwise the methods are similar to Everaert et al. (2018, 2020). These studies concluded a low impact from microplastics however, they used a quotient method to estimate risk relying on species sensitivity distributions and predicted no-effect concentrations. Quotients are not necessarily probabilistic, the use of a single

number (a quotient) underrepresents variability and may not adequately describe an exposure-response relationships (Dale et al., 2008). Coffin et al. (2022) used rescaled microplastic monitoring data from surface water samples in the San Francisco Bay and then compared these data to the management thresholds developed by Mehinto et al. (2022). Mehinto et al. (2022) proposed a microplastic monitoring framework that included four management threshold calculated using species sensitivity distributions. Coffin et al. (2022) concluded that current microplastic concentrations in some parts of the San Francisco Bay exceed risk thresholds. Unlike other studies mentioned here, they included probability distributions, a sensitivity analysis, and an uncertainty analysis but they still relied on sensitivity distributions to determine risk thresholds. Species sensitivity distributions have a number of weaknesses. They assume that the hazardous concentration for five percent of the species (HC5) is an adequate endpoint. Although widely used to approximate impact, the HC5 lacks specificity. Species sensitivity distributions also are impacted by sample number and model choice and may be limited in their ecological relevance (Fox et al., 2021).

A number of these studies also focus on global or continental-scale risk does not allow for consideration of microplastic concentrations gradients, that may exhibit patchy occurrences in the field. The patchiness of the distribution of the particles leads to an underestimate of the uncertainty in the exposure estimation. Xu et al. (2018) also attempted a risk assessment for microplastics. The study is geographically constrained, which allowed them to conduct a finer grain assessment however, they never actually calculated risk. Instead, they performed a hazard assessment to compare the relative concentrations of microplastics in the Changjiang Estuary to that of the adjacent sea. A difference in exposure does not necessarily mean an increase in risk depending on the exposure to the key endpoints specific to that habitat. A hazard assessment is a useful initial step, but it does not meet current risk assessment practice. Although attempts have been made, an ecological risk assessment using current methods has not yet been conducted for microplastics or nanoplastics.

6 Conclusion on data gaps to prioritize

Though existing knowledge in the microplastic and nanomaterials fields can be used to inform nanoplastic risk assessment (Table 1), there are large data gaps on nanoplastic sources, transport, and toxicological impacts that drive uncertainty to levels that make it difficult to perform a robust ecological risk assessment. While the BN-RRM can perform a robust risk assessment where data are limited, collection of data for plastic debris, specifically accounting for the nanoplastic contributions, should continue to be prioritized (Granek et al., 2020). A conceptual framework and preliminary risk assessments can help to identify these gaps helping to highlight future research needs. The data gaps specific to the needs of risk assessment are discussed in greater detail below.

Toxicity studies for nanoplastics do not provide exposure-response information suitable for modeling risk. The typical design of the current generation of toxicity tests has been screening level designs using concentrations a factor of ten apart and the use of hypothesis testing to produce single values such as no/lowest observed effect concentrations (NOEC/LOEC). This type of study design does not map the exposure-response curve, the exposure at which toxic effects are first seen, the concentration that exhibits the maximum response, and the changing slopes of the curve. In contrast, experimental designs that map the exposure-response curve provide information on the shape of the relationship, generate a mathematical description, and generate both confidence and predictive intervals to illustrate uncertainty. In addition, exposure-response curves show variability, patterns in the data, generate confidence and predictive intervals, and place a priority on the testing of more exposures to better map the relationship rather that prioritizing a null hypothesis statistical test result. The advantages described make curve-fitting the method that should be used in risk assessments (Landis and Chapman, 2011; Fox and Landis, 2016).

Quantification of exposure to microplastics and nanoplastics to a broad range of endpoints is lacking. Exposure is quantified as the probability of an endpoint being exposed to a stressor. For ecological risk assessment, it is critical to know or predict exposure concentrations so that exposure-response relationships can be used to determine toxic effects. Derivation of probability distributions for exposure requires knowledge about how nanoplastics move in the environment, where they concentrate, the rate of uptake, and physiological transport. Waldschläger and Schü;ttrumpf (2019) address part of this question by testing microplastics of various compositions, sizes, and shapes and determined settling and rising velocities for each plastic type. This information was then used in conjunction with a site-specific hydrodynamic model to develop a microplastic transport for the San Francisco Bay (Sutton et al., 2019). While this model has limitations, it is the best example of an exposure assessment. Transport mechanisms for nanoplastics likely differ in many ways from microplastics, so any transport model should be specific to nanoplastics.

A risk assessment for microplastics and nanoplastics has not been conducted but is a central priority. The assessment it will aid in determining critical data gaps to aid in making key management decisions. Any ecological risk assessment conducted for nanoplastics (1) should be site-specific, (2) consider the complex interactions that nanoplastics have with other nanoplastics, other stressors (pesticides, PCBs, metals), environmental factors (temperature, dissolved oxygen) and organisms that are exposed to them. To be a risk assessment the process be probabilistic, quantitative and descriptive of uncertainty.

Author contributions

Conceptualization, SB, WL, and SH; Literature review, manuscript writing, figure creation, BC; Risk assessment section and figure, WL, ES; review and editing, BC, ES, WL, SB, and SH; supervision, project administration, funding acquisition, SH (principle investigator).

Funding

This work was funded by the National Science Foundation Growing Convergence Research Big Idea, 1935028 (to SH and SB) and 1935018 (to WL).

Acknowledgments

Research reported in this publication was also supported by the National Institute of Environmental Health Sciences of the National Institutes of Health under Award Number T32ES007060. The content is solely the responsibility of the authors and does not necessarily represent the official views of the National Institutes of Health.

Conflict of interest

The authors declare that the research was conducted in the absence of any commercial or financial relationships that could be construed as a potential conflict of interest.

Publisher's note

All claims expressed in this article are solely those of the authors and do not necessarily represent those of their affiliated organizations, or those of the publisher, the editors and the reviewers. Any product that may be evaluated in this article, or claim that may be made by its manufacturer, is not guaranteed or endorsed by the publisher.

Supplementary material

The Supplementary material for this article can be found online at: https://www.frontiersin.org/articles/10.3389/ftox.2023.1154538/full#supplementary-material

References

Accinelli, C., Abbas, H. K., Shier, W. T., Vicari, A., Little, N. S., Aloise, M. R., et al. (2019). Degradation of microplastic seed film-coating fragments in soil. *Chemosphere* 226, 645–650. doi:10.1016/j.chemosphere.2019.03.161

Adam, V., von Wyl, A., and Nowack, B. (2021). Probabilistic environmental risk assessment of microplastics in marine habitats. *Aquat. Toxicol.* 230, 105689. doi:10.1016/j.aquatox.2020.105689

al-Sid-Cheikh, M., Rouleau, C., and Pelletier, E. (2013). Tissue distribution and kinetics of dissolved and nanoparticulate silver in Iceland scallop (Chlamys islandica). *Mar. Environ. Res.* 86, 21–28. doi:10.1016/j.marenvres.2013.02.003

al-Sid-Cheikh, M., Rowland, S. J., Stevenson, K., Rouleau, C., Henry, T. B., and Thompson, R. C. (2018). Uptake, Whole-body distribution, and depuration of nanoplastics by the scallop pecten maximus at environmentally realistic concentrations. *Environ. Sci. Technol.* 52, 14480–14486. doi:10.1021/acs.est.8b05266

Allen, S., Allen, D., Phoenix, V. R., le Roux, G., Jiménez, P. D., Simonneau, A., et al. (2019). Atmospheric transport and deposition of microplastics in a remote mountain catchment. *Nat. Geosci.* 12, 339–344. doi:10.1038/s41561-019-0335-5

Andrady, A. L. (2015). *Marine anthropogenic litter*. Cham: Springer.Persistence of plastic litter in the oceans

Ashton, K., Holmes, L., and Turner, A. (2010). Association of metals with plastic production pellets in the marine environment. *Mar. Pollut. Bull.* 60, 2050–2055. doi:10.1016/j.marpolbul.2010.07.014

Avio, C. G., Gorbi, S., and Regoli, F. (2017). Plastics and microplastics in the oceans: From emerging pollutants to emerged threat. *Mar. Environ. Res.* 128, 2–11. doi:10.1016/j.marenvres.2016.05.012

Babaei, A. A., Rafiee, M., Khodagholi, F., Ahmadpour, E., and Amereh, F. (2021). Nanoplastics-induced oxidative stress, antioxidant defense, and physiological response in exposed Wistar albino rats. *Environ. Sci. Pollut. Res.* 29, 11332–11344. doi:10.1007/s11356-021-15920-0

Balbi, T., Camisassi, G., Montagna, M., Fabbri, R., Franzellitti, S., Carbone, C., et al. (2017). Impact of cationic polystyrene nanoparticles (PS-NH2) on early embryo development of *Mytilus galloprovincialis*: Effects on shell formation. *Chemosphere* 186, 1–9. doi:10.1016/j.chemosphere.2017.07.120

Barnes, D. K., Galgani, F., Thompson, R. C., and Barlaz, M. (2009). Accumulation and fragmentation of plastic debris in global environments. *Philosophical Trans. R. Soc. B Biol. Sci.* 364, 1985–1998. doi:10.1098/rstb.2008.0205

Bergami, E., Bocci, E., Vannuccini, M. L., Monopoli, M., Salvati, A., Dawson, K. A., et al. (2016). Nano-sized polystyrene affects feeding, behavior and physiology of brine shrimp Artemia franciscana larvae. *Ecotoxicol. Environ. Saf.* 123, 18–25. doi:10.1016/j.ecoenv.2015.09.021

Bergami, E., Pugnalini, S., Vannuccini, M., Manfra, L., Faleri, C., Savorelli, F., et al. (2017). Long-term toxicity of surface-charged polystyrene nanoplastics to marine planktonic species Dunaliella tertiolecta and Artemia franciscana. *Aquat. Toxicol.* 189, 159–169. doi:10.1016/j.aquatox.2017.06.008

Besseling, E., Wang, B., LüRling, M., and Koelmans, A. A. (2014). Nanoplastic affects growth of S. obliquus and reproduction of D. magna. *Environ. Sci. Technol.* 48, 12336–12343. doi:10.1021/es503001d

Bhargava, S., Chen Lee, S. S., Min Ying, L. S., Neo, M. L., Lay-Ming Teo, S., and Valiyaveettil, S. (2018). Fate of nanoplastics in marine larvae: A case study using barnacles, amphibalanus amphitrite. *ACS Sustain. Chem. Eng.* 6, 6932–6940. doi:10.1021/acssuschemeng.8b00766

Bläsing, M., and Amelung, W. (2018). Plastics in soil: Analytical methods and possible sources. *Sci. Total Environ.* 612, 422–435. doi:10.1016/j.scitotenv.2017.08.086

Booth, A. M., Hansen, B. H., Frenzel, M., Johnsen, H., and Altin, D. (2016). Uptake and toxicity of methylmethacrylate-based nanoplastic particles in aquatic organisms. *Environ. Toxicol. Chem.* 35, 1641–1649. doi:10.1002/etc.3076

Bouwmeester, H., Hollman, P. C., and Peters, R. J. (2015). Potential health impact of environmentally released micro-and nanoplastics in the human food production chain: Experiences from nanotoxicology. *Environ. Sci. Technol.* 49, 8932–8947. doi:10.1021/acs.est.5b01090

Brahney, J., Hallerud, M., Heim, E., Hahnenberger, M., and Sukumaran, S. (2020). Plastic rain in protected areas of the United States. *Science* 368, 1257–1260. doi:10.1126/science.aaz5819

Brahney, J., Mahowald, N., Prank, M., Cornwell, G., Klimont, Z., Matsui, H., et al. (2021). Constraining the atmospheric limb of the plastic cycle. *Proc. Natl. Acad. Sci.* 118, e2020719118. doi:10.1073/pnas.2020719118

Brander, S. M., Renick, V. C., Foley, M. M., Steele, C., Woo, M., Lusher, A., et al. (2020). Sampling and quality assurance and quality control: A guide for scientists investigating the occurrence of microplastics across matrices. *Appl. Spectrosc.* 74, 1099–1125. doi:10.1177/0003702820945713

Brandts, I., Garcia-Ordoñez, M., Tort, L., Teles, M., and Roher, N. (2020). Polystyrene nanoplastics accumulate in ZFL cell lysosomes and in zebrafish larvae after acute exposure, inducing a synergistic immune response *in vitro* without affecting larval survival *in vivo*. *Environ. Sci. Nano* 7, 2410–2422. doi:10.1039/d0en00553c

Brandts, I., Teles, M., Tvarijonaviciute, A., Pereira, M., Martins, M., Tort, L., et al. (2018). Effects of polymethylmethacrylate nanoplastics on *Dicentrarchus labrax*. *Genomics* 110, 435–441. doi:10.1016/j.ygeno.2018.10.006

Brun, N. R., Beenakker, M. M., Hunting, E. R., Ebert, D., and Vijver, M. G. (2017). Brood pouch-mediated polystyrene nanoparticle uptake during Daphnia magna embryogenesis. *Nanotoxicology* 11, 1059–1069. doi:10.1080/17435390.2017.1391344

Cai, H., Chen, M., du, F., Matthews, S., and Shi, H. (2021). Separation and enrichment of nanoplastics in environmental water samples via ultracentrifugation. *Water Res.* 203, 117509. doi:10.1016/j.watres.2021.117509

Caputo, F., Vogel, R., Savage, J., Vella, G., Law, A., della Camera, G., et al. (2021). Measuring particle size distribution and mass concentration of nanoplastics and microplastics: Addressing some analytical challenges in the sub-micron size range. *J. Colloid Interface Sci.* 588, 401–417. doi:10.1016/j.jcis.2020.12.039

Carpenter, E. J., and Smith, K. (1972). Plastics on the sargasso sea surface. *Science* 175, 1240–1241. doi:10.1126/science.175.4027.1240

Carr, S. A., Liu, J., and Tesoro, A. G. (2016). Transport and fate of microplastic particles in wastewater treatment plants. *Water Res.* 91, 174–182. doi:10.1016/j.watres.2016.01.002

Casado, M. P., Macken, A., and Byrne, H. J. (2013). Ecotoxicological assessment of silica and polystyrene nanoparticles assessed by a multitrophic test battery. *Environ. Int.* 51, 97–105. doi:10.1016/j.envint.2012.11.001

Catarino, A. I., Frutos, A., and Henry, T. B. (2019). Use of fluorescent-labelled nanoplastics (NPs) to demonstrate NP absorption is inconclusive without adequate controls. *Sci. Total Environ.* 670, 915–920. doi:10.1016/j.scitotenv.2019.03.194

Cedervall, T., Hansson, L.-A., Lard, M., Frohm, B., and Linse, S. (2012). Food chain transport of nanoparticles affects behaviour and fat metabolism in fish. *PloS one* 7, e32254. doi:10.1371/journal.pone.0032254

Chae, Y., Kim, D., Kim, S. W., and An, Y.-J. (2018). Trophic transfer and individual impact of nano-sized polystyrene in a four-species freshwater food chain. *Sci. Rep.* 8, 284–311. doi:10.1038/s41598-017-18849-y

Chen, Q., Gundlach, M., Yang, S., Jiang, J., Velki, M., Yin, D., et al. (2017). Quantitative investigation of the mechanisms of microplastics and nanoplastics toward zebrafish larvae locomotor activity. *Sci. total Environ.* 584, 1022–1031. doi:10.1016/j.scitotenv.2017.01.156

Coffin, S., Bouwmeester, H., Brander, S., Damdimopoulou, P., Gouin, T., Hermabessiere, L., et al. (2022). Development and application of a health-based framework for informing regulatory action in relation to exposure of microplastic particles in California drinking water. *Microplastics Nanoplastics* 2, 12. doi:10.1186/s43591-022-00030-6

Cole, M., and Galloway, T. S. (2015). Ingestion of nanoplastics and microplastics by Pacific oyster larvae. *Environ. Sci. Technol.* 49, 14625–14632. doi:10.1021/acs.est.5b04099

Cole, M., Lindeque, P., Halsband, C., and Galloway, T. S. (2011). Microplastics as contaminants in the marine environment: A review. *Mar. Pollut. Bull.* 62, 2588–2597. doi:10.1016/j.marpolbul.2011.09.025

Colton, J. B., Knapp, F. D., and Burns, B. R. (1974). Plastic particles in surface waters of the northwestern Atlantic. *Science* 185, 491–497. doi:10.1126/science.185.4150.491

Corradini, F., Meza, P., Eguiluz, R., Casado, F., Huerta-Lwanga, E., and Geissen, V. (2019). Evidence of microplastic accumulation in agricultural soils from sewage sludge disposal. *Sci. Total Environ.* 671, 411–420. doi:10.1016/j.scitotenv.2019.03.368

Cowger, W., Steinmetz, Z., Gray, A., Munno, K., Lynch, J., Hapich, H., et al. (2021). Microplastic spectral classification needs an open source community: Open specy to the rescue. *Anal. Chem.* 93, 7543–7548. doi:10.1021/acs.analchem.1c00123

Cox, K. D., Covernton, G. A., Davies, H. L., Dower, J. F., Juanes, F., and Dudas, S. E. (2019). *Human consumption of microplastics*. Washington, DC: Environmental Science & Technology is published by ACS. doi:10.1021/acs.est.9b01517

Cózar, A., Echevarría, F., González-Gordillo, J. I., Irigoien, X., Úbeda, B., Hernández-León, S., et al. (2014). Plastic debris in the open ocean. *Proc. Natl. Acad. Sci.* 111, 10239–10244. doi:10.1073/pnas.1314705111

Crossman, J., Hurley, R. R., Futter, M., and Nizzetto, L. (2020). Transfer and transport of microplastics from biosolids to agricultural soils and the wider environment. *Sci. Total Environ.* 724, 138334. doi:10.1016/j.scitotenv.2020.138334

Cui, R., Kim, S. W., and An, Y.-J. (2017). Polystyrene nanoplastics inhibit reproduction and induce abnormal embryonic development in the freshwater crustacean Daphnia galeata. *Sci. Rep.* 7, 12095. doi:10.1038/s41598-017-12299-2

Cunningham, B., Harper, B., Brander, S., and Harper, S. (2022). Toxicity of micro and nano tire particles and leachate for model freshwater organisms. *J. Hazard. Mater.* 429, 128319. doi:10.1016/j.jhazmat.2022.128319

Dale, V. H., Biddinger, G. R., Newman, M. C., Oris, J. T., Suter, G. W., Thompson, T., et al. (2008). Enhancing the ecological risk assessment process. *Integr. Environ. Assess. Manag.* 4, 306–313. doi:10.1897/IEAM_2007-066.1

de Frond, H., Cowger, W., Renick, V., Brander, S., Primpke, S., Sukumaran, S., et al. (2023). What determines accuracy of chemical identification when using microspectroscopy for the analysis of microplastics? *Chemosphere* 313, 137300. doi:10.1016/j.chemosphere.2022.137300

Derraik, J. G. (2002). The pollution of the marine environment by plastic debris: A review. *Mar. Pollut. Bull.* 44, 842–852. doi:10.1016/s0025-326x(02)00220-5

Dong, Z., Zhu, L., Zhang, W., Huang, R., Lv, X., Jing, X., et al. (2019). Role of surface functionalities of nanoplastics on their transport in seawater-saturated sea sand. *Environ. Pollut.* 255, 113177. doi:10.1016/j.envpol.2019.113177

Dris, R., Gasperi, J., Saad, M., Mirande, C., and Tassin, B. (2016). Synthetic fibers in atmospheric fallout: A source of microplastics in the environment? *Mar. Pollut. Bull.* 104, 290–293. doi:10.1016/j.marpolbul.2016.01.006

Eriksen, M., Lebreton, L. C., Carson, H. S., Thiel, M., Moore, C. J., Borerro, J. C., et al. (2014). Plastic pollution in the world's oceans: More than 5 trillion plastic pieces weighing over 250,000 tons afloat at sea. *PloS one* 9, e111913. doi:10.1371/journal.pone.0111913

Everaert, G., de Rijcke, M., Lonneville, B., Janssen, C., Backhaus, T., Mees, J., et al. (2020). Risks of floating microplastic in the global ocean. *Environ. Pollut.* 267, 115499. doi:10.1016/j.envpol.2020.115499

Everaert, G., van Cauwenberghe, L., de Rijcke, M., Koelmans, A. A., Mees, J., Vandegehuchte, M., et al. (2018). Risk assessment of microplastics in the ocean: Modelling approach and first conclusions. *Environ. Pollut.* 242, 1930–1938. doi:10.1016/j.envpol.2018.07.069

Farré, M., Gajda-Schrantz, K., Kantiani, L., and Barceló, D. (2009). Ecotoxicity and analysis of nanomaterials in the aquatic environment. *Anal. Bioanal. Chem.* 393, 81–95. doi:10.1007/s00216-008-2458-1

Forrest, A. K., and Hindell, M. (2018). Ingestion of plastic by fish destined for human consumption in remote South Pacific Islands. *Aust. J. Marit. Ocean Aff.* 10, 81–97. doi:10.1080/18366503.2018.1460945

Fox, D. R., and Landis, W. G. (2016). Don't be fooled—a no-observed-effect concentration is no substitute for a poor concentration–response experiment. *Environ. Toxicol. Chem.* 35, 2141–2148. doi:10.1002/etc.3459

Fox, D., van Dam, R., Fisher, R., Batley, G., Tillmanns, A., Thorley, J., et al. (2021). Recent developments in species sensitivity distribution modeling. *Environ. Toxicol. Chem.* 40, 293–308. doi:10.1002/etc.4925

Frydkjær, C. K., Iversen, N., and Roslev, P. (2017). Ingestion and egestion of microplastics by the cladoceran Daphnia magna: Effects of regular and irregular shaped plastic and sorbed phenanthrene. *Bull. Environ. Contam. Toxicol.* 99, 655–661. doi:10.1007/s00128-017-2186-3

Geyer, R., Gavigan, J., Jackson, A. M., Saccomanno, V. R., Suh, S., and Gleason, M. G. (2022). Quantity and fate of synthetic microfiber emissions from apparel washing in California and strategies for their reduction. *Environ. Pollut.* 298, 118835. doi:10.1016/j.envpol.2022.118835

Geyer, R., Jambeck, J. R., and Law, K. L. (2017). Production, use, and fate of all plastics ever made. *Sci. Adv.* 3, e1700782. doi:10.1126/sciadv.1700782

Gigault, J., el Hadri, H., Nguyen, B., Grassl, B., Rowenczyk, L., Tufenkji, N., et al. (2021). Nanoplastics are neither microplastics nor engineered nanoparticles. *Nat. Nanotechnol.* 16, 501–507. doi:10.1038/s41565-021-00886-4

Gigault, J., Ter Halle, A., Baudrimont, M., Pascal, P.-Y., Gauffre, F., Phi, T.-L., et al. (2018). Current opinion: What is a nanoplastic? *Environ. Pollut.* 235, 1030–1034. doi:10.1016/j.envpol.2018.01.024

Gomes, T., Almeida, A. C., and Georgantzopoulou, A. (2020). Characterization of cell responses in Rhodomonas baltica exposed to PMMA nanoplastics. *Sci. Total Environ.* 726, 138547. doi:10.1016/j.scitotenv.2020.138547

Gomes, T., Bour, A., Coutris, C., Almeida, A. C., Bråte, I. L., Wolf, R., et al. (2022). "Ecotoxicological impacts of micro-and nanoplastics in terrestrial and aquatic environments," in *Microplastic in the environment: Pattern and process*. (Switzerland: Environmental Contamination Remediation and Management is published by Springer), 199–260. doi:10.1007/978-3-030-78627-4_7

Gonçalves, J. M., Sousa, V. S., Teixeira, M. R., and Bebianno, M. J. (2022). Chronic toxicity of polystyrene nanoparticles in the marine mussel *Mytilus galloprovincialis*. *Chemosphere* 287, 132356. doi:10.1016/j.chemosphere.2021.132356

González-Pleiter, M., Tamayo-Belda, M., Pulido-Reyes, G., Amariei, G., Leganés, F., Rosal, R., et al. (2019). Secondary nanoplastics released from a biodegradable microplastic severely impact freshwater environments. *Environ. Sci. Nano* 6, 1382–1392. doi:10.1039/c8en01427b

Granek, E., Brander, S., and Holland, E. (2020). Microplastics in aquatic organisms: Improving understanding and identifying research directions for the next decade. *Limnol. Oceanogr. Lett.* 5, 1–4. doi:10.1002/lol2.10145

Gray, A. D., and Weinstein, J. E. (2017). Size-and shape-dependent effects of microplastic particles on adult daggerblade grass shrimp (Palaemonetes pugio). *Environ. Toxicol. Chem.* 36, 3074–3080. doi:10.1002/etc.3881

Greven, A. C., Merk, T., Karagöz, F., Mohr, K., Klapper, M., Jovanović, B., et al. (2016). Polycarbonate and polystyrene nanoplastic particles act as stressors to the innate immune system of fathead minnow (*Pimephales promelas*). *Environ. Toxicol. Chem.* 35, 3093–3100. doi:10.1002/etc.3501

Hans, M. L., and Lowman, A. M. (2002). Biodegradable nanoparticles for drug delivery and targeting. *Curr. Opin. Solid State Mater. Sci.* 6, 319–327. doi:10.1016/s1359-0286(02)00117-1

Hassan, P. A., Rana, S., and Verma, G. (2014). Making sense of brownian motion: Colloid characterization by dynamic light scattering. *Langmuir* 31, 3–12. doi:10.1021/la501789z

Heinlaan, M., Kasemets, K., Aruoja, V., Blinova, I., Bondarenko, O., Lukjanova, A., et al. (2020). Hazard evaluation of polystyrene nanoplastic with nine bioassays did not show particle-specific acute toxicity. *Sci. Total Environ.* 707, 136073. doi:10.1016/j.scitotenv.2019.136073

Hermabessiere, L., Himber, C., Boricaud, B., Kazour, M., Amara, R., Cassone, A.-L., et al. (2018). Optimization, performance, and application of a pyrolysis-GC/MS method for the identification of microplastics. *Anal. Bioanal. Chem.* 410, 6663–6676. doi:10.1007/s00216-018-1279-0

Hernandez, L. M., Yousefi, N., and Tufenkji, N. (2017). Are there nanoplastics in your personal care products? *Environ. Sci. Technol. Lett.* 4, 280–285. doi:10.1021/acs.estlett.7b00187

Huang, W., Zhao, T., Zhu, X., Ni, Z., Guo, X., Tan, L., et al. (2021). *The effects and mechanisms of polystyrene and polymethyl methacrylate with different sizes and concentrations on Gymnodinium aeruginosum*. United Kingdom: Environmental Pollution is published by Elsevier, 117626.

Hurley, R. R., and Nizzetto, L. (2018). Fate and occurrence of micro (nano) plastics in soils: Knowledge gaps and possible risks. *Curr. Opin. Environ. Sci. Health* 1, 6–11. doi:10.1016/j.coesh.2017.10.006

Jambeck, J. R., Geyer, R., Wilcox, C., Siegler, T. R., Perryman, M., Andrady, A., et al. (2015). Marine pollution. Plastic waste inputs from land into the ocean. *Science* 347, 768–771. doi:10.1126/science.1260352

Kaikkonen, L., Parviainen, T., Rahikainen, M., Uusitalo, L., and Lehikoinen, A. (2021). Bayesian networks in environmental risk assessment: A review. *Integr. Environ. Assess. Manag.* 17, 62–78. doi:10.1002/ieam.4332

Kashiwada, S. (2006). Distribution of nanoparticles in the see-through medaka (*Oryzias latipes*). *Environ. health Perspect.* 114, 1697–1702. doi:10.1289/ehp.9209

Kelpsiene, E., Torstensson, O., Ekvall, M. T., Hansson, L.-A., and Cedervall, T. (2020). Long-term exposure to nanoplastics reduces life-time in Daphnia magna. *Sci. Rep.* 10, 5979–5987. doi:10.1038/s41598-020-63028-1

Kolandhasamy, P., Su, L., Li, J., Qu, X., Jabeen, K., and Shi, H. (2018). Adherence of microplastics to soft tissue of mussels: A novel way to uptake microplastics beyond ingestion. *Sci. Total Environ.* 610, 635–640. doi:10.1016/j.scitotenv.2017.08.053

Kotar, S., Mcneish, R., Murphy-Hagan, C., Renick, V., Lee, C.-F. T., Steele, C., et al. (2022). Quantitative assessment of visual microscopy as a tool for microplastic research: Recommendations for improving methods and reporting. *Chemosphere* 308, 136449. doi:10.1016/j.chemosphere.2022.136449

Kwak, J. I., and An, Y.-J. (2021). Microplastic digestion generates fragmented nanoplastics in soils and damages earthworm spermatogenesis and coelomocyte viability. *J. Hazard. Mater.* 402, 124034. doi:10.1016/j.jhazmat.2020.124034

Lambert, S., and Wagner, M. (2016). Characterisation of nanoplastics during the degradation of polystyrene. *Chemosphere* 145, 265–268. doi:10.1016/j.chemosphere.2015.11.078

Landis, W. G. (2021). The origin, development, application, lessons learned, and future regarding the Bayesian network relative risk model for ecological risk assessment. *Integr. Environ. Assess. Manag.* 17, 79–94. doi:10.1002/ieam.4351

Landis, W. G., and Chapman, P. M. (2011). *Well past time to stop using NOELs and LOELs*. Wiley Online Library.

Landis, W. G., Markiewicz, A. J., Ayre, K. K., Johns, A. F., Harris, M. J., Stinson, J. M., et al. (2017). A general risk-based adaptive management scheme incorporating the Bayesian Network Relative Risk Model with the South River, Virginia, as case study. *Integr. Environ. Assess. Manag.* 13, 115–126. doi:10.1002/ieam.1800

Landis, W. G., and Wiegers, J. A. (1997). Design considerations and a suggested approach for regional and comparative ecological risk assessment. *Hum. Ecol. Risk Assess.* 3, 287–297. doi:10.1080/10807039709383685

Landis, W. G., and Wiegers, J. A. (2007). Ten years of the relative risk model and regional scale ecological risk assessment. *Hum. Ecol. Risk Assess.* 13, 25–38. doi:10.1080/10807030601107536

Lee, K.-W., Shim, W. J., Kwon, O. Y., and Kang, J.-H. (2013). Size-dependent effects of micro polystyrene particles in the marine copepod Tigriopus japonicus. *Environ. Sci. Technol.* 47, 11278–11283. doi:10.1021/es401932b

Lee, W. S., Cho, H.-J., Kim, E., Huh, Y. H., Kim, H.-J., Kim, B., et al. (2019). Bioaccumulation of polystyrene nanoplastics and their effect on the toxicity of Au ions in zebrafish embryos. *Nanoscale* 11, 3173–3185. doi:10.1039/c8nr09321k

Lehner, R., Weder, C., Petri-Fink, A., and Rothen-Rutishauser, B. (2019). Emergence of nanoplastic in the environment and possible impact on human health. *Environ. Sci. Technol.* 53, 1748–1765. doi:10.1021/acs.est.8b05512

Li, L., Luo, Y., Li, R., Zhou, Q., Peijnenburg, W. J., Yin, N., et al. (2020a). Effective uptake of submicrometre plastics by crop plants via a crack-entry mode. *Nat. Sustain.* 3, 929–937. doi:10.1038/s41893-020-0567-9

Li, W. C., Tse, H., and Fok, L. (2016). Plastic waste in the marine environment: A review of sources, occurrence and effects. *Sci. Total Environ.* 566, 333–349. doi:10.1016/j.scitotenv.2016.05.084

Li, Z., Li, R., Li, Q., Zhou, J., and Wang, G. (2020b). Physiological response of cucumber (Cucumis sativus L.) leaves to polystyrene nanoplastics pollution. *Chemosphere* 255, 127041. doi:10.1016/j.chemosphere.2020.127041

Lim, D., Jeong, J., Song, K. S., Sung, J. H., Oh, S. M., and Choi, J. (2021). Inhalation toxicity of polystyrene micro (nano) plastics using modified OECD TG 412. *Chemosphere* 262, 128330. doi:10.1016/j.chemosphere.2020.128330

Lim, S. L., Ng, C. T., Zou, L., Lu, Y., Chen, J., Bay, B. H., et al. (2019). Targeted metabolomics reveals differential biological effects of nanoplastics and nanoZnO in human lung cells. *Nanotoxicology* 13, 1117–1132. doi:10.1080/17435390.2019.1640913

Liu, Z., Cai, M., Wu, D., Yu, P., Jiao, Y., Jiang, Q., et al. (2020a). Effects of nanoplastics at predicted environmental concentration on *Daphnia pulex* after exposure through multiple generations. *Environ. Pollut.* 256, 113506. doi:10.1016/j.envpol.2019.113506

Liu, Z., Cai, M., Yu, P., Chen, M., Wu, D., Zhang, M., et al. (2018). Age-dependent survival, stress defense, and AMPK in *Daphnia pulex* after short-term exposure to a polystyrene nanoplastic. *Aquat. Toxicol.* 204, 1–8. doi:10.1016/j.aquatox.2018.08.017

Liu, Z., Huang, Y., Jiao, Y., Chen, Q., Wu, D., Yu, P., et al. (2020b). Polystyrene nanoplastic induces ROS production and affects the MAPK-HIF-1/NFkB-mediated antioxidant system in *Daphnia pulex*. *Aquat. Toxicol.* 220, 105420. doi:10.1016/j.aquatox.2020.105420

Liu, Z., Jiao, Y., Chen, Q., Li, Y., Tian, J., Huang, Y., et al. (2020c). Two sigma and two mu class genes of glutathione S-transferase in the waterflea *Daphnia pulex*: Molecular characterization and transcriptional response to nanoplastic exposure. *Chemosphere* 248, 126065. doi:10.1016/j.chemosphere.2020.126065

Liu, Z., Li, Y., Pérez, E., Jiang, Q., Chen, Q., Jiao, Y., et al. (2021). Polystyrene nanoplastic induces oxidative stress, immune defense, and glycometabolism change in *Daphnia pulex*: Application of transcriptome profiling in risk assessment of nanoplastics. *J. Hazard. Mater.* 402, 123778. doi:10.1016/j.jhazmat.2020.123778

Liu, Z., Yu, P., Cai, M., Wu, D., Zhang, M., Huang, Y., et al. (2019). Polystyrene nanoplastic exposure induces immobilization, reproduction, and stress defense in the freshwater cladoceran *Daphnia pulex*. *Chemosphere* 215, 74–81. doi:10.1016/j.chemosphere.2018.09.176

Lu, Y., Zhang, Y., Deng, Y., Jiang, W., Zhao, Y., Geng, J., et al. (2016). Uptake and accumulation of polystyrene microplastics in zebrafish (*Danio rerio*) and toxic effects in liver. *Environ. Sci. Technol.* 50, 4054–4060. doi:10.1021/acs.est.6b00183

Maas, S., Daphi, D., Lehmann, A., and Rillig, M. C. (2017). Transport of microplastics by two collembolan species. *Environ. Pollut.* 225, 456–459. doi:10.1016/j.envpol.2017.03.009

Magrì, D., Sanchez-Moreno, P., Caputo, G., Gatto, F., Veronesi, M., Bardi, G., et al. (2018). Laser ablation as a versatile tool to mimic polyethylene terephthalate nanoplastic pollutants: Characterization and toxicology assessment. *ACS Nano* 12, 7690–7700. doi:10.1021/acsnano.8b01331

Mattsson, K., Johnson, E. V., Malmendal, A., Linse, S., Hansson, L.-A., and Cedervall, T. (2017). Brain damage and behavioural disorders in fish induced by plastic nanoparticles delivered through the food chain. *Sci. Rep.* 7, 11452. doi:10.1038/s41598-017-10813-0

Mehinto, A. C., Coffin, S., Koelmans, A. A., Brander, S. M., Wagner, M., Thornton Hampton, L. M., et al. (2022). Risk-based management framework for microplastics in aquatic ecosystems. *Microplastics Nanoplastics* 2, 17–10. doi:10.1186/s43591-022-00033-3

Meyer, W., Gurman, P., Stelinski, L., and Elman, N. (2015). Functional nano-dispensers (FNDs) for delivery of insecticides against phytopathogen vectors. *Green Chem.* 17, 4173–4177. doi:10.1039/c5gc00717h

Mohamed Nor, N. H., Kooi, M., Diepens, N. J., and Koelmans, A. A. (2021). Lifetime accumulation of microplastic in children and adults. *Environ. Sci. Technol.* 55, 5084–5096. doi:10.1021/acs.est.0c07384

Moore, C. J. (2008). Synthetic polymers in the marine environment: A rapidly increasing, long-term threat. *Environ. Res.* 108, 131–139. doi:10.1016/j.envres.2008.07.025

Moser, M. L., and Lee, D. S. (1992). A fourteen-year survey of plastic ingestion by Western North Atlantic seabirds. *Colon. Waterbirds* 15, 83–94. doi:10.2307/1521357

Murphy, F., Ewins, C., Carbonnier, F., and Quinn, B. (2016). Wastewater treatment works (WwTW) as a source of microplastics in the aquatic environment. *Environ. Sci. Technol.* 50, 5800–5808. doi:10.1021/acs.est.5b05416

NATIONAL ACADEMIES OF SCIENCES (2016). *Gene drives on the horizon: Advancing science, navigating uncertainty, and aligning research with public values*.

Ng, E.-L., Lwanga, E. H., Eldridge, S. M., Johnston, P., Hu, H.-W., Geissen, V., et al. (2018). An overview of microplastic and nanoplastic pollution in agroecosystems. *Sci. Total Environ.* 627, 1377–1388. doi:10.1016/j.scitotenv.2018.01.341

Nizzetto, L., Bussi, G., Futter, M. N., Butterfield, D., and Whitehead, P. G. (2016a). A theoretical assessment of microplastic transport in river catchments and their retention by soils and river sediments. *Environ. Sci. Process. Impacts* 18, 1050–1059. doi:10.1039/c6em00206d

Nizzetto, L., Futter, M., and Langaas, S. (2016b). *Are agricultural soils dumps for microplastics of urban origin?*. Washington, DC published in Environmental Science & Technology by ACS. doi:10.1021/acs.est.6b04140

O'Connor, D., Pan, S., Shen, Z., Song, Y., Jin, Y., Wu, W.-M., et al. (2019). Microplastics undergo accelerated vertical migration in sand soil due to small size and wet-dry cycles. *Environ. Pollut.* 249, 527–534. doi:10.1016/j.envpol.2019.03.092

Obbard, R. W. (2018). Microplastics in polar regions: The role of long range transport. *Curr. Opin. Environ. Sci. Health* 1, 24–29. doi:10.1016/j.coesh.2017.10.004

Pinsino, A., Bergami, E., della Torre, C., Vannuccini, M. L., Addis, P., Secci, M., et al. (2017). Amino-modified polystyrene nanoparticles affect signalling pathways of the sea urchin (*Paracentrotus lividus*) embryos. *Nanotoxicology* 11, 201–209. doi:10.1080/17435390.2017.1279360

Pitt, J. A., Kozal, J. S., Jayasundara, N., Massarsky, A., Trevisan, R., Geitner, N., et al. (2018a). Uptake, tissue distribution, and toxicity of polystyrene nanoparticles in developing zebrafish (*Danio rerio*). *Aquat. Toxicol.* 194, 185–194. doi:10.1016/j.aquatox.2017.11.017

Pitt, J. A., Trevisan, R., Massarsky, A., Kozal, J. S., Levin, E. D., and di Giulio, R. T. (2018b). Maternal transfer of nanoplastics to offspring in zebrafish (*Danio rerio*): A case study with nanopolystyrene. *Sci. Total Environ.* 643, 324–334. doi:10.1016/j.scitotenv.2018.06.186

Plasticseurope (2020). *Plastics-the Facts 2020.* An analysis of European plastics production, demand and waste data.

Poma, A., Vecchiotti, G., Colafarina, S., Zarivi, O., Aloisi, M., Arrizza, L., et al. (2019). *In vitro* genotoxicity of polystyrene nanoparticles on the human fibroblast Hs27 cell line. *Nanomaterials* 9, 1299. doi:10.3390/nano9091299

Primpke, S., Christiansen, S. H., Cowger, W., de Frond, H., Deshpande, A., Fischer, M., et al. (2020). Critical assessment of analytical methods for the harmonized and cost-efficient analysis of microplastics. *Appl. Spectrosc.* 74, 1012–1047. doi:10.1177/0003702820921465

Qi, Y., Yang, X., Pelaez, A. M., Lwanga, E. H., Beriot, N., Gertsen, H., et al. (2018). Macro-and micro-plastics in soil-plant system: Effects of plastic mulch film residues on wheat (*Triticum aestivum*) growth. *Sci. Total Environ.* 645, 1048–1056. doi:10.1016/j.scitotenv.2018.07.229

Qiao, R., Deng, Y., Zhang, S., Wolosker, M. B., Zhu, Q., Ren, H., et al. (2019). Accumulation of different shapes of microplastics initiates intestinal injury and gut microbiota dysbiosis in the gut of zebrafish. *Chemosphere* 236, 124334. doi:10.1016/j.chemosphere.2019.07.065

Rafiee, M., Dargahi, L., Eslami, A., Beirami, E., Jahangiri-Rad, M., Sabour, S., et al. (2018). Neurobehavioral assessment of rats exposed to pristine polystyrene nanoplastics upon oral exposure. *Chemosphere* 193, 745–753. doi:10.1016/j.chemosphere.2017.11.076

Redondo-Hasselerharm, P. E., Vink, G., Mitrano, D. M., and Koelmans, A. A. (2021). Metal-doping of nanoplastics enables accurate assessment of uptake and effects on Gammarus pulex. *Environ. Sci. Nano* 8, 1761–1770. doi:10.1039/d1en00068c

Renner, G., Schmidt, T. C., and Schram, J. (2018). Analytical methodologies for monitoring micro (nano) plastics: Which are fit for purpose? *Curr. Opin. Environ. Sci. Health* 1, 55–61. doi:10.1016/j.coesh.2017.11.001

Rillig, M. C., Ziersch, L., and Hempel, S. (2017). Microplastic transport in soil by earthworms. *Sci. Rep.* 7, 1362–1366. doi:10.1038/s41598-017-01594-7

Rist, S., Baun, A., Almeda, R., and Hartmann, N. B. (2019). Ingestion and effects of micro-and nanoplastics in blue mussel (*Mytilus edulis*) larvae. *Mar. Pollut. Bull.* 140, 423–430. doi:10.1016/j.marpolbul.2019.01.069

Rist, S., Baun, A., and Hartmann, N. B. (2017). Ingestion of micro-and nanoplastics in Daphnia magna–Quantification of body burdens and assessment of feeding rates and reproduction. *Environ. Pollut.* 228, 398–407. doi:10.1016/j.envpol.2017.05.048

Rist, S., and Hartmann, N. B. (2018). *Freshwater Microplastics*. Cham: Springer.Aquatic ecotoxicity of microplastics and nanoplastics: Lessons learned from engineered nanomaterials

Rochman, C. M., Browne, M. A., Halpern, B. S., Hentschel, B. T., Hoh, E., Karapanagioti, H. K., et al. (2013). Policy: Classify plastic waste as hazardous. *Nature* 494, 169–171. doi:10.1038/494169a

Rosenkranz, P., Chaudhry, Q., Stone, V., and Fernandes, T. F. (2009). A comparison of nanoparticle and fine particle uptake by Daphnia magna. *Environ. Toxicol. Chem. Int. J.* 28, 2142–2149. doi:10.1897/08-559.1

Ross, P. S., Chastain, S., Vassilenko, E., Etemadifar, A., Zimmermann, S., Quesnel, S.-A., et al. (2021). Pervasive distribution of polyester fibres in the Arctic Ocean is driven by Atlantic inputs. *Nat. Commun.* 12, 106. doi:10.1038/s41467-020-20347-1

Rossi, G., Barnoud, J., and Monticelli, L. (2013). Polystyrene nanoparticles perturb lipid membranes. *J. Phys. Chem. Lett.* 5, 241–246. doi:10.1021/jz402234c

Ryan, P. G., Moore, C. J., van Franeker, J. A., and Moloney, C. L. (2009). Monitoring the abundance of plastic debris in the marine environment. *Philosophical Trans. R. Soc. B Biol. Sci.* 364, 1999–2012. doi:10.1098/rstb.2008.0207

Sarasamma, S., Audira, G., Siregar, P., Malhotra, N., Lai, Y.-H., Liang, S.-T., et al. (2020). Nanoplastics cause neurobehavioral impairments, reproductive and oxidative damages, and biomarker responses in zebrafish: Throwing up alarms of wide spread health risk of exposure. *Int. J. Mol. Sci.* 21, 1410. doi:10.3390/ijms21041410

Schür, C., Rist, S., Baun, A., Mayer, P., Hartmann, N. B., and Wagner, M. (2019). *Environmental toxicology and chemistry*.WHEN Fluorescence is not a particle: The tissue translocation of microplastics in Daphnia magna seems an artIfact

Sendra, M., Carrasco-Braganza, M. I., Yeste, P. M., Vila, M., and Blasco, J. (2020a). Immunotoxicity of polystyrene nanoplastics in different hemocyte subpopulations of *Mytilus galloprovincialis*. *Sci. Rep.* 10, 8637–8714. doi:10.1038/s41598-020-65596-8

Sendra, M., Saco, A., Yeste, M. P., Romero, A., Novoa, B., and Figueras, A. (2020b). Nanoplastics: From tissue accumulation to cell translocation into *Mytilus galloprovincialis* hemocytes. resilience of immune cells exposed to nanoplastics and nanoplastics plus Vibrio splendidus combination. *J. Hazard. Mater.* 388, 121788. doi:10.1016/j.jhazmat.2019.121788

Sharpe, E. E. (2022). *Ecological risk assessment of tire wear particles in the san Francisco Bay using a bayesian network relative risk model.*

Shupe, H. J., Boenisch, K. M., Harper, B. J., Brander, S. M., and Harper, S. L. (2021). Effect of nanoplastic type and surface chemistry on particle agglomeration over a salinity gradient. *Environ. Toxicol. Chem.* 40, 1822–1828. doi:10.1002/etc.5030

Siddiqui, S., Dickens, J. M., Cunningham, B. E., Hutton, S. J., Pedersen, E. I., Harper, B. J., et al. (2022). Internalization, reduced growth, and behavioral effects following exposure to micro and nano tire particles in two estuarine indicator species. *Chemosphere* 296, 133934. doi:10.1016/j.chemosphere.2022.133934

Sigler, M. (2014). The effects of plastic pollution on aquatic wildlife: Current situations and future solutions. *Water, Air, & Soil Pollut.* 225, 2184. doi:10.1007/s11270-014-2184-6

Sjollema, S. B., Redondo-Hasselerharm, P., Leslie, H. A., Kraak, M. H., and Vethaak, A. D. (2016). Do plastic particles affect microalgal photosynthesis and growth? *Aquat. Toxicol.* 170, 259–261. doi:10.1016/j.aquatox.2015.12.002

Snell, T. W., and Hicks, D. G. (2011). Assessing toxicity of nanoparticles using Brachionus manjavacas (Rotifera). *Environ. Toxicol.* 26, 146–152. doi:10.1002/tox.20538

Sobhani, Z., Zhang, X., Gibson, C., Naidu, R., Megharaj, M., and Fang, C. (2020). Identification and visualisation of microplastics/nanoplastics by Raman imaging (i): Down to 100 nm. *Water Res.* 174, 115658. doi:10.1016/j.watres.2020.115658

Sökmen, T. Ö., Sulukan, E., Türkoğlu, M., Baran, A., Özkaraca, M., and Ceyhun, S. B. (2020). Polystyrene nanoplastics (20 nm) are able to bioaccumulate and cause oxidative DNA damages in the brain tissue of zebrafish embryo (*Danio rerio*). *Neurotoxicology* 77, 51–59. doi:10.1016/j.neuro.2019.12.010

Steinmetz, Z., Wollmann, C., Schaefer, M., Buchmann, C., David, J., Tröger, J., et al. (2016). Plastic mulching in agriculture. Trading short-term agronomic benefits for long-term soil degradation? *Sci. total Environ.* 550, 690–705. doi:10.1016/j.scitotenv.2016.01.153

Stephens, B., Azimi, P., el Orch, Z., and Ramos, T. (2013). Ultrafine particle emissions from desktop 3D printers. *Atmos. Environ.* 79, 334–339. doi:10.1016/j.atmosenv.2013.06.050

Sun, J., Dai, X., Wang, Q., van Loosdrecht, M. C., and Ni, B.-J. (2019). *Microplastics in wastewater treatment plants: Detection, occurrence and removal*. United Kingdom: Water Research is published by Elsevier. doi:10.1016/j.watres.2018.12.050

Sun, L., Liao, K., and Wang, D. (2021). Comparison of transgenerational reproductive toxicity induced by pristine and amino modified nanoplastics in *Caenorhabditis elegans*. *Sci. Total Environ.* 768, 144362. doi:10.1016/j.scitotenv.2020.144362

Sun, X.-D., Yuan, X.-Z., Jia, Y., Feng, L.-J., Zhu, F.-P., Dong, S.-S., et al. (2020). Differentially charged nanoplastics demonstrate distinct accumulation in *Arabidopsis thaliana*. *Nat. Nanotechnol.* 15, 755–760. doi:10.1038/s41565-020-0707-4

Sun, X., Chen, B., Li, Q., Liu, N., Xia, B., Zhu, L., et al. (2018). Toxicities of polystyrene nano-and microplastics toward marine bacterium Halomonas alkaliphila. *Sci. Total Environ.* 642, 1378–1385. doi:10.1016/j.scitotenv.2018.06.141

Sutton, R., Franz, A., Gilbreath, A., Lin, D., Miller, L., Sedlak, M., et al. (2019). *Understanding microplastic levels, pathways, and transport in the San Francisco Bay region*. San Francisco, CA: San Fransisco Estuary Institute, SFEI-ASC Publication# 950.

Szule, J. A., Curtis, L. R., Sharpton, T. J., Löhr, C. V., Brander, S. M., Harper, S. L., et al. (2022). *Early enteric and hepatic responses to ingestion of polystyrene nanospheres from water in C BL/mice*.

Tamis, J. E., Koelmans, A. A., Dröge, R., Kaag, N. H., Keur, M. C., Tromp, P. C., et al. (2021). Environmental risks of car tire microplastic particles and other road runoff pollutants. *Microplastics Nanoplastics* 1, 10–17. doi:10.1186/s43591-021-00008-w

Ter Halle, A., Jeanneau, L., Martignac, M., Jardé, E., Pedrono, B., Brach, L., et al. (2017). Nanoplastic in the north atlantic subtropical gyre. *Environ. Sci. Technol.* 51, 13689–13697. doi:10.1021/acs.est.7b03667

Thornton Hampton, L. M., Brander, S. M., Coffin, S., Cole, M., Hermabessiere, L., Koelmans, A. A., et al. (2022). Characterizing microplastic hazards: Which concentration metrics and particle characteristics are most informative for understanding toxicity in aquatic organisms? *Microplastics Nanoplastics* 2, 20–16. doi:10.1186/s43591-022-00040-4

van Sebille, E., Wilcox, C., Lebreton, L., Maximenko, N., Hardesty, B. D., van Franeker, J. A., et al. (2015). A global inventory of small floating plastic debris. *Environ. Res. Lett.* 10, 124006. doi:10.1088/1748-9326/10/12/124006

Venâncio, C., Savuca, A., Oliveira, M., Martins, M., and Lopes, I. (2021). Polymethylmethacrylate nanoplastics effects on the freshwater cnidarian *Hydra viridissima*. *J. Hazard. Mater.* 402, 123773. doi:10.1016/j.jhazmat.2020.123773

von Moos, N., Burkhardt-Holm, P., and KöHler, A. (2012). Uptake and effects of microplastics on cells and tissue of the blue mussel *Mytilus edulis* L. after an experimental exposure. *Environ. Sci. Technol.* 46, 11327–11335. doi:10.1021/es302332w

Wabnitz, C., and Nichols, W. J. (2010). Plastic pollution: An ocean emergency. *Mar. Turt. Newsl.* 1.

Wagner, M., Lambert, S., and Lambert, M. W. (2018). *Freshwater microplastics*. Switzerland: Springer International Publishing Cham.

Wahl, A., le Juge, C., Davranche, M., el Hadri, H., Grassl, B., Reynaud, S., et al. (2021). Nanoplastic occurrence in a soil amended with plastic debris. *Chemosphere* 262, 127784. doi:10.1016/j.chemosphere.2020.127784

WaldschläGer, K., and SchüTtrumpf, H. (2019). Effects of particle properties on the settling and rise velocities of microplastics in freshwater under laboratory conditions. *Environ. Sci. Technol.* 53, 1958–1966. doi:10.1021/acs.est.8b06794

Wang, H.-T., Ma, L., Zhu, D., Ding, J., Li, G., Jin, B.-J., et al. (2021). *Responses of earthworm Metaphire vulgaris gut microbiota to arsenic and nanoplastics contamination*. Netherlands: Science of The Total Environment is published by Elsevier, 150279. doi:10.1016/j.scitotenv.2021.150279

Wang, J., Lv, S., Zhang, M., Chen, G., Zhu, T., Zhang, S., et al. (2016). Effects of plastic film residues on occurrence of phthalates and microbial activity in soils. *Chemosphere* 151, 171–177. doi:10.1016/j.chemosphere.2016.02.076

Ward, J. E., and Kach, D. J. (2009). Marine aggregates facilitate ingestion of nanoparticles by suspension-feeding bivalves. *Mar. Environ. Res.* 68, 137–142. doi:10.1016/j.marenvres.2009.05.002

Wegner, A., Besseling, E., Foekema, E. M., Kamermans, P., and Koelmans, A. A. (2012). Effects of nanopolystyrene on the feeding behavior of the blue mussel (*Mytilus edulis* L.). *Environ. Toxicol. Chem.* 31, 2490–2497. doi:10.1002/etc.1984

Wiegers, J. K., Feder, H. M., Mortensen, L. S., Shaw, D. G., Wilson, V. J., and Landis, W. G. (1998). A regional multiple-stressor rank-based ecological risk assessment for the

fjord of Port Valdez, Alaska. *Hum. Ecol. Risk Assess.* 4, 1125–1173. doi:10.1080/10807039891285036

Wright, S., Ulke, J., Font, A., Chan, K., and Kelly, F. (2020). Atmospheric microplastic deposition in an urban environment and an evaluation of transport. *Environ. Int.* 136, 105411. doi:10.1016/j.envint.2019.105411

Wu, B., Wu, X., Liu, S., Wang, Z., and Chen, L. (2019a). Size-dependent effects of polystyrene microplastics on cytotoxicity and efflux pump inhibition in human Caco-2 cells. *Chemosphere* 221, 333–341. doi:10.1016/j.chemosphere.2019.01.056

Wu, J., Jiang, R., Lin, W., and Ouyang, G. (2019b). Effect of salinity and humic acid on the aggregation and toxicity of polystyrene nanoplastics with different functional groups and charges. *Environ. Pollut.* 245, 836–843. doi:10.1016/j.envpol.2018.11.055

Xu, M., Halimu, G., Zhang, Q., Song, Y., Fu, X., Li, Y., et al. (2019). Internalization and toxicity: A preliminary study of effects of nanoplastic particles on human lung epithelial cell. *Sci. Total Environ.* 694, 133794. doi:10.1016/j.scitotenv.2019.133794

Xu, P., Peng, G., Su, L., Gao, Y., Gao, L., and Li, D. (2018). Microplastic risk assessment in surface waters: A case study in the Changjiang estuary, China. *Mar. Pollut. Bull.* 133, 647–654. doi:10.1016/j.marpolbul.2018.06.020

Yee, M. S.-L., Hii, L.-W., Looi, C. K., Lim, W.-M., Wong, S.-F., Kok, Y.-Y., et al. (2021). Impact of microplastics and nanoplastics on human health. *Nanomaterials* 11, 496. doi:10.3390/nano11020496

Yoo, J.-W., Cho, H., Jeon, M., Jeong, C.-B., Jung, J.-H., and Lee, Y.-M. (2021). Effects of polystyrene in the brackish water flea Diaphanosoma celebensis: Size-dependent acute toxicity, ingestion, egestion, and antioxidant response. *Aquat. Toxicol.* 235, 105821. doi:10.1016/j.aquatox.2021.105821

Zhang, W., Liu, Z., Tang, S., Li, D., Jiang, Q., and Zhang, T. (2020). Transcriptional response provides insights into the effect of chronic polystyrene nanoplastic exposure on *Daphnia pulex*. *Chemosphere* 238, 124563. doi:10.1016/j.chemosphere.2019.124563

Zhou, X.-X., Liu, R., Hao, L.-T., and Liu, J.-F. (2021). Identification of polystyrene nanoplastics using surface enhanced Raman spectroscopy. *Talanta* 221, 121552. doi:10.1016/j.talanta.2020.121552

Zhu, B.-K., Fang, Y.-M., Zhu, D., Christie, P., Ke, X., and Zhu, Y.-G. (2018). Exposure to nanoplastics disturbs the gut microbiome in the soil oligochaete Enchytraeus crypticus. *Environ. Pollut.* 239, 408–415. doi:10.1016/j.envpol.2018.04.017

frontiers | Frontiers in Toxicology

TYPE Original Research
PUBLISHED 02 May 2023
DOI 10.3389/ftox.2023.1176172

OPEN ACCESS

EDITED BY
Iseult Lynch,
University of Birmingham,
United Kingdom

REVIEWED BY
Andi Alijagic,
Örebro University, Sweden
Changjian Xie,
Shandong University of Technology,
China

*CORRESPONDENCE
Suanne Bosch,
bosch.suanne@gmail.com

RECEIVED 28 February 2023
ACCEPTED 11 April 2023
PUBLISHED 02 May 2023

CITATION
Bosch S, Botha TL and Wepener V (2023), Influence of different functionalized CdTe quantum dots on the accumulation of metals, developmental toxicity and respiration in different development stages of the zebrafish (*Danio rerio*). *Front. Toxicol.* 5:1176172. doi: 10.3389/ftox.2023.1176172

Influence of different functionalized CdTe quantum dots on the accumulation of metals, developmental toxicity and respiration in different development stages of the zebrafish (*Danio rerio*)

Suanne Bosch[1]*, Tarryn Lee Botha[1,2] and Victor Wepener[1]

[1]Water Research Group, School of Biological Sciences, North-West University, Potchefstroom, South Africa, [2]Department of Zoology, University of Johannesburg, Johannesburg, South Africa

Introduction: The bioaccumulation and differential effects of cadmium tellurium quantum dot (CdTe QDs) nanomaterials with different functional groups are poorly understood in aquatic organisms. This study aimed to investigate the metal uptake, developmental effects, and respiratory effects of CdTe QDs with different functional groups (COOH, NH3, and PEG) on zebrafish embryos.

Methods: Zebrafish embryos were exposed to carboxylate (COOH), ammonia (NH3), and polyethylene glycol (PEG) functionalized CdTe QDs at nominal concentrations of 0.5, 2, 4, 6, and 20 mg QDs/L. The materials were characterized in E3 exposure media and the metal uptake, developmental effects, and respiratory effects of zebrafish embryos were recorded.

Results: The total Cd or Te concentrations in the larvae could not be explained by the metal concentrations or dissolution of the materials in the exposure media. The metal uptake in the larvae was not dose-dependent, except for the QD-PEG treatment. The QD-NH3 treatment caused respiration inhibition at the highest exposure concentration and hatching delays and severe malformations at low concentrations. The toxicities observed at low concentrations were attributed to particles crossing the pores in the chorion, and toxicities at higher concentrations were linked to the aggregation of particle agglomerates to the surface of the chorion impairing respiration. Developmental defects were recorded following exposure to all three functional groups, but the QD-NH3 group had the most severe response. The LC50 values for embryo development of QD-COOH and QD-PEG groups were higher than 20 mg/L, and the LC50 of the QD-NH3 group was 20 mg/L.

Discussion: The results of this study suggest that CdTe QDs with different functional groups have differential effects on zebrafish embryos. The QD-NH3 treatment caused the most severe effects, including respiration inhibition and developmental defects. These findings provide valuable information for understanding the effects of CdTe QDs on aquatic organisms and highlight the need for further investigation.

KEYWORDS

metal uptake, oxygen consumption, carboxylate (COOH), ammonia (NH_3), polyethylene glycol (PEG)

1 Introduction

Quantum dots (QDs) are fluorescent nanocrystals with a semiconductor metal core, which is usually comprised of CdSe or CdTe (King-Heiden et al., 2009; Zheng et al., 2021). Due to their small size and unique composition, they absorb and emit light at different wavelengths making them ideal as contrasting agents for bio-imaging applications (Michalet et al., 2005). Besides cellular imaging, QDs can be used for a wide range of other applications, such as fixed tissue analysis, spectral encoding of microparticles, and quantitative analysis of ions (Åkerman et al., 2002; Jason et al., 2009). Even though QDs have many advantageous properties they are essentially inorganic semiconductor materials that can be toxic to living organisms (Jason et al., 2009). Many studies report no or little toxicity to living organisms (Jaiswal et al., 2003; Larson et al., 2003; Chen and Gerion, 2004; Voura et al., 2004; Zhang et al., 2013), however, some studies have seen cytotoxicity and other toxic outcomes from exposure to QDs leading to the development of surface coatings and functionalization to minimize toxicity (Derfus et al., 2004; Lovrić et al., 2005; Jason et al., 2009; Zhang et al., 2012b; Hsu et al., 2012). Surface functionalization with organic molecules increases their dispensability in water, making them more biologically compatible and prevents metal core leaching (Medintz et al., 2005; Michalet et al., 2005; Ron, 2006; King-Heiden et al., 2009).

Given their wide range of applications, the substantial growth in production volumes of QDs is predicted and thus entry of QDs and their by-products into waterways is likely (Singh et al., 2020). Even though the exact concentration of QDs in the environment is unknown, this potentially poses risks to aquatic biota. The coatings that make them unique and useful could also be their weakness. As they end up in the environment the coating could become compromised and reveal a possibly toxic core or cause the dissolution of metals from the core (Ron, 2006; Rocha et al., 2017). As QDs degrade they could also react in undesirable ways *in vivo*. It is said that the estimated environmental residence times for QDs range from months to years (Ron, 2006). From this, it is evident that their physicochemical properties and surface functionalization are fundamental in understanding their potential toxicity.

In the aquatic environment processes such as agglomeration patterns, settling, oxidation, interaction with organic material and biotransformation can influence the fate, behaviour and uptake of any nanomaterial (Rocha et al., 2017; Mishra et al., 2021). These aspects are determined by the physicochemical properties of the environment, particle size, shape, coating, and functionalization. Studies have found that particle size and functionalization determine the interaction with biological membranes (such as cell membranes as well as the chorion of an embryo) and biodistribution in the organism (Paatero et al., 2017). Not many studies have looked at the effect of QDs with the same core size and composition but different functionalization on their toxicity, especially in zebrafish (Rocha et al., 2017; Gallud et al., 2020). The zebrafish (*Danio rerio*) is an established bioindicator to study nanoparticle toxicity (Zhu et al., 2007; Martinez et al., 2019; Mishra et al., 2021). The specie is small in size, has good reproducibility and has a fast embryonic development. The embryo is transparent and thus the development of organs can be visualized during development (Wang et al., 2012; Paatero et al., 2017). Different parameters can be assessed, such as hatching, organ development, respiration, behaviour, immunotoxicity, and genotoxicity, in addition to reproductive toxicity and mortality.

Accordingly, the present study aimed to determine the embryotoxicity induced by three CdTe QDs functionalized with carboxylate (COOH), ammonia (NH_3), and polyethylene glycol (PEG) using zebrafish embryo test (ZET) as a model. The authors conducted a sequence of assessments for embryonic developmental toxicity including embryonic mortality, hatching rate, malformation percentage, respiration rates and Cd/Te uptake from QDs exposure. Combining embryonic toxicity, metal body burden and respiration rates as indicators of evaluating QDs toxicity will give a clearer indication of the toxicity (nano-specific or metal-based) which is important for safety by design for biomedical application.

2 Materials and methods

2.1 Chemicals

Quantum dot nanopowders with 3–5 nm primary particle size were produced by PlasmaChem GmbH (Lot# YF140402) and supplied by the Nanosolutions EU FP7 project (Project ID: 309329). The stock suspensions (100 mg/L) were freshly prepared by directly dispersing the three types of QDs (5 mg) in 50 mL of ultrapure water individually (18.2 MΩ/cm, Millipore, Billerica, MA). The 50 mL nano stock solutions were sonicated at 60°C in a bath ultra-sonicator (Model E-UC6-HD-D, Scientech, India) for 1 h at 20 Hz prior to dilution in E3 media for exposure and characterization.

2.2 Preparation and characterization of quantum dots

Characterization was done in two batches. Firstly, the 100 mg/L NM stocks in ultrapure were characterised by the University of Plymouth as part of the Nanosolutions project. Secondly, QDs in E3 media at concentrations used for this study was characterized at the North-West University.

Characterization of 100 mg/L stock CdTe QDs data were obtained from the Nanosolutions project data sheets since they were the same batches that were used in this study (Nanosolutions., 2013; Vassallo et al., 2018; Tatsi et al., 2020). Briefly the hydrodynamic size distribution of stock solutions was determined by Nanoparticle Tracking Analysis (NTA) using Nanosight LM 10 (Nanosight, Salisbury, United Kingdom, laser output set at 30 mW at 640 nm) and methods described by Besinis et al. (2014). Material dissolution was measured using dialysis bags containing 700 µL of the appropriate stock solution. Briefly, 8 mL of a sonicated stock of

each material was added to a dialysis tube (product code: D9777, cellulose membrane with molecular weight cut off at 12,000 Da, Sigma-Aldrich Ltd., Dorset, United Kingdom) which was then secured on both ends using cable ties to prevent leakage. Each bag was then placed in a beaker containing 492 mL of ultrapure water. Samples (15 mL) of the external water from each beaker was taken after 24 h. Each material was analysed in duplicate on a shaker (IKA Labortechnik, KS250 basic). Samples of 15 mL where acidified with 300 µL of 65% nitric acid. Metal concentrations were measured by inductively coupled plasma optical emission spectrophotometry (ICP-OES, ICAP 7400) and inductively coupled plasma optical mass spectrophotometry (ICP-MS, Thermoscientific, X Series 2).

The primary particle diameter of initial nanomaterial particles was determined using transmission electron microscopy (TEM) (FEI Tecnai G2). One drop of 100 mg/L solution of each individual nanomaterial was added to a carbon grid separately, allowed to settle and dried, thereafter it was examined at high resolution (200 kV).

For exposures, standard E3 media was used. The media was constituted by dissolving 34.8 g NaCl, 1.6 g KCl, 5.8 g $CaCl_2.2H_2O$, and 9.78 g $MgCl_2.6H_2O$ in 2 L reverse osmosis water. The pH of approximately 7.6 remained stable at 7.65. To make up the desired exposure concentrations the relevant volumes of sonicated nanomaterial stock solutions (100 mg/L) were added to the exposure media. Six different concentrations were selected for each nanomaterial with 5 replicates of each. Nominal exposure concentrations were 0, 0.5, 2, 4, 6, and 20 mg/L QDs.

Further characterization of exposure solutions in E3 media was conducted at the North-West University. Hydrodynamic size distribution in E3 media was measured using Dynamic Light Scattering (DLS) and stability were examined with a zeta-sizer (Malvern, Zetasizer Nano-ZS). The total metal content of solutions was determined by acidifying solutions (10 µL 65% HNO_3 per 10 mL) and measuring Cd and Te concentrations using standard ICP-MS techniques.

2.3 Zebrafish maintenance and embryo exposure

Long-fin wild-type adult *D. rerio* breeding stocks were kept in a ZebTEC recirculating aquarium system in an environmentally controlled room (28°C). Adult *D. rerio* breeding stocks were bred in Tecniplast iSpawn spawning chambers (Tecniplast, Italy) in a ratio of two males to three females. After approximately 2 h post fertilization (hpf) eggs were collected and placed in an incubator at 27°C for another 2 h (Martinez et al., 2019; Kumar et al., 2020). The *D. rerio* embryo acute toxicity test (OECD 236—OECD, 2013) was carried out using 4 hpf embryos. Viable fertilized eggs were sorted using a stereo microscope and separated from unhealthy eggs. Healthy fertilized eggs were then treated with QD-NH_3, QD-PEG, and QD-COOH (0.5, 2, 4, 6, and 20 mg/L) respectively. Test concentrations of each material were prepared by adding the required amount of the stock solution to each well in a 6-well plate and filling it to 5 mL with E3 media. Negative controls consisted of E3 media with no material added. Five viable eggs were then transferred to each well, thus for each treatment consisted of four replicates of five eggs (n = 20). The six-well plates were sealed with self-adhesive, oxygen-permeable sealing film (BRAND®, Sigma Aldrich, Merck, Darmstadt, Germany) to prevent evaporation from taking place. Unless otherwise stated, data for the QDs are shown as a nominal mass concentration of QD per unit volume and not normalized to the concentration of metal in the particle. This is because the dissolution rates of QDs were very low and therefore the particles were the predominant form in which the metal occurred in the media throughout the exposures. The plates were then incubated for 96 h at 27°C at a 12: 12 dark-light cycle. Mortality, hatching rate and malformations were noted every 24 h. Observations performed on each tested embryo included: Coagulation of embryos, lack of somite formation, non-detachment of the tail, spinal deformation, pericardial edema and lack of heartbeat.

2.4 Embryo respiration

Respiration was measured at 24 h and 48 h by removing embryos from exposure media, washing them twice with clean E3 media and placing 5 embryos per replicate in each well of a 12-well Loligo® microplate system containing 80 µL of aerated E3 media. Three replicates were assessed at each concentration (n = 3). Measurements were taken every 5 s for at least 30 min, where after embryos were carefully removed from the wells and returned to the exposure media and incubated to continue with the test. Data are expressed as mg oxygen per embryo per minute.

2.5 Metal uptake in larvae

A parallel exposure was carried out concomitantly in E3 media to obtain enough biomass for metal analysis. Fertilised eggs were exposed in groups of 20 in 30 mL of exposure media. After 96 h, larvae were collected and larvae that were not hatched yet were manually dechorionated using a pair of forceps to eliminate possible QDs adhering to the chorion surface. Larvae were humanely killed in ice water, washed twice in ultrapure water and 10 individuals were pooled to represent a replicate sample. A minimum of three replicates per treatment was immediately frozen at −20°C until analyses.

Thawed samples were weighed and digested for 24 h in a Teflon heatblock with 1 mL nitric acid (65%, suprapure, Merck) at 65°C. Metal concentrations were measured using standard ICP-MS. Untreated organisms were used as negative controls and the natural background concentrations were subtracted from the concentrations measured in the exposed organisms. Concentrations are expressed as the total metal concentration on a wet weight basis. Analytical quality control was assured using certified reference materials (DORM-4 fish tissue) and is presented with instrumental detection limits in Table 1.

2.6 Statistical analysis

The dose-response function, namely, effect concentration where 50% of the population died (LC_{50} values) was calculated using non-

TABLE 1 Recovery rates (%) and detection limits of cadmium and tellurium from larval tissue and E3 media samples.

Metal ion from QD treatment	Recovery rates (%) Dorm-4 certified reference material	Detection limits in larvae tissue (μg/g dw)	Detection limits in E3 media (μg/L)
Cd	99 ± 5	0.30	0.11
Te	Not available	2.1	1.38

TABLE 2 Hydrodynamic size (nm) distribution, zeta potential (mV) and metal concentrations (mg/L) of CdTe QDs in E3 media (±SD) measured at the North-West University.

Material	Endpoint	Time point (h)	Exposure concentration (mg/L)				
			0.5	2	4	6	20
QD-COOH	Hydrodynamic size (nm)	0	1,068 ± 345	704 ± 148	699 ± 79	649 ± 92	156 ± 31
		48	710 ± 91	1,212 ± 15	779 ± 49	782 ± 82	226 ± 36
	Zeta potential (mV)	0	−22 ± 3	−18 ± 13	−23 ± 1	−23 ± 0.6	−17 ± 10
		48	−24 ± 1	−13 ± 9	−22 ± 2	−23 ± 2	−19 ± 5
	Cadmium concentration (mg/L)	0	0.19 ± 0.03	0.9 ± 0.1	1.6 ± 0.05	2.5 ± 0.06	8.1 ± 0.3
	Tellurium concentration (mg/L)	0	0.034 ± 0.005	0.2 ± 0.03	0.3 ± 0.01	0.56 ± 0.02	1.6 ± 0.07
QD-PEG	Hydrodynamic size (nm)	0	697 ± 38	801 ± 43	682 ± 22	459 ± 21	93 ± 14
		48	1,003 ± 23	1,026 ± 156	924 ± 81	630 ± 69	163 ± 16
	Zeta potential (mV)	0	−22 ± 4	−15 ± 4	−15 ± 10	−14 ± 2	−9 ± 5
		48	−22 ± 1	−22 ± 1	−22 ± 1	−22 ± 2	−14 ± 7
	Cadmium concentration (mg/L)	0	0.2 ± 0.03	0.8 ± 0.05	1.6 ± 0.1	1.7 ± 0.5	6.9 ± 0.2
	Tellurium concentration (mg/L)	0	0.05 ± 0.006	0.15 ± 0.01	0.36 ± 0.02	0.44 ± 0.2	1.7 ± 0.05
QD-NH_3	Hydrodynamic size (nm)[a]	0	880 ± 91	643 ± 12	489 ± 46	436 ± 17	84 ± 21
		48	769 ± 54	697 ± 50	690 ± 69	492 ± 12	120 ± 25
	Zeta potential (mV)	0	−22 ± 4	−21 ± 3	−21 ± 0.7	−7 ± 10	−7 ± 6
		48	−22 ± 2	−23 ± 0.5	−17 ± 11	−23 ± 0.4	−22 ± 2
	Cadmium concentration (mg/L)	0	0.04 ± 0.002	0.15 ± 0.04	0.33 ± 0.03	0.46 ± 0.02	1.6 ± 0.05
	Tellurium concentration (mg/L)	0	0.002 ± 0.0002	0.005 ± 0.001	0.006 ± 0.0002	0.01 ± 0.003	0.056 ± 0.005

[a]Data refer to aggregate hydrodynamic diameters from particle size distribution measurements made by DLS, at the North-West University.

linear regression analysis in ToxRat® software. Effect data are expressed as mean ± standard error. Significance between controls and treatments and functionalised groups were determined by using One-way analysis of variance (ANOVA) and Tukey's *post hoc* test. All data were tested for normality using the Shapiro-Wilk test. Data that did not meet the normality assumption were log-transformed prior to analyses. Differences were considered significant at $p < 0.05$.

3 Results

3.1 Characterization

The primary particle size of all three QDs was 3–5 nm as described by the manufacturers. Nanoparticle tracking analysis performed at the University of Plymouth (as part of the Nanosolutions project) on 100 mg/L stock solutions indicated that QD-PEG had the largest hydrodynamic size distribution in ultra-pure water (Table 3).

Dynamic light scattering analysis of exposure concentration in E3 media conducted at the North-West University indicated that QD-COOH produced the largest hydrodynamic size distribution in E3 media and a decline in hydrodynamic size distribution as concentrations increased could be seen in all three materials. There was also a time-dependent agglomeration of particles (Table 2). Large agglomerates were observed settling out in exposure vessels at the 20 mg/L concentration. Hydrodynamic particle size was smaller in ultrapure water compared to concentrations made in E3 media (Tables 2, 3). The zeta potential of QDs were measured in E3 media to provide quantitative information on the stability of QDs in this study.

TABLE 3 Hydrodynamic size (nm) distribution and metal dissolution (mg/L) of 100 mg/L CdTe QDs stock solutions after 24 h in ultrapure water as analysed by Plymouth University for the Nanosolutions project (±SD).

Material		QD-COOH	QD-PEG	QD-NH_3
Mean hydrodynamic size (nm)[a]		84 ± 58	159 ± 72	75 ± 50
Dissolution (%)[b]	Cd	0.74	2.43	2.10
	Te	0.39	3.23	23.69

[a]Data refer to aggregate hydrodynamic diameters from particle size distribution measurements made by NTA, at Plymouth University.
[b]The values have been calculated taking into account the degree of functionalization or impurities content as reported by Nanosolutions.

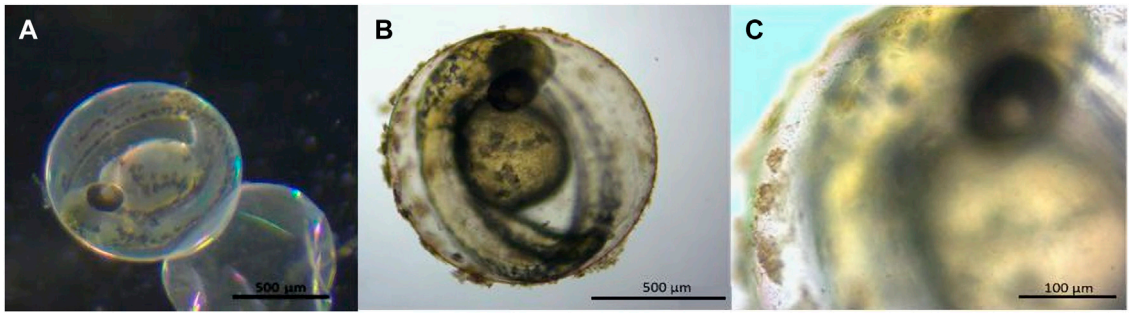

FIGURE 1
Stereo microscope images of 48 hpf *Danio rerio* embryos indicating no particle agglomerates on the chorion of the control **(A)** and QD agglomerates covering the outside of the chorion **(B, C)** during exposure to QD-NH_3 20 mg/L.

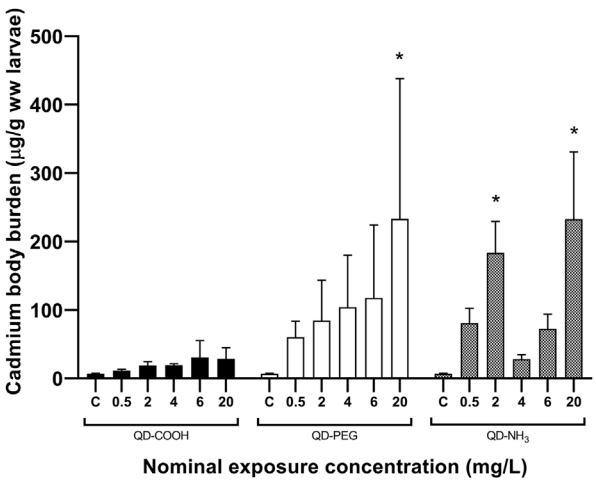

FIGURE 2
Total Cd concentrations (mean ± standard error expressed as µg/g ww larvae) in *Danio rerio* larvae after exposure to increasing concentrations of QD-COOH, QD-PEG and QD-NH_3. Asterisk (*) indicates significance from control ($p < 0.05$, T-tests).

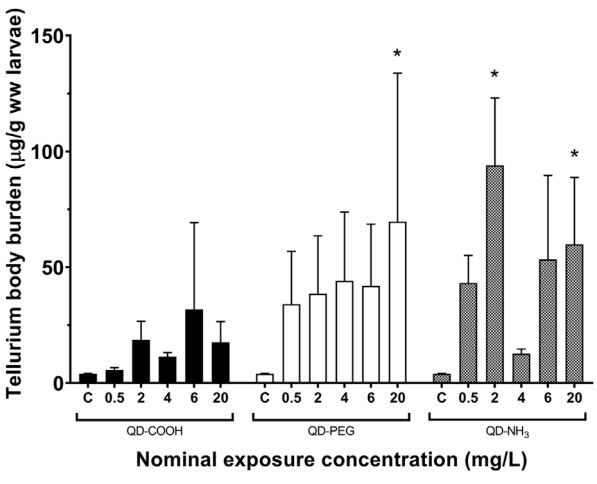

FIGURE 3
Total Te concentrations (mean ± standard error expressed as µg/g ww larvae) in *Danio rerio* larvae after exposure to increasing concentrations of QD-COOH, QD-PEG and QD-NH_3. Single asterisk (*) indicates significance from control ($p < 0.05$, *T*-tests).

Overall no significant effects on zeta potential were observed. Dissolution was also measured as part of the Nanosolutions project, and it was established that all three groups had less than 4% metal dissolution in ultra-pure water, only the QD-NH_3 group had a larger dissolution of Te at 23.69% (Table 3). Based on the total metal content of each concentration of QDs the Cd concentration was between 3.8 and 5.5-fold higher than the Te concentration in QD-COOH and QD-PEG but between 28 and 55-fold higher in QD-NH_3. The QD-COOH group has the highest overall metal content and the QD-NH_3 group the lowest. There was also an increase in total metal content as exposure concentrations increased.

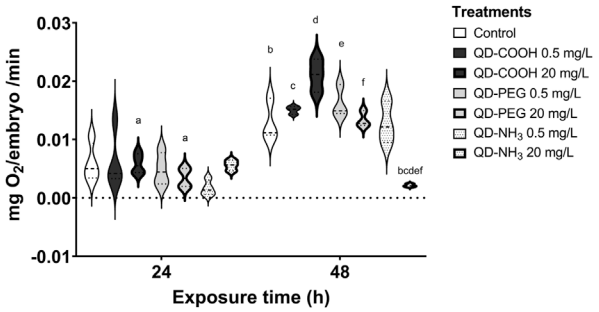

FIGURE 4
Respiration of *Danio rerio* embryos 24 hpf and 48 hpf. The graph represents the replicates and mean of each treatment. The same letters in superscript denotes a significant difference between treatments ($p < 0.05$, *T*-tests).

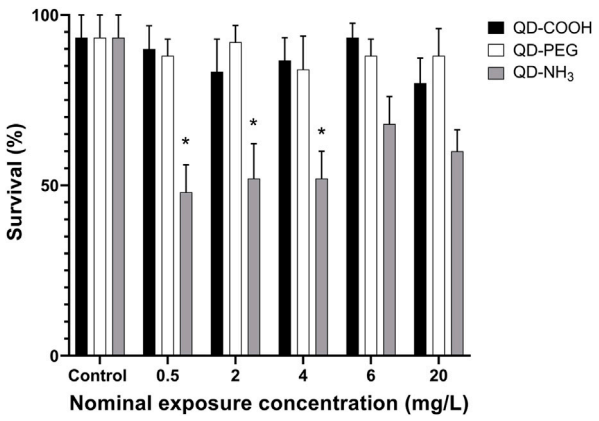

FIGURE 5
Survival of *Danio rerio* larvae after 96 h of exposure to QD-COOH, QD-PEG and QD-NH_3. Error bars represent standard deviation. Single asterisk (*) indicates differences from control ($p < 0.05$).

3.2 Metal uptake

Particle agglomerates adhered to the surface of the embryo chorion in only the QD-NH_3 group (Figure 1). Thus, for metal uptake, only hatched larvae after 96 h of exposure were used to avoid any metal from the chorion surface being included in uptake results.

Body burden of Cd after 96 h of exposure showed no significant uptake of Cd from the QD-COOH group and the QD-PEG group showed a concentration dependant increase in Cd uptake with the only significant increase compared to control was seen at the highest exposure concentration (20 mg/L) (Figure 2). The QD-NH_3 group showed no dose-dependent increase in Cd uptake. The only two exposure concentrations that showed significant uptake was 2 mg/L and 20 mg/L.

Similar uptake patterns were seen for Te but at lower concentrations (Figure 3). A significant uptake of 70 µg/g was found in the 20 mg/L exposure concentration of the QD-COOH group and the QD-NH_3 group caused uptake of 94 µg/g and 60 µg/g in the 2 and 20 mg/L exposure concentrations.

3.3 Respiration

After 24 h there was no significant effect on the respiration of embryos (Figure 4). However, after 48 h the highest concentration of the QD-NH_3 group caused a significant decrease in respiration compared to the control. The highest QD-COOH exposure group concentration (20 mg/L) resulted in a significant increase in respiration compared to the control.

3.4 Developmental toxicity

Exposure to QD-COOH and QD-PEG groups did not produce any significant decrease in embryo survival (Figure 5). It was therefore not possible to calculate LC_{50} values for these groups, however the LOEC was calculated as ≥ 20 mg/L. Exposure to the QD-NH_3 group caused significant mortality (i.e., > 50%) at the low concentrations of 0.5, 2, and 4 mg/L, while no mortality was observed at the higher exposure concentrations.

Two low concentrations (2 and 4 mg/L) of the QD-NH_3 group caused a significant ($p < 0.05$) delay in the hatching of surviving embryos (Figure 6). No significant effect on hatching success during the exposure period was observed at the other exposure concentrations.

Exposure to all concentrations, except for the highest exposure (20 mg/L), of QD-PEG and QD-NH_3 resulted in significant increases in pericardial edemas (Figure 7A). All concentrations of the QD-COOH group also resulted in significant pericardial edemas (Figure 7A). No significant occurrence of spinal deformations was observed in embryos exposed to QD-COOH (Figure 7B). The QD-PEG group showed significant spinal deformations compared to the control at all exposure concentrations except he 4 mg/L exposure. The QD-NH_3 group also showed a significant occurrence of spinal deformations at all concentrations, with the lowest concentration (0.5 mg/L) having the highest effect.

4 Discussion

Nanomaterials have many beneficial properties and as their daily use is increasing it is inevitable that this will lead to the exposure of humans and other organisms to these materials (Ghobadian et al., 2015). The size and functionalization of these materials influence their toxicity and thus it is important to investigate and compare the toxicity of different functionalized QDs with the same primary particle size. In this study, we showed that there are clear differences of particle behaviour in exposure media influencing toxicity, metal uptake and respiration effects to the zebrafish embryo's during exposure. Overall, the QD-NH_3 group resulted in the most significant negative effects to the developing embryos causing severe malformations, hatching delay and mortality at low concentrations, and respiration inhibition at the highest concentration (20 mg/L). This contrasts with findings by Zheng et al. (2021) that showed exposure to CdSe/ZnS QDs with COOH functionalization was more toxic to developing zebrafish than NH_3

10.3389/ftox.2023.1176172

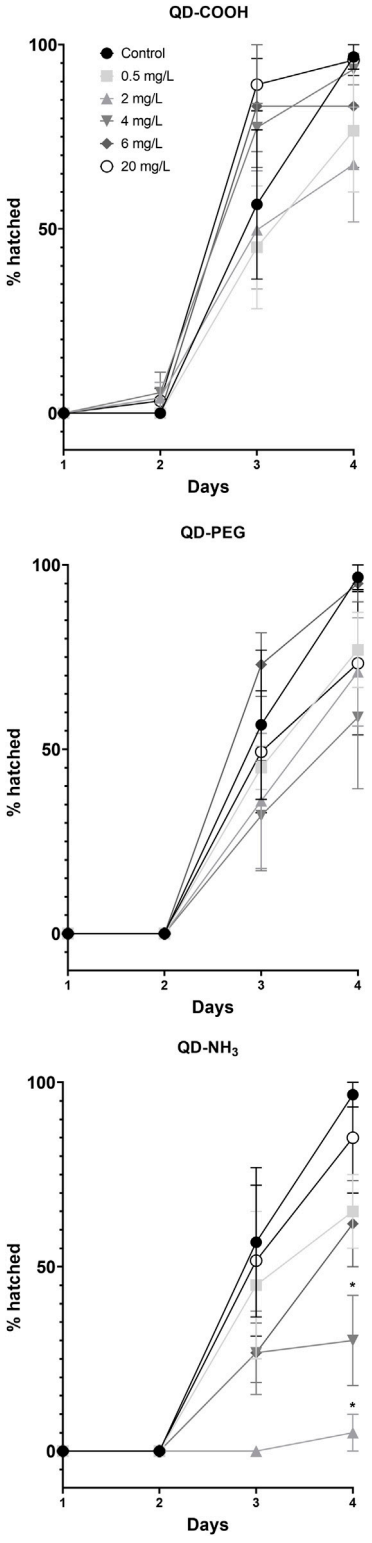

FIGURE 6
Percentage hatched *Danio rerio* larvae at different time points during the exposure to QD-COOH, QD-PEG and QD-NH_3. Error bars represent standard deviation. Single asterisk (*) differences from control ($p < 0.05$, *T*-tests).

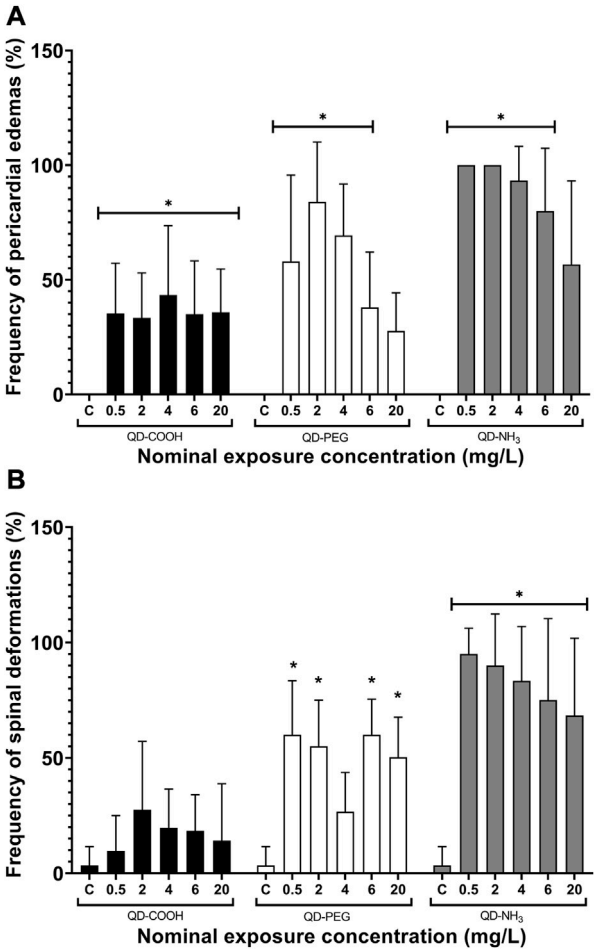

FIGURE 7
Spinal deformations **(A)** and pericardial edemas **(B)** of *Danio rerio* embryos exposed to QD-COOH, QD-PEG, and QD-NH_3 expressed as a percentage of surviving embryos. Error bars represent standard deviation. Single asterisk (*) denotes significant differences from control ($p < 0.05$, *T*-tests).

functionalized material. The QD-PEG group caused significant edema and spinal deformations in a bimodal pattern, caused no respiration effects and no significant mortality, while the QD-COOH group showed the least toxic effects with only significant cardiac edema and increased respiration rate the lowest exposure concentration.

4.1 Dissolution and colloidal activity of particles

The colloidal activity of these particles can be described by the DLVO theory. This suggests that both van der Waals forces and electrostatic forces cause aggregation of particles in a suspension (Adair et al., 2001). At higher concentrations van der Waals forces between the large number of particles cause higher aggregation of nanoparticles. At a certain point the aggregates and agglomerates

become too large to remain in suspension causing them to settle out. This makes them less bioavailable and influences toxicity. In the present study it was seen that QD-COOH caused the largest aggregates in the exposure media. This can be attributed to Mg and Ca ions in the media that reduce the electrostatic double layer initiating binding with the negatively charged COOH chain on the nanomaterial (Deerfield et al., 1989). However, these interactions are dynamic and size, temperature, time and concentration dependent. Thus, bioavailability and toxicity and change over time and concentration, leading to the bimodal and effects at lower concentrations seen in the present study.

Dissolution is a fundamental parameter to be considered when nanomaterial toxicity is assessed, as it can lead to highly toxic ions interacting with target sites (Zolotarev et al., 2012). The QDs used in this study have a very low dissolution potential (<4%) in ultra-pure water and decreases in solutions with higher pH such as E3 media that was used in this study (Boyle et al., 2020). Thus, the effects of dissolution metal ions from these materials were not considered to be significant. The highest dissolution of Te was from the QD-NH_3 group (i.e., 23%) meaning that there would only be 13 µg/L Te ions in the highest exposure concentration of 20 mg/L. This is less than 10% of the NOEC derived for Te in algae and freshwater fish (ECHA, 2022). Total body metal concentrations for both Cd and Te increased in a dose-dependent manner only in the QD-PEG group. There were however no clear dose-response relationships between the body burdens and the effects observed, suggesting mechanisms other than dissolved metal content and total internal exposure (as reflected in the body burdens).

However, it may be possible that despite the insignificant dissolution of metals in exposure media, *in vivo* QD degradation may expose embryos to Cd and Te (Gao et al., 2019). This would be expected to produce endpoints of Cd toxicity in zebrafish embryos exposed to sublethal QD concentrations. King-Heiden et al. (2009) found that CdSe QDs with different chain lengths did degrade internally into Cd^{2+} ions. The only toxicity parameter that can be linked to total metal uptake in our study was hatching success. A study by Zolotarev et al. (2012) also found hatching success impacted by Cd^{2+} ions dissociating from Cdse/Cds/Zns/S,S-Dihydrolipoic acid/Polyacrylic acid QDs, but also found edemas and spinal deformations associated with Cd^{2+} ions. Boyle et al. (2020) and Vicario-Parés et al. (2014) suggest that metal ions from nanomaterials bind to the hatching enzyme sites resulting in delayed or non-hatching of embryos. Delayed hatching in the present study (in the case of QD-NH_3 exposures) also lead to decreased interaction of the larvae with the media thereby decreased uptake of nanomaterials due to the prolonged protection of the chorion; this was seen for the 4 mg/L concentration but not for the 2 mg/L concentration in the present study.

4.2 Embryo developmental toxicity

Hatching success has been linked to increased occurrence of developmental defects following exposure to metal nanomaterials (King-Heiden et al., 2009; Asharani et al., 2011; Zhao et al., 2013; Ghobadian et al., 2015; Zheng et al., 2021). In this study malformations were more prevalent in the QD-NH_3 group at the lower exposure concentrations. This contrasts with studies by Duan et al. (2013), that found a very strong dose-response relationship between exposure concentrations and developmental toxicity. These contrasting findings are probably related to the difference in materials with Duan et al. (2013) using water-soluble CdTe QDs as opposed to the three functionalised groups used in this study. Pericardial edemas were the most common malformation observed, consistent with previous results (Zhang et al., 2012a; Xu et al., 2012; Duan et al., 2013; Jin et al., 2017). Cellular studies have also shown that NH_3 functionalized graphene oxide nanoparticles were more cytotoxic than pristine particles and mammalian studies exploring PEG functionalized gold nanoparticles found that these PEGylated particles were toxic to rats when injected intravenously (Cho et al., 2009; Keremidarska-Markova et al., 2018). Tang et al. (2013) reported that QDs enter cells through endocytosis and cause the formation of reactive oxygen species (ROS), which result in ROS-mediated genotoxicity leading to malformations. Studies have also concluded that QDs and Cd ions cause pericardial edemas and in turn, impaired cardiac function via bradycardia (Zhu et al., 2009; Duan et al., 2013; Krzykwa et al., 2019; Zheng et al., 2021).

Since the cardiac function influences the respiration rate, we established whether exposure to the three different functionalised QDs influenced the oxygen consumption of zebrafish embryos. Data showed that the embryo oxygen consumption displayed a different trend from the other effects recorded. The QD-NH_3 group had the greatest effects but only at the highest exposure concentration (20 mg/L). Large agglomerates formed and adhered to the chorion of the embryos. This was also reported in other studies (Sun et al., 2013; Petushkova et al., 2015; Zheng et al., 2021). The agglomerations were the result of increased ZP at the highest exposure concentration and settling out of suspension. Lower dispersions ZP values will lead to aggregation, coagulation, or flocculation due to van der Waals interparticle attraction (Joseph and Singhvi, 2019; Shnoudeh et al., 2019), as is the case in the present study where all ZP values were in the non-stable range.

The chorion consists of two membranes, namely, the chorion membrane and the vitelline, it also has pores running through it to assist in gas exchange, as gills only develop after 2 weeks (Pelster and Bagatto, 2010). The pore canals are between 0.5 and 0.7 µm in diameter, this means that small particles can permeate these canals and enter the larvae. However, larger agglomerates can also block these canals causing hypoxic conditions for the embryo (Lee et al., 2007; Vicario-Parés et al., 2014; Samaee et al., 2015; Lacave et al., 2016). Even though embryos were washed in clean media before respiration measurements were taken there still could have been residual agglomerates blocking pore canals and impairing respiration in the 20 mg/L QD-NH_3 treatment embryos. Increased oxygen consumption is most likely due to stress, increased activity or increased metabolic activity seen in the 20 mg/L QD-COOH group, as no agglomerates on the embryo surface were observed in this treatment. Increased oxygen requiring activities were observed as severe hyperactivity in larvae exposed to low doses (2.5 nM) of uncoated CdTe QDs (Duan et al., 2013), as well as anxiety-related swimming behaviour changes after exposure to CdSe QDs (Zonouzi-Marand et al., 2022).

By comparing responses of zebrafish embryos following exposure to different functional groups QDs, it was evident that developmental and respiratory effects could not solely be attributed to metal ion toxicity. This supports findings by Tang et al. (2013) that reported effects of free Cd could not adequately explain QD toxicity in zebrafish embryos. Endpoints assessed in the present study also indicated a clear difference in the severity of responses between functionalized groups. Bimodal responses in metal uptake and malformations were observed

for QD-PEG and QD-COOH treatments. This is most likely attributed to smaller NMs crossing the chorion membrane and eliciting direct toxicological responses, whereas larger agglomerates at higher exposure concentrations blocking the membrane pores and eliciting indirect toxicity. Bioaccumulation and elimination rates are important parameters in QD toxicokinetics and merit examination (King-Heiden et al., 2009). The QD-COOH and QD-PEG groups may be less bioavailable compared to the QD-NH_3 group. Work by King-Heiden et al. (2009) found that QD-PEG with different chain lengths did exhibit toxicity towards zebrafish embryos but these effects were less severe than non-functionalized QDs. Several studies suggest that the terminal functional group of QDs and surface chemistry influences tissue distribution (Hardman, 2006). Thus, it is likely that surface chemistry, surface charge, and particle size influenced particle bioavailability and mode of toxicity, accounting for the differences observed in this study.

5 Conclusion

In summary, this study demonstrates that CdTe QDs cause developmental embryonic toxicity, resulting in persistent effects on larval development and respiration. We also established that different functionalized CdTe QDs materials tended to agglomerate and react differently in exposure media, which in turn influenced the toxicity. The QD-NH_3-were the most toxic of the three tested QDs in this study. It was also seen that lower exposure concentrations were more toxic to survival and spinal deformations compared to high exposure concentrations, and no dose dependent effects were observed for all three materials in this study regardless of metal uptake. This was attributed to changes in the agglomerate sizes and colloidal behaviour of the particles in the media. This was evident in larger agglomerates forming at the high exposure concentrations, which resulted in decreased respiration rates, such as for the QD-NH_3 group. It is thus concluded that three differently functionalized quantum dots with the same primary particle size can have different toxicities due to the particles characteristics, and that the toxicity observed is not solely due to metal body burden but rather a combination of particle specific effects due to aggregation, such as respiration impairment and metal uptake at lower concentrations. This highlights the need for further investigation.

Data availability statement

The raw data supporting the conclusion of this article will be made available by the authors, without undue reservation.

Ethics statement

The animal study was reviewed and approved by NWU-Animcare animal research ethics committee, North-West University, South Africa. Study NWU-00173-18-A5.

Author contributions

SB, TLB, and VW contributed to the conception and design of the study. SB wrote the first draft of the manuscript and performed the statistical analysis. All authors contributed to the manuscript revision, and read, and approved the submitted version.

Funding

The study was funded through the Health, Safety and Environmental Risk of Nanotechnology research platform of the South African Department of Science and Innovation (DSI). Funding for SBM through the National Research Foundation (NRF) (UID: 131561) is acknowledged. Opinions expressed and conclusions arrived at, are those of the authors and are not necessarily to be attributed to the NRF.

Acknowledgments

This is contribution number 754 of the North-West University (NWU) Water Research Group.

Conflict of interest

The authors declare that the research was conducted in the absence of any commercial or financial relationships that could be construed as a potential conflict of interest.

Publisher's note

References

Adair, J., Suvaci, E., and Sindel, J. (2001). Surface and colloid chemistry. *Encycl. Mater. Sci. Technol.* (2), 1–10. doi:10.1016/b0-08-043152-6/01622-3

Åkerman, M. E., Chan, W. C. W., Laakkonen, P., Bhatia, S. N., and Ruoslahti, E. (2002). Nanocrystal targeting *in vivo*. *Proc. Natl. Acad. Sci.* 99, 12617–12621. doi:10.1073/pnas.152463399

Asharani, P. V., Lianwu, Y., Gong, Z., and Valiyaveettil, S. (2011). Comparison of the toxicity of silver, gold and platinum nanoparticles in developing zebrafish embryos. *Nanotoxicology* 5, 43–54. doi:10.3109/17435390.2010.489207

Besinis, A., Van Noort, R., and Martin, N. (2014). Remineralization potential of fully demineralized dentin infiltrated with silica and hydroxyapatite nanoparticles. *Dent. Mat.* 30, 249–262. doi:10.1016/j.dental.2013.11.014

Boyle, D., Clark, N. J., and Handy, R. D. (2020). Toxicities of copper oxide nanomaterial and copper sulphate in early life stage zebrafish: Effects of pH and intermittent pulse exposure. *Ecotoxicol. Environ. Saf.* 190, 109985. doi:10.1016/j.ecoenv.2019.109985

Chen, F., and Gerion, D. (2004). Fluorescent CdSe/ZnS nanocrystal–peptide conjugates for long-term, nontoxic imaging and nuclear targeting in living cells. *Nano Lett.* 4, 1827–1832. doi:10.1021/nl049170q

Cho, W. S., Cho, M., Jeong, J., Choi, M., Cho, H. Y., Han, B. S., et al. (2009). Acute toxicity and pharmacokinetics of 13 nm-sized PEG-coated gold nanoparticles. *Toxicol. Appl. Pharmacol.* 236, 16–24. doi:10.1016/j.taap.2008.12.023

Deerfield, D. W., 2nd, Lapadat, M. A., Spremulli, L. L., Hiskey, R. G., and Pedersen, L. G. (1989). The role of hydrated divalent metal ions in the bridging of two anionic groups. An *ab initio* quantum chemical and molecular mechanics study of dimethyl phosphate and formate bridged by calcium and magnesium ions. *J. Biomol. Struct. Dyn.* 6 (6), 1077–1091. doi:10.1080/07391102.1989.10506538

Derfus, A. M., Chan, W. C. W., and Bhatia, S. N. (2004). Probing the cytotoxicity of semiconductor quantum dots. *Nano Lett.* 4, 11–18. doi:10.1021/nl0347334

Duan, J., Yu, Y., Li, Y., Yu, Y., Li, Y., Huang, P., et al. (2013). Developmental toxicity of CdTe QDs in zebrafish embryos and larvae. *J. Nanoparticle Res.* 15, 1700. doi:10.1007/s11051-013-1700-8

ECHA (2022). Tellurium European chemicals agency (ECHA) registration dossier. Available at: https://echa.europa.eu/fr/registrationdossier/-/registered-dossier/14525/6/2/2

Gallud, A., Delaval, M., Kinaret, P., Marwah, V. S., Fortino, V., Ytterberg, J., et al. (2020). Multiparametric profiling of engineered nanomaterials: Unmasking the surface coating effect. *Adv. Sci.* 7, 2002221. doi:10.1002/advs.202002221

Gao, Y., Xie, Z., Feng, J., Ma, W., and Zhu, L. (2019). Different factors determined the toxicokinetics of organic chemicals and nanomaterials exposure to zebrafish (Danio Rerio). *Ecotoxicol. Environ. Saf.* 186, 109810. doi:10.1016/j.ecoenv.2019.109810

Ghobadian, M., Nabiuni, M., Parivar, K., Fathi, M., and Pazooki, J. (2015). Toxic effects of magnesium oxide nanoparticles on early developmental and larval stages of zebrafish (*Danio rerio*). *Ecotoxicol. Environ. Saf.* 122, 260–267. doi:10.1016/j.ecoenv.2015.08.009

Hardman, R. (2006). A toxicologic review of quantum dots: Toxicity depends on physicochemical and environmental factors. *Environ. Health Perspect.* 114, 165–172. doi:10.1289/ehp.8284

Hsu, P. C., O'Callaghan, M., Al-Salim, N., and Hurst, M. R. (2012). Quantum dot nanoparticles affect the reproductive system of *Caenorhabditis elegans*. *Environ. Toxicol. Chem.* 31, 2366–2374. doi:10.1002/etc.1967

Jaiswal, J. K., Mattoussi, H., Mauro, J. M., and Simon, S. M. (2003). Long-term multiple color imaging of live cells using quantum dot bioconjugates. *Nat. Biotechnol.* 21, 47–51. doi:10.1038/nbt767

Jason, R. E. S., Jennifer, A. N., and Maureen, A. W. (2009). Quantum dots for live cell and *in vivo* imaging. *Int. J. Mol. Sci.* 10, 441–491. doi:10.3390/ijms10020441

Jin, Y., Wu, S., Zeng, Z., and Fu, Z. (2017). Effects of environmental pollutants on gut microbiota. *Environ. Pollut.* 222, 1–9. doi:10.1016/j.envpol.2016.11.045

Joseph, E., and Singhvi, G. (2019). "Chapter 4 - multifunctional nanocrystals for cancer therapy: A potential nanocarrier," in *Nanomaterials for drug delivery and therapy*. Editor A. M. Grumezescu (William Andrew Publishing).

Keremidarska-Markova, M., Hristova, K., Andreeva, T., Speranza, G., Wang, D., and Krasteva, N. (2018). Cytotoxicity evaluation of ammonia-modified graphene oxide particles in lung cancer cells and embryonic stem cells. *Adv. Condens. Matter Phys.*, 2018, 1–11. doi:10.1155/2018/9571828

King-Heiden, T. C., Wiecinski, P. N., Mangham, A. N., Metz, K. M., Nesbit, D., Pedersen, J. A., et al. (2009). Quantum dot nanotoxicity assessment using the zebrafish embryo. *Environ. Sci. Technol.* 43, 1605–1611. doi:10.1021/es801925c

Krzykwa, J. C., Saeid, A., and Jeffries, M. K. S. (2019). Identifying sublethal endpoints for evaluating neurotoxic compounds utilizing the fish embryo toxicity test. *Ecotoxicol. Environ. Saf.* 170, 521–529. doi:10.1016/j.ecoenv.2018.11.118

Kumar, N., Willis, A., Satbhai, K., Ramalingam, L., Schmitt, C., Moustaid-Moussa, N., et al. (2020). Developmental toxicity in embryo-larval zebrafish (*Danio rerio*) exposed to strobilurin fungicides (azoxystrobin and pyraclostrobin). *Chemosphere* 241, 124980. doi:10.1016/j.chemosphere.2019.124980

Lacave, J. M., Retuerto, A., Vicario-Parés, U., Gilliland, D., Oron, M., Cajaraville, M. P., et al. (2016). Effects of metal-bearing nanoparticles (Ag, Au, CdS, ZnO, SiO2) on developing zebrafish embryos. *Nanotechnology* 27, 325102. doi:10.1088/0957-4484/27/32/325102

Larson, D. R., Zipfel, W. R., Williams, R. M., Clark, S. W., Bruchez, M. P., Wise, F. W., et al. (2003). Water-soluble quantum dots for multiphoton fluorescence imaging *in vivo*. *Science* 300, 1434–1436. doi:10.1126/science.1083780

Lee, K. J., Nallathamby, P. D., Browning, L. M., Osgood, C. J., and Xu, X.-H. N. (2007). *In vivo* imaging of transport and biocompatibility of single silver nanoparticles in early development of zebrafish embryos. *ACS Nano* 1, 133–143. doi:10.1021/nn700048y

Lovrić, J., Bazzi, H. S., Cuie, Y., Fortin, G. R., Winnik, F. M., and Maysinger, D. (2005). Differences in subcellular distribution and toxicity of green and red emitting CdTe quantum dots. *J. Mol. Med. Berl.* 83, 377–385. doi:10.1007/s00109-004-0629-x

Martinez, C. S., Igartua, D. E., Czarnowski, I., Feas, D. A., Alonso, S. D., and Prieto, M. J. (2019). Biological response and developmental toxicity of zebrafish embryo and larvae exposed to multi-walled carbon nanotubes with different dimension. *Heliyon* 5, e02308. doi:10.1016/j.heliyon.2019.e02308

Medintz, I. L., Uyeda, H. T., Goldman, E. R., and Mattoussi, H. (2005). Quantum dot bioconjugates for imaging, labelling and sensing. *Nat. Mater.* 4, 435–446. doi:10.1038/nmat1390

Michalet, X., Pinaud, F. F., Bentolila, L. A., Tsay, J. M., Doose, S., Li, J. J., et al. (2005). Quantum dots for live cells, *in vivo* imaging, and diagnostics. *Science* 307, 538–544. doi:10.1126/science.1104274

Mishra, Y. K., Verma, S. K., Nandi, A., Sinha, A., Patel, P., Jha, E., et al. (2021). Zebrafish (*Danio rerio*) as an ecotoxicological model for nanomaterial induced toxicity profiling. *Precis. Nanomedicine* 4 (1), 750–782. doi:10.33218/001c.21978

NANOSOLUTIONS (2013). *Biological foundation for the safety classification of engineered nanomaterials (ENM): Systems biology approaches to understand interactions of enm with living organisms and the environment*. D3.2 Particle behaviour in exposure media (report on task 3.4). Project ID: 309329. Funded under: FP7-NM. 2013-04-01 to 2017-03-31.

Paatero, I., Casals, E., Niemi, R., Özliseli, E., Rosenholm, J. M., and Sahlgren, C. (2017). Analyses in zebrafish embryos reveal that nanotoxicity profiles are dependent on surface-functionalization controlled penetrance of biological membranes. *Sci. Rep.* 7, 8423. doi:10.1038/s41598-017-09312-z

Pelster, B., and Bagatto, B. (2010). "7 - respiration," in *Fish physiology*. Editors S. F. Perry, M. Ekker, A. P. Farrell, and C. J. brauner (Academic Press).

Petushkova, N. A., Kuznetsova, G. P., Larina, O. V., Kisrieva, Y. S., Samenkova, N. F., Trifonova, O. P., et al. (2015). One-dimensional proteomic profiling of *Danio rerio* embryo vitellogenin to estimate quantum dot toxicity. *Proteome Sci.* 13, 17. doi:10.1186/s12953-015-0072-7

Rocha, T. L., Mestre, N. C., Sabóia-Morais, S. M. T., and Bebianno, M. J. (2017). Environmental behaviour and ecotoxicity of quantum dots at various trophic levels: A review. *Environ. Int.* 98, 1–17. doi:10.1016/j.envint.2016.09.021

Ron, H. (2006). A toxicologic review of quantum dots: Toxicity depends on physicochemical and environmental factors. *Environ. Health Perspect.* 114, 165–172. doi:10.1289/ehp.8284

Samaee, S.-M., Rabbani, S., Jovanović, B., Mohajeri-Tehrani, M. R., and Haghpanah, V. (2015). Efficacy of the hatching event in assessing the embryo toxicity of the nano-sized TiO_2 particles in zebrafish: A comparison between two different classes of hatching-derived variables. *Ecotoxicol. Environ. Saf.* 116, 121–128. doi:10.1016/j.ecoenv.2015.03.012

Shnoudeh, A. J., Hamad, I., Abdo, R. W., Qadumii, L., Jaber, A. Y., Surchi, H. S., et al. (2019). "Chapter 15 - synthesis, characterization, and applications of metal nanoparticles," in *Biomaterials and bionanotechnology*. Editor R. K. Tekade (Academic Press).

Singh, S., Dhawan, A., Karhana, S., Bhat, M., and Dinda, A. K. (2020). Quantum dots: An emerging tool for point-of-care testing. *Micromachines* 11 (12), 1058. doi:10.3390/mi11121058

Sun, J., Zhang, Q., Wang, Z., and Yan, B. (2013). Effects of nanotoxicity on female reproductivity and fetal development in animal models. *Int. J. Mol. Sci.* 14, 9319–9337. doi:10.3390/ijms14059319

Tang, S., Cai, Q., Chibli, H., Allagadda, V., Nadeau, J. L., and Mayer, G. D. (2013). Cadmium sulfate and CdTe-quantum dots alter DNA repair in zebrafish (*Danio rerio*) liver cells. *Toxicol. Appl. Pharmacol.* 272, 443–452. doi:10.1016/j.taap.2013.06.004

Tatsi, K., Hutchinson, T. H., and Handy, R. D. (2020). Consequences of surface coatings and soil ageing on the toxicity of cadmium telluride quantum dots to the earthworm *Eisenia fetida*. *Ecotoxicol. Environ. Saf.* 201, 110813. doi:10.1016/j.ecoenv.2020.110813

Vassallo, J., Besinis, A., Boden, R., and Handy, R. D. (2018). The minimum inhibitory concentration (MIC) assay with *Escherichia coli*: An early tier in the environmental hazard assessment of nanomaterials? *Ecotoxicol. Environ. Saf.* 162, 633–646. doi:10.1016/j.ecoenv.2018.06.085

Vicario-Parés, U., Castañaga, L., Lacave, J. M., Oron, M., Reip, P., Berhanu, D., et al. (2014). Comparative toxicity of metal oxide nanoparticles (CuO, ZnO and TiO_2) to developing zebrafish embryos. *J. Nanoparticle Res.* 16, 2550. doi:10.1007/s11051-014-2550-8

Voura, E. B., Jaiswal, J. K., Mattoussi, H., and Simon, S. M. (2004). Tracking metastatic tumor cell extravasation with quantum dot nanocrystals and fluorescence emission-scanning microscopy. *Nat. Med.* 10, 993–998. doi:10.1038/nm1096

Wang, J., Zhu, X., Chen, Y., and Chang, Y. (2012). "Application of embryonic and adult zebrafish for nanotoxicity assessment," in *Nanotoxicity. Methods in molecular biology (methods and protocols)*. Editor J. Reineke (Totowa, NJ: Humana Press).

Xu, Z., Zhang, Y.-L., Song, C., Wu, L.-L., and Gao, H.-W. (2012). Interactions of hydroxyapatite with proteins and its toxicological effect to zebrafish embryos development. *PLOS ONE* 7, e32818. doi:10.1371/journal.pone.0032818

Zhang, W., Lin, K., Miao, Y., Dong, Q., Huang, C., Wang, H., et al. (2012). Toxicity assessment of zebrafish following exposure to CdTe QDs. *J. Hazard Mater* 213-214, 413–420. doi:10.1016/j.jhazmat.2012.02.014

Zhang, X.-Q., Xu, X., Bertrand, N., Pridgen, E., Swami, A., and Farokhzad, O. C. (2012). Interactions of nanomaterials and biological systems: Implications to personalized nanomedicine. *Adv. Drug Deliv. Rev.* 64, 1363–1384. doi:10.1016/j.addr.2012.08.005

Zhang, S., Jiang, Y., Chen, C.-S., Creeley, D., Schwehr, K. A., Quigg, A., et al. (2013). Ameliorating effects of extracellular polymeric substances excreted by *Thalassiosira pseudonana* on algal toxicity of CdSe quantum dots. *Aquat. Toxicol.* 126, 214–223. doi:10.1016/j.aquatox.2012.11.012

Zhao, X., Wang, S., Wu, Y., You, H., and Lv, L. (2013). Acute ZnO nanoparticles exposure induces developmental toxicity, oxidative stress and DNA damage in embryo-larval zebrafish. *Aquat. Toxicol.* 136-137, 49–59. doi:10.1016/j.aquatox.2013.03.019

Zheng, N., Yan, J., Qian, W., Song, C., Zuo, Z., and He, C. (2021). Comparison of developmental toxicity of different surface modified CdSe/ZnS QDs in zebrafish embryos. *J. Environ. Sci.* 100, 240–249. doi:10.1016/j.jes.2020.07.019

Zhu, X., Zhu, L., Li, Y., Duan, Z., Chen, W., and Alvarez, P. J. (2007). Developmental toxicity in zebrafish (*Danio rerio*) embryos after exposure to manufactured nanomaterials: Buckminsterfullerene aggregates (nC60) and fullerol. *Environ. Toxicol. Chem.* 26, 976–979. doi:10.1897/06-583.1

Zhu, X., Wang, J., Zhang, X., Chang, Y., and Chen, Y. (2009). The impact of ZnO nanoparticle aggregates on the embryonic development of zebrafish (*Danio rerio*). *Nanotechnology* 20, 195103. doi:10.1088/0957-4484/20/19/195103

Zolotarev, K., Kashirtseva, V., Mishin, A., Belyaeva, N., Medvedeva, N., and Ipatova, O. (2012). Assessment of toxicity of Cdse/Cds/Zns/S,S-Dihydrolipoic Acid/Polyacrylic acid quantum dots at *Danio rerio* embryos and larvae. *ISRN Nanotechnol.*, 2012, 1, 5. doi:10.5402/2012/914636

Zonouzi-Marand, M., Naderi, M., and Kwong, R. W. M. (2022). Toxicological assessment of cadmium-containing quantum dots in developing zebrafish: Physiological performance and neurobehavioral responses. *Aquat. Toxicol.* 247, 106157. doi:10.1016/j.aquatox.2022.106157

frontiers | Frontiers in Toxicology

TYPE Mini Review
PUBLISHED 23 June 2023
DOI 10.3389/ftox.2023.1233854

OPEN ACCESS

EDITED BY
Dilek Battal,
Mersin University, Türkiye

REVIEWED BY
Changjian Xie,
Shandong University of Technology, China

*CORRESPONDENCE
Dhruv Menon,
dm958@cam.ac.uk
Swaroop Chakraborty,
s.chakraborty@bham.ac.uk

RECEIVED 02 June 2023
ACCEPTED 16 June 2023
PUBLISHED 23 June 2023

CITATION
Menon D and Chakraborty S (2023), How safe are nanoscale metal-organic frameworks?
Front. Toxicol. 5:1233854.
doi: 10.3389/ftox.2023.1233854

How safe are nanoscale metal-organic frameworks?

Dhruv Menon[1]* and Swaroop Chakraborty[2]*

[1]Cavendish Laboratory, Department of Physics, University of Cambridge, Cambridge, United Kingdom, [2]School of Geography, Earth and Environmental Sciences, The University of Birmingham, Birmingham, United Kingdom

Owing to the size scales that can be accessed, the nanoscale has opened doors to new physical and chemical properties, not seen in the bulk. These properties are leveraged by nanomaterials (NMs) across a plethora of applications. More recently, nanoscale metal-organic frameworks (nMOFs) have witnessed explosive growth due to the modularity of their chemical constituents, the ability to modify their composition and structure, and exceptional properties such as permanent porosity and high surface areas. These properties have prompted the investigation of these materials for applications in biological and environmental contexts. However, one aspect that is often ignored in these discussions is their safety at a nanoscale. In this mini review, we aim to initiate a discussion on the safety and toxicity of nMOFs, drawing parallels with the existing guidelines and literature on the safety of inorganic NMs. We first describe why nMOFs are of considerable interest to the scientific community followed by a discussion on routes through which they can be exposed to the environment and living organisms, particularly shedding light on their transformation mechanisms. The review also discusses the factors affecting toxicity of nMOFs, such as their size, shape, morphology, and composition. We briefly highlight potential mechanisms of toxicity and conclude with describing the need to transition towards data-intensive computational approaches such as machine learning to establish nMOFs as credible materials for their envisioned applications.

KEYWORDS

metal organic framework (MOF), nanosafety, safe by design, machine learning, toxicology

Introduction

Humanity's quest towards pushing the boundaries of science has led to the nanoscale, where exciting physical and chemical phenomena have been unlocked owing solely to the size scales that can be accessed (generally <100 nm, however these definitions are arbitrary and often flexible) (Silva, 2004). The observation of these phenomena at these length-scales has not only advanced fundamental understanding of science, but has also served as the basis for emergent applications with far-reaching consequences. These unusual properties can be ascribed to the size of nanomaterials, where they tend to behave more like molecules and less as bulk materials (nanomaterials act as a bridge between the bulk and atomic scale) (Nel et al., 2006). Nanomaterials have a significantly higher proportion of surface atoms than bulk materials. These surface atoms have fewer neighbors than their bulk counterparts, leading to a higher free energy (Figure 1A). Since high free energies are unfavourable, these materials tend to be highly reactive and either bind to other species or undergo specific interactions in order to stabilise themselves (Fruk and Kerbs, 2021).

The engineering of materials at the nanoscale leverages the emergence of these unusual properties across consumer products, electronics and more recently, in medicine (Nel et al.,

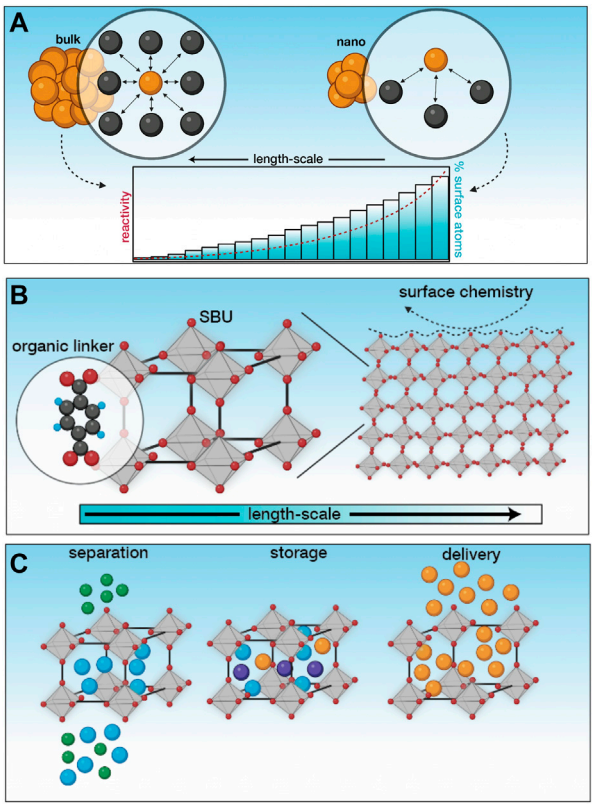

FIGURE 1
An introduction to nMOFs. **(A)** At the nanoscale, there is a higher proportion of surface atoms leading to higher surface energies, which in turn facilitates higher reactivity. This unlocks exciting physical and chemical phenomena not observed in bulk. **(B)** MOFs are hybrid inorganic-organic crystalline materials composed of secondary building units connected via organic linkers. Owing to the way that they are connected, these materials have high porosity and surface area. Often, the external surface of MOFs are modified through functional molecules to enhance their properties, making them more suitable for the task at hand. **(C)** By virtue of their properties, these materials are used for applications pertaining to separation, storage and delivery, in both biological and environmental contexts. Created using BioRender.

2006; Valsami-Jones and Lynch, 2015). While the initial focus was on inorganic NMs, a hybrid inorganic-organic class of NMs known as metal-organic frameworks (or porous coordination polymers) have witnessed explosive growth owing to the modularity of their constituents and the ability to modify their composition and structure with relative ease. At the simplest level, these crystalline materials are composed of metallic centers (known as secondary building units) connected via organic linkers using relatively strong bonds (Figure 1B). Owing to the strength of the bonds and the use of relatively long organic molecules, the material formed has significant void space, making them permanently porous (Furukawa et al., 2013). Given the virtually infinite chemical space, a careful selection of MOF building blocks can undergo temperature induced self-assembly that can be modulated to facilitate a fine control over phase purity, porosity, particle size, morphology and surface chemistry (Figure 1B); (Forgan, 2020). In most applications, it is the ultrahigh porosity (>90%) and high specific surface area (>7,000 m^2/g) that is made use of, for sensing, separation, removal or delivery of specific species (Figure 1C). We have previously used these materials for the removal of toxic metal contaminants (such as Pb(II)) from wastewater (Goyal et al., 2022a; Goyal et al., 2023), which is a very small subset of their applications in biological and environmental contexts. A common observation across applications, however, is the stability of MOFs, which is poor at operating conditions. While the bond between the secondary building units and the linkers are strong enough to allow modulated self-assembly, they are not strong enough to withstand most operating conditions such as moderately high temperatures or interactions with water (Ding et al., 2019). As a result, a third component is often introduced to functionalise the MOF to improve its stability and augment its applicability for the task at hand (Cohen, 2012; Menon and Bhatia, 2022). The flexibility of secondary building units, organic linkers and functional molecules make MOFs incredibly diverse, which is promising from an application standpoint, but makes one process increasingly challenging; assessing and quantifying their safety.

A similar discussion was initiated in the early 2000s for engineered NMs, where there were worries that the environmental impact of NMs would outweigh their benefits, especially since no guidelines were in place to assess them (Colvin, 2003). It was abundantly clear that NMs could not be treated in the same way as bulk materials, as their smaller size gives them additional capabilities such as penetrating cell membranes and causes functional alteration in cells. Several studies point towards a strong correlation between toxicity and physical parameters such as size and shape, and chemical properties such as ability to agglomerate or transform. New phenomena such as the "Trojan horse" are observed at the nanoscale, where nanoparticles are internalised in cells, and dissolve in cellular environments leading to the release of toxic metals inside cells (Valsami-Jones and Lynch, 2015). In a recent study, we tried to observe correlations between a NM's ability to dissolve and the toxicity it induces. While there was a strong correlation for some NMs, the analysis was much more challenging for others (Chakraborty et al., 2023). Despite the apparent complexities, the nanosafety community has rallied to develop advanced tools for the assessment of the toxic potential of engineered NMs (Fadeel et al., 2018) and there are well-defined regulations and guidelines set in place (Rasmussen et al., 2016). That brings us to an important question; would the same guidelines and regulations serve nanoscale MOFs (nMOFs) well? This review is intended to initiate a discussion on the safety of nMOFs by relating their properties with that of engineered NMs, with a focus on nMOFs physicochemical properties, their impact on biological responses. We also discussed upon the application of computational modelling in making these promising set of materials safer-by-design.

Parallels between engineered NMs and nMOFs

Several similarities can be drawn between engineered inorganic NMs and nMOFs, primarily with regards to their sizes, shapes, morphology, and intended applications. As mentioned previously, due to high surface energy, these materials are highly reactive,

forming more stable phases either through aggregation or dissolution (Casals et al., 2012). From a biological context, this increased reactivity facilitates stronger interactions between these NMs and biomolecules (such as proteins) and machinery (such as cells). It is important to note that it is not the nanoparticle itself that cells interact with, but rather a nanoparticle coated with biomolecules (a "corona"). These proteins associate to the nanoparticle as soon as it is introduced into physiological environments (Lynch and Dawson, 2008; Casals et al., 2010). There exists a very complex interplay between the size of the nanoparticle (due to agglomeration), the rates of binding and unbinding of proteins on the nanoparticle surface during the corona formation, and potential release of metallic ions that would ultimately dictate the interactions of these NMs with cells. Despite their apparent similarities, it is worth noting that the diversities and complexities of engineered NMs pales in comparison to nMOFs. Apart from focusing on physical parameters such as size and shape, one must consider the effect of virtually infinite individual nMOF pre-cursors and their interactions with their immediate environment. This inherent diversity forces a need to go "above-and-beyond" standard nanosafety protocols. Nonetheless, there are several lessons that can be learnt from the work on engineered NMs, and several parallels can be drawn as we navigate the nanoscale MOF landscape.

Toxicity at the nanoscale affects both ecosystems and living organisms. Once released into the environment, nanoparticles tend to interact with the air, soil and water (Elsaesser and Howard, 2012). The ecotoxicity of NMs is most often studied on aquatic organisms, with several correlations drawn to mammalian studies. Taking note of lung damage during studies on mammals, injury to the gills and intestine were predicted for aquatic organisms upon exposure, due to the presence of similar epithelial tissues. Similar studies have since been conducted for assessing the fate, transformation and toxicity of nMOFs when exposed to aquatic organisms such as *Daphnia magna* (Li and Wang, 2022) and *C. elegans* (Goyal et al., 2022b). Commonly studied exposure routes were aqueous exposure (Handy et al., 2008), natural feeding mechanisms (Goyal et al., 2022b) and trophic transfer. (Li and Wang, 2022). In these cases, there are concerns of long-term health implications even after short exposure, albeit at higher concentrations likely only during accidental spills (Handy et al., 2008).

The behaviour of inorganic NMs and nMOFs in colloidal dispersions are critical towards understanding their fate, transformation and resultant toxicity. Due to particle-particle collisions, dispersions are thermodynamically unstable, tending to aggregate and separate. The rate of aggregation is higher for particles of different sizes (polydisperse) and have implications on their interactions with organisms (Handy et al., 2008). Several theories such as Derjaguin and Landau (Derjaguin and Landau, 1941), and Verwey et al. (1948) (DLVO) account for attractive and repulsive interactions between closely adjacent particles. In-depth insights of these theories and their shortcomings in predicting the behaviour of nanoparticles in the environment has been discussed by Handy et al. (2008).

With regards to exposure from a biological context, nMOFs can be treated akin to engineered NMs due to similarities in size (dimensions of the order of 100 nm) and the applications for which they are employed. Here it is important to differentiate

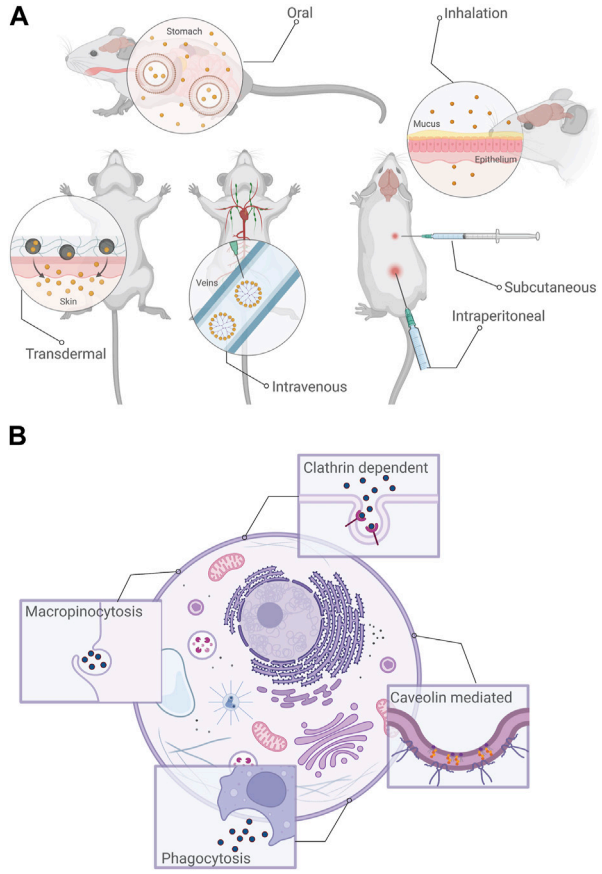

FIGURE 2
(A) Common routes of exposure to nMOFs. Depending upon the applications for which they are used, nMOF exposure to living organisms would be most likely through intravenous, transdermal, subcutaneous, inhalation, intraperitoneal or oral routes. **(B)** Routes of endocytosis most commonly reported for nMOFs: Clathrin-dependent, Caveolin mediated, phagocytosis and macropinocytosis. Created using BioRender.

between engineered NMs and ultrafine polydispersed particulates. In a seminal communication on nanomaterial toxicity, Colvin argues that engineered NMs in general should not be compared to these particulates. This is because particulates are generated as aerosols, and the most likely exposure route is through the same medium. Since aerosols are highly dilute, agglomeration is not commonly observed. In contrast, engineered NMs and nMOFs alike, are most usually synthesized in a liquid phase, and are used for applications in a solid state. In these phases, the concentrations are high enough to allow particle-particle interactions leading to the formation of aggregates which behave very differently during exposure and uptake (Colvin, 2003).

The most likely cause of human exposure to nMOFs is intentional, i.e., nMOFs being used as carriers for biomedical applications such as drug delivery, biosensing or bioimaging (Menon and Bhatia, 2022). It is important to understand that nMOFs are being used as carriers to improve the biodistribution of the therapeutic agents for enhanced targeting of diseased cells (Simon-Yarza et al., 2018). In the context of their applications, there are six possible routes for the exposure to nMOFs (as is the case with

NMs being used for biomedical applications): intravenous (within a vein), transdermal (across the skin), subcutaneous (through the fatty tissues below the skin), inhalation, intraperitoneal (within the peritoneal cavity) and oral (Simon-Yarza et al., 2018); (Sharifi et al., 2012) Among these exposure routes, inhalation, ingestion, contact with the skin and intravenous injection are more likely, again depending on the application (Figure 2A); (Sharifi et al., 2012). For example, if the nanoscale MOFs are being used for environmental remediation applications, the likely exposure routes would be inhalation, ingestion or through skin contact, whereas for biomedical applications, intravenous injection, ingestion or inhalation are more likely.

Post-exposure, the interactions of the NMs with blood is critical towards understanding its fate and resultant toxicity. A lack of compatibility with blood leads to the formation of clots or blood coagulation due to adsorption of proteins onto the NMs surface in order to minimise surface energies. NMs surface gets rapidly coated with specific proteins present in the blood leading to the formation of an entity known as the "protein corona." In case the nanomaterial has to overcome additional physiological barriers before entering the blood stream, it adsorbs additional biomolecules (Sharifi et al., 2012); (Cedervall et al., 2007). The entity formed post adsorption of the relevant biomolecules dictates the interaction of the nanomaterial with cells, and the resulting fate and biodistribution in the body. Interestingly, in the case of MOFs, this phenomenon (sometimes referred to as opsonisation) often rendered them unusable for drug delivery-based applications. As a solution, studies used functional molecules such as polyethylene glycol (PEG) to render MOFs undetectable to these proteins (Chen et al., 2021). Unfortunately studies pertaining to the adsorption of biomolecules onto the surface of nMOFs, their biodistribution and metabolism are sparse.

From the literature that does exist, it is observed that nMOFs tend to aggregate and accumulate in the lungs, which make them good candidates for drug delivery to the lungs, but also raises concerns of respiratory toxicity (Simon-Yarza et al., 2018); (Baati et al., 2013). Specifically with regards to engineered NMs, nMOFs have three specific advantages for pulmonary drug delivery as highlighted by Zheng et al. (2022), (a) a richer elemental composition and variable porosity allowing diverse structures with varying attributes (b) high void space allowing rapid diffusion of high amounts of drugs (c) the ability to post-synthetically modify the outer surface. With regards to bio-compatibility however, while many studies do highlight favourable outcomes (increased bio-compatibility), most of them focus on *in vivo* or *ex vivo* studies. Studies at both a molecular level and epidemiological level are yet to be conducted, making it difficult to draw clear conclusions.

Additionally, reversible accumulation is observed in the liver and the spleen, and depending on the chemistry of the linker, in some cases, slight accumulation is also observed in the brain. Interestingly, the biodistribution changes upon loading the nMOFs with drugs, making it difficult to extrapolate distribution profiles. These profiles also change depending on the guest molecule that is loaded (Simon-Yarza et al., 2018). A better understanding of these phenomena are crucial before these materials can be considered as serious candidates for biological applications at a clinical level. Simon-Yarza et al. (2018) provide a framework to gauge the suitability of a platform from a safety perspective for drug delivery applications.

Factors affecting the toxicity of nMOFs

When it comes to the factors that affect the toxicity of nMOFs, the discussion tends to diverge from conventional wisdom surrounding engineered NMs, due to the inorganic-organic crystalline nature of the former. An obvious starting point for these discussions would be the inherent toxicity of the building blocks. When it comes to the inorganic metallic cluster, the commonly used metallic centers are Al, Co, Cr, Cu, Fe, Mg, Mn, Ni, Zn, and Zr, among which MOFs containing Al, Co, Cr, and Fe have relatively lower toxicity, Mg, Ni, Zn, and Zr have moderate toxicity while Cu and Mn have relatively high toxicity. These observations point towards an inverse correlation between the stability of the MOFs in biological media and toxicity, implying that a higher release of metallic ions leads to a higher toxicity. However, this correlation is not linear as one might expect. Similarly, when it comes to the organic linker, the inherent toxicity does seem to have a correlation with the resulting toxicity of the MOF. Factors such as the hydrophobicity of the organic linker dictates the rate of clearance from the body. While the inherent toxicity of building blocks does not necessarily paint a clear picture of the toxicity of the MOF, as a general rule of thumb, the lower the toxicity of the precursors, the lower the toxicity of the MOF (Baati et al., 2013); (Ruyra et al., 2015) As pointed out earlier, the introduction of a functional molecule adds a third order of complexity to the mix, as it could either accelerate or decelerate the release of the metallic center into the biological media and could either be in compliance with or counteract the effect of the organic linker. In the context of biological applications, nMOFs are usually functionalized using nucleic acids, lipids, aptamers, and enzymes to either maintain or improve bio-compatibility while enhancing applicability (Menon and Bhatia, 2022). For environmental applications, the scope of functionalization is much broader, as there are no constraints such as bio-compatibility. Functionalization is carried out either during synthesis or post-synthesis depending on the reaction conditions involved and the strength of the interaction required between the functional molecule and the nMOF. That being said, most applications rely on post-synthetic modifications. Post-synthetic modifications can further be broken down into two broad categories of covalent and non-covalent functionalization, depending on the type of interaction, relative strength and ease of assembly. For a more detailed discussion on methods of functionalization, readers are directed to Cohen (Cohen, 2012).

Considering the building blocks as the first layer of complexity, the physicochemical properties of the material can be visualised as the second layer. Consider the size of the MOF; as size decreases, the ability of the MOF to penetrate physiological barriers such as cell membranes and the blood-brain barrier increases significantly, which in turn, increases its ability to cause severe damage at a cellular level (Baati et al., 2013); (Ettlinger et al., 2022). However, the analysis is not so straightforward, as at smaller sizes (as discussed earlier), surface energies are so high that particles tend to agglomerate to stabilise, which in turn leads to a more rapid clearance from the system. When it comes to the shape of the

MOF on the other hand, Wuttke and others (Ettlinger et al., 2022) argue that shape or topology might not have a major role to play in overall toxicity, citing a lack of evidence to the contrary. This is particularly surprising, as shape does tend to have a sizable contribution to toxicity in the case of a wide-array of engineered NMs (Aillon et al., 2009).

A majority of the applications of MOFs rely on their remarkable surface properties, which implies that surface chemistry controls a majority of the interactions. The ability to control the surface chemistry of MOFs thus presents itself as a promising route towards controlling its toxicity, and applicability (McGuire and Forgan, 2015). All put together, there seems to be a complex interplay between the inherent toxicity of the metallic secondary building unit, organic linker, functional molecule, the size, surface chemistry, and colloidal stability of the MOF. Understandably, experimental approaches towards the optimisation of MOFs both from an application and toxicity standpoint seem to be increasingly complex.

Potential mechanisms of toxicity

The trafficking of species of biological interest into the cell through highly controlled and regulated mechanisms is formally termed "endocytosis". In the context of cellular function, endocytosis regulates nutrient uptake and cell signaling among other crucial tasks. In nMOFs, it is this mechanism (or rather set of mechanisms) that regulate their internalization whether for intended applications (such as drug delivery or bioimaging) or unintended/accidental exposure. (Linnane et al., 2022). In the simplest possible terms, when nMOFs reach the cellular environment, they interact with the extracellular matrix and the cell membrane. Membrane invaginations engulf the material, leading to the formation of vesicles which are then transported through specialised compartments into the cell (Figure 2B). Based on the specific mechanism, the processes can be described as clathrin-mediated, calveolin-mediated, cathrin/calveolin independent, phagocytosis and macropinocytosis (Behzadi et al., 2017). While an in-depth discussion of these pathways is outside the scope of this review, briefly, most mechanisms are classified on the basis of the proteins involved in the trafficking process. In the case of clathrin-mediated endocytosis, the protein clathrin forms pits along the cell membrane which through a scission process forms vesicles that are trafficked inside the cell. Caveolin-mediated endocytosis involves the protein caveolin forming an invagination along the cell membrane. Clathrin-/caveolin-independent pathways involve other specialised proteins, macropinocytosis involves endocytosis of materials that are soluble and phagocytosis involves the internalization of larger particles (Figure 2B); (Linnane et al., 2022).

Among mechanisms of toxicity, one that is very commonly observed in the context of nMOFs (and engineered NMs in general) is the generation of excessive reactive oxygen species (ROS). ROS are oxygen radicals, with one or more unpaired electrons, for example, superoxide (O^-), hydroxyl (OH^-), hydroperoxyl (HO^-), and certain oxidizing agents such as hydrogen peroxide (H_2O_2) and ozone (O_3) (Bayr, 2005). In the presence of redox-active metal (released from MOFs), there is a steep increase in the concentration of these species (much high than normal physiological conditions) leading to an increased oxidative stress. This increase in stress in turn leads to DNA/RNA damage, modifications of proteins and oxidation of lipid membrane constituents, having a major effect on cell viability (Ettlinger et al., 2022). It should be noted that in most cases, the toxicity of the organic linker and functional molecules are not well explored or explained, presenting itself as a critical bottleneck for establishing standard protocols for the testing of nMOFs.

Towards a computational future

A key takeaway from the previous discussions is that safety-by-design is particularly challenging in the context of nMOFs owing to the sheer diversity of pre-cursors. It is evident that there is a complex interplay between several factors such as the chemistry of the individual building blocks, strength of interactions, shape and size, porosity and morphology, among several other features. Unfortunately, this suggests that an understanding of the potential toxicity of the individual building blocks does not necessarily dictate the toxicity of the resulting MOF. This also implies that relying purely on experimental approaches would be unfeasible owing to the associated timescales, costs and resources. This sets the stage for transitioning towards a computational future.

Given that fundamentally, MOFs are composed of organic and inorganic pre-cursors, in theory it is possible to leverage the well-established chemistry of each component to gain insights into the molecular and solid-state chemistry of MOFs. In a review by Mancuso et al. (2020), the authors suggest that in a majority of cases, MOFs can be considered to be an array of ordered molecules (treated as a sum of their parts). This simplification has allowed density functional theory (DFT) to make major in-roads into the MOF ecosystem. DFT is used for the electronic structure modelling of MOFs, which can be used to calculate the energetics of MOF interactions with the environment. For example, in a previous study, we leveraged DFT calculations to compare the interactions of different MOFs with water, allowing us to gauge their suitability for toxic metal removal from water (Goyal et al., 2023). In the context of toxicity and safety, DFT in particular can be used to analyse dissolution and degradation when subjected to operating conditions, which as we discussed earlier, majorly contributes to toxicity. Another set of computational approaches are molecular dynamics (MD) and grand canonical Monte Carlo (GCMC) simulations, which allow the exploration of larger length-scales and timescales as compared to DFT. These techniques are better suited for assessing the suitability of MOFs for adsorption, storage and separation-based applications (Bernini et al., 2014).

Despite these promises, the computational costs and timescales associated with the methods discussed above make them unsuitable for large-scale chemical space exploration and screening. This is where, given ample amounts of "good" data, machine learning comes to the rescue. In the context of MOFs, we envision that machine learning can make in-roads in three ways: (I) screening large databases to identify ideal MOF candidates with low toxicity for the application at hand. Researchers have previously had success in using these techniques for the screening of MOFs for storage applications (Borboudakis et al., 2017). (II) For the prediction of MOF toxicity (we however acknowledge that the available data is sparse and biased, making this more challenging to tackle).

Researchers have previously been able to develop accurate predictive algorithms for the water stability (Batra et al., 2020), pore guest accessibility (Pétuya et al., 2022) and adsorption (Pardakhti et al., 2017). (III) The more ambitious, inverse design of low toxicity MOF candidates for the application at hand. Generative modelling has only recently been introduced in the context of materials science (Menon and Ranganathan, 2022), and preliminary work on MOFs has begun (Yao et al., 2021), (Kim et al., 2020) As a word of caution however, it is important to have a fundamental understanding of the working of machine learning models, good quality data and accurate checks and balances in place, to get reliable, meaningful and useful outputs from these models.

Conclusion and perspectives

From an application point-of-view, it is evident that nMOFs have the potential to be useful at a large-scale across biological and environmental applications. The existing literature on nMOFs raise concerns of their adverse effects if present at significant concentrations. There exist significant knowledge gaps both in the ecotoxicology and biological toxicology of these materials, that stand in the way of large-scale adoption. It is therefore time that the MOF community begins to ponder about regulations and standards when it comes to their safety. Luckily, the community does not have to start from scratch, but rather build on the foundations set by the decades of work done on engineered NMs. Given the immense compositional diversity of MOFs, it is necessary to go above and beyond the state-of-the-art for engineered NMs.

To understand the toxicology of nMOFs, it is crucial to understand their biochemical transformation and reactivities. In environmental contexts, this refers to phenomenon such as agglomeration, dissolution, sedimentation, speciation and precipitation while in biological contexts, this refers to formation of biomolecular corona, intra/extracellular dissolution and manymore. In either case, not just the pristine nMOFs, their transformed form could interact with organisms, leading to biological responses. For biomedical applications such as drug delivery, considerations must be given to the route of nMOF administration, dosage, biodistribution and pharmacokinetic profiles. As is the case with inorganic NMs, the physicochemical properties are very crucial for understanding the interactions of nanoparticles with biological entities. In the case of nMOFs, the problem is made more complex due to the presence of guest molecules and functional molecules that have a significant impact on the resultant properties and thus, interactions. Given the compositional diversity, it is evident that relying solely on experimental approaches is unfeasible, and the focus should transition towards an increased dependence on computational approaches. Through community-driven efforts, a large-scale responsible adoption of computational methods such as machine learning, would go a long way towards realizing the true potential of these materials.

Author contributions

DM: conceptualisation, writing, and editing; SC: conceptualisation, writing, and editing. All authors contributed to the article and approved the submitted version.

Funding

SC acknowledges the NERC-Discovery Sciences-Discipline Hopping project (Grant number: NE/X017559/1).

Acknowledgments

DM acknowledges the Trinity Henry-Barlow Scholarship, University of Cambridge.

Conflict of interest

The authors declare that the research was conducted in the absence of any commercial or financial relationships that could be construed as a potential conflict of interest.

Publisher's note

References

Aillon, K. L., Xie, Y., El-Gendy, N., Berkland, C. J., and Forrest, M. L. (2009). Effects of nanomaterial physicochemical properties on *in vivo* toxicity. *Adv. Drug Deliv. Rev.* 61, 457–466. doi:10.1016/j.addr.2009.03.010

Baati, T., Njim, L., Neffati, F., Kerkeni, A., Bouttemi, M., Gref, R., et al. (2013). In depth analysis of the *in vivo* toxicity of nanoparticles of porous iron(iii) metal–organic frameworks. *Chem. Sci.* 4, 1597–1607. doi:10.1039/c3sc22116d

Batra, R., Chen, C., Evans, T. G., Walton, K. S., and Ramprasad, R. (2020). Prediction of water stability of metal–organic frameworks using machine learning. *Nat. Mach. Intell.* 2, 704–710. doi:10.1038/s42256-020-00249-z

Bayr, H. (2005). Reactive oxygen species. *Crit. Care Med.* 33, S498–S501. doi:10.1097/01.ccm.0000186787.64500.12

Behzadi, S., Serpooshan, V., Tao, W., Hamaly, M. A., Alkawareek, M. Y., Dreaden, E. C., et al. (2017). Cellular uptake of nanoparticles: journey inside the cell. *Chem. Soc. Rev.* 46, 4218–4244. doi:10.1039/c6cs00636a

Bernini, M. C., Fairen-Jimenez, D., Pasinetti, M., Ramirez-Pastor, A. J., and Snurr, R. Q. (2014). Screening of bio-compatible metal–organic frameworks as potential drug carriers using Monte Carlo simulations. *J. Mat. Chem. B* 2, 766–774. doi:10.1039/c3tb21328e

Borboudakis, G., Stergiannakos, T., Frysali, M., Klontzas, E., Tsamardinos, I., and Froudakis, G. E. (2017). Chemically intuited, large-scale screening of MOFs by machine learning techniques. *npj Comput. Mat.* 3, 40. doi:10.1038/s41524-017-0045-8

Casals, E., Gonzalez, E., and Puntes, V. F. (2012). Reactivity of inorganic nanoparticles in biological environments: insights into nanotoxicity mechanisms. *J. Phys. D. Appl. Phys.* 45, 443001. doi:10.1088/0022-3727/45/44/443001

Casals, E., Pfaller, T., Duschl, A., Oostingh, G. J., and Puntes, V. (2010). Time evolution of the nanoparticle protein corona. *ACS Nano* 4, 3623–3632. doi:10.1021/nn901372t

Cedervall, T., Lynch, I., Lindman, S., Berggård, T., Thulin, E., Nilsson, H., et al. (2007). Understanding the nanoparticle–protein corona using methods to quantify exchange rates and affinities of proteins for nanoparticles. *Proc. Natl. Acad. Sci.* 104, 2050–2055. doi:10.1073/pnas.0608582104

Chakraborty, S., Menon, D., Akhil Varri, V. S., Sahoo, M., Ranganathan, R., Zhang, P., et al. (2023). Does the doping strategy of ferrite nanoparticles create a correlation between reactivity and toxicity? *Environ. Sci. Nano* 10, 1553–1569. doi:10.1039/d3en00076a

Chen, X., Zhuang, Y., Rampal, N., Hewitt, R., Divitini, G., O'Keefe, C. A., et al. (2021). Formulation of metal–organic framework-based drug carriers by controlled coordination of methoxy PEG phosphate: Boosting colloidal stability and redispersibility. *J. Am. Chem. Soc.* 143, 13557–13572. doi:10.1021/jacs.1c03943

Cohen, S. M. (2012). Postsynthetic methods for the functionalization of metal–organic frameworks. *Chem. Rev.* 112, 970–1000. doi:10.1021/cr200179u

Colvin, V. L. (2003). The potential environmental impact of engineered nanomaterials. *Nat. Biotechnol.* 21, 1166–1170. doi:10.1038/nbt875

Derjaguin, B., and Landau, L. D. (1941). Theory of the stability of strongly charged lyophobic sols and of the adhesion of strongly charged particles in solutions of electrolytes. *Acta Phys. chim. URSS* 14, 633–662.

Ding, M., Cai, X., and Jiang, H.-L. (2019). Improving MOF stability: approaches and applications. *Chem. Sci.* 10, 10209–10230. doi:10.1039/c9sc03916c

Elsaesser, A., and Howard, C. V. (2012). Toxicology of nanoparticles. *Adv. Drug Deliv. Rev.* 64, 129–137. doi:10.1016/j.addr.2011.09.001

Ettlinger, R., Lächelt, U., Gref, R., Horcajada, P., Lammers, T., Serre, C., et al. (2022). Toxicity of metal–organic framework nanoparticles: From essential analyses to potential applications. *Chem. Soc. Rev.* 51, 464–484. doi:10.1039/d1cs00918d

Fadeel, B., Farcal, L., Hardy, B., Vázquez-Campos, S., Hristozov, D., Marcomini, A., et al. (2018). Advanced tools for the safety assessment of nanomaterials. *Nat. Nanotechnol.* 13, 537–543. doi:10.1038/s41565-018-0185-0

Forgan, R. S. (2020). Modulated self-assembly of metal–organic frameworks. *Chem. Sci.* 11, 4546–4562. doi:10.1039/d0sc01356k

Fruk, L., and Kerbs, A. (2021). *Bionanotechnology: concepts and applications*. Cambridge University Press.

Furukawa, H., Cordova, K. E., O'Keeffe, M., and Yaghi, O. M. (2013). The chemistry and applications of metal-organic frameworks. *Science* 341, 1230444. doi:10.1126/science.1230444

Goyal, P., Menon, D., Jain, P., Prakash, P., and Misra, S. K. (2023). Linker mediated enhancement in reusability and regulation of Pb(II) removal mechanism of Cu-centered MOFs. *Sep. Purif. Technol.*, 123941. doi:10.1016/j.seppur.2023.123941

Goyal, P., Paruthi, A., Menon, D., Behara, R., Jaiswal, A., V, K., et al. (2022a). Fe doped bimetallic HKUST-1 MOF with enhanced water stability for trapping Pb(II) with high adsorption capacity. *Chem. Eng. J.* 430, 133088. doi:10.1016/j.cej.2021.133088

Goyal, P., Soppina, P., Misra, S. K., Valsami-Jones, E., Soppina, V., and Chakraborty, S. 2022b, Toxicological impact and *in vivo* tracing of rhodamine functionalised ZIF-8 nanoparticles. *Front. Toxicol.*, 4, 917749, doi:10.3389/ftox.2022.917749

Handy, R. D., von der Kammer, F., Lead, J. R., Hassellöv, M., Owen, R., and Crane, M. (2008). The ecotoxicology and chemistry of manufactured nanoparticles. *Ecotoxicology* 17, 287–314. doi:10.1007/s10646-008-0199-8

Kim, B., Lee, S., and Kim, J. (2020). Inverse design of porous materials using artificial neural networks. *Sci. Adv.* 6, eaax9324. doi:10.1126/sciadv.aax9324

Li, Y., and Wang, W.-X. (2022). Internalization of the metal–organic framework MIL-101(Cr)-NH_2 by a freshwater alga and transfer to zooplankton. *Environ. Sci. Technol.* 57, 118–127. doi:10.1021/acs.est.2c03780

Linnane, E., Haddad, S., Melle, F., Mei, Z., and Fairen-Jimenez, D. (2022). The uptake of metal–organic frameworks: A journey into the cell. *Chem. Soc. Rev.* 51, 6065–6086. doi:10.1039/d0cs01414a

Lynch, I., and Dawson, K. A. (2008). Protein-nanoparticle interactions. *Nano Today* 3, 40–47. doi:10.1016/s1748-0132(08)70014-8

Mahmoudi, M., Lynch, I., Ejtehadi, M. R., Monopoli, M. P., Bombelli, F. B., and Laurent, S. (2011). Protein-nanoparticle interactions: opportunities and challenges. *Chem. Rev.* 111, 5610–5637. doi:10.1021/cr100440g

Mancuso, J. L., Mroz, A. M., Le, K. N., and Hendon, C. H. (2020). Electronic structure modeling of metal–organic frameworks. *Chem. Rev.* 120, 8641–8715. doi:10.1021/acs.chemrev.0c00148

McGuire, C. V., and Forgan, R. S. (2015). The surface chemistry of metal–organic frameworks. *Chem. Commun.* 51, 5199–5217. doi:10.1039/c4cc04458d

Menon, D., and Bhatia, D. (2022). Biofunctionalized metal–organic frameworks and host–guest interactions for advanced biomedical applications. *J. Mat. Chem. B* 10, 7194–7205. doi:10.1039/d2tb00459c

Menon, D., and Ranganathan, R. (2022). A generative approach to materials discovery, design, and optimization. *ACS Omega* 7, 25958–25973. doi:10.1021/acsomega.2c03264

Nel, A., Xia, T., Madler, L., and Li, N. (2006). Toxic potential of materials at the nanolevel. *Ccience* 311, 622–627. doi:10.1126/science.1114397

Pardakhti, M., Moharreri, E., Wanik, D., Suib, S. L., and Srivastava, R. (2017). Machine learning using combined structural and chemical descriptors for prediction of methane adsorption performance of metal organic frameworks (mofs). *ACS Comb. Sci.* 19, 640–645. doi:10.1021/acscombsci.7b00056

Pétuya, R., Durdy, S., Antypov, D., Gaultois, M. W., Berry, N. G., Darling, G. R., et al. (2022). Machine-learning prediction of metal–organic framework guest accessibility from linker and metal chemistry. *Angew. Chem. Int. Ed.* 61, e202114573. doi:10.1002/anie.202114573

Rasmussen, K., González, M., Kearns, P., Sintes, J. R., Rossi, F., and Sayre, P. (2016). Review of achievements of the OECD working party on manufactured nanomaterials' testing and assessment programme. From exploratory testing to test guidelines. *Regul. Toxicol. Pharmacol.* 74, 147–160. doi:10.1016/j.yrtph.2015.11.004

Ruyra, À., Yazdi, A., Espín, J., Carné-Sánchez, A., Roher, N., Lorenzo, J., et al. (2015). Synthesis, culture medium stability, and *in vitro* and *in vivo* zebrafish embryo toxicity of metal–organic framework nanoparticles. *Chem. Eur. J.* 21, 2508–2518. doi:10.1002/chem.201405380

Sharifi, S., Behzadi, S., Laurent, S., Forrest, M. L., Stroeve, P., and Mahmoudi, M. (2012). Toxicity of nanomaterials. *Chem. Soc. Rev.* 41, 2323–2343. doi:10.1039/c1cs15188f

Silva, G. A. (2004). Introduction to nanotechnology and its applications to medicine. *Surg. Neurol.* 61, 216–220. doi:10.1016/j.surneu.2003.09.036

Simon-Yarza, T., Mielcarek, A., Couvreur, P., and Serre, C. (2018). Nanoparticles of metal-organic frameworks: On the road to *in vivo* efficacy in biomedicine. *Adv. Mat.* 30, 1707365. doi:10.1002/adma.201707365

Valsami-Jones, E., and Lynch, I. (2015). How safe are nanomaterials? *Science* 350, 388–389. doi:10.1126/science.aad0768

Verwey, E., Overbeek, J. T. G., and Nes, K. V. (1948). *Theory of the stability of lyophobic colloids: The interaction of sol particles having an electric double layer*.

Yao, Z., Sánchez-Lengeling, B., Bobbitt, N. S., Bucior, B. J., Kumar, S. G. H., Collins, S. P., et al. (2021). Inverse design of nanoporous crystalline reticular materials with deep generative models. *Nat. Mach. Intell.* 3, 76–86. doi:10.1038/s42256-020-00271-1

Zheng, Y., Zhao, Y., Bai, M., Gu, H., and Li, X. (2022). Metal-organic frameworks as a therapeutic strategy for lung diseases. *J. Mat. Chem. B* 10, 5666–5695. doi:10.1039/d2tb00690a

frontiers | Frontiers in Toxicology

TYPE Review
PUBLISHED 31 August 2023
DOI 10.3389/ftox.2023.1242634

OPEN ACCESS

EDITED BY
Marina Trevizan Guerra,
Federal University of Mato Grosso do Sul, Brazil

REVIEWED BY
Geraldine Delbes,
Institut National de la Recherche Scientifique, Canada
Jasim Khan,
University of Alabama at Birmingham, United States

*CORRESPONDENCE
Martine Culty,
culty@usc.edu

RECEIVED 19 June 2023
ACCEPTED 18 August 2023
PUBLISHED 31 August 2023

CITATION
Cui H and Culty M (2023), Do macrophages play a role in the adverse effects of endocrine disrupting chemicals (EDCs) on testicular functions?
Front. Toxicol. 5:1242634.
doi: 10.3389/ftox.2023.1242634

Do macrophages play a role in the adverse effects of endocrine disrupting chemicals (EDCs) on testicular functions?

Haoyi Cui and Martine Culty*

Department of Pharmacology and Pharmaceutical Sciences, Alfred E. Mann School of Pharmacy and Pharmaceutical Sciences, University of Southern California, Los Angeles, CA, United States

During the past decades, several endocrine disrupting chemicals (EDCs) have been confirmed to affect male reproductive function and fertility in animal studies. EDCs are suspected to exert similar effects in humans, based on strong associations between levels of antiandrogenic EDCs in pregnant women and adverse reproductive effects in infants. Testicular macrophages (tMΦ) play a vital role in modulating immunological privilege and maintaining normal testicular homeostasis as well as fetal development. Although tMΦ were not historically studied in the context of endocrine disruption, they have emerged as potential targets to consider due to their critical role in regulating cells such as spermatogonial stem cells (SSCs) and Leydig cells. Few studies have examined the impact of EDCs on the ability of testicular cells to communicate and regulate each other's functions. In this review, we recapitulate what is known about tMΦ functions and interactions with other cell types in the testis that support spermatogenesis and steroidogenesis. We also surveyed the literature for reports on the effects of the EDCs genistein and DEHP on tMΦ, SSCs, Sertoli and Leydig cells. Our goal is to explore the possibility that EDC disruption of tMΦ interactions with other cell types may play a role in their adverse effects on testicular developmental programming and functions. This approach will highlight gaps of knowledge, which, once resolved, should improve the risk assessment of EDC exposure and the development of safeguards to protect male reproductive functions.

KEYWORDS

endocrine disrupting chemicals, testis, macrophages, germ cells, Leydig cells, genistein, DEHP, cell-cell interactions

1 Introduction

The most recent data from WHO reports a global infertility lifetime prevalence at 17.5% of the adult population worldwide (Infertility prevalence estimates, 1990–2021. Geneva: World Health Organization; 2023. Licence: CC BY-NC-SA 3.0 IGO). Among those, half of infertility cases are attributable to male factor (Agarwal et al., 2015). Concern has risen in recent decades about the increasing incidence of male reproductive disorders, including hypospadias and cryptorchidism in newborns, testicular cancer starting in adolescence, and a global decline in sperm counts and quality potentially linked to male infertility (Merzenich et al., 2010; Toppari et al., 2010; Agarwal et al., 2015; Barati et al., 2020; Levine et al., 2022). Testicular germ cell tumors (TGCTs) are the most common malignancies observed in young men from 15 to 44 years, including in USA where Hispanics are the most affected (Ghazarian

et al., 2017). Studies have shown that early-life negative effects can lead to permanent changes in physiology and disease predisposition in adult life, which has been described as 'developmental origins of adult disease hypothesis' (de Boo and Harding, 2006; Arima and Fukuoka, 2020). This hypothesis also applies to diseases of the reproductive system, based on studies in which endocrine disrupting chemicals (EDCs) with antiandrogenic or estrogenic properties were found to affect sperm quality negatively and/or to be associated with male reproductive symptoms/disorders. Perinatal exposures EDCs are believed to play a major role in the etiology of these male reproductive disorders, classified under the umbrella term of testicular dysgenesis syndrome (TDS) (Skakkebaek, 2003; Skakkebaek et al., 2016). Overall, EDCs alter endocrine functions, body homeostasis, reproduction, and development by interfering with hormone function, synthesis, secretion, transport, metabolism, and elimination, exerting broad and long-term adverse effects (Diamanti-Kandarakis et al., 2009; Gore et al., 2015). EDCs that alter fetal androgens levels, androgen/estrogen balance or actions in the male reproductive tract, can impair the development and maintenance of male reproductive system during the masculinization programming window, resulting in TDS, as reported in the literature by us and others (Jones et al., 2014; Jones et al., 2015; Kilcoyne and Mitchell, 2019a).

A growing interest in the potential risk of exposure to EDCs and their association with adverse effects on infants, as well as children and adults has risen in recent years (Sun et al., 2013). Indeed, humans are subjected to multiple anthropogenic and natural EDCs from fetal life through adulthood (Diamanti-Kandarakis et al., 2009). Findings that fetal and neonatal exposures to EDCs in animal models result in a decline of male reproductive potential and genital birth defects have been substantiated in humans by epidemiological studies (Swan et al., 2005; Kalfa et al., 2015; Kilcoyne and Mitchell, 2019b). Although the current increased incidence of testicular cancer could relate to perinatal EDC exposure (Kristensen et al., 2008), it has not been experimentally demonstrated, due to most rodents models not developing testicular cancer, and to the difficulty of establishing strong associations between fetal/perinatal exposures to chemicals and a disease occurring later in life, in adolescent and young adults, who might have been exposed to many cancer-initiators, promoters and/or progressors in the years preceding the cancer diagnostic. Several studies have shown detectable levels of EDCs in breast milk, amniotic fluid, cord blood, urine and semen in humans (Adibi et al., 2009; Jones et al., 2014). Two common EDCs, the phytoestrogen genistein (GEN) and the plasticizer di-(2-ethylhexyl) phthalate (DEHP), and its bioactive metabolite mono-(2-ethylhexyl) phthalate (MEHP), are found in cord blood, amniotic fluid and breast milk (Jefferson and Williams, 2011; Lin et al., 2011; Wen et al., 2017). Fetal exposure to GEN was found to cause transient alterations in rat testes (Thuillier et al., 2009). Maternal exposure to GEN was reported to result in adverse effects on male reproductive system, including changes in spermatogenesis and steroidogenesis and reduced fertility in male offspring (Meena et al., 2017). Studies have also shown adverse effects of DEHP/MEHP on male reproductive system, including a decline in Leydig cell function, especially testosterone biosynthesis (Culty et al., 2008; Martinez-Arguelles et al., 2013).

The mammalian testis contains seminiferous tubules surrounded by the interstitium and performs two essential functions: spermatogenesis and steroidogenesis. The interstitial compartment comprises fibroblasts, blood vessels, leukocytes, mast cells, tMΦ, and steroidogenic Leydig cells. Spermatogenesis occurs in seminiferous tubules that contain germ cells (GCs) and somatic Sertoli cells (SCs), and are surrounded by peritubular myoid smooth muscle cells (PMCs) (Riccioli et al., 2006). EDCs can have differential effects on these various cell types, either by interfering with sex hormone homeostasis, by disrupting the factors they produce or by targeting cell-specific genes involved in critical interactions between cell types. The importance of these interactions is illustrated by the adverse impact of reduced testosterone production by Leydig cell on spermatogenesis. Similar to the central position exerted by Leydig cells on other testicular cell types, testicular macrophages (tMΦ) have been shown to interact with several cell types such as Leydig cells, but also spermatogonia, which rely on tMΦ for their survival and maintenance (DeFalco et al., 2015). However, there has been limited research on the effects of EDC exposures on such cell-cell interactions in testis, and more studies are needed to examine whether EDC deleterious effects could be due in part to the disruption of tMΦ interactions with other testicular cells. Understanding the impact of EDCs on tMΦ immunoregulation and cell interactions could shed light on some of the toxic mechanisms of action of EDC in testis. The present review addresses this possibility by (A) Providing a general overview of macrophages and their multiple functions. (B) Surveying what is known on tMΦ interactions with other testicular cells, with a particular focus on the role of tMΦ in the development and homeostasis of male reproductive system; (C) Review reported adverse effects of GEN and DEHP/MEHP, used as estrogenic and anti-androgenic prototypes, on tMΦ interactions with other testicular cell types.

2 The role of macrophages goes far beyond their innate immune functions

Macrophages are part of the body's immune system, and secrete pro- and anti-inflammatory cytokines and chemokines, are ubiquitous and comprise two classes: resident macrophages and blood-borne infiltrating macrophages (circulating macrophages) (Liao et al., 2018). Studies have shown that most tissue-resident MΦ stem directly from yolk sac-derived erythromyeloid progenitors (EMPs) without monocyte intermediates and from fetal blood monocytes produced in the fetal liver (Liao et al., 2018). Another study has shown that circulating monocytes often arise from bone marrow progenitors and can derive from spleen under abnormal circumstances (during tumor development, or extramedullary hematopoiesis) (Qian et al., 2011). In the mouse, monocytes can be divided into two populations based on their Ly6C expression levels: Classical Ly6C^{high} monocytes and non-classical Ly6C^{low} monocytes (Honold and Nahrendorf, 2018). Classical Ly6C^{high} monocytes are derived from Ly6C^{high} bone marrow progenitors, mediated by chemokine receptor CCR2, while the non-classical Ly6C^{low} monocytes differentiate from classic Ly6C^{high} monocytes under the control of orphan nuclear receptor Nr4a17 (Serbina and

Pamer, 2006; Hanna et al., 2011). Under healthy conditions, Ly6C^{low} monocytes exert a protective or anti-inflammatory effect during tissue injury or autoimmune joint inflammation (Misharin et al., 2014). "Classical" Ly6C^{high} monocytes can extravate and infiltrate tissues under homeostatic conditions to become resident MΦ, which have been shown to resolve tissue injury (Liao et al., 2018). Additionally, tissue-resident MΦ are differentiated immune cells that mature differently in particular tissues of the developing fetus, acquiring tissue-specific functional properties and changing their gene expression profiles accordingly (Hashimoto et al., 2013; Gomez Perdiguero et al., 2015; Song et al., 2017). Tissue-resident MΦ are long-lived, essential for tissue differentiation, physiology and homeostasis and can self-renew locally (Sieweke and Allen, 2013).

Tissue-resident MΦ, including tMΦ and monocyte-derived MΦ, are not only critical for tissue homeostasis, but they also play important roles in stress-induced responses and immune functions, including responses to infections and injury (Italiani and Boraschi, 2014; Italiani and Boraschi, 2017). Phagocytosis is an essential property of MΦ, supporting their role of "scavengers" to remove dead cells and other debris, important for healing processes (Seljelid and Eskeland, 1993). Given their rapid changes in accordance with different environmental stimulations, MΦ have been classified into classically activated (M1) and alternatively activated (M2) macrophages (Gordon, 2003; Martinez et al., 2009). M1 MΦ can be activated by interferon-γ (IFN-γ), lipopolysaccharide (LPS), granulocyte-macrophage colony-stimulating factor (GM-CSF) or other microbial stimuli, and can produce strong pro-inflammatory cytokines such as tumor necrosis factor (TNF α), Interleukin 1 beta (IL1b), and interleukin (IL 6) (Winnall et al., 2011). M1 MΦ produce nitric oxide (NO) to protect against bacteria and viruses and contribute to the clearance of microbial pathogens (Mosser and Edwards, 2008). In contrast, M2 MΦ are stimulated by IL-4, glucocorticoids, macrophage colony-stimulating factor (M-CSF), different inflammatory stimuli, and some immune complexes (Bode et al., 2012; Lee et al., 2014). M2 MΦ typically secrete anti-inflammatory cytokines, including interleukin (IL 10) or transforming growth factor (TGF β), and have distinct phenotypes (Gordon, 2003; Winnall et al., 2011; Sica and Mantovani, 2012). M2 MΦ can produce ornithine to promote proliferation and are associated with wound healing, tissue repair, parasite resistance, immuno-regulation. M2 MΦ are also able to attenuate the detrimental immune response (Sica and Mantovani, 2012). An important regulator of myeloid progenitors and monocyte and MΦ recruitment and differentiation that encapsulates well the broad role of MΦ beyond their immune function is Macrophage colony-stimulating factor (CSF1), a secreted cytokine exerting its action via binding on its receptor CSF1R, found to regulate non-immune cells expressing CSF1R, such as SSCs in testis (Stanley and Chitu, 2014; DeFalco et al., 2015).

3 Testicular macrophages and their interaction with other testicular cells

3.1 Characteristics of testicular macrophages

Testicular macrophages (tMΦ) are the most abundant immune cells in the mammalian testis (Mossadegh-Keller et al., 2017; Hosseini et al., 2022), where they play a critical role in controlling innate immune responses in infection and sterile inflammation via secreting pro-inflammatory and anti-inflammatory cytokines (Hedger, 2002). They can produce inflammatory responses to pathogens and bacteria by expressing major histocompatibility complex (MHC) class II antigens and Fc receptors in rodents (Rival et al., 2008). TMΦ can establish and maintain testicular immune privilege by protecting developing germ cells from immune assaults and preventing spermatogenesis from auto-immune assault and detrimental effects of autoimmunity (Mossadegh-Keller and Sieweke, 2018). In addition to their immune functions, tMΦ contribute to organogenesis, supporting fetal testis development and vascularization, the formation and normal functioning of SSCs, and tissue homeostasis (DeFalco et al., 2014; Potter and DeFalco, 2017; Mossadegh-Keller and Sieweke, 2018). Indeed, due to their immunosuppressive and testis-specific roles mentioned above, tMΦ are considered as the "guardians of fertility (Mossadegh-Keller and Sieweke, 2018). Two main subpopulations of tMΦ have been reported in rat testis: Resident testicular macrophages (Resident tMΦ) and Newly arrived testicular macrophages (Newly arrived tMΦ). This classification is characterized by the expression of a lysosomal antigen, CD68 (expressed in circulating monocytes and found in M1 and intermediary resident MΦ), and a scavenger receptor, marker, CD163 (expressed in tissue-resident M2 MΦ, and intermediary resident MΦ) (Table1) (Winnall et al., 2011; Winnall and Hedger, 2013). Resident M2 tMΦ are derived from precursor macrophages through local proliferation and were described as CD163+ tMΦ. TMΦ can also be distinguished by their localization either in the interstitium or at the periphery of the seminiferous tubules, defining different types of interactions with other types of testicular cells (Mossadegh-Keller et al., 2017; Potter and DeFalco, 2017). Besides newly-arrived tMΦ, defined as CD68^{+} CD163^{-} tMΦ that differentiated from infiltrated monocytes, other populations of tMΦ were identified as derived directly from bone-marrow progenitors, those derived from fetal BM progenitors forming interstitial tMΦ, whereas those derived from postnatal/prepubertal BM progenitors forming peritubular tMΦ (Hume, 2008; Winnall et al., 2011; Mossadegh-Keller et al., 2017). Studies have shown that tMΦ can produce high amounts of anti-inflammatory cytokine IL 10, as well as CXCL2, which is produced by both inflammatory and alternative tMΦ; and low amounts of pro-inflammatory factors TNF α and IL 1b when stimulated by LPS, IFN-γ in the case of pro-inflammatory tMΦ, or by IL 4 for alternative tMΦ (Winnall and Hedger, 2013). TMΦ maintain immune tolerance and the complex testicular microenvironment necessary for testis development and life-long testicular functions by communicating with other critical testicular cell types through cell-cell interactions via spatially associating with SSCs, SCs and Leydig cells (Skinner et al., 1991; Hales, 2002; DeFalco et al., 2014). Any disruption to these interactions could disrupt androgen synthesis and sperm production, potentially leading to hypogonadism-related disorders and male infertility (Skinner et al., 1991; Hales, 2002; DeFalco et al., 2014; Potter and DeFalco, 2017; Mossadegh-Keller and Sieweke, 2018).

TABLE 1 Origins, types, and main functions of testicular macrophages. Testicular macrophages can be distinguished by their origins, their polarization status, the cytokines they produce and their functions. The table summarizes the information collected from three references (Williams et al., 2018; Shi et al., 2022; Mass et al., 2023).

Origins	Age range	Macrophage polarization type	Main cytokines	Main function/targets
Yolk sac monocyte - fetal-derived macrophages	fetal/prenatal	M1	IL1b CD68	Pro-inflammatory functions
			CXCL2 CXCL10 IL1 IL6	Regulate B cell differentiation, T cell antibody secretion, killing activity of natural killer cells (NK cells)
			IL12 IL23 TNF-α	Regulate the permeability of the blood-testis barrier (BTB)
			MCP-1 NO	Regulate spermatogenic cell apoptosis
Bone marrow monocytes - hematopoietic stem cells - common myeloid progenitor cells - monocyte-derived macrophages	postnatal/ prepubertal	M2	TGFb	Anti-inflammatory and immune tolerance functions, Self-maintain
			IL10	
			CD163	

TABLE 2 Summary of reported effects of GEN-DEHP/MEHP mixtures on testicular cells in mammalian species. tMΦ: testicular macrophages; GCs: germ cells; SCs: Sertoli cells; Leydig cells: LCs.

Cell type	Species	Main results	Study type	Ref
TMΦ	Rat	Increased mRNA expression of macrophage markers	*In vivo*	Walker et al. (2020)
GCs	Rat	Altered mRNA expression of undifferentiated GC (Thy1, Sox17) and differentiated (Kit, Sohlh2) markers	*In vivo*	Jones et al. (2014)
GCs	Rat	Altered mRNA expression of undifferentiated GC markers Plzf, Foxo1; differentiated GC marker Sohlh2	*In vivo*	Jones et al. (2015)
SCs	Rat	Altered mRNA expression of Wt1, Abp	*In vivo*	Jones et al. (2014)
SCs	Rat	Altered mRNA of differentiated SC gene marker Abp	*In vivo*	Jones et al. (2015)
SCs	Rat	Induced abnormal testicular phenotypes	*In vivo*	Walker et al. (2020)
SCs	Rat	GEN partially attenuated DEHP-induced SC toxicity	*In vivo*	Zhang et al. (2017)
SCs	Mouse	Induced histological abnormality (tubular vacuolation)	*In vivo*	Xie et al. (2014)
LCs	Rat	Altered expression of Hsd3b, Anxa1, Foxa3, and Pdgfra	*In vivo*	Jones et al. (2014)
LCs	Rat	Altered expression of Cyp11a1, Hsd3b	*In vivo*	Jones et al. (2015)
LCs	Rat	GEN normalized DEHP-induce testosterone changes	*In vivo*	Jones et al. (2015)
LCs	Rat	Long-term alterations in adult Leydig cell function	*In vivo*	Walker et al. (2020)
LCs	Mouse	Decreased gene expression of Insl3	*In vitro*	Jones et al. (2016)
LCs	Mouse	Altered steroid production and lipid homeostasis	*In vitro*	Jones et al. (2016)

3.2 Cell-cell interaction between testicular macrophages and germ cells

The main interaction tMΦ have with germ cells is that with spermatogonia, which are in direct contact with the basement membrane of the seminiferous tubules. SSCs, the stem cells of the germline, are undifferentiated spermatogonia with pluripotent potential that form in early postnatal life (weeks 8–12 postnatal in human; ~ PND6 in rodents) from their precursors, neonatal gonocytes (also called pre-/pro-spermatogonia) (Culty, 2013). In contrast to the first wave of spermatogonia which contribute only to the first round of spermatogenesis (Busada et al., 2016), SSCs sustain steady-state spermatogenesis after puberty, and as such they are essential to spermatogenesis and lifelong male fertility (Mei et al., 2015; Phillips et al., 2010). Similar to other stem cells, the SSCs have the ability to self-renewal and differentiate into other GCs, enabling

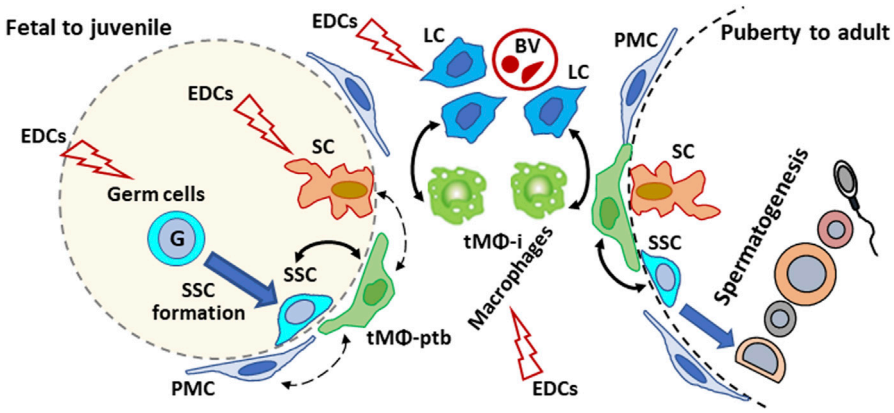

FIGURE 1
Schematic illustration of the proposed effects of endocrine disrupting chemicals (EDCs) on testicular cells interactions in mammalian testis from development to adulthood. Plain arrows: Direct interactions with macrophages. Dotted arrow: indirect/unreported interactions with macrophages. G: gonocyte; SSC: spermatogonial Stem Cell; tMΦ: testicular macrophages; tMΦ-ptb: peritubular tMΦ; tMΦ-i: interstitial tMΦ; PMC: peritubular myoid cells; SCs: Sertoli cells; Leydig cells: LCs; BV: blood vessels.

the production and supply of sperm (Vlajković et al., 2012). Studies of SSCs transplantation in animals have shown an improvement of fertility, indicating that auto-transplantation of SSCs may be a promising therapeutic approach after fertility-ablative treatments in young males (Vlajković et al., 2012; Forbes et al., 2018; David and Orwig, 2020). Macrophage colony-stimulating factor (CSF1) is a secreted cytokine that has a significant role in the regulation of myeloid progenitor cells, and CSF1/CSF1R signaling is associated with the recruitment and differentiation of monocytes and macrophages (Stanley and Chitu, 2014; DeFalco et al., 2015). Interestingly, studies have shown that CSF1 promotes cell proliferation in primary cultures of isolated spermatogonia and SSCs, and that tMΦ express CSF1 that regulates the proliferation and differentiation of isolated type A spermatogonia and the spermatogonial-derived cell line C18–4 in culture, via local macrophage-spermatogonial interactions (DeFalco et al., 2015). The exact nature of this interaction does not seem resolved, but it could involve the diffusion of molecules secreted by tMΦ into adjacent SSCs in the intratubular space. The possibility that processes extending from peritubular tMΦ might directly contact SSCs would imply that the processes passed across the basement membrane. However, this was not observed in the study (DeFalco et al., 2015). *CSF1R* is expressed on both MΦ and SSCs. The role of CSF1/CSF1R signaling has also been shown to promote *in vitro* spermatogonial proliferation through the activation of mitogen-activated protein kinase (MAPK) (Kokkinaki et al., 2009). However, few studies have investigated the effects of EDCs on the interaction between tMΦ and spermatogonia. Besides the role of tMΦ in the maintenance of the spermatogonial niche, recent studies have identified the possible role of MΦ in regulating testicular germ cell tumors (TGCTs). A study examining the tumor microenvironment of metastatic vs. non-metastatic TGCTs reported increased levels of tumor-associated MΦ expressing Programmed death ligand 1 (PD-L1) in seminoma in comparison to non-metastatic TGCTs, proposing that PD-L1$^+$ MΦ influenced the aggressive behavior of the tumors (Sadigh et al., 2020). Considering the established role of MΦ on SSC functions and their potential role on TGCT behavior, it would be interesting to explore the possibility that the disruption of tMΦ following early exposure to EDCs could contribute to the development or progression on TGCTs later in life.

3.3 Cell-cell interaction between testicular macrophages and Leydig cells

Steroidogenic Leydig cells, located between seminiferous tubules, produce and secrete testicular androgens, mainly testosterone, making them essential for the development of male reproductive tissues, sexual development, spermatogenesis and normal male reproductive function, (Zhou et al., 2019). Infertile men who are diagnosed with non-obstructive azoospermia (NOA) have hypertrophic Leydig cells with altered ultrastructure (Tash et al., 2002). Studies have shown altered production of testosterone and abnormal intratubular location of Leydig cells in men with cryptorchidism or Klinefelter's syndrome (Regadera et al., 1991). Therefore, defective Leydig cell activity resulted in reduced testosterone production, increased follicle stimulating hormone (FSH) and luteinizing hormone (LH), impaired testis function, spermatogenesis failure, azoospermia and decreased fertility (Jezek et al., 1998; Joensen et al., 2008; Zirkin and Papadopoulos, 2018; Adamczewska et al., 2022).

The physical association between tMΦ and Leydig cells in the interstitium of the adult rat testis was first recognized in the late 1960s and extensively studied over the years (Christensen, 1969; Hutson, 1998). Morphological studies revealed this direct structural interaction via morphological contact sites between the membranes of macrophages and Leydig cells, known as "digitations" (Hutson et al., 1994). These digitations formed when interstitial tMΦ incorporated into clusters of Leydig cells upon puberty (Hutson, 1992), which is required for Leydig cell development and function during postnatal testicular maturation, as shown in macrophage-depleted transgenic csfm (op)/csfm (op) mice lacking CSF1 and in mice lacking macrophages after treatment with dichloromethylene diphosphonate (Gaytan et al., 1994a; Cohen et al., 1996; Cohen et al.,

1997; Hutson, 2006). A study by Bergh found that the average volume density and total cell mass per testis of both macrophages and Leydig cells were reduced in cryptorchid testes (Bergh, 1985). This coordination of morphological changes of interstitial tMΦ and Leydig cells suggested that they were functionally related, further supporting a functional coupling between these 2 cell populations (Bergh, 1985; Bergh, 1987). In the rat testis, Leydig cells extended slender cytoplasmic processes to channels within an electron-dense network of adjacent macrophage membrane invaginations (Miller et al., 1983). It is believed that an intensive exchange of molecules and signals can occur in these channels between tMΦ and Leydig cells in both juvenile and adult testis through unique intercellular contacts or by secreting paracrine factors throughout development (Christensen, 1969; Miller et al., 1983; Hutson, 1992; Nes et al., 2000). Failure of this intimate communication between the 2 cell populations has been associated with azoospermia (Goluža et al., 2014). Moreover, the presence of tMΦ was necessary for rat Leydig cell differentiation in prepubertal rat and regeneration after ip injection of 75 mg/kg body weight ethylene dimethane sulfonate (EDS)-induced depletion in adult rats, whereas the ablation of tMΦ had no effect on Leydig cell number in intact adult testes (Gaytan et al., 1994a; Gaytan et al., 1994b). TMΦ and Leydig cells interact with each other through the secretion of cytokines and growth factors. Under normal physiological and non-inflammatory conditions, tMΦ secrete several essential cytokines, growth and differentiation factors to offer a proper microenvironment and extracellular milieu that regulates the development and differentiation of immature Leydig cells (Khan et al., 1992; Cohen et al., 1996; Cohen et al., 1997; Hales, 2002).

In inflammatory conditions, tMΦ are activated and provide several factors, including reactive oxygen species (ROS) and pro-inflammatory cytokines like interleukin-1 (IL-1) and tumor necrosis factor-alpha (TNF-α) to inhibit steroidogenesis in Leydig cells (Hales, 2002). However, excessive activation of tMΦ can cause chronic inflammation, even resulting in damaged Leydig cells, reduced testosterone production, and impaired testicular function. Moreover, tMΦ have been found to produce paracrine factors, such as 25-hydroxycholesterol (25-HC), acting as steroidogenic substrates for side chain cleavage, testosterone biosynthesis and steroidogenic functions in Leydig cells (Nes et al., 2000; Lukyanenko et al., 2001; Hutson, 2006; Singh et al., 2021). In turn, Leydig cells produce growth factors like insulin-like growth factor-1 (IGF-1) (Cailleau et al., 1990), which was found to be act as an anti-inflammatory cytokine (Nederlof et al., 2022) thereby may affect the inflammatory responses in tMΦ. An interesting local feedback interaction between mouse tMΦ and Leydig cells was recently reported, based on the *de novo* production of progesterone by tMΦ in mixed testicular interstitial co-cultures upon treatment with cAMP, known to be produced by Leydig cells, postulated to act on tMΦ via gap junction observed between the 2 cell types, whereas treating tMΦ with a M1-inducer mixture of LPS and interferon-γ inhibited progesterone synthesis by MΦ (Yamauchi et al., 2022).

Overall, the macrophage-Leydig cell interaction is a complicated process involving the secretion of several cytokines and growth factors. It is crucial for maintaining normal testicular steroidogenesis, Leydig cell function and male lifelong fertility, and disruptions in this unique interaction can result in testicular dysfunction and reduced fertility. Further research identifying the mechanism underlying the developmental and functional links between macrophages and Leydig cells could provide new insights into potential therapeutic options for male infertility.

3.4 Is there evidence of cell-cell interactions between testicular macrophages and Sertoli cells?

In contrast to spermatogonia and Leydig cells, which have well established interactions with tMΦ, to the best of our knowledge, there is no study demonstrating the existence of cell-cell interaction between tMΦ and Sertoli cells (SCs). SCs are the only somatic cells in the seminiferous epithelium, where they provide physical and nutritional support to the survival and differentiation of germ cells, starting in fetal testis and throughout mammalian spermatogenesis, via regulated cell junctions, cell-cell interactions, and biochemical components by secreting lactate, cytokines, and hormones. SCs also form an immune-protective environment for autoantigenic germ cells via physically inhibiting the invasion of harmful substances by the blood-testis barrier (BTB) and secreting immunomodulatory factors. Studies have also shown that SCs play a crucial role in the phagocytosis of the elongated spermatids' cytoplasm by engulfing dead or dying spermatogenic cells (Shiratsuchi et al., 2013). These cell-cell interactions are important for the development, homeostasis, and regulation of male reproductive system (O'Donnell et al., 2000). Sertoli cells support, nourish, and protect spermatogenic cells by various signal pathways. The TGF-β/Smad, AMPK and MAPK signaling pathways are involved in immature Sertoli cell proliferation and in the dynamics of tight junctions and adherent junctions in mature Sertoli cells to support spermatogenesis. The MAPK and AMPK signaling pathways also regulate the lactate production of Sertoli cells to maintain normal carbohydrate metabolism of germ cells, while the MAPK signaling pathway also exerts a dominant role in regulating SSCs self-renewal. A recent study found that the activities of these signaling pathways were abnormal in the Sertoli cells of testicular cancer or infertile patients (Ni et al., 2019). In addition, mature Sertoli cells produce androgen-binding protein (Abp), transferrin, proteases, and protease inhibitors, all of which are essential for maintaining spermatogenesis, sperm maturation, the tight SCs junctions, and the seminiferous remodeling processes. Moreover, SCs can secrete growth factors, such as TGF-β, PDGF, VEGF, stem cell factor, and express glycoproteins that are necessary for the structure of the basement membranes between the SCs and peritubular cells (Luca et al., 2018).

Although these studies do not demonstrate an interaction between tMΦ and Sertoli cells, there are several studies suggesting that Sertoli cells may indirectly participate to macrophages role in testis. Mouse and human Sertoli cells express CXCL12 (Chen et al., 2015; Westernstroer et al., 2015; Guo et al., 2018), facilitating the maintenance of $CXCR4^{+}$ spermatogonia by producing CXCL12, the ligand of CXCR4, a receptor expressed in both human macrophages and spermatogonia (Guo et al., 2018). Taken together with the immunomodulator role of Sertoli cells, it is reasonable to think

that both Sertoli cells and tMΦ may modulate or support their respective effects on testicular inflammation and spermatogenesis. A more direct interaction between the 2 cell types cannot be excluded. Therefore, clarifying the effects of EDCs on potential interactions between macrophages and Sertoli cells could contribute to a better understanding of their toxicological mechanisms of signaling pathways in male reproduction and provide novel insights into identifying potential therapeutic targets of reproductive disorders. More recently, hematopoietic lineage-tracing studies in mice depleted in Sertoli cells, using Sertoli-specific Amh-cre mice, revealed that Sertoli cells are critical in recruiting monocytes originating from fetal hematopoietic stem cells to become tMΦ in the developing gonads (Gu et al., 2023).

4 Comparison of GEN and DEHP/MEHP effects on macrophages and other testicular cells

4.1 GEN and DEHP/MEHP as EDC prototypes

EDCs include widely used man-made compounds used in the production of plastics, pesticides, lubricants, preservatives, fungicides, medical devices, and additives in consumer products such as cosmetics and personal care products, as well as natural substances, such as phytoestrogens that are found in food (Gore et al., 2015). Human exposure to EDCs has been well documented through multiple studies measuring the parent compounds and/or metabolites in human body, such as in semen, breast milk, amniotic fluid, and cord blood (Adibi et al., 2009). Moreover, many EDCs have high fat-solubility and low water-solubility facilitating their accumulation in body tissues (Diamanti-Kandarakis et al., 2009). Exposure to EDCs, particularly those with antiandrogenic or estrogenic properties, during the masculinization programming window, can perturb fetal programming and gonadal development, leading to testicular dysgenesis syndrome (TDS), as demonstrated in animal models, including our own studies (DiVall, 2013; Jones et al., 2014; Jones et al., 2015).

Genistein, the main phytoestrogen in soy, has extensive biochemical properties, in addition of its estrogenicity via binding to estrogen receptors (ERs), mainly ESR1 and 2 (Erα and Erβ), exerting also direct or indirect antioxidant action and activating peroxisome proliferator-activated receptor (PPAR), as well as inhibiting tyrosine kinases (Jones et al., 2015). Estrogens play an essential role in the regulation of testis development and the male reproductive tract, which express estrogen receptors and are responsive to estrogens from fetal life to adulthood (Lehraiki et al., 2011). Fetal exposure to genistein occurs mainly through maternal uptake of soy-derived products and then undergoes placental transfer. Soy-based formula-fed infants have high circulating GEN levels of up to 9 mg/kg/day, with urine concentration levels around 500 times higher than that of infants fed cow milk-based formula (Setchell et al., 1997; Cao et al., 2009). Studies have also measured GEN blood levels up to 10.2 μM in 4-year-old infants (Jefferson and Williams, 2011). By mimicking the structure of estradiol and binding to ERs at inappropriate times during development, GEN can produce adverse effects on male fertility (Cederroth et al., 2010). Studies have shown that fetal and neonatal exposures of rats to GEN induced transient changes in intracellular signaling (such as MAPK, PDGFR) in neonatal gonocytes and alterations in spermatogenesis (Thuillier et al., 2003; Wang et al., 2004; Thuillier et al., 2009).

Humans are chronically exposed to DEHP, the most used phthalate plasticizer, which leaches from plastics and other consumer products to which it is added but not covalently bound (Gore et al., 2015; Walker et al., 2021). Fetal exposure to DEHP is predominantly through maternal ingestion, dermal contact, or inhalation. Neonatal exposure to DEHP takes place mainly through ingestion by infants, such as drinking contaminated breast milk (Zhu et al., 2006). Studies have found measurable amounts of DEHP or its metabolites in human blood, amniotic fluid, cord blood, and urine (Calafat et al., 2004). In rodents, DEHP or its metabolites, including its main bioactive metabolite Mono-(2-ethylhexyl) phthalate (MEHP) have also been found in amniotic fluid and urine following ingestion (Calafat et al., 2006). DEHP and MEHP can produce androgen receptor-independent antiandrogen effects through biding on *PPAR*s, but have also been shown to alter DNA methylation status and affect estradiol-regulated proteins, all of which could impair testosterone biosynthesis in fetal and adult mice (Culty et al., 2008).

Several *in vivo* and *in vitro* studies have examined the effects of DEHP/MEHP and other phthalates on MΦs, using concentrations ranging from 10^{-8} to 10^{-3} M for *in vitro studies*, and from 1 to 1,000 mg/kg/day for *in vivo* and *ex-vivo* studies. These studies, including some using the human THP-1 cell line, reported variable effects of MEHP, from decreased to increased cytokine production and phagocytosis depending on the concentrations and macrophage cell lines used (Li et al., 1998; Bennasroune et al., 2012; Hansen et al., 2015). Few studies also tested the effects of genistein on MΦ cell lines, using concentrations from 50 nM to 100 μM and reporting mostly anti-inflammatory effects (Mueller et al., 2010). However, these studies did not address the possibility that exposure of MΦ to these chemicals could alter cellular networks and the biological responses of tissues such as the testis.

4.2 Can GEN and DEHP/MEHP alter macrophages and germ cells interactions?

Although there is no study reporting direct or indirect effects of GEN and DEHP/MEHP on MΦ and germ cells interactions, or on Csf1 signaling pathway, critical for MΦ-SSC interactions, the possibility can be inferred from studies describing the disruption of both cell types upon exposure to these EDCs. Caspase-3-positive immunostaining studies of human fetal testes demonstrated that MEHP treatment decreased germ cell number by inducing germ cell apoptosis *in vitro* (Lambrot et al., 2009). Previous work from our laboratory have shown that *in-utero* exposure of rats to 10 mg/kg/day of GEN and DEHP mixtures (GEN-DEHP) altered short- and long-term gene expression and protein levels of germ and somatic cell markers, and increased incidence of infertility in rats exposed to GEN-DEHP mix at this human-relevant dose, differently from exposure to individual EDCs (Jones et al., 2014; Jones et al., 2015). Additionally, *in-utero* exposures to 0.1 and 10 mg/kg/day of GEN-DEHP induced alterations in testicular macrophages, both in neonatal and adult rats, with transcriptome analyses pointing at genes and pathways uniquely altered by GEN-DEHP mixtures, while others were common between mixtures and single EDCs at

the same low doses (Walker et al., 2020). Peroxisome proliferator-activated receptors gamma (PPAR g) is expressed in monocytes and MΦ, regulating fatty acid synthesis, glucose metabolism, and the immune inflammatory (anti-inflammatory) response (Chinetti et al., 2003). Moreover, PPAR g agonists have been shown to inhibit pro-inflammatory cytokines (TNF α, IL 1β, and IL 6) synthesis in a dose-dependent manner (Heming et al., 2018). Moreover, GEN was reported to impede CSF1 action in osteoclast homeostasis, providing a model in support of the possible disruption of MΦ-SSC interactions by GEN (Amano et al., 1998). Thus, we predicted that fetal tMΦs could be direct targets of GEN and/or DEHP in our *in-utero* exposure model, permanently disrupting their interaction with testicular cells such as spermatogonia after birth. However, our studies did not resolve the mechanisms by which the two EDCs affected mechanisms underlying these interactions and spermatogonia postnatally, and whether such effects could be triggered by postnatal exposures.

In view of these studies, one can reasonably predict that the perturbation of MΦ-SSC interactions may contribute to the adverse effects of EDCs on spermatogenesis and male fertility. For example, considering the key role played by tMΦs-produced CSF1, if *in vivo* exposure to GEN-DEHP mixtures (or other EDCs with equivalent mechanism of action and molecular targets) inhibited the production of CSF1, disrupting its signaling on SSC-expressed CSF1R and altering the tyrosine kinases downstream of CSF1R, which could result in inadequate SSC pool, failure of spermatogenesis and infertility, as observed in ours and others animal studies of EDC exposures. It is therefore important to investigate the biological effect and molecular mechanisms of GEN, DEHP/MEHP and their mixtures on immune and inflammatory processes and spermatogenesis.

4.3 Can GEN and DEHP/MEHP alter macrophages and Leydig cells interactions?

A number of studies have shown that Leydig cells are direct targets of EDC mixtures (Svechnikov et al., 2010; Walker et al., 2021), and that EDCs can disrupt steroidogenesis in prepubertal Leydig cells (Akingbemi et al., 2004; Li et al., 2013; Yawer et al., 2020). In prepubertal Leydig TM3 cells, EDCs have been shown to affect the expression of gap junctional protein connexin 43 (Cx43) and intercellular signaling (Yawer et al., 2020). Consistent with this finding, a recent meta-analysis of the literature on the effects of isoflavone on Leydig cells found that GEN, administered during the perinatal period to mice at doses ranging from 50 to 1,000 mg/L or 10–600 mg/kg, depending of the studies, exerted overall adverse effects on Leydig cells, downregulating gene expression, alter protein-protein interactions, interfering with androgen biosynthesis and luteinizing hormone-dependent signaling and reducing the protein expression of adiponectin and AdipoR2, suggesting an impaired endocrine function (Hancock et al., 2009; Lozi et al., 2021). In Leydig cells, both GEN and MEHP individual exposures are reported to decrease the gene expression of steroidogenic acute regulatory protein StAR (Enangue Njembele and Tremblay, 2021; Lozi et al., 2021). DEHP and MEHP exposures both decreased cell viability and steroidogenic potential in mouse MA-10 cells (Piché et al., 2012). Microarray analysis of cultured rat fetal testis revealed that MEHP altered the gene expression of Cyp17a1, which is involved in Leydig cell steroidogenesis, while reducing testosterone production in a dose-dependent manner (Chauvigné et al., 2011). DEHP was found to have a deleterious impact on cell proliferation and testosterone production during development (Ge et al., 2007). In our own studies, *in utero* exposure to various doses of DEHP was found to reduce both fetal and adult Leydig cell testosterone production in rats, with concomitant decrease in steroidogenic enzymes in fetal testis, but not in the adult, leading to the subsequent discovery of an additional effect of fetal DEHP exposure on testis via altered aldosterone production in adrenal glands in the adult (Culty et al., 2008; Martinez-Arguelles et al., 2011). Adding 10 μM MEHP to organ cultures of fetal rat testes treated with the LH analog hCG reduced testosterone production (Boisvert et al., 2016), similarly to the *in vivo* effects of DEHPs. However, when PND3 rat testis were used instead of fetal testes, the production of basal, but not hormone-induced testosterone, was increased by 10 μM MEHP (Jones et al., 2015). In the same study, co-treatment of MEHP and GEN brought down basal testosterone to control level, indicating that GEN countered MEHP stimulatory effects on Leydig cells. Interestingly, treating mouse tumoral MA-10 Leydig cells with 10 μM GEN-MEHP mixtures increased steroid production in basal condition, but decrease it the presence of hCG, further indicating that Leydig cells may respond differently to EDCs according to their hormonal status (Jones et al., 2016). Concurrently, 10 μM GEN-MEHP mixture altered lipid profiles and decreased Insl3 mRNA, a functional marker of Leydig cells, suggesting endocrine disruption and Leydig cell dysfunction (Jones et al., 2016). Recent studies suggested that the pro-inflammatory effects of tMΦ may affect testosterone synthesis and metabolic processes in Leydig cells (Harris et al., 2016; Ye et al., 2021; Gabriela et al., 2022). These results imply that Leydig cell functions can be impacted by testicular macrophages responses to EDC mixtures under inflammatory conditions. Furthermore, a study performed on 514 mothers and their infants (Hokkaido Study Sapporo Cohort Study) reported that maternal blood levels of DEHP and MEHP were associated with hormonal changes in their infants blood, including altered testosterone/estradiol ratio, progesterone levels, and Insulin like 3 (INSL3) levels, indicative of Leydig cell functional disruption in the infants (Araki et al., 2014).

All together, these studies support the possibility that the disruption of Leydig cell-tMΦ play a role in the adverse effects of EDCs on testicular function. However, this has been poorly investigated. Understanding the impact of EDCs on the signaling pathways involved in macrophage-Leydig interactions and the mechanisms underlying these interactions should help us gain insight into the risk of such exposures on male reproductive functions.

4.4 Are there common threads between GEN and DEHP/MEHP effects on macrophages and Sertoli cells?

To our knowledge, there is no study examining the effects of DEHP/MEHP on tMΦ and Sertoli cell interactions, but there are

studies reporting effects of these EDCs on Sertoli cells. Early studies reported that DEHP induced morphologic changes in prepubertal Sertoli cells, and to inhibit cAMP accumulation and intracellular ATP levels in immature Sertoli cells by changing FSH receptor signaling in rats (Creasy et al., 1983; Heindel and Powell, 1992; Richburg and Boekelheide, 1996; Lee et al., 1997). DEHP treatment increased the mRNA expression of PPARα and PPARγ but decreased the protein levels of phosphorylated mitogen-activated protein kinase (activated MAPK) in Sertoli cells (Bhattacharya et al., 2005). In another study, exposure of pregnant mice to 2 mg/kg/day DEHP was found to disrupt the differentiation of fetal Sertoli cells and subsequent postnatal immature Sertoli cells by altering the regulation of sex determination genes (Wang et al., 2016). In addition, treating mice from conception to lactation with a diet containing 40 mg/kg GEN increased seminiferous tubule diameter and testosterone production, whereas treatment with 800 mg/kg GEN, a dose exceeding human exposure levels, reduced seminiferous tubule diameter and decreased the gene expression of the Sertoli cell marker SOX9, indicating opposite effects of GEN on Sertoli cells depending of the doses, and Sertoli cell toxic effects for the high GEN concentration (Shi et al., 2020). In our own *in utero* exposure studies using the human-relevant dose of 10 mg/kg/day GEN and DEHP, we found that Abp gene expression was reduced in juvenile rat Sertoli cell by DEHP and GEN-DEHP, while Amh and Wt1 transcripts were reduced only by GEN-DEHP mixture in adult rat offspring, indicating a predominantly inhibitory effect of GEN on Sertoli cells (Jones et al., 2014; Jones et al., 2015). Additionally, MEHP treatment had an adverse effect on prepubertal Sertoli cell development in rat testes via stimulating Sertoli cell apoptosis and oxidative damages, and this effect could be partially counteracted by GEN through antioxidative action (Zhang et al., 2017). Several animal studies confirmed that Sertoli cells showed abnormal testicular phenotypes when mice or rats were exposed to GEN and DEHP mixtures (Xie et al., 2014; Walker et al., 2020). A recent study showed that MEHP at 0.1 μmol/L induced mitochondria swelling in Sertoli cells after 4 days of exposure, while no alterations in normal ultrastructure were observed following the GEN and DEHP combination (Zhang et al., 2022). Furthermore, Sertoli cells were found to be altered by MEHP in cultured human fetal testes, where MEHP treatment decreased the expression of Amh, a characteristic marker of Sertoli cells (Lambrot et al., 2009).

Compelling human data were reported in the analyses of maternal blood samples of pregnant women and infant in the Hokkaido Study. Looking at reproductive hormones, this epidemiological study unveiled a robust correlation between DEHP exposure *in utero* and impaired Sertoli and Leydig cell functions in male offspring (Araki et al., 2014). The study reported that *in utero* DEHP exposure reduced the concentration of Inhibin B, a hormone produced by Sertoli cells, in a dose-dependent manner, indicating an adverse effects of maternal phthalate exposure on Sertoli cell function in male infants (Araki et al., 2014).

Collectively, these findings strongly suggest that GEN and DEHP/MEHP mixtures have negative effects on Sertoli cell differentiation and function, with the predictable consequence of jeopardizing spermatogenesis. However, more investigations are needed to understand whether Genistein and DEHP, including their mixtures, affect macrophages - Sertoli cell interactions, that could contribute to male infertility.

5 Discussion

Testicular macrophages (tMΦ) are critical in maintaining immunological privilege in mammalian testis and contribute to tissue homeostasis, organogenesis, and normal testicular function via interactions with several types of testicular cells. Testicular development and function have an absolute requirement for androgens and estrogens, which are produced in a tightly regulated spaciotemporal way. Thus, these processes are prime targets of EDCs that disrupt androgen and estrogen homeostasis. The phytoestrogen GEN and the anti-androgenic phthalates DEHP and its metabolite MEHP were shown to hamper the development and function of critical testicular cell types in fetal to adult offspring, following perinatal exposures. We propose that these deleterious effects might be due to GEN, DEHP/MEHP or their mixtures interfering with the interactions between tMΦ and germ cells, Sertoli cells, or Leydig cells, at fetal to juvenile ages, thereby adversely affecting the development, homeostasis, and function of these cells and ultimately leading to male infertility.

Since infants can be exposed via maternal diet or baby formula to GEN in early life, and DEHP is ubiquitous, leaching out from consumer products, medical devices, cosmetics and other man-made products, early exposure to GEN and DEHP have high chance to happen and exert adverse effects on testicular function. GEN and DEHP may alter testicular developmental programs and functions by disrupting cell interactions in the testis. Moreover, mixtures may have unique effects not predicted by toxicological studies using single compounds (see Table 2). At present, there is clear evidence of tMΦ interactions with SSCs and Leydig cells, and the importance of these interactions for testicular function. The question remains about the possibility that tMΦ may interact directly or indirectly with Sertoli cells, as they do with SSCs, by communicating across the basement membrane of seminiferous tubules. We hypothesize that EDCs could directly target tMΦ in fetal to juvenile testis, disrupting their interactions with germ cells, Leydig cells and Sertoli cells, which would lead to impaired testicular functions. Intercellular communication depends on the secretion of various growth factors and signaling molecules. The interaction between tMΦ and SCCs has been shown to rely on the CSF1/CSF1R pathway. Thus, the EDC-driven dysregulation of CSF1 production in testicular macrophages could hamper SSC pool maintenance. Taken CSF1 as example, one could determine its expression levels using *in vitro* settings (e.g. organ on a chip; cell models) to screen novel EDCs with suspected male reproductive toxicity. One may also be able to use CSF1 or CSF1R downstream molecules for diagnostics purpose. Lastly, if CSF1 reduction is confirmed as one of the culprits in the adverse effects of EDCs, it could be used as target for the development of novel therapeutic agents to treat cases of deficient spermatogenesis or infertility, by researching pharmacological ways to palliate or prevent CSF1 decrease in testis and restore or support tMΦ-SSCs interactions.

6 Conclusion

EDC can interfere with sex hormone homeostasis, disrupt the factors produced by testicular cells and their interactions with cells. Although tMΦ, SSCs, SCs, and Leydig cells have been the subject of experimental studies using *in vivo*, organ cultures or single-cell models to determine EDCs risk on male reproduction, information is lacking on whether disrupting cell-cell interactions could affect male reproductive functions and fertility. Future studies should examine the effects of EDCs such as GEN and DEHP, including mixtures at doses meaningful for human exposures and doses judged as non-toxic from single toxicant studies, on the interactions between macrophages and other testicular cell types. Moreover, studies mentioned in this review highlight the fact that determining reproductive risk based on a single EDC compound may not provide an adequate prediction of the reproductive toxicity of EDC mixtures to which humans are exposed. Comparing the impact of EDCs, individually and in mixtures, on testicular cell interactions should provide more insight into the toxicological mechanism of EDCs in male reproduction. As tMΦ are at the center of intricate cell-cell interactions (see Figure 1), encompassing multiple signaling molecules and signaling pathways, a first step could be to identify genes and signaling pathways dysregulated by EDCs in association with abnormal tMΦ functions, disrupted spermatogenesis and/or steroid production. Then, one could determine if treating tMΦ with EDCs would influence the behavior and functions of the other cell types, using *in vitro* approaches.

The ultimate goal of this strategy is to identify new targets of EDCs that could help in preventing testicular dysgenesis syndrome, by providing ways to assess risk more accurately, generate early interventions models to reduce the risk of hypospadias, infertility and testicular cancer. Ideally, this could lead to developing new diagnostic tools and/or therapies focusing on reestablishing healthy cell-cell interactions in the testis.

Author contributions

HC contribution includes the literature search, writing the first draft of the manuscript, and preparing the tables and figure. MC contribution is to participate to the design and concept of the review, literature search, and working with HC on the contents of the manuscript, table and figure, to generate the final review article. All authors contributed to the article and approved the submitted version.

Funding

This work was supported by funds from the University of Southern California Alfred E. Mann School of Pharmacy and Pharmaceutical Sciences to MC; and did not receive any grant from funding agencies.

Conflict of interest

The authors declare that the research was conducted in the absence of any commercial or financial relationships that could be construed as a potential conflict of interest.

Publisher's note

References

Adamczewska, D., Słowikowska-Hilczer, J., and Walczak-Jędrzejowska, R. (2022). The fate of Leydig cells in men with spermatogenic failure. *Life (Basel)* 12 (4), 570. doi:10.3390/life12040570

Adibi, J. J., Hauser, R., Williams, P. L., Whyatt, R. M., Calafat, A. M., Nelson, H., et al. (2009). Maternal urinary metabolites of Di-(2-Ethylhexyl) phthalate in relation to the timing of labor in a US multicenter pregnancy cohort study. *Am. J. Epidemiol.* 169 (8), 1015–1024. doi:10.1093/aje/kwp001

Agarwal, A., Mulgund, A., Hamada, A., and Chyatte, M. R. (2015). A unique view on male infertility around the globe. *Reprod. Biol. Endocrinol.* 13, 37. doi:10.1186/s12958-015-0032-1

Akingbemi, B. T., Sottas, C. M., Koulova, A. I., Klinefelter, G. R., and Hardy, M. P. (2004). Inhibition of testicular steroidogenesis by the xenoestrogen bisphenol A is associated with reduced pituitary luteinizing hormone secretion and decreased steroidogenic enzyme gene expression in rat Leydig cells. *Endocrinology* 145 (2), 592–603. doi:10.1210/en.2003-1174

Amano, H., Yamada, S., and Felix, R. (1998). Colony-stimulating factor-1 stimulates the fusion process in osteoclasts. *J. Bone Min. Res.* 13 (5), 846–853. doi:10.1359/jbmr.1998.13.5.846

Araki, A., Mitsui, T., Miyashita, C., Nakajima, T., Naito, H., Ito, S., et al. (2014). Association between maternal exposure to di(2-ethylhexyl) phthalate and reproductive hormone levels in fetal blood: the hokkaido study on environment and children's health. *PLoS One* 9 (10), e109039. doi:10.1371/journal.pone.0109039

Arima, Y., and Fukuoka, H. (2020). Developmental origins of health and disease theory in cardiology. *J. Cardiol.* 76 (1), 14–17. doi:10.1016/j.jjcc.2020.02.003

Barati, E., Nikzad, H., and Karimian, M. (2020). Oxidative stress and male infertility: current knowledge of pathophysiology and role of antioxidant therapy in disease management. *Cell Mol. Life Sci.* 77 (1), 93–113. doi:10.1007/s00018-019-03253-8

Bennasroune, A., Rojas, L., Foucaud, L., Goulaouic, S., Laval-Gilly, P., Fickova, M., et al. (2012). Effects of 4-nonylphenol and/or diisononylphthalate on THP-1 cells: impact of endocrine disruptors on human immune system parameters. *Int. J. Immunopathol. Pharmacol.* 25 (2), 365–376. doi:10.1177/039463201202500206

Bergh, A. (1985). Effect of cryptorchidism on the morphology of testicular macrophages: evidence for a Leydig cell-macrophage interaction in the rat testis. *Int. J. Androl.* 8 (1), 86–96. doi:10.1111/j.1365-2605.1985.tb00821.x

Bergh, A. (1987). Treatment with hCG increases the size of Leydig cells and testicular macrophages in unilaterally cryptorchid rats. *Int. J. Androl.* 10 (6), 765–772. doi:10.1111/j.1365-2605.1987.tb00380.x

Bhattacharya, N., Dufour, J. M., Vo, M. N., Okita, J., Okita, R., and Kim, K. H. (2005). Differential effects of phthalates on the testis and the liver. *Biol. Reproduction* 72 (3), 745–754. doi:10.1095/biolreprod.104.031583

Bode, J. G., Ehlting, C., and Häussinger, D. (2012). The macrophage response towards LPS and its control through the p38(MAPK)-STAT3 axis. *Cell Signal* 24 (6), 1185–1194. doi:10.1016/j.cellsig.2012.01.018

Boisvert, A., Jones, S., Issop, L., Erythropel, H. C., Papadopoulos, V., and Culty, M. (2016). *In vitro* functional screening as a means to identify new plasticizers devoid of reproductive toxicity. *Environ. Res.* 150, 496–512. doi:10.1016/j.envres.2016.06.033

Busada, J. T., Velte, E. K., Serra, N., Cook, K., Niedenberger, B. A., Willis, W. D., et al. (2016). Rhox13 is required for a quantitatively normal first wave of spermatogenesis in mice. *Reproduction* 152 (5), 379–388. doi:10.1530/REP-16-0268

Cailleau, J., Vermeire, S., and Verhoeven, G. (1990). Independent control of the production of insulin-like growth factor I and its binding protein by cultured testicular cells. *Mol. Cell. Endocrinol.* 69 (1), 79–89. doi:10.1016/0303-7207(90)90091-l

Calafat, A. M., Brock, J. W., Silva, M. J., Gray, L. E., Reidy, J. A., Barr, D. B., et al. (2006). Urinary and amniotic fluid levels of phthalate monoesters in rats after the oral administration of di(2-ethylhexyl) phthalate and di-n-butyl phthalate. *Toxicology* 217 (1), 22–30. doi:10.1016/j.tox.2005.08.013

Calafat, A. M., Slakman, A. R., Silva, M. J., Herbert, A. R., and Needham, L. L. (2004). Automated solid phase extraction and quantitative analysis of human milk for 13 phthalate metabolites. *J. Chromatogr. B Anal. Technol. Biomed. Life Sci.* 805 (1), 49–56. doi:10.1016/j.jchromb.2004.02.006

Cao, Y., Calafat, A. M., Doerge, D. R., Umbach, D. M., Bernbaum, J. C., Twaddle, N. C., et al. (2009). Isoflavones in urine, saliva, and blood of infants: data from a pilot study on the estrogenic activity of soy formula. *J. Expo. Sci. Environ. Epidemiol.* 19 (2), 223–234. doi:10.1038/jes.2008.44

Cederroth, C. R., Auger, J., Zimmermann, C., Eustache, F., and Nef, S. (2010). Soy, phyto-oestrogens and male reproductive function: A review. *Int. J. Androl.* 33 (2), 304–316. doi:10.1111/j.1365-2605.2009.01011.x

Chauvigné, F., Plummer, S., Lesné, L., Cravedi, J. P., Dejucq-Rainsford, N., Fostier, A., et al. (2011). Mono-(2-ethylhexyl) phthalate directly alters the expression of Leydig cell genes and CYP17 lyase activity in cultured rat fetal testis. *PLoS One* 6 (11), e27172. doi:10.1371/journal.pone.0027172

Chen, S. R., Tang, J. X., Cheng, J. M., Li, J., Jin, C., Li, X. Y., et al. (2015). Loss of Gata4 in Sertoli cells impairs the spermatogonial stem cell niche and causes germ cell exhaustion by attenuating chemokine signaling. *Oncotarget* 6 (35), 37012–37027. doi:10.18632/oncotarget.6115

Chinetti, G., Fruchart, J. C., and Staels, B. (2003). Peroxisome proliferator-activated receptors and inflammation: from basic science to clinical applications. *Int. J. Obes. Relat. Metab. Disord.* 27 (3), S41–S45. doi:10.1038/sj.ijo.0802499

Christensen, A. K. (1969). The correlation of fine structure and function in the steroid-secreting cells with emphasis on those of the gonads. *gonads*, 415–488.

Cohen, P. E., Chisholm, O., Arceci, R. J., Stanley, E. R., and Pollard, J. W. (1996). Absence of colony-stimulating factor-1 in osteopetrotic (csfmop/csfmop) mice results in male fertility defects. *Biol. Reproduction* 55 (2), 310–317. doi:10.1095/biolreprod55.2.310

Cohen, P. E., Hardy, M. P., and Pollard, J. W. (1997). Colony-stimulating factor-1 plays a major role in the development of reproductive function in male mice. *Mol. Endocrinol.* 11 (11), 1636–1650. doi:10.1210/mend.11.11.0009

Creasy, D. M., Foster, J. R., and Foster, P. M. (1983). The morphological development of di-N-pentyl phthalate induced testicular atrophy in the rat. *J. Pathol.* 139 (3), 309–321. doi:10.1002/path.1711390307

Culty, M. (2013). Gonocytes, from the fifties to the present: is there a reason to change the name? *Biol. Reprod.* 89 (2), 46. doi:10.1095/biolreprod.113.110544

Culty, M., Thuillier, R., Li, W., Wang, Y., Martinez-Arguelles, D. B., Benjamin, C. G., et al. (2008). *In utero* exposure to di-(2-ethylhexyl) phthalate exerts both short-term and long-lasting suppressive effects on testosterone production in the rat. *Biol. Reprod.* 78 (6), 1018–1028. doi:10.1095/biolreprod.107.065649

David, S., and Orwig, K. E. (2020). Spermatogonial stem cell culture in oncofertility. *Urol. Clin. North Am.* 47 (2), 227–244. doi:10.1016/j.ucl.2020.01.001

de Boo, H. A., and Harding, J. E. (2006). The developmental origins of adult disease (Barker) hypothesis. *Aust. N. Z. J. Obstet. Gynaecol.* 46 (1), 4–14. doi:10.1111/j.1479-828X.2006.00506.x

DeFalco, T., Bhattacharya, I., Williams, A. V., Sams, D. M., and Capel, B. (2014). Yolk-sac-derived macrophages regulate fetal testis vascularization and morphogenesis. *Proc. Natl. Acad. Sci. U. S. A.* 111 (23), E2384–E2393. doi:10.1073/pnas.1400057111

DeFalco, T., Potter, S. J., Williams, A. V., Waller, B., Kan, M. J., and Capel, B. (2015). Macrophages contribute to the spermatogonial niche in the adult testis. *Cell Rep.* 12 (7), 1107–1119. doi:10.1016/j.celrep.2015.07.015

Diamanti-Kandarakis, E., Bourguignon, J. P., Giudice, L. C., Hauser, R., Prins, G. S., Soto, A. M., et al. (2009). Endocrine-disrupting chemicals: an endocrine society scientific statement. *Endocr. Rev.* 30 (4), 293–342. doi:10.1210/er.2009-0002

DiVall, S. A. (2013). The influence of endocrine disruptors on growth and development of children. *Curr. Opin. Endocrinol. Diabetes Obes.* 20 (1), 50–55. doi:10.1097/MED.0b013e32835b7ee6

Enangue Njembele, A. N., and Tremblay, J. J. (2021). Mechanisms of MEHP inhibitory action and analysis of potential replacement plasticizers on Leydig cell steroidogenesis. *Int. J. Mol. Sci.* 22 (21), 11456. doi:10.3390/ijms222111456

Forbes, C. M., Flannigan, R., and Schlegel, P. N. (2018). Spermatogonial stem cell transplantation and male infertility: current status and future directions. *Arab. J. Urol.* 16 (1), 171–180. doi:10.1016/j.aju.2017.11.015

Gabriela, C. S., Leticia, N. T., Margarita, C. R., Nicté, X. A., María de Lourdes, A. C., Elena, Z., et al. (2022). Maternal and offspring sugar consumption increases perigonadal adipose tissue hypertrophy and negatively affects the testis histological organization in adult rats. *Front. Cell Dev. Biol.* 10, 893099. doi:10.3389/fcell.2022.893099

Gaytan, F., Bellido, C., Aguilar, E., and van Rooijen, N. (1994a). Requirement for testicular macrophages in Leydig cell proliferation and differentiation during prepubertal development in rats. *J. Reprod. Fertil.* 102 (2), 393–399. doi:10.1530/jrf.0.1020393

Gaytan, F., Bellido, C., Morales, C., Reymundo, C., Aguilar, E., and van Rooijen, N. (1994b). Selective depletion of testicular macrophages and prevention of Leydig cell repopulation after treatment with ethylene dimethane sulfonate in rats. *J. Reprod. Fertil.* 101 (1), 175–182. doi:10.1530/jrf.0.1010175

Ge, R. S., Chen, G. R., Tanrikut, C., and Hardy, M. P. (2007). Phthalate ester toxicity in Leydig cells: developmental timing and dosage considerations. *Reprod. Toxicol.* 23 (3), 366–373. doi:10.1016/j.reprotox.2006.12.006

Ghazarian, A. A., Kelly, S. P., Altekruse, S. F., Rosenberg, P. S., and McGlynn, K. A. (2017). Future of testicular germ cell tumor incidence in the United States: forecast through 2026. *Cancer* 123 (12), 2320–2328. doi:10.1002/cncr.30597

Goluža, T., Boscanin, A., Cvetko, J., Kozina, V., Kosović, M., Bernat, M. M., et al. (2014). Macrophages and Leydig cells in testicular biopsies of azoospermic men. *Biomed. Res. Int.* 2014, 828697. doi:10.1155/2014/828697

Gomez Perdiguero, E., Klapproth, K., Schulz, C., Busch, K., Azzoni, E., Crozet, L., et al. (2015). Tissue-resident macrophages originate from yolk-sac-derived erythro-myeloid progenitors. *Nature* 518 (7540), 547–551. doi:10.1038/nature13989

Gordon, S. (2003). Alternative activation of macrophages. *Nat. Rev. Immunol.* 3 (1), 23–35. doi:10.1038/nri978

Gore, A. C., Chappell, V. A., Fenton, S. E., Flaws, J. A., Nadal, A., Prins, G. S., et al. (2015). Executive summary to EDC-2: the endocrine society's second scientific statement on endocrine-disrupting chemicals. *Endocr. Rev.* 36 (6), 593–602. doi:10.1210/er.2015-1093

Gu, X., Heinrich, A., Li, S. Y., and DeFalco, T. (2023). Testicular macrophages are recruited during a narrow fetal time window and promote organ-specific developmental functions. *Nat. Commun.* 14 (1), 1439. doi:10.1038/s41467-023-37199-0

Guo, J., Grow, E. J., Mlcochova, H., Maher, G. J., Lindskog, C., Nie, X., et al. (2018). The adult human testis transcriptional cell atlas. *Cell Res.* 28 (12), 1141–1157. doi:10.1038/s41422-018-0099-2

Hales, D. B. (2002). Testicular macrophage modulation of Leydig cell steroidogenesis. *J. Reprod. Immunol.* 57 (1-2), 3–18. doi:10.1016/s0165-0378(02)00020-7

Hancock, K. D., Coleman, E. S., Tao, Y. X., Morrison, E. E., Braden, T. D., Kemppainen, B. W., et al. (2009). Genistein decreases androgen biosynthesis in rat Leydig cells by interference with luteinizing hormone-dependent signaling. *Toxicol. Lett.* 184 (3), 169–175. doi:10.1016/j.toxlet.2008.11.005

Hanna, R. N., Carlin, L. M., Hubbeling, H. G., Nackiewicz, D., Green, A. M., Punt, J. A., et al. (2011). The transcription factor NR4A1 (Nur77) controls bone marrow differentiation and the survival of Ly6C- monocytes. *Nat. Immunol.* 12 (8), 778–785. doi:10.1038/ni.2063

Hansen, J. F., Bendtzen, K., Boas, M., Frederiksen, H., Nielsen, C. H., Rasmussen, Å. K., et al. (2015). Influence of phthalates on cytokine production in monocytes and macrophages: A systematic review of experimental trials. *PLoS One* 10 (3), e0120083. doi:10.1371/journal.pone.0120083

Harris, S., Shubin, S. P., Wegner, S., Van Ness, K., Green, F., Hong, S. W., et al. (2016). The presence of macrophages and inflammatory responses in an *in vitro* testicular co-culture model of male reproductive development enhance relevance to *in vivo* conditions. *Toxicol Vitro* 36, 210–215. doi:10.1016/j.tiv.2016.08.003

Hashimoto, D., Chow, A., Noizat, C., Teo, P., Beasley, M. B., Leboeuf, M., et al. (2013). Tissue-resident macrophages self-maintain locally throughout adult life with minimal contribution from circulating monocytes. *Immunity* 38 (4), 792–804. doi:10.1016/j.immuni.2013.04.004

Hedger, M. P. (2002). Macrophages and the immune responsiveness of the testis. *J. Reprod. Immunol.* 57 (1-2), 19–34. doi:10.1016/s0165-0378(02)00016-5

Heindel, J. J., and Powell, C. J. (1992). Phthalate ester effects on rat Sertoli cell function *in vitro*: effects of phthalate side chain and age of animal. *Toxicol. Appl. Pharmacol.* 115 (1), 116–123. doi:10.1016/0041-008x(92)90374-2

Heming, M., Gran, S., Jauch, S. L., Fischer-Riepe, L., Russo, A., Klotz, L., et al. (2018). Peroxisome proliferator-activated receptor-γ modulates the response of macrophages to lipopolysaccharide and glucocorticoids. *Front. Immunol.* 9, 893. doi:10.3389/fimmu.2018.00893

Honold, L., and Nahrendorf, M. (2018). Resident and monocyte-derived macrophages in cardiovascular disease. *Circ. Res.* 122 (1), 113–127. doi:10.1161/CIRCRESAHA.117.311071

Hosseini, S., Moody, S. C., Fietz, D., Indumathy, S., Schuppe, H. C., Hedger, M. P., et al. (2022). The changing landscape of immune cells in the fetal mouse testis. *Histochem Cell Biol.* 158 (4), 345–368. doi:10.1007/s00418-022-02129-6

Hume, D. A. (2008). Differentiation and heterogeneity in the mononuclear phagocyte system. *Mucosal Immunol.* 1 (6), 432–441. doi:10.1038/mi.2008.36

Hutson, J. C. (1992). Development of cytoplasmic digitations between Leydig cells and testicular macrophages of the rat. *Cell Tissue Res.* 267 (2), 385–389. doi:10.1007/BF00302977

Hutson, J. C. (1998). Interactions between testicular macrophages and Leydig cells. *J. Androl.* 19 (4), 394–398.

Hutson, J. C. (2006). Physiologic interactions between macrophages and Leydig cells. *Exp. Biol. Med. (Maywood)* 231 (1), 1–7. doi:10.1177/153537020623100101

Hutson, J. C. (1994). "Testicular macrophages," in *International review of cytology*. Editors K. W. Jeon and J. Jarvik (Cambridge, MA, United States: Academic Press), 99–143.

Italiani, P., and Boraschi, D. (2017). Development and functional differentiation of tissue-resident versus monocyte-derived macrophages in inflammatory reactions. *Results Probl. Cell Differ.* 62, 23–43. doi:10.1007/978-3-319-54090-0_2

Italiani, P., and Boraschi, D. (2014). From monocytes to M1/M2 macrophages: phenotypical vs. functional differentiation. *Front. Immunol.* 5, 514. doi:10.3389/fimmu.2014.00514

Jefferson, W. N., and Williams, C. J. (2011). Circulating levels of genistein in the neonate, apart from dose and route, predict future adverse female reproductive outcomes. *Reprod. Toxicol.* 31 (3), 272–279. doi:10.1016/j.reprotox.2010.10.001

Jezek, D., Knuth, U. A., and Schulze, W. (1998). Successful testicular sperm extraction (TESE) in spite of high serum follicle stimulating hormone and azoospermia: correlation between testicular morphology, tese results, semen analysis and serum hormone values in 103 infertile men. *Hum. Reprod.* 13 (5), 1230–1234. doi:10.1093/humrep/13.5.1230

Joensen, U. N., Jørgensen, N., Rajpert-De Meyts, E., and Skakkebaek, N. E. (2008). Testicular dysgenesis syndrome and Leydig cell function. *Basic Clin. Pharmacol. Toxicol.* 102 (2), 155–161. doi:10.1111/j.1742-7843.2007.00197.x

Jones, S., Boisvert, A., Duong, T. B., Francois, S., Thrane, P., and Culty, M. (2014). Disruption of rat testis development following combined *in utero* exposure to the phytoestrogen genistein and antiandrogenic plasticizer di-(2-ethylhexyl) phthalate. *Biol. Reprod.* 91 (3), 64. doi:10.1095/biolreprod.114.120907

Jones, S., Boisvert, A., Francois, S., Zhang, L., and Culty, M. (2015). *In utero* exposure to di-(2-ethylhexyl) phthalate induces testicular effects in neonatal rats that are antagonized by genistein cotreatment. *Biol. Reprod.* 93 (4), 92. doi:10.1095/biolreprod.115.129098

Jones, S., Boisvert, A., Naghi, A., Hullin-Matsuda, F., Greimel, P., Kobayashi, T., et al. (2016). Stimulatory effects of combined endocrine disruptors on MA-10 Leydig cell steroid production and lipid homeostasis. *Toxicology* 355-356, 21–30. doi:10.1016/j.tox.2016.05.008

Kalfa, N., Paris, F., Philibert, P., Orsini, M., Broussous, S., Fauconnet-Servant, N., et al. (2015). Is hypospadias associated with prenatal exposure to endocrine disruptors? A French collaborative controlled study of a cohort of 300 consecutive children without genetic defect. *Eur. Urol.* 68 (6), 1023–1030. doi:10.1016/j.eururo.2015.05.008

Khan, S., Teerds, K., and Dorrington, J. (1992). Growth factor requirements for DNA synthesis by Leydig cells from the immature rat. *Biol. Reproduction* 46 (3), 335–341. doi:10.1095/biolreprod46.3.335

Kilcoyne, K. R., and Mitchell, R. T. (2019a). Effect of environmental and pharmaceutical exposures on fetal testis development and function: A systematic review of human experimental data. *Hum. Reprod. Update* 25 (4), 397–421. doi:10.1093/humupd/dmz004

Kilcoyne, K. R., and Mitchell, R. T. (2019b). Effect of environmental and pharmaceutical exposures on fetal testis development and function: A systematic review of human experimental data. *Hum. Reprod. update* 25 (4), 397–421. doi:10.1093/humupd/dmz004

Kokkinaki, M., Lee, T. L., He, Z., Jiang, J., Golestaneh, N., Hofmann, M. C., et al. (2009). The molecular signature of spermatogonial stem/progenitor cells in the 6-day-old mouse testis. *Biol. Reprod.* 80 (4), 707–717. doi:10.1095/biolreprod.108.073809

Kristensen, D. M., Sonne, S. B., Ottesen, A. M., Perrett, R. M., Nielsen, J. E., Almstrup, K., et al. (2008). Origin of pluripotent germ cell tumours: the role of microenvironment during embryonic development. *Mol. Cell Endocrinol.* 288 (1-2), 111–118. doi:10.1016/j.mce.2008.02.018

Lambrot, R., Muczynski, V., Lécureuil, C., Angenard, G., Coffigny, H., Pairault, C., et al. (2009). Phthalates impair germ cell development in the human fetal testis *in vitro* without change in testosterone production. *Environ. Health Perspect.* 117 (1), 32–37. doi:10.1289/ehp.11146

Lee, J., Richburg, J. H., Younkin, S. C., and Boekelheide, K. (1997). The Fas system is a key regulator of germ cell apoptosis in the testis. *Endocrinology* 138 (5), 2081–2088. doi:10.1210/endo.138.5.5110

Lee, M., Park, C. S., Lee, Y. R., Im, S. A., Song, S., and Lee, C. K. (2014). Resiquimod, a TLR7/8 agonist, promotes differentiation of myeloid-derived suppressor cells into macrophages and dendritic cells. *Arch. Pharm. Res.* 37 (9), 1234–1240. doi:10.1007/s12272-014-0379-4

Lehraiki, A., Chamaillard, C., Krust, A., Habert, R., and Levacher, C. (2011). Genistein impairs early testosterone production in fetal mouse testis via estrogen receptor alpha. *Toxicol Vitro* 25 (8), 1542–1547. doi:10.1016/j.tiv.2011.05.017

Levine, H., Jørgensen, N., Martino-Andrade, A., Mendiola, J., Weksler-Derri, D., Mindlis, I., et al. (2022). Temporal trends in sperm count: A systematic review and meta-regression analysis. *Hum. Reprod. Update* 23, 646–659. doi:10.1093/humupd/dmx022

Li, D., Sekhon, P., Barr, K. J., Márquez-Rosado, L., Lampe, P. D., and Kidder, G. M. (2013). Connexins and steroidogenesis in mouse Leydig cells. *Can. J. Physiol. Pharmacol.* 91 (2), 157–164. doi:10.1139/cjpp-2012-0385

Li, L. H., Jester, W. F., Jr., and Orth, J. M. (1998). Effects of relatively low levels of mono-(2-ethylhexyl) phthalate on cocultured Sertoli cells and gonocytes from neonatal rats. *Toxicol. Appl. Pharmacol.* 153 (2), 258–265. doi:10.1006/taap.1998.8550

Liao, X., Shen, Y., Zhang, R., Sugi, K., Vasudevan, N. T., Alaiti, M. A., et al. (2018). Distinct roles of resident and nonresident macrophages in nonischemic cardiomyopathy. *Proc. Natl. Acad. Sci. U. S. A.* 115 (20), E4661-E4669–e4669. doi:10.1073/pnas.1720065115

Lin, S., Ku, H. Y., Chen, J. W., Huang, P. C., and Angerer, J., (2011). Phthalate exposure in pregnant women and their children in central Taiwan. *Chemosphere* 82 (7), 947–955. doi:10.1016/j.chemosphere.2010.10.073

Lozi, A. A., Pinto da Matta, S. L., Sarandy, M. M., Silveira Alves de Melo, F. C., Araujo, D. C., Novaes, R. D., et al. (2021). Relevance of the isoflavone absorption and testicular function: A systematic review of preclinical evidence. *Evid. Based Complement. Altern. Med.* 2021, 8853172. doi:10.1155/2021/8853172

Luca, G., Arato, I., Sorci, G., Cameron, D. F., Hansen, B. C., Baroni, T., et al. (2018). Sertoli cells for cell transplantation: pre-clinical studies and future perspectives. *Andrology* 6 (3), 385–395. doi:10.1111/andr.12484

Lukyanenko, Y. O., Chen, J.-J., and Hutson, J. C. (2001). Production of 25-hydroxycholesterol by testicular macrophages and its effects on Leydig cells. *Biol. Reproduction* 64 (3), 790–796. doi:10.1095/biolreprod64.3.790

Martinez, F. O., Helming, L., and Gordon, S. (2009). Alternative activation of macrophages: an immunologic functional perspective. *Annu. Rev. Immunol.* 27, 451–483. doi:10.1146/annurev.immunol.021908.132532

Martinez-Arguelles, D. B., Campioli, E., Culty, M., Zirkin, B. R., and Papadopoulos, V. (2013). Fetal origin of endocrine dysfunction in the adult: the phthalate model. *J. Steroid Biochem. Mol. Biol.* 137, 5–17. doi:10.1016/j.jsbmb.2013.01.007

Martinez-Arguelles, D. B., Guichard, T., Culty, M., Zirkin, B. R., and Papadopoulos, V. (2011). *In utero* exposure to the antiandrogen di-(2-ethylhexyl) phthalate decreases adrenal aldosterone production in the adult rat. *Biol. Reprod.* 85 (1), 51–61. doi:10.1095/biolreprod.110.089920

Mass, E., Nimmerjahn, F., Kierdorf, K., and Schlitzer, A. (2023). Tissue-specific macrophages: how they develop and choreograph tissue biology. *Nat. Rev. Immunol.*, 1–17. doi:10.1038/s41577-023-00848-y

Meena, R., Supriya, C., Pratap Reddy, K., and Sreenivasula Reddy, P. (2017). Altered spermatogenesis, steroidogenesis and suppressed fertility in adult male rats exposed to genistein, a non-steroidal phytoestrogen during embryonic development. *Food Chem. Toxicol.* 99, 70–77. doi:10.1016/j.fct.2016.11.020

Mei, X. X., Wang, J., and Wu, J. (2015). Extrinsic and intrinsic factors controlling spermatogonial stem cell self-renewal and differentiation. *Asian J. Androl.* 17 (3), 347–354. doi:10.4103/1008-682X.148080

Merzenich, H., Zeeb, H., and Blettner, M. (2010). Decreasing sperm quality: A global problem? *BMC Public Health* 10, 24. doi:10.1186/1471-2458-10-24

Miller, S. C., Bowman, B. M., and Rowland, H. G. (1983). Structure, cytochemistry, endocytic activity, and immunoglobulin (Fc) receptors of rat testicular interstitial-tissue macrophages. *Am. J. Anat.* 168 (1), 1–13. doi:10.1002/aja.1001680102

Misharin, A. V., Cuda, C. M., Saber, R., Turner, J. D., Gierut, A. K., Haines, G. K., et al. (2014). Nonclassical Ly6C(-) monocytes drive the development of inflammatory arthritis in mice. *Cell Rep.* 9 (2), 591–604. doi:10.1016/j.celrep.2014.09.032

Mossadegh-Keller, N., Gentek, R., Gimenez, G., Bigot, S., Mailfert, S., and Sieweke, M. H. (2017). Developmental origin and maintenance of distinct testicular macrophage populations. *J. Exp. Med.* 214 (10), 2829–2841. doi:10.1084/jem.20170829

Mossadegh-Keller, N., and Sieweke, M. H. (2018). Testicular macrophages: guardians of fertility. *Cell Immunol.* 330, 120–125. doi:10.1016/j.cellimm.2018.03.009

Mosser, D. M., and Edwards, J. P. (2008). Exploring the full spectrum of macrophage activation. *Nat. Rev. Immunol.* 8 (12), 958–969. doi:10.1038/nri2448

Mueller, M., Hobiger, S., and Jungbauer, A. (2010). Red clover extract: A source for substances that activate peroxisome proliferator-activated receptor alpha and ameliorate the cytokine secretion profile of lipopolysaccharide-stimulated macrophages. *Menopause* 17 (2), 379–387. doi:10.1097/gme.0b013e3181c94617

Nederlof, R., Reidel, S., Spychala, A., Gödecke, S., Heinen, A., Lautwein, T., et al. (2022). Insulin-like growth factor 1 attenuates the pro-inflammatory phenotype of neutrophils in myocardial infarction. *Front. Immunol.* 13, 908023. doi:10.3389/fimmu.2022.908023

Nes, W. D., Lukyanenko, Y. O., Jia, Z. H., Quideau, S., Howald, W. N., Pratum, T. K., et al. (2000). Identification of the lipophilic factor produced by macrophages that stimulates steroidogenesis. *Endocrinology* 141 (3), 953–958. doi:10.1210/endo.141.3.7350

Ni, F. D., Hao, S. L., and Yang, W. X. (2019). Multiple signaling pathways in Sertoli cells: recent findings in spermatogenesis. *Cell Death Dis.* 10 (8), 541. doi:10.1038/s41419-019-1782-z

O'Donnell, L., Stanton, P., and de Kretser, D. M., (2000). "Endocrinology of the male reproductive system and spermatogenesis,". Editor K. R. Feingold Endotext (South Dartmouth, MA, USA: MDText.com, Inc.).

Phillips, B. T., Gassei, K., and Orwig, K. E. (2010). Spermatogonial stem cell regulation and spermatogenesis. *Philos. Trans. R. Soc. Lond B Biol. Sci.* 365 (1546), 1663–1678. doi:10.1098/rstb.2010.0026

Piché, C. D., Sauvageau, D., Vanlian, M., Erythropel, H. C., Robaire, B., and Leask, R. L. (2012). Effects of di-(2-ethylhexyl) phthalate and four of its metabolites on steroidogenesis in MA-10 cells. *Ecotoxicol. Environ. Saf.* 79, 108–115. doi:10.1016/j.ecoenv.2011.12.008

Potter, S. J., and DeFalco, T. (2017). Role of the testis interstitial compartment in spermatogonial stem cell function. *Reproduction* 153 (4), R151-R162–r162. doi:10.1530/REP-16-0588

Qian, B. Z., Li, J., Zhang, H., Kitamura, T., Zhang, J., Campion, L. R., et al. (2011). CCL2 recruits inflammatory monocytes to facilitate breast-tumour metastasis. *Nature* 475 (7355), 222–225. doi:10.1038/nature10138

Regadera, J., Codesal, J., Paniagua, R., Gonzalez-Peramato, P., and Nistal, M. (1991). Immunohistochemical and quantitative study of interstitial and intratubular Leydig cells in normal men, cryptorchidism, and Klinefelter's syndrome. *J. Pathol.* 164 (4), 299–306. doi:10.1002/path.1711640405

Riccioli, A., Starace, D., Galli, R., Fuso, A., Scarpa, S., Palombi, F., et al. (2006). Sertoli cells initiate testicular innate immune responses through TLR activation. *J. Immunol.* 177 (10), 7122–7130. doi:10.4049/jimmunol.177.10.7122

Richburg, J. H., and Boekelheide, K. (1996). Mono-(2-ethylhexyl) phthalate rapidly alters both Sertoli cell vimentin filaments and germ cell apoptosis in young rat testes. *Toxicol. Appl. Pharmacol.* 137 (1), 42–50. doi:10.1006/taap.1996.0055

Rival, C., Theas, M. S., Suescun, M. O., Jacobo, P., Guazzone, V., van Rooijen, N., et al. (2008). Functional and phenotypic characteristics of testicular macrophages in experimental autoimmune orchitis. *J. Pathol.* 215 (2), 108–117. doi:10.1002/path.2328

Sadigh, S., Farahani, S. J., Shah, A., Vaughn, D., and Lal, P. (2020). Differences in PD-L1-expressing macrophages and immune microenvironment in testicular germ cell tumors. *Am. J. Clin. Pathol.* 153 (3), 387–395. doi:10.1093/ajcp/aqz184

Seljelid, R., and Eskeland, T. (1993). The biology of macrophages: I. General principles and properties. *Eur. J. Haematol.* 51 (5), 267–275. doi:10.1111/j.1600-0609.1993.tb01607.x

Serbina, N. V., and Pamer, E. G. (2006). Monocyte emigration from bone marrow during bacterial infection requires signals mediated by chemokine receptor CCR2. *Nat. Immunol.* 7 (3), 311–317. doi:10.1038/ni1309

Setchell, K. D., Zimmer-Nechemias, L., Cai, J., and Heubi, J. E. (1997). Exposure of infants to phyto-oestrogens from soy-based infant formula. *Lancet* 350 (9070), 23–27. doi:10.1016/S0140-6736(96)09480-9

Shi, X., Zhao, H., Kang, Y., Dong, X., Yu, C., Xie, Q., et al. (2022). The role of mononuclear phagocytes in the testes and epididymis. *Int. J. Mol. Sci.* 24 (1), 53. doi:10.3390/ijms24010053

Shi, Z., Lv, Z., Hu, C., Zhang, Q., Wang, Z., Hamdard, E., et al. (2020). Oral exposure to genistein during conception and lactation period affects the testicular development of male offspring mice. *Anim. (Basel)* 10 (3), 377. doi:10.3390/ani10030377

Shiratsuchi, A., Osada, Y., and Nakanishi, Y. (2013). Differences in the mode of phagocytosis of bacteria between macrophages and testicular Sertoli cells. *Drug Discov. Ther.* 7 (2), 73–77. doi:10.5582/ddt.2013.v7.2.73

Sica, A., and Mantovani, A. (2012). Macrophage plasticity and polarization: *in vivo* veritas. *J. Clin. Invest.* 122 (3), 787–795. doi:10.1172/JCI59643

Sieweke, M. H., and Allen, J. E. (2013). Beyond stem cells: self-renewal of differentiated macrophages. *Science* 342 (6161), 1242974. doi:10.1126/science.1242974

Singh, V., Tripathy, M., and Rai, U. (2021). Testicular 25-hydroxycholesterol: an alternate substrate for steroidogenesis in reptiles. *Gen. Comp. Endocrinol.* 314, 113906. doi:10.1016/j.ygcen.2021.113906

Skakkebaek, N. E., Rajpert-De Meyts, E., Buck Louis, G. M., Toppari, J., Andersson, A. M., Eisenberg, M. L., et al. (2016). Male reproductive disorders and fertility trends: influences of environment and genetic susceptibility. *Physiol. Rev.* 96 (1), 55–97. doi:10.1152/physrev.00017.2015

Skakkebaek, N. E. (2003). Testicular dysgenesis syndrome. *Horm. Res.* 60 (3), 49. doi:10.1159/000074499

Skinner, M. K., Norton, J. N., Mullaney, B. P., Rosselli, M., Whaley, P. D., and Anthony, C. T. (1991). Cell-cell interactions and the regulation of testis function. *Ann. N. Y. Acad. Sci.* 637, 354–363. doi:10.1111/j.1749-6632.1991.tb27322.x

Song, W., Mazzieri, R., Yang, T., and Gobe, G. C. (2017). Translational significance for tumor metastasis of tumor-associated macrophages and epithelial-mesenchymal transition. *Front. Immunol.* 8, 1106. doi:10.3389/fimmu.2017.01106

Stanley, E. R., and Chitu, V. (2014). CSF-1 receptor signaling in myeloid cells. *Cold Spring Harb. Perspect. Biol.* 6 (6), a021857. doi:10.1101/cshperspect.a021857

Sun, Y., Huang, H., Wang, C., Shi, X. L., and Hu, H. Y., (2013). Ecological risk of estrogenic endocrine disrupting chemicals in sewage plant effluent and reclaimed water. *Environ. Pollut.* 180, 339–344. doi:10.1016/j.envpol.2013.05.006

Svechnikov, K., Izzo, G., Landreh, L., Weisser, J., and Söder, O. (2010). Endocrine disruptors and Leydig cell function. *J. Biomed. Biotechnol.* 2010, 684504. doi:10.1155/2010/684504

Swan, S. H., Main, K. M., Liu, F., Stewart, S. L., Kruse, R. L., Calafat, A. M., et al. (2005). Decrease in anogenital distance among male infants with prenatal phthalate exposure. *Environ. Health Perspect.* 113 (8), 1056–1061. doi:10.1289/ehp.8100

Tash, J. A., McCallum, S., Hardy, M. P., Knudsen, B., and Schlegel, P. N. (2002). Men with nonobstructive azoospermia have Leydig cell hypertrophy but not hyperplasia. *J. Urol.* 168 (3), 1068–1070. doi:10.1097/01.ju.0000026414.68954.d1

Thuillier, R., Manku, G., Wang, Y., and Culty, M. (2009). Changes in MAPK pathway in neonatal and adult testis following fetal estrogen exposure and effects on rat testicular cells. *Microsc. Res. Tech.* 72 (11), 773–786. doi:10.1002/jemt.20756

Thuillier, R., Wang, Y., and Culty, M. (2003). Prenatal exposure to estrogenic compounds alters the expression pattern of platelet-derived growth factor receptors alpha and beta in neonatal rat testis: identification of gonocytes as targets of estrogen exposure. *Biol. Reproduction* 68 (3), 867–880. doi:10.1095/biolreprod.102.009605

Toppari, J., Virtanen, H. E., Main, K. M., and Skakkebaek, N. E. (2010). Cryptorchidism and hypospadias as a sign of testicular dysgenesis syndrome (TDS): environmental connection. *Birth Defects Res. A Clin. Mol. Teratol.* 88 (10), 910–919. doi:10.1002/bdra.20707

Vlajković, S., Cukuranović, R., Bjelaković, M. D., and Stefanović, V. (2012). Possible therapeutic use of spermatogonial stem cells in the treatment of male infertility: A brief overview. *ScientificWorldJournal* 2012, 374151. doi:10.1100/2012/374151

Walker, C., Garza, S., Papadopoulos, V., and Culty, M. (2021). Impact of endocrine-disrupting chemicals on steroidogenesis and consequences on testicular function. *Mol. Cell Endocrinol.* 527, 111215. doi:10.1016/j.mce.2021.111215

Walker, C., Ghazisaeidi, S., Collet, B., Boisvert, A., and Culty, M. (2020). *In utero* exposure to low doses of genistein and di-(2-ethylhexyl) phthalate (DEHP) alters innate immune cells in neonatal and adult rat testes. *Andrology* 8 (4), 943–964. doi:10.1111/andr.12840

Wang, Y., Thuillier, R., and Culty, M. (2004). Prenatal estrogen exposure differentially affects estrogen receptor-associated proteins in rat testis gonocytes. *Biol. Reproduction* 71 (5), 1652–1664. doi:10.1095/biolreprod.104.030205

Wang, Y., Yang, Q., Liu, W., Yu, M., Zhang, Z., and Cui, X. (2016). Di(2-Ethylhexyl) phthalate exposure in utero damages Sertoli cell differentiation via disturbance of sex determination pathway in fetal and postnatal mice. *Toxicol. Sci.* 152 (1), 53–61. doi:10.1093/toxsci/kfw063

Wen, H. J., Sie, L., Chuang, C. J., Chen, H. Y., and Sun, C. W., (2017). Prenatal and childhood exposure to phthalate diesters and sex steroid hormones in 2-5-8-and 11-year-old children: A pilot study of the taiwan maternal and infant cohort study. *J. Epidemiol.* 27 (11), 516–523. doi:10.1016/j.je.2016.10.009

Westernstroer, B., Langenstroth, D., Kliesch, S., Troppmann, B., Redmann, K., Macdonald, J., et al. (2015). Developmental expression patterns of chemokines CXCL11, CXCL12 and their receptor CXCR7 in testes of common marmoset and human. *Cell Tissue Res.* 361 (3), 885–898. doi:10.1007/s00441-015-2164-1

Williams, J. W., Giannarelli, C., Rahman, A., Randolph, G. J., and Kovacic, J. C. (2018). Macrophage biology, classification, and phenotype in cardiovascular disease: JACC macrophage in CVD series (Part 1). *J. Am. Coll. Cardiol.* 72 (18), 2166–2180. doi:10.1016/j.jacc.2018.08.2148

Winnall, W. R., and Hedger, M. P. (2013). Phenotypic and functional heterogeneity of the testicular macrophage population: A new regulatory model. *J. Reprod. Immunol.* 97 (2), 147–158. doi:10.1016/j.jri.2013.01.001

Winnall, W. R., Muir, J. A., and Hedger, M. P. (2011). Rat resident testicular macrophages have an alternatively activated phenotype and constitutively produce interleukin-10 *in vitro*. *J. Leukoc. Biol.* 90 (1), 133–143. doi:10.1189/jlb.1010557

Xie, B. G., Li, J., and Zhu, W. J. (2014). Pathological changes of testicular tissue in normal adult mice: A retrospective analysis. *Exp. Ther. Med.* 7 (3), 654–656. doi:10.3892/etm.2014.1481

Yamauchi, S., Yamamoto, K., and Ogawa, K. (2022). Testicular macrophages produce progesterone de novo promoted by cAMP and inhibited by M1 polarization inducers. *Biomedicines* 10 (2), 487. doi:10.3390/biomedicines10020487

Yawer, A., Sychrová, E., Labohá, P., Raška, J., Jambor, T., Babica, P., et al. (2020). Endocrine-disrupting chemicals rapidly affect intercellular signaling in Leydig cells. *Toxicol. Appl. Pharmacol.* 404, 115177. doi:10.1016/j.taap.2020.115177

Ye, L., Huang, W., Liu, S., Cai, S., Hong, L., Xiao, W., et al. (2021). Impacts of immunometabolism on male reproduction. *Front. Immunol.* 12, 658432. doi:10.3389/fimmu.2021.658432

Zhang, L., Gao, M., Zhang, T., Chong, T., Wang, Z., Zhai, X., et al. (2017). Protective effects of genistein against mono-(2-ethylhexyl) phthalate-induced oxidative damage in prepubertal Sertoli cells. *Biomed. Res. Int.* 2017, 2032697. doi:10.1155/2017/2032697

Zhang, T. D., Ma, Y. B., Gao, M., Li, H. C., Wang, Z. M., Chong, T., et al. (2022). 10(-7) M genistein partially alleviates 10(-7) M MEHP unfavorable effects in a new modified fetal rat testis culture system. *Front. Cell Dev. Biol.* 10, 987928. doi:10.3389/fcell.2022.987928

Zhou, R., Wu, J., Liu, B., Jiang, Y., Chen, W., Li, J., et al. (2019). The roles and mechanisms of Leydig cells and myoid cells in regulating spermatogenesis. *Cell Mol. Life Sci.* 76 (14), 2681–2695. doi:10.1007/s00018-019-03101-9

Zhu, J., Phillips, S. P., Feng, Y. L., and Yang, X. (2006). Phthalate esters in human milk: concentration variations over a 6-month postpartum time. *Environ. Sci. Technol.* 40 (17), 5276–5281. doi:10.1021/es060356w

Zirkin, B. R., and Papadopoulos, V. (2018). Leydig cells: formation, function, and regulation. *Biol. Reprod.* 99 (1), 101–111. doi:10.1093/biolre/ioy059

frontiers | Frontiers in Toxicology

TYPE Original Research
PUBLISHED 25 September 2023
DOI 10.3389/ftox.2023.1237819

OPEN ACCESS

EDITED BY
Takamitsu A. Kato,
Colorado State University, United States

REVIEWED BY
Changjian Xie,
Shandong University of Technology, China
Khursheed Ali,
University of Washington, United States

*CORRESPONDENCE
Masakazu Umezawa,
masa-ume@rs.tus.ac.jp

RECEIVED 10 June 2023
ACCEPTED 13 September 2023
PUBLISHED 25 September 2023

CITATION
Umezawa M, Itano R, Sakaguchi N and Kawasaki T (2023), Infrared spectroscopy analysis determining secondary structure change in albumin by cerium oxide nanoparticles.
Front. Toxicol. 5:1237819.
doi: 10.3389/ftox.2023.1237819

Infrared spectroscopy analysis determining secondary structure change in albumin by cerium oxide nanoparticles

Masakazu Umezawa[1,2]*, Ryodai Itano[2], Naoya Sakaguchi[2] and Takayasu Kawasaki[3]

[1]Department of Medical and Robotic Engineering Design, Faculty of Advanced Engineering, Tokyo University of Science, Tokyo, Japan, [2]Department of Materials Science and Technology, Graduate School of Advanced Engineering, Tokyo University of Science, Tokyo, Japan, [3]Accelerator Laboratory, High Energy Accelerator Research Organization, Tsukuba, Japan

Cerium oxide (CeO_2) nanoparticles are expected to have applications in the biomedical field because of their antioxidative properties. Inorganic nanoparticles interact with proteins at the nanoparticle surface and change their conformation when administered; however, the principle underlying this interaction is still unclear. This study aimed to investigate the secondary structural changes occurring in bovine serum albumin (BSA) mixed with CeO_2 nanoparticles having different surface modifications using Fourier transform infrared spectroscopy. CeO_2 nanoparticles (diameter: 240 nm) were synthesized from an aqueous cerium (III) nitrate solution using a homogeneous precipitation method. The surfaces of the nanoparticles were modified by the catechol compounds dopamine and 3,4-dihydroxyhydrocinnamic acid (DHCA). In the presence of these CeO_2 nanoparticles (0.11–0.43 mg/mL), β-sheet formation of BSA (30 mg/mL) was promoted especially on the amine-modified (positively charged) nanoparticles. The local concentration of BSA on the surface of the positively charged nanoparticles may have resulted in structural changes due to electrostatic and other interactions with BSA. Further investigations of the interaction mechanism between nanoparticles and proteins are expected to lead to the safe biomedical applications of inorganic nanoparticles.

KEYWORDS

nanotoxicology, protein corona, protein conformation, albumin, infrared spectrometry, β-sheet

1 Introduction

Recent advances in nanotechnology offer applications of various nanoparticles (NPs) for targeted drug delivery, bioimaging, and biosensing by utilizing their enhanced magnetic, antibacterial, and other bioactive properties (McNamara and Tofail, 2017). Cerium oxide (CeO_2) NPs are crucial industrial materials, including polishing materials in the glass and optics industry (Dahle and Arai, 2015). In addition, they have gained much interest for biological applications owing to their antioxidant properties. Because of the quick conversion of the oxidation state between Ce^{3+} and Ce^{4+}, CeO_2 NPs exhibit anti-oxidative activities, including superoxide oxidase and catalase mimetic properties to scavenge excess reactive oxygen and nitric species in biological tissues (Korsvik et al., 2007; Heckert et al., 2008; Caputo et al., 2014; Xu and Qu, 2014). These properties of CeO_2 NPs may contribute to the

regulation and maintenance of cell proliferation in tissue engineering (Hosseini and Mozafari, 2020). Previous studies have shown that CeO_2 NPs ameliorate neurodegeneration in a Parkinson's disease model (Hegazy et al., 2017) and drug-induced keratinocyte cytotoxicity (Singh et al., 2016), oxidative brain injury (Elshony et al., 2021), reproductive toxicity (Saleh et al., 2020), and hepatic steatosis (Wasef et al., 2021).

When NPs are applied to *in vivo* tissues, biomolecules, such as proteins, interact with the particle surface. Protein adsorption to NPs (corona formation) depends on the charge (Aramesh et al., 2015) and chemical modification (Galdino et al., 2020) of the NP surface and salts coexisting in the dispersant (Givens et al., 2019). This interaction is not limited to simple adsorption (corona formation) and desorption, but can cause conformational changes in proteins (Lynch et al., 2006; Khanal et al., 2016; Onoda et al., 2017) and following cellular responses (Onoda et al., 2020). In this context, the NP surface can act as a catalyst to provide a high-energy activated state for the stable secondary structure of proteins. Dysregulation of the conformation (misfolding) of proteins reduces their solubility and degradability, and in some cases, causes tissue dysfunction and diseases (Zerovnik, 2002; Gidalevitz et al., 2010). The potential for such conformational changes was indicated by the Raman shift in the amide I region of bovine serum albumin (BSA) interacting with zinc oxide NPs (Žūkienė and Snitka, 2015). Based on the Fourier transform infrared (FT-IR) spectra of the amide I band (Sakaguchi et al., 2022), we recently reported that concentrating amyloid β peptides on the NP surface may enhance the formation and stacking of their β-sheet structure. The coexistence of ions that can interact with peptides also modifies the interaction between the NPs and peptides (Sakaguchi et al., 2022). Some other studies reported a potential of secondary structure (conformational) changes of albumin by metal oxide NPs such as titanium dioxide, zinc oxide, CeO_2, (Simón-Vázquez et al., 2014; Ranjan et al., 2016; Bukackova and Marsalek, 2020), and iron oxide (Mehrabi et al., 2021; Nisar et al., 2022).

In general, forces such as hydrophobic interactions, hydrogen bonding, and electrostatic interactions act between the NPs and biomolecules. The interaction pattern can be predicted to some extent based on the forces between functional groups at the NP surface, that is, at the interface, and biomolecules, including proteins (Co and Li, 2021). However, because proteins are constantly adsorbing and desorbing at the surface of NPs and the interactions between NPs and proteins are constantly changing (Saptarshi et al., 2013), it is difficult to accurately predict the complex effects of these interactions on protein conformations. Furthermore, the effect on protein conformation depends not only on the physicochemical properties of NPs but also on their concentration (Wangoo et al., 2008). When NPs are administered to living organisms for biomedical and pharmaceutical purposes, it is necessary to screen for conformational changes in proteins at the NP surface to prevent unintentional and toxic reactions. Surface modification to tune the properties of NPs is an effective measure for the systematic study of these interactions. Here, we used CeO_2 NPs as a model of metal oxide whose surface can be easily modified. The present study aimed to investigate the changes in protein secondary structure due to interactions with CeO_2 NPs, an inorganic material expected to be used in the biomedical field. BSA, which is abundant in the blood of humans and animals, was used as a model protein.

2 Materials and methods

2.1 Materials

Cerium (III) nitrate hexahydrate ($Ce(NO_3)_3$ $6H_2O$; product No. CEH09XB) was purchased from Kojundo Chemical Laboratory Co., Ltd. (Saitama, Japan). Urea (product No. 219-00175) was purchased from Fujifilm Wako Pure Chemical Co. (Osaka, Japan). BSA (product No. A2153), dopamine hydrochloride (product No. H8502), 3,4-dihydroxyhydrocinnamic acid (DHCA; product No. 102601), and deuterium oxide (D_2O; product No. 151890) were purchased from Sigma-Aldrich Co. (St Louis, MO, USA). All the reagents were used without further purification.

2.2 Synthesis and characterization of CeO_2 NPs

CeO_2 NPs were synthesized using a homogeneous precipitation method. $Ce(NO_3)_3$ $6H_2O$ (4 mmol) and urea (50 g) were mixed and dissolved in distilled water (300 mL) and heated at 90°C for 60 min in a hot water bath. After cooling to 20°C, the precipitate was collected as a precursor by centrifugation (10,000 g, 10 min) and washed with distilled water (10,000 g, 10 min, ×3). After drying the precursor at 80°C for 24 h, it was calcined by increasing the temperature to 800°C at a rate of 10°C/min and maintaining it at 800°C for 1 h in an electric furnace (NHK-170; Nitto Kagaku Co., Ltd., Nagoya, Japan). Calcined samples (1 g) were milled using Pulverrisette 7 Classic Line (Fritsch GmbH, Idar-Oberstein, Germany) at 250 rpm for 60 min. The obtained samples were analyzed using an FT-IR spectrometer (FT/IR-6000; JASCO Co., Tokyo, Japan), X-ray diffraction (XRD; RINT-TTR III; Rigaku Co., Tokyo, Japan), dynamic light scattering (DLS; ELSZ-2000ZS; Otsuka Electronics Co., Ltd., Osaka, Japan), and scanning electron microscopy (SEM; S-4200; Hitachi High-Tech Co., Tokyo, Japan). The crystalline size of samples was also determined by the half-width of XRD peaks according to the Scherrer formula (Patterson, 1939).

2.3 Surface modification of CeO_2 NPs

The surfaces of CeO_2 NPs can be modified by catechol compounds, as described previously (Togashi et al., 2011; Hayat et al., 2014). The samples of CeO_2 NPs (1.7 mg) were mixed and stirred for 48 h with dopamine (0.25 mM) or DHCA (0.25 mM) in distilled water (5 mL) for surface modification of the particles. The suspension was then washed four times with distilled water and collected via centrifugation (5,000 g et al., 2 min) on an Amicon Ultra centrifugal filter device (MWCO 100 k; Merck KGaA, Darmstadt, Germany) to remove excess dopamine and DHCA. Finally, the dispersion medium was replaced with D_2O via centrifugal washing on the filter device.

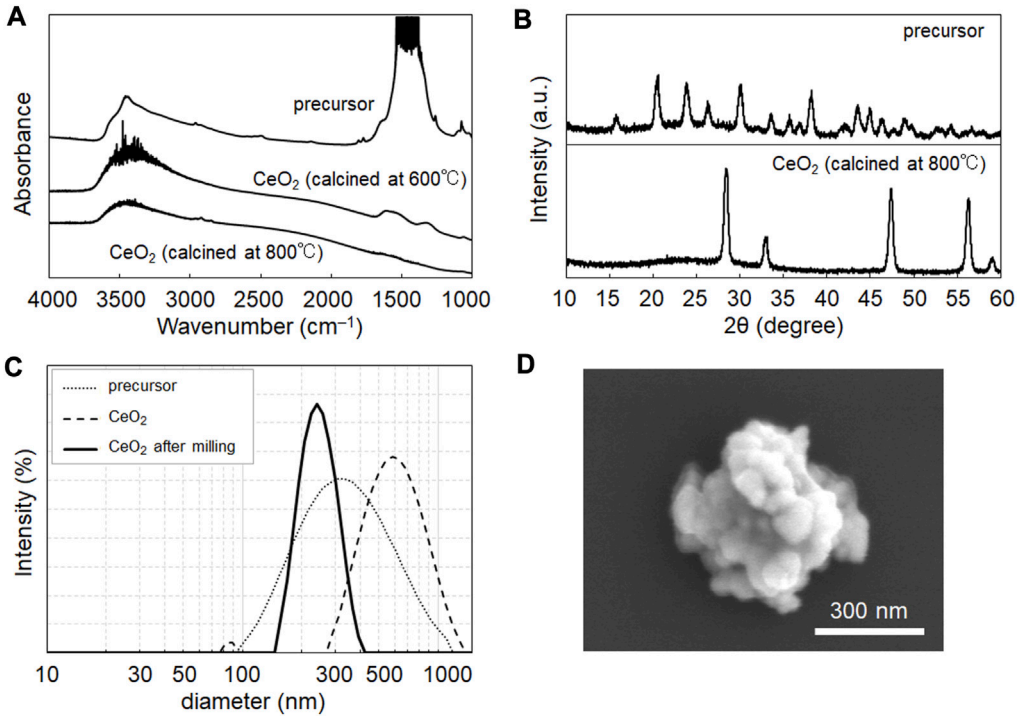

FIGURE 1
Characterization of CeO_2 nanoparticles (NPs) synthesized in this study. **(A)** Fourier transform infrared (FT-IR) spectra of NP samples before and after calcination at 600°C and 800°C. **(B)** X-ray diffraction pattern of NP samples before and after calcination at 800°C. The pattern of the calcined sample showed the characteristics of CeO_2 (JCPDS no. 43-1,002). **(C)** Size distribution data from dynamic light scattering of samples before and after milling treatment (250 rpm, 60 min). **(D)** SEM image of the obtained NP samples after the milling treatment.

2.4 Fourier transform infrared spectroscopy of Protein-NP mixtures

The BSA solution (40 mg/mL) in D_2O was mixed with CeO_2 NPs dispersed in D_2O at a 3:1 volume ratio; thus, the final concentration of BSA in the mixed samples was 30 mg/mL. The final concentration of NPs in the mixture was 0, 0.11, and 0.43 mg/mL. The BSA solutions with and without NPs in D_2O were sandwiched between two CaF_2 plate windows (spacer, 0.025 mm). D_2O was used as the solvent instead of water because the IR absorption peak at 1,600–1,650 cm^{-1} derived from O-H bonding in water overlaps with the peak of the amide I band and disturbs the analysis. FT-IR spectra, including amide bands, were recorded using an FT/IR-6200 spectrometer (JASCO Co., Tokyo, Japan) for samples set between the CaF_2 windows.

3 Results and discussion

CeO_2 NPs were prepared via the homogenous precipitation method (Venkatachalam et al., 2009), which enables the synthesis of products with homogeneous particle sizes and high yields. Figure 1A shows the FT-IR spectra used to evaluate the chemical composition of the NPs after calcination. The peaks at 3,300 and 1,500 cm^{-1} indicate the presence of hydroxides and carbonates in the NP samples. In homogeneous precipitation (Venkatachalam et al., 2009), urea is converted to ions of ammonium (NH_4^+), hydroxide (OH^-), and hydrogen carbonate (HCO_3^-) in a cerium solution at 80°C. The $OH^-$and HCO_3^- produced precursor NP composed of cerium hydroxide and cerium hydrogen carbonate. This precursor was converted into CeO_2 via calcination. As shown in Figure 1A, hydrogen carbonate was removed by calcination at 800°C, but remained after treatment at 600°C. Thus, similar to the case of yttria reported previously (Venkatachalam et al., 2009), calcination at 800°C is suitable for yielding an oxide (ceria).

The samples were characterized using XRD (Figure 1B), DLS (Figure 1C), and SEM (Figure 1D). Figure 1B shows the characteristic XRD pattern of CeO_2 in the samples obtained after calcination. DLS showed a peak in the size distribution of calcined CeO_2 at 550 nm, with a wide distribution from 350 to 1,000 nm (Figure 1C), which shows their agglomeration in dispersion in water. Therefore, milling was performed to prevent the agglomeration of the samples. The milling treatment yielded CeO_2 NPs with a size distribution peak at 240 nm (Figure 1C), which was validated using SEM (Figure 1D). XRD data suggested the crystalline size of CeO_2 was 15.8 nm. The mass of a CeO_2 NP (density: 7.22 mg/cm^3) could be calculated as 5.22×10^{-14} g; thus, the particle concentrations of the CeO_2 dispersions at 0.11 and 0.43 mg/mL were 2.11 and 8.24×10^9 particles/mL, respectively.

The surface of the synthesized CeO_2 NPs was modified with the catechol compounds, which can form strong bonds with hydroxy groups on the surface of metal oxides (cerium oxide, iron oxide, and gadolinium oxide, *etc.*) (Togashi et al., 2011; Hayat et al., 2014). Dopamine and DHCA were used as catechol compounds with

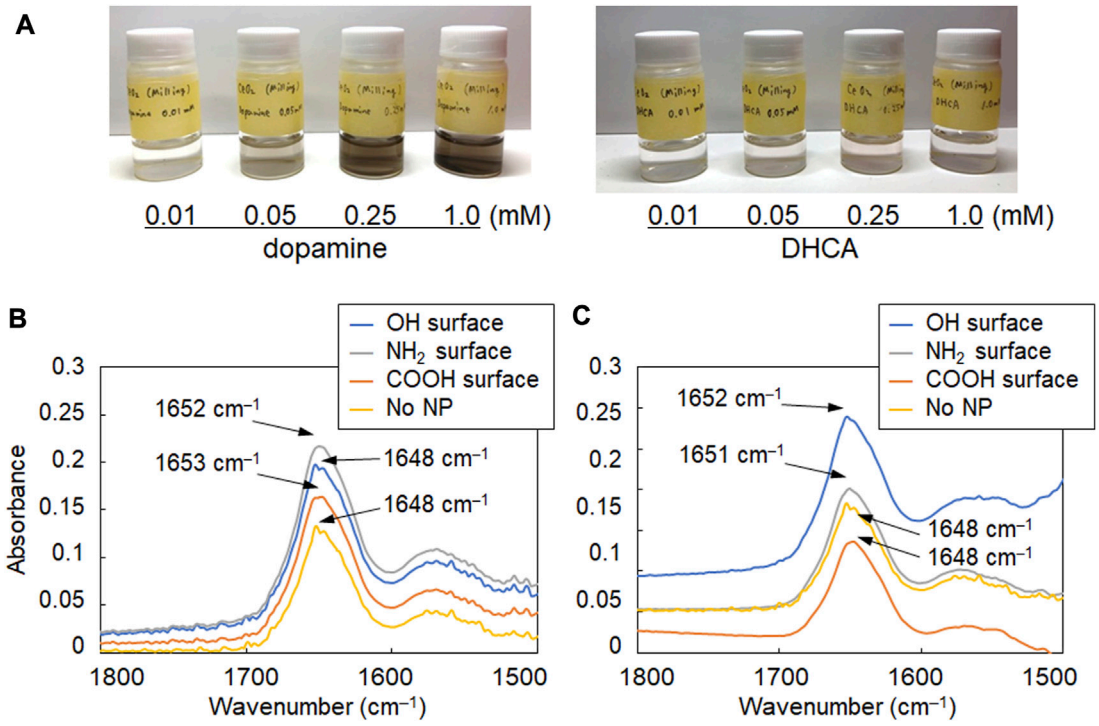

FIGURE 2
FT-IR spectra of albumin reacted with CeO_2 NPs having different surface modifications. **(A)** Images of aqueous suspensions of CeO_2 NPs modified with dopamine and 3,4-dihydroxyhydrocinnamic acid (DHCA). **(B, C)** FT-IR spectra of albumin (30 mg/mL) incubated with **(B)** 0.11 mg/mL and **(C)** 0.43 mg/mL of NPs with plain (OH, bare NPs) and modified NH_2 and COOH surfaces.

amino and carboxy groups, respectively, to analyze the changes in the secondary structure of albumin due to the difference in the surfaces of CeO_2 NPs. When the NPs were mixed and stirred with each catechol solution, the surface modification was confirmed by the colorimetric change in the dispersion (Figure 2A), as reported previously (Hayat et al., 2014). Such colorimetric change is observed due to the formation of dopaquinone structure on the NPs (Hayat et al., 2014). BSA, which is abundant in the blood and other body fluids and is highly similar to human albumin, was used as a model protein. The mixture ratio was set considering the number concentration of the NPs and BSA molecules to ensure that the particle concentration was not too high relative to BSA to unrealistic levels. The number concentration of BSA (30 mg/mL; Mw: 66,500) was 2.72×10^{17} molecules/mL; therefore, the number ratios of BSA/CeO_2 NPs were 1.3×10^8 and 3.3×10^7 per CeO_2 NP in this study. The FT-IR spectra of albumin and NP samples mixed in D_2O were analyzed to investigate the secondary structure of albumin. The amide I band (around 1,650 cm^{-1}), attributed to C=O stretching, was focused on because it is hardly affected by the nature of the side chains but depends on the secondary structure of the backbone (Jiang et al., 2011) and therefore, it is applicable to both *in vitro* (Barth and Zscherp, 2002) and *in situ* (Onoda et al., 2017) analyses of the protein secondary structure. Because water molecules (H_2O) show peaks at 3,300 cm^{-1} as well as 1,650 cm^{-1} that interferes with those of the amide I band, which was the target of analysis in this study, D_2O was used for incubating BSA with NPs instead of H_2O.

As shown in Figures 2B,C, the amide I band in the FT-IR spectrum of BSA shifted to a slightly higher wavenumber in the presence of CeO_2 NPs. In addition, the shape of the low-wavenumber side of the amide I band peak changed when BSA was mixed with CeO_2 NPs. The minor shoulder of the low-wavenumber side tended to be slightly larger in the presence of NPs. Deconvolution analysis using Gaussian fitting showed that the FT-IR spectra of BSA included, in addition to the major peak at 1,650 cm^{-1}, a minor peak corresponding to protein β-sheet formation at 1,618 cm^{-1} (Barth and Zscherp, 2002) (Figure 3). The results showed that the ratio of β-sheets did not change upon mixing with the NPs having plain or carboxylate surfaces at lower concentration, but increased 1.1-fold by reacting with the NPs having an amine surface (Figure 4). On the other hand, α-helix slightly decreased with the increase in the β-sheet structure by the amine-modified NPs (Figure 4). At higher concentration (0.43 mg/mL of NPs), all the three NPs affected the β-sheet structure. The change in BSA was due to whole NPs because it was incubated with NP samples after the purification with the centrifugal filter membrane to remove the excess catechol compounds unbound to the NPs.

The primary interaction between NPs and protein molecules depends on the size and morphology of the NPs and the strength of their affinity (Co and Li, 2021). In addition to hydrophobic interaction (Roach et al., 2006), electrostatic interaction also works; the contribution of electrostatic interaction is considered to be significant because the increase rate of β-sheet was larger when incubated with the amine-modified NPs in this study. The surfaces of the amine-modified NPs are positively charged in the dispersion. In contrast, BSA, which has an isoelectric point of 4.9, is positively

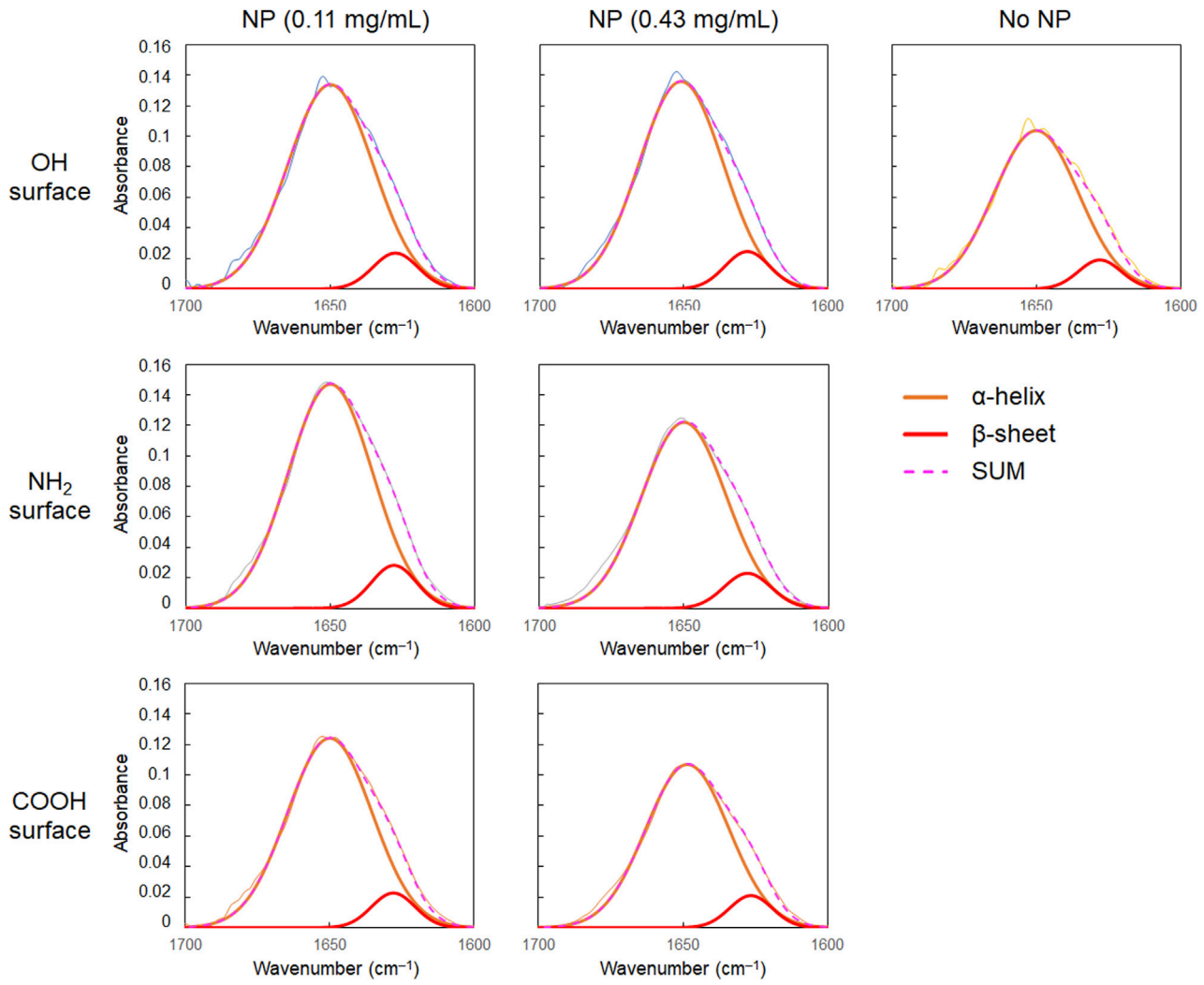

FIGURE 3
Results of the deconvolution analysis of FT-IR spectra of albumin (30 mg/mL) with CeO_2 NPs.

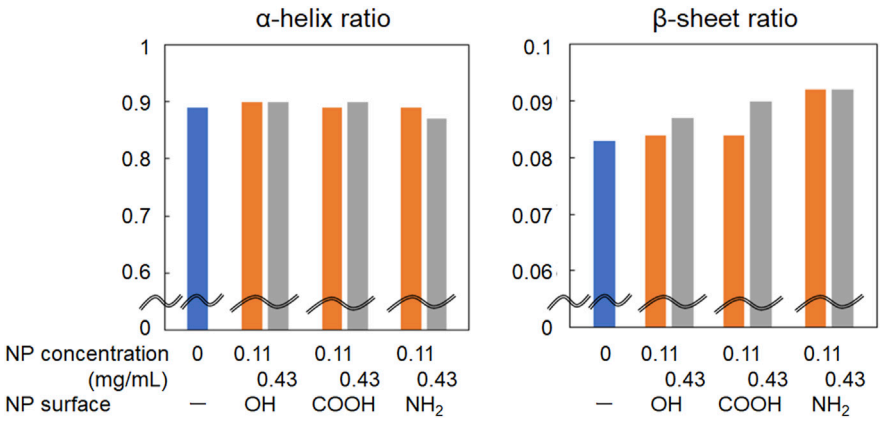

FIGURE 4
Change in the ratio of α-helix and β-sheet in the amide I band of FT-IR spectra of albumin reacted with CeO_2 NPs.

charged as a whole molecule in a neutral pH environment. Protein adsorption onto NPs is dependent on the surface charge of the NPs (Aramesh et al., 2015; Yadav et al., 2017). Under neutral conditions, the amine-modified NPs attracted BSA through electrostatic interactions and concentrated locally near the NP surface causing secondary structure changes. Further interactions of the concentrated BSA molecules with each other via forces such as hydrogen bonding may change the folding state and increase the ratio of the β-sheet structure in BSA. Differences in such interaction the different surface modifications of NPs with proteins may contribute to modulation of their toxicity. Although the toxicity of these NPs with different surfaces was not compared in the present study, the amine-modified NPs with cationic surface generally show higher membrane permeability and toxicity. Further investigation of the method to separate the protein and NPs after their reaction is underway to study the effect of the deconformed proteins by NPs on toxicity to cells and animals.

This paper focused on the method of FT-IR data for secondary structural analysis of proteins with NPs. In addition to FT-IR, analysis of circular dichroism (CD) data in ultraviolet (UV) is also useful for validating the secondary structure of proteins in the liquid phase. Our preliminary data showed a quite large difference in the optical absorbance of proteins between UV and IR, and therefore, a need to investigate using protein samples with very different concentrations. Care should be taken for the possible changes in the secondary structure due to differences in concentration of proteins for analysis in future studies. In addition, zeta potential data to evaluate the surface modification could not be obtained due to the low concentration of well-dispersed particle samples obtained after the final centrifugation on the centrifugal filter device (see section 2.3). Further investigations are needed to obtain a method of NP preparation to analyze such secondary structure changes with zeta potential data of NPs.

Overall, we present an IR spectroscopy-based method for evaluating changes in the secondary structure of proteins interacting with NPs, having large liquid–solid interfaces, using albumin, which is abundant in body fluids, as a model. Changes in the secondary structure of BSA were induced by a reaction with amine-modified NPs, which increased the β-sheet structure. Further investigations are needed to clarify the effects of NPs on the secondary structure of other proteins and their dependence on particle size. Moreover, the effects of coexisting molecules and ions on NP–protein interactions, together with other methods such as molecular dynamics simulations, are of interest for elucidating the details of the mechanisms underlying the interactions in an *in vivo* environment. This approach will contribute to the safe biomedical application of inorganic nanomaterials by providing a mechanistic understanding of the interactions between biomolecules and inorganic nanomaterials designed for future applications.

Data availability statement

The raw data supporting the conclusions of this article will be made available by the authors, without undue reservation.

Author contributions

MU was the main project leader and conceived the overall research idea. RI performed all the experiments and data collection. RI, NS, TK, and MU were substantially involved in data analysis and interpretation. MU and RI drafted the manuscript. All authors contributed to the article and approved the submitted version.

Funding

This work was supported by JSPS KAKENHI Grant Numbers 22K06565 and 22H03335.

Acknowledgments

The authors thank Hikaru Haraguchi, Junsuke Katayama, and Hiroyuki Kurahashi (Tokyo University of Science) for technical assistance of synthesis and characterization of CeO_2 NPs. The authors would like to acknowledge Faculty of Advanced Engineering of Tokyo University of Science to provide additional financial resources of this study through a Young Scientist Collaborative Research Grant.

Conflict of interest

The authors declare that the research was conducted in the absence of any commercial or financial relationships that could be construed as a potential conflict of interest.

Publisher's note

References

Aramesh, M., Shimori, O., Ostrikov, K., Prawer, S., and Cervenka, J. (2015). Surface charge effects in protein adsorption on nanodiamonds. *Nanoscale* 7, 5726–5736. doi:10.1039/c5nr00250h

Barth, A., and Zscherp, C. (2002). What vibrations tell us about proteins. *Rev. Biophys.* 35, 369–430. doi:10.1017/s0033583502003815

Bukackova, M., and Marsalek, R. (2020). Interaction of BSA with ZnO, TiO_2, and CeO_2 nanoparticles. *Biophys. Chem.* 267, 106475. doi:10.1016/j.bpc.2020.106475

Caputo, F., De Nicola, M., and Ghibelli, L. (2014). Pharmacological potential of bioactive engineered nanomaterials. *Biochem. Pharm.* 92, 112–130. doi:10.1016/j.bcp.2014.08.015

Co, N. T., and Li, M. S. (2021). Effect of surface roughness on aggregation of polypeptide chains: a Monte Carlo study. *Biomolecules* 11, 596. doi:10.3390/biom11040596

Dahle, J. T., and Arai, Y. (2015). Environmental geochemistry of cerium: applications and toxicology of cerium oxide nanoparticles. *Int. J. Environ. Res. Public Health* 12, 1253–1278. doi:10.3390/ijerph120201253

Elshony, N., Nassar, A. M., El-Sayed, Y. S., Samak, D., Noreldin, A., Wasef, L., et al. (2021). Ameliorative role of cerium oxide nanoparticles against fipronil impact on brain function, oxidative stress, and apoptotic cascades in albino rats. *Front. Neurosci.* 15, 651471. doi:10.3389/fnins.2021.651471

Galdino, F. E., Picco, A. S., Sforca, M. L., Cardoso, M. B., and Loh, W. (2020). Effect of particle functionalization and solution properties on the adsorption of bovine serum albumin and lysozyme onto silica nanoparticles. *Colloids Surf. B Biointerfaces* 186, 110677. doi:10.1016/j.colsurfb.2019.110677

Gidalevitz, T., Kikis, E. A., and Morimoto, R. I. (2010). A cellular perspective on conformational disease: the role of genetic background and proteostasis networks. *Curr. Opin. Struct. Biol.* 20, 23–32. doi:10.1016/j.sbi.2009.11.001

Givens, B. E., Wilson, E., and Fiegel, J. (2019). The effect of salts in aqueous media on the formation of the BSA corona on SiO_2 nanoparticles. *Colloids Surf. B Biointerfaces* 179, 374–381. doi:10.1016/j.colsurfb.2019.04.012

Hayat, A., Andreescu, D., Bulbul, G., and Andreescu, S. (2014). Redox reactivity of cerium oxide nanoparticles against dopamine. *J. Colloid Interface Sci.* 418, 240–245. doi:10.1016/j.jcis.2013.12.007

Heckert, E., Karakoti, A. S., Seal, S., and Self, W. T. (2008). The role of cerium redox state in the SOD mimetic activity of nanoceria. *Biomaterials* 29, 2705–2709. doi:10.1016/j.biomaterials.2008.03.014

Hegazy, M. A. E., Maklad, H. M., Elmonsif, D. A. A., Elnozhy, F. Y., Alqubiea, M. A., Alenezi, F. A., et al. (2017). The possible role of cerium oxide (CeO_2) nanoparticles in prevention of neurobehavioral and neurochemical changes in 6-hydroxydopamine induced parkinsonian disease. *Alex. J. Med.* 53, 351–360. doi:10.1016/j.ajme.2016.12.006

Hosseini, M., and Mozafari, M. (2020). Cerium oxide nanoparticles: recent advances in tissue engineering. *Materials* 13, 3072. doi:10.3390/ma13143072

Jiang, Y., Li, C., Nguyen, X., Muzammil, S., Towers, E., Gabrielson, J., et al. (2011). Qualification of FTIR spectroscopic method for protein secondary structural analysis. *J. Pharm. Sci.* 100, 4631–4641. doi:10.1002/jps.22686

Khanal, D., Kondyurin, A., Hau, H., Knowles, J. C., Levinson, O., Ramzan, I., et al. (2016). Biospectroscopy of nanodiamond-induced alterations in conformation of intra- and extracellular proteins: a nanoscale IR study. *Anal. Chem.* 88, 7530–7538. doi:10.1021/acs.analchem.6b00665

Korsvik, C., Patil, S., Seal, S., and Self, W. T. (2007). Superoxide dismutase mimetic properties exhibited by vacancy-engineered ceria nanoparticles. *Chem. Commun.* 10, 1056–1058. doi:10.1039/b615134e

Lynch, I., Dawson, K. A., and Linse, S. (2006). Detecting cryptic epitopes created by nanoparticles. *Sci. STKE* 327, pe14. doi:10.1126/stke.3272006pe14

McNamara, K., and Tofail, S. A. M. (2017). Nanoparticles in biomedical applications. *Adv. Phys. X* 2, 54–88. doi:10.1080/23746149.2016.1254570

Mehrabi, M., Ghasemi, M. F., Rasti, B., Falahati, M., Mirzaie, A., and Hasan, A. (2021). Nanoporous iron oxide nanoparticle: hydrothermal fabrication, human serum albumin interaction and potential antibacterial effects. *J. Biomol. Struct. Dyn.* 39, 2595–2606. doi:10.1080/07391102.2020.1751296

Nisar, A., Ajabia, D. K., Agrawal, S. B., Varma, S., Chaudhari, B. P., and Tupe, R. S. (2022). Mechanistic insight into differential interactions of iron oxide nanoparticles with native, glycated albumin and their effect on erythrocytes parameters. *Int. J. Biol. Macromol.* 212, 232–247. doi:10.1016/j.ijbiomac.2022.05.106

Onoda, A., Kawasaki, T., Tsukiyama, K., Takeda, K., and Umezawa, M. (2020). Carbon nanoparticles induce endoplasmic reticulum stress around blood vessels with accumulation of misfolded proteins in the developing brain of offspring. *Sci. Rep.* 10, 10028. doi:10.1038/s41598-020-66744-w

Onoda, A., Kawasaki, T., Tsukiyama, K., Takeda, K., and Umezawa, M. (2017). Perivascular accumulation of β-sheet-rich proteins in offspring brain following maternal exposure to carbon black nanoparticles. *Front. Cell. Neurosci.* 11, 92. doi:10.3389/fncel.2017.00092

Patterson, A. L. (1939). The scherrer formula for X-ray particle size determination. *Phys. Rev.* 56, 978–982. doi:10.1103/physrev.56.978

Ranjan, S., Dasgupta, N., Srivastava, P., and Ramalingam, C. (2016). A spectroscopic study on interaction between bovine serum albumin and titanium dioxide nanoparticle synthesized from microwave-assisted hybrid chemical approach. *J. Photochem. Photobiol. B.* 161, 472–481. doi:10.1016/j.jphotobiol.2016.06.015

Roach, P., Farrar, D., and Perry, C. C. (2006). Surface tailoring for controlled protein adsorption: effect of topography at the nanometer scale and chemistry. *J. Am. Chem. Soc.* 128, 3939–3945. doi:10.1021/ja056278e

Sakaguchi, N., Kaumbekova, S., Itano, R., Amouei Torkmahalleh, M., Shah, D., and Umezawa, M. (2022). Changes in the secondary structure and assembly of proteins on fluoride ceramic (CeF_3) nanoparticle surfaces. *ACS Appl. Bio Mat.* 5 (6), 2843–2850. doi:10.1021/acsabm.2c00239

Saleh, H., Nassar, A. M. K., Noreldin, A. E., Samak, D., Elshony, N., Wasef, L., et al. (2020). Chemo-protective potential of cerium oxide nanoparticles against fipronil-induced oxidative stress, apoptosis, inflammation and reproductive dysfunction in male white albino rats. *Molecules* 25, 3479. doi:10.3390/molecules25153479

Saptarshi, S. R., Duschl, A., and Lopata, A. L. (2013). Interaction of nanoparticles with proteins: relation to bio-reactivity of the nanoparticle. *J. Nanobiotechnol.* 11, 26. doi:10.1186/1477-3155-11-26

Simón-Vázquez, R., Lozano-Fernández, T., Peleteiro-Olmedo, M., and González-Fernández, A. (2014). Conformational changes in human plasma proteins induced by metal oxide nanoparticles. *Colloids Surf. B. Biointerfaces* 113, 198–206. doi:10.1016/j.colsurfb.2013.08.047

Singh, R., Karakoti, A. S., Self, W., Seal, S., and Singh, S. (2016). Redox-sensitive cerium oxide nanoparticles protect human keratinocytes from oxidative stress induced by glutathione depletion. *Langmuir* 32, 12202–12211. doi:10.1021/acs.langmuir.6b03022

Togashi, T., Naka, T., Asahina, S., Sato, K., Takami, S., and Adschiri, T. (2011). Surfactant-assisted one-pot synthesis of superparamagnetic magnetite nanoparticle clusters with tunable cluster size and magnetic field sensitivity. *Dalton Trans.* 40, 1073–1078. doi:10.1039/c0dt01280g

Venkatachalam, N., Saito, Y., and Soga, K. (2009). Synthesis of Er^{3+} doped Y_2O_3 nanophosphors. *J. Am. Ceram. Soc.* 92, 1006–1010. doi:10.1111/j.1551-2916.2009.02986.x

Wangoo, N., Suri, C. R., and Shekhawat, G. (2008). Interaction of gold nanoparticles with protein: a spectroscopic study to monitor protein conformational changes. *Appl. Phys. Lett.* 92, 133104. doi:10.1063/1.2902302

Wasef, L., Nassar, A. M. K., El-Sayed, Y. S., Samak, D., Noreldin, A., Elshony, N., et al. (2021). The potential ameliorative impacts of cerium oxide nanoparticles against fipronil-induced hepatic steatosis. *Sci. Rep.* 11, 1310. doi:10.1038/s41598-020-79479-5

Xu, C., and Qu, X. (2014). Cerium oxide nanoparticle: a remarkably versatile rare earth nanomaterial for biological applications. *NPG Asia Mater* 6, e90. doi:10.1038/am.2013.88

Yadav, I., Kumar, S., Aswal, V. K., and Kohlbrecher, J. (2017). Structure and interaction in the pH-dependent phase behavior of nanoparticle-protein systems. *Langmuir* 33, 1227–1238. doi:10.1021/acs.langmuir.6b04127

Zerovnik, E. (2002). Amyloid-fibril formation. Proposed mechanisms and relevance to conformational disease. *Eur. J. Biochem.* 269, 3362–3371. doi:10.1046/j.1432-1033.2002.03024.x

Žūkienė, R., and Snitka, V. (2015). Zinc oxide nanoparticle and bovine serum albumin interaction and nanoparticles influence on cytotoxicity *in vitro*. *Colloids Surf. B Biointerfaces* 135, 316–323. doi:10.1016/j.colsurfb.2015.07.054

Frontiers in Toxicology

Explores the effects of toxins from molecular to population level

A multidisciplinary journal which presents the latest research on the adverse effects of substances, particles and mixtures on living organisms.

Discover the latest Research Topics

See more →

Frontiers

Avenue du Tribunal-Fédéral 34
1005 Lausanne, Switzerland
frontiersin.org

Contact us

+41 (0)21 510 17 00
frontiersin.org/about/contact